Molecular and cellular determinants of Cardiac tachyarrhythmias:

From trigger to therapy

B.O. Bingen

Colophon
The studies described in this thesis were performed at the department of Cardiology of the Leiden University Medical Center, Leiden, the Netherlands.
Thesis, Leiden University, the Netherlands

Printed by: Gildeprint Enschede
ISBN: 978-94-6233354-3
Cover: B.O. Bingen

Molecular and cellular determinants of Cardiac tachyarrhythmias:

From trigger to therapy

PROEFSCHRIFT

ter verkrijging van
de graad van doctor aan de Universiteit Leiden,
op gezag van Rector Magnificus prof. mr. C.J.J.M. Stolker
volgens besluit van het College voor Promoties
te verdedigen op woensdag 5 oktober 2016
klokke 15.00 uur

door

Brian Oscar Bingen

Geboren te Den Helder

In 1987

Promotor:
Prof. dr. M.J. Schalij
Co-Promotores:
Dr. D.A. Pijnappels
Dr. A.A.F. de Vries

Leden promotiecommissie:
Prof. dr. D.E. Atsma
Prof. dr. K. Zeppenfeld
Prof. dr. M.J. Goumans
Prof. dr. A.V. Panfilov (Universiteit van Gent)
Prof. dr. U. Schotten (Universiteit van Maastricht)

The research described in this thesis was supported by a grant of the
Dutch Heart Foundation (DHF-2012T023*)*

TABLE OF CONTENTS

Chapter I

General introduction and outline of thesis

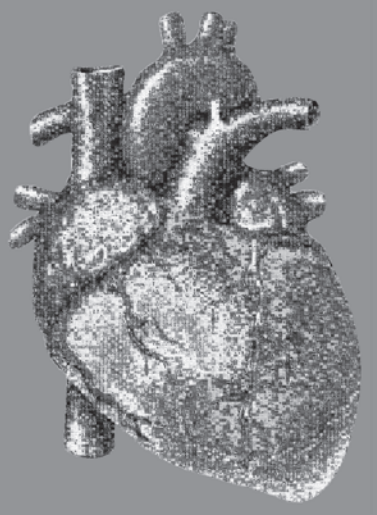

BACKGROUND

The human heart several billion cells of which the main functional or contractile unit is the cardiomyocyte.[1] For the heart to function normally (*i.e.* to deliver oxygenated blood, nutrients, immune cells and regulatory molecules to the organs and tissues) it relies on the coordinated rhythmic contractions of these cardiomyocytes upon electrical activation. In theory, given the large amount of cardiomyocytes constituting the heart, the number of sequences in which these cells could contract is enormous. However, only a small fraction of these theoretical sequences lead to the physiological forceful extrusion of blood from the heart.[2] Hence, tightly regulated electrical activation of these cardiomyocytes (cardiac electrophysiology) is essential for proper cardiac function. Concordantly, any significant perturbation of this regulation can, in theory, lead to dyssynchronous, irregular, overly fast or slow cardiac contractions, which are referred to as cardiac arrhythmias.

Cardiac arrhythmias are a major cause of morbidity and mortality throughout the world.[3, 4] Over the past decades, significant improvements have been made in anti-arrhythmic therapy. However, due to our incomplete understanding of the mechanisms underlying cardiac arrhythmias, treatment options are still far from optimal: Anti-arrhythmic drugs for instance, while sometimes effective in suppressing one arrhythmia, can display a tendency to provoke new/other arrhythmias.[5, 6] Furthermore, ablation techniques, whichrely on the intentional damaging of myocardium to prevent arrhythmias, are prone to complications due to the invasive nature of the techniques, while data on long-term outcome is currently lacking.[7, 8] Moreover, implantable devices, although effective, employ electric shocks to terminate arrhythmias, which are painful, traumatizing and cause tissue damage, while the use of this technology is limited by the high costs and complications such as infections and lead failures.[9-12] The limited preventive efficacy, the often invasive nature and the risk of adverse events/complications of current anti-arrhythmic treatment warrants a search for more specific, substrate-oriented treatment options. Hence, it is of critical importance to better understand the mechanisms underlying cardiac arrhythmias if we are to make progress in their treatment. In order to provide such understanding one should start by dissecting the basics of cardiac electrophysiology.

BASICS OF CARDIAC ELECTROPHYSIOLOGY

The cardiac cycle

During the normal cardiac cycle, deoxygenated blood from the body (systemic circulation) is collected in the right atrium, and pumped to the lungs by the right ventricles (the pulmonary circulation) where carbon dioxide is exchanged for oxygen. Subsequently, oxygenated blood is collected into the left atrium and pumped back into the systemic circulation by the left ventricle.

In order to complete this cycle to maximal efficiency, ventricular contraction must be delayed until the atria have completely emptied their contents into the ventricles to allow sufficient ventricular filling. Moreover, contraction of cardiomyocytes in the ventricles has to be coordinated so that ventricular contraction proceeds from apex to base to build up sufficient systolic pressure.[2]

The action potential

The initiation and coordination of cardiomyocyte contraction is governed by electrical signals called action potentials, which activate/excite the cardiomyocytes and stimulate contraction through a process called excitation-contraction coupling. Under normal conditions, action potentials develop spontaneously in the sinoatrial (or, in brief: sinus) node (the physiological cardiac pacemaker, located in the right atrium) and are propagated uniformly over both atria. Subsequently, the action potential travels through the atrioventricular node, where it slows down providing the critical delay between atrial and ventricular contraction, after which the ventricles are activated from apex to base through a specialized conduction network consisting of the His-bundle, left and right bundle branches and the Purkinje network.

The action potentials themselves are the result of the precisely timed opening and closing of mainly voltage-gated ion channels, located in the outer membrane (sarcolemma) of the cardiomyocyte. These ion channels allow selective passage of certain an- or cations across the sarcolemma down their electrochemical gradient. The difference in charge between the extracellular and intracellular environment of the cardiomyocyte (the transmembrane voltage or membrane potential) determines the conformation (*i.e.* open, closed or inactivated state) of the voltage-gated ion channels

and its consequent ionic conductance.[13-15] Under normal conditions, the cardiomyocyte membrane potential is negative at rest. However, action potentials propagated from neighboring cells can depolarize the cardiomyocyte until the threshold transmembrane voltage at which voltage-gated Na^+ (sodium) channels change from a closed state to an opened state, causing influx of Na^+.[16] The consequent, rapid further depolarization of the cardiomyocyte membrane (phase 0), marks the beginning of a new action potential. In turn, threshold voltages for several Ca^{2+} (calcium, inward current) and K^+ (potassium, outward current) channels are reached while the Na^+ channels are entering the inactivated state (phase 1)[16], leading to a transient plateau in membrane voltage (phase 2), characteristic for the cardiomyocyte action potential. As the main inward currents are inactivated at these depolarized membrane potentials, cardiomyocytes are resistant to new excitations (*i.e.* refractory), during this phase. Finally, when the outward current outweighs the inward current the cell repolarizes (phase 3) to its resting state (phase 4), enabling subsequent excitation by a new action potential (Figure 1).[14, 15]

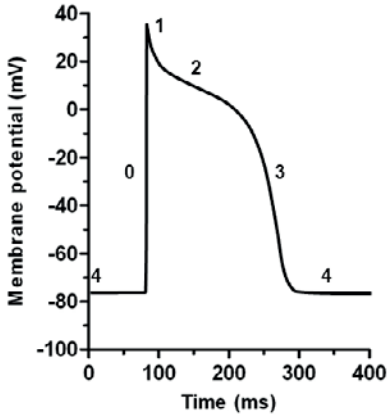

Figure 1. *Schematic representation of the action potential phases. 0: rapid depolarization of membrane potential caused by Na-⁺influx. 1: early repolarization caused by Na+ channel inactivation. 2: plateau phase resulting from calcium channel opening. 3: repolarization as a consequence of potassium channel activation. 4: resting phase*

Excitation contraction-coupling

The Ca^{2+} entering the cell during the action potential is a key regulating element for excitation-contraction coupling, serving as a signal for Ca^{2+}-induced Ca^{2+} release from an intracellular Ca^{2+} store called the sarcoplasmatic reticulum (SR) through specialized Ca^{2+} channels called ryanodine receptors located in the SR membrane.[17] Inside the sarcomere (the contractile element of the cardiomyocyte consisting of a multitude of proteins including troponins, tropomyosin, myosin and actin) the resulting increase in cytoplasmic Ca^{2+}, through its binding to tropinin-c, causes a conformational change in the tropomyosin complex enabling binding of the myosin head to the actin filament. This allows a conformational change in the myosin to occur, which pulls the actin filaments towards the centre of the sarcomere causing contraction of the cardiomyocyte.[18, 19] Upon hydrolysis of ATP bound to myosin, myosin releases its binding to actin, after which it reverts to its initial configuration. Simultaneously, intracellular Ca^{2+} is transported back to the SR by the sarco/endoplasmatic reticulum ATPase, moving the tropomyosin complex back in its original position, while preparing the SR for the next cycle.

Intercellular communication

To coordinate contraction throughout the entire heart, action potentials are propagated between cardiomyocytes by specialized intracellular channels called gap junctions.[20, 21] Gap junctions consist of hexamers of proteins called connexins that form transmembrane hemichannels (connexons) which connect to connexons of juxtaposed cells.[22] Different subtypes of connexins make up gap junctions in a tissue- and site-specific fashion. In mammalian hearts, ventricles mainly express connexin43 and connexin45, whereas connexin40, connexin43 and connexin45 are found in the atria and conduction system.[23] The resistance provided by the gap junctions, which are clustered together at the intercalated discs (the microscopic cross bands that connect the opposing short

ends of cardiomyocytes), roughly approximates the resistance provided by the cytosol. Gap junctions thus allow the passing of depolarizing current from activated cardiomyocytes to resting cardiomyocytes in order to trigger new action potentials. This causes the action potential to propagate as a wave of excitation.[14]

In summary, during normal cardiac rhythm, action potentials are initiated at the sinus node and propagated from cardiomyocyte to cardiomyocyte throughout the heart via gap junctions, stimulating the near simultaneous contraction of cardiomyocytes in the atrium followed by those in the ventricles. Any disruption in this sequence at the molecular, cellular or tissue level can disrupt normal cardiac electrophysiology and potentially lead to cardiac arrhythmias.

CARDIAC ARRHYTHMIAS

Cardiac arrhythmias comprise a wide range of conditions which can be subdivided into two categories by heart rate being either too low (*i.e.* bradyarrhythmias), or too high (*i.e.* tachyarrhythmias). The altered rhythm, especially when irregular, can lead to an abnormal awareness of the heartbeat (palpitations). More importantly, as the cardiac output is determined by the stroke volume × heart rate, both bradyarrhythmias (though limiting heart rate) and tachyarrhythmias (through limiting diastolic filling and thereby stroke volume) can severely impair cardiac function. In addition, stasis of blood secondary to the arrhythmia can lead to potentially lethal thromboembolic events. As such, cardiac arrhythmias provide a significant contribution to morbidity and mortality throughout the world.[3, 4]

Bradyarrhythmias arise when impulse generation at the sinus node is abnormally slow or atrioventricular conduction is impaired. Tachyarrhythmias, which are the main focus of this thesis, can also occur through altered (fast) impulse generation at the sinus node (sinus tachycardia). Sinus tachycardias, however, are usually the result of an increase in the body's oxygen demand, and are therefore benign. The most dangerous tachyarrhythmias originate from outside the sinus node and can occur as a consequence of alterations in impulse initiation and conduction, resulting in either high-frequency focal or reentrant activation.[14, 24]

FOCAL TACHYARRHYTHMIAS

Focal tachyarrhythmias are rhythm disturbances in which a single focus or multiple ectopic (*i.e.* outside the normal dominant pacemaker site, the sinus node) foci residing in the atria or the ventricles override the activity from the sinoatrial node by firing action

potentials at a higher frequency, resulting in tachycardia. Several theories regarding the mechanisms underlying the spontaneous firing from ectopic foci have been postulated during the past decades, which include enhanced automaticity, abnormal automaticity and triggered activity.

Enhanced automaticity

Enhanced automaticity occurs when cells with pacemaking ability, such as those in the sinus node, increases their rate of spontaneous discharge. In these pacemaker cells, the so-called "funny current" (I_f, governed by the HCN family of ion channels), causes periodic diastolic depolarisations in resting membrane potential, which lead to action potential generation if the threshold voltage is reached.[25] Hence, enhanced automaticity can occur through an increase in the slope of diastolic depolarization (by increased HCN channel activity), lowering of the threshold voltage, or depolarization of the maximal diastolic membrane potential (MDP). The presence of I_f and enhanced automaticity in cardiomyocytes in the pulmonary vein sleeves (probably because of shared embryonic origin between pulmonary vein and nodal myocytes) has been suggested as a mechanism in the initiation of atrial fibrillation.[26] However, further evidence for enhanced automaticity as a mechanism of tachyarrhythmias is lacking.

Abnormal automaticity

Abnormal automaticity can arise in cells lacking pacemaking ability, when the MDP is depolarized to the threshold voltage for inward currents. MDP depolarization however precludes inward currents through the fast Na^+ channels as these are inactivated at depolarized MDPs.[16] Hence, the upstroke of action potentials generated through abnormal automaticity relies on Ca^{2+} currents. Abnormal automaticity is suggested to play a role in for example post-myocardial infarction ventricular tachycardias, as a consequence of depolarized surviving subendocardial Purkinje fiber cardiomyocytes.[27]

Triggered activity

During triggered activity, single action potentials generated in a normal fashion "trigger" a second (ectopic) action potential in the absence of an extra-stimulus. Afterdepolarizations, which can be categorized as early or late, are regarded as the prime mechanisms underlying the double activations characterizing triggered activity.

During an early afterdepolarization (EAD), depolarizing force is reactivated during phase 2 (the plateau phase) or phase 3 (the repolarizing phase) of the action potential, reversing repolarization. EADs occur if the net outward current, required to repolarize the cardiomyocyte, during phase 2 or 3 of the action potential is diminished. Given this reduced repolarization reserve, currents that can increase progressively as the membrane potential depolarizes allow the generation of the early afterdepolarization

upstroke. For phase-2 EADs, currents that meet this criterion in the voltage range of action potential phase-2 (approximately -30 to 0 mV) are the L-type Ca^{2+} current (I_{CaL}), the Na^{+}-Ca^{2+} exchanger current (I_{NCX}) and the late Na^{+} current (I_{Na}).

I_{CaL} can exhibit this property because at membrane potentials between -30 and 0 mV the steady state activation and inactivation curves (plotting the state of the activation gate and the inactivation gate as values between open and closed as a function of the membrane potential) of I_{CaL} overlap (I_{CaL} window current).[28] In other words, within this window the probability of the Ca^{2+} to be open and not inactivated are both greater than 0 at steady state. As such, if the membrane potential lingers between these values, I_{CaL} is allowed to recover from inactivation.[28, 29] Reduced repolarization reserve is in this case essential as deinactivation of the I_{CaL} is in part time-dependent.

In forward mode, NCX transports one Ca^{2+} ion out of the cell in exchange for the import of three Na^{+} ions. During repolarization when intracellular Ca^{2+} is elevated through sarcoplasmatic reticulum Ca^{2+} release, inward I_{NCX} increases, impairing repolarization. However, as inward I_{NCX} becomes smaller when the membrane potential increases, I_{NCX} alone is unsufficient for EAD induction. Yet, if through reduced repolarization reserve I_{CaL} increases, further Ca^{2+} release from the sarcoplasmatic reticulum is stimulated, in turn stimulating I_{NCX} forward mode. Hence, synergistic interaction between I_{CaL} and I_{NCX} during phase 2 of the action potential provides an additional mechanism opposing repolarization during phase 2 of the action potential.[29] The resulting net depolarizing current can generate a triggered beat in adjacent tissue, given sufficient local excitability.

Finally, the Na^{+}-current has been suggested to play a role in EADs including those occurring during phase 3 of the action potential. Although, under normal conditions I_{Na} is inactivated during the repolarization and plateau phases of the action potential,[16] in several diseased states sustained channel activity been observed. This sustained activity is ascribed to three mechanisms being failure to inactivate (called channel bursting),[30] increase of the (normally very narrow) I_{Na} window current,[31, 32] and an increase in the rate of channel recovery from inactivation relative to deactivation (referred to as non-equilibrium).[32, 33] Through these channel gating abnormalities the so-called late I_{Na} can also lead to reactivation of depolarizing current and subsequent triggered action potentials.

In contrast to EADs, delayed afterdepolarizations (DADs) occur after full repolarization of the action potential (*i.e.* in phase 4). DADs are thought to depend on spontaneous sarcoplasmatic reticulum Ca^{2+} release events (SCREs). In the case of SCREs, Ca^{2+}-dependent currents such as the I_{NCX} and the Ca^{2+}-activated Cl^{-} (chloride, outward) current are activated upon the increase of cytosolic Ca^{2+}.[29] Again, if the resulting current depolarizes the cell and adjacent tissue to threshold voltage an action potential is triggered.

REENTRANT TACHYARRHYTHMIAS

As mentioned earlier, during normal heart rhythm, action potentials (starting at the sinus node) are uniformly propagated from right to left atrium, and from apex to base in the ventricles. Next, the cardiomyocytes repolarize after which any subsequent activation is again dependent on the pacemaker activity of the sinus node. However, under specific conditions, the action potential can follow an alternative route, which loops back upon itself. As such, subsequent activations are no longer dependent on the sinus node, but on the action potential returning at the beginning of the loop. The resulting self-perpetuating high-frequency activation is referred to as a reentrant tachyarrhythmia.

Unidirectional block

Paramount to the initiation of reentrant tachyarrhythmias is the occurrence of unidirectional conduction block, where antegrade propagation of the action potential is (partially) blocked but retrograde propagation through the same area is not. If after reexcitation of the previously blocked area, the area in which antegrade propagation occurred is repolarized (hence no longer refractory) the wavefront of excitation propagated from the retrogradely activated tissue can enter the self-perpetuating reentrant loop. Unidirectional block can occur as a consequence of source-sink mismatches, anatomical obstacles or critically timed extra-stimuli.[14]

Source-sink mismatching

If an action potential is to propagate between cardiomyocytes, the charge provided by the first cell in the sequence should exceed the charge required to excite subsequent cells. If this condition is met, the so-called safety factor of conduction (SF) exceeds 1. Permutations of the required relation between tsource and sink (*i.e.* the charge required exceeds the charge provided, referred to as source-sink mismatch), cause the SF to fall below 1, and conduction block to occur.[14]

As myocardial tissue structure is inherently heterogeneous (owing to varying wall thickness, trabeculation, [micro]vascularization), which is emphasized in the diseased heart (as a result of fibrosis), the heart contains multiple area in which thin pathways (isthmuses) lead into large expansions. These areas are prone to antegrade conduction block as cells at the leading tip of the wavefront have to activate more cells in front of it, resulting in local small source/sink ratios.[34] Here, conduction block will be unidirectional as current provided by cells at the expansion will be relatively large compared to the charge necessary to excite cells at isthmus during retrograde conduction (Figure 2). Moreover, as the area connecting the isthmus to the expansion is prone to EAD formation (as a consequence of electrotonic current [*i.e.* passive spread of charge] flowing from expansion to isthmus during the activation of the expansion and early repolarization of

the isthmus leading to local prolongation of the action potential plateau),[35] conduction through isthmuses provide an important substrate for arrhythmia initiation.

Logically, source-sink mismatches can also occur through areas of decreased excitability (*i.e.* a reduction in the provided charge) at the source. The consequent conduction block will be unidirectional if in this area excitability is asymmetrically decreased, such that a gradient in excitability exists in one direction, while excitability abruptly decreases in the opposite direction. Action potentials entering from the gradient side (anterograde) are blocked because when the wavefront arrives at the area of least excitability (most sink), the excitability of the source is lowest as well. In retrograde direction, excitability of the source will be maximal when arriving at the point of least excitability allowing retrograde action potential propagation. As such, impulses are conducted more easily from a rapidly conducting tissue to a slowly conducting tissue than in the opposite direction (Figure 2).[14, 36]

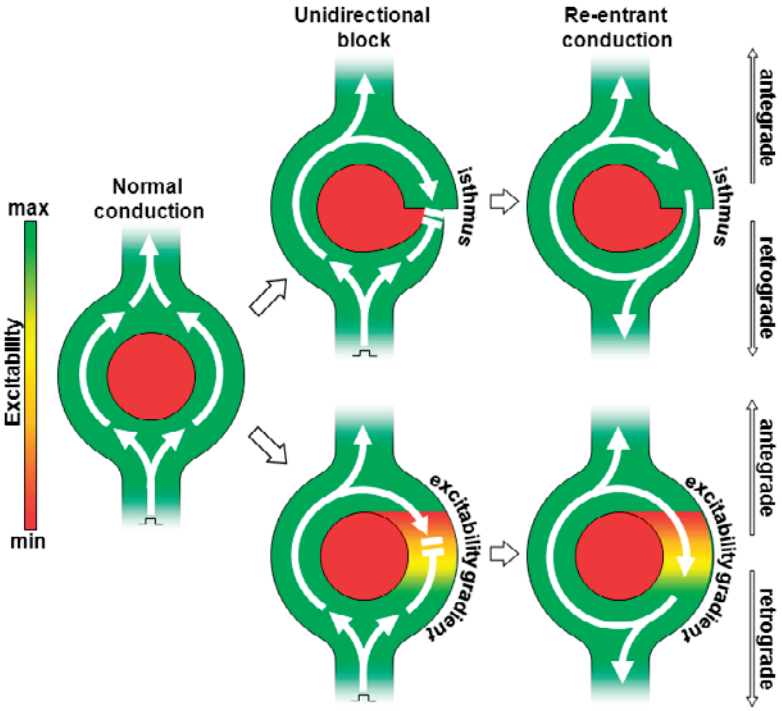

Figure 2. *Schematic representation of a myocardial tissue containing an anatomical obstacle during normal AP propagation (left panel), unidirectional block caused by a critical isthmus (upper middle panel) or an excitability gradient (lower middle panel) followed by reentrant conduction (right panels). Arrows indicate direction of AP propagation, double white lines indicate conduction block.*

Anatomical obstacles

Reentry can be induced when the wavefront of action potential propagation interacts with an anatomical (inexcitable) obstacle (*e.g.* fibrotic strands of myocardium or coronary vasculature) through a process called vortex shedding. Vortex shedding depends on the fact that conduction velocity relies on the curvature of the wavefront, such that increased wavefront curvature decreases conduction velocity (strongly curved wavefronts require an increased number of cells to be activated from a single source, leading to relative mismatching in the source-sink relationship, reducing conduction velocity).[34] At the critical wavefront curvature, absolute source-sink mismatching occurs and conduction velocity becomes zero. Logically, the value of the critical wavefront curvature depends on local excitability (*i.e.* the source). For an action potential wavefront to propagate towards tissue behind an anatomical obstacle, the wavefront has to curve around the obstacle. If at a certain local excitability, the wavefront curvature necessary to excite all tissue behind the obstacle is below the critical curvature, the wavefront will circumnavigate the obstacle to proceed in the initial antegrade direction. However, if the wavefront curvature necessary to excite all tissue behind the obstacle exceeds the critical curvature (*i.e.* if the obstacle has sharp edges, or excitability is locally decreased), propagation will only proceed distal from the obstacle at a wavefront curvature that allows the SF to be >1. Hence, the wavefront detaches from the obstacle (*i.e.* the obstacle sheds the wavefront), after which tissue behind the obstacle can be activated in a retrograde fashion, allowing formation of a reentrant loop (*i.e.* vortex).[34, 37]

Extra-stimuli in the vulnerable window

Structural heterogeneities are no prerequisite for the induction of reentrant conduction. The classical method to induce reentrant conduction in homogenously behaving myocardial tissue involves provoking the collision of a wavefront (from an extra-stimulus) with the wavetail of another perpendicularly conducted wave (*i.e.* crossfield stimulation). During crossfield stimulation, anterograde action potential propagation of the extra-stimulus is blocked where it meets refractory tissue from the wavetail of the preceding action potential. However, behind the wavetail of the first action potential, the wavefront of the extra-stimulus will encounter excitable tissue. As a result, the second wave can turn retrogradely into the recovering cells at the area previously blocking antegrade conduction, forming an reentrant loop. As such, extra-stimuli (arising from sites with enhanced automaticity, triggered activity or external electrical stimulation), when applied in the vulnerable window (*i.e.* the time, space or voltage window in the action potential in which unidirectionality can be induced; stimuli applied before or after the vunerable window will culminate in bidirectional block and conduction, respectively) can underlie reentry in the absence of structural heterogeneities (*i.e.* functional reentry) (Figure 3A-E).[38] However, it should be noted that the presence of structural heterogene-

ities in repolarization will significantly prolong the vulnerable window, increasing the chance of reentry initiation in the presence of abnormal extra-stimuli.

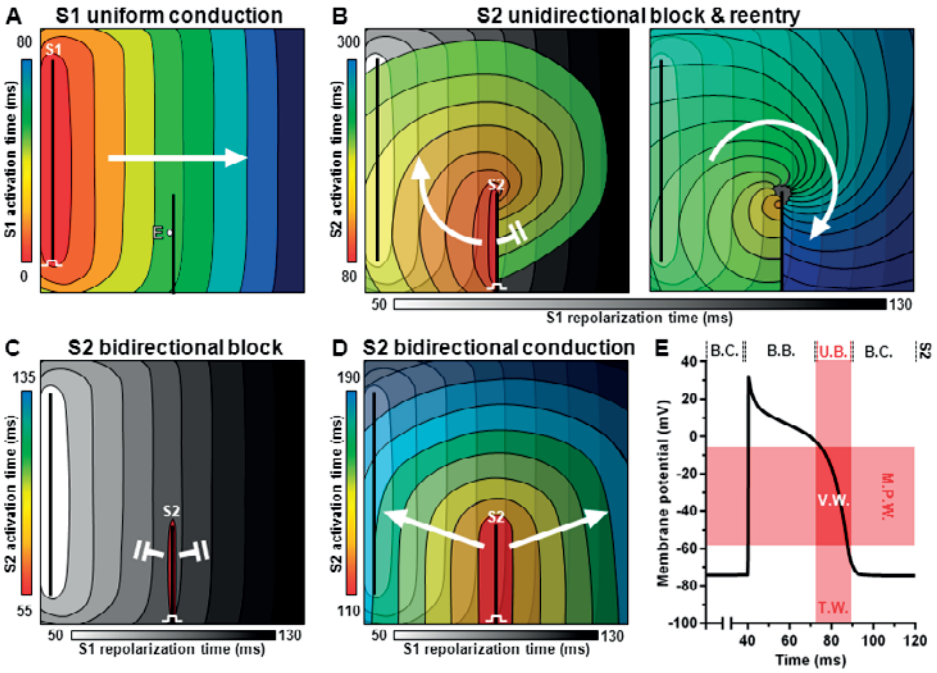

Figure 3. *Schematic representation of a myocardial tissue square during (A) an S1 stimulus from a line shaped electrode leading (left black line) to uniform conduction and subsequent S2 stimulus from a line shaped electrode (right black line) timed during (B) the vulnerable window, leading to reentry, (C) before the vulnerable window, leading to bi-directional block or (D) after the vulnerable window, leading to bidirectional conduction. (E) Schematic representation of the action potential in point E in subfigure A. V.W.: Vulnerable window. M.P.W.: membrane potential window. T.W.: Time window. B.C.: Bidirectional conduction. B.B.: Bidirectional block. U.B.: Unidirectional block. All indicated times represent the time from the start of the S1 pacing stimulus. Isochrones are spaced 10ms apart. White arrows indicate the direction of AP conduction, double white lines indicate conduction block.*

Anatomical and functional reentry

For many years it has been known that reentrant conduction can occur around an anatomical (inexcitable) obstacle, such as a post-myocardial infarction scar.[39] To allow its maintenance, in such an anatomical reentrant circuit (*i.e.* circus movement reentry), reentry cycle length has to exceed a critical value to prevent wavefront-wavetail interaction, and consequent spontaneous reentry termination. Therefore, reentrant conduction depends on conduction velocity and refractory period, in such a way that the path length of the reentrant circuit must exceed the wavelength of excitation (*i.e.* conduction velocity×refractory period, which determines the size of the refractory zone behind the wavefront). Under such conditions, an area of excitable tissue (*i.e.* an excitable gap) is

present between the wavetail and the wavefront.[40] The anatomical fixation of the reentrant circuit gives rise to a monomorphic appearance of the resultant tachyarrhythmia on electrograms.[41] These characteristics can hold true for, for example, atrioventricular reentrant tachycardias, and macroreentrant atrial and monomorphic ventricular tachycardias.

As indicated above reentry can also occur without any anatomical obstacle, giving rise to the term functional reentry. Due to the source-sink relationship, the maximal velocity of a convex wave can never exceed that of a flat front. Hence, in case of homogeneous basal excitability and stable reentry cycle lengths throughout the tissue, wavefront curvature increases (*i.e.* making sharper curves), while conduction velocity has to decrease from the periphery towards the center of a rotating wave. As such, functional reentry acquires the form of an Archimedean spiral.[34]

The functional core (center of rotation) is formed where the wavefront curvature hits the critical value and conduction velocity becomes zero.[34] Since functional reentry does not rely on an anatomical obstacle, during such reentrant activation the functional core can meander throughout the tissue, giving rise to polymorphic electrograms as can be seen in polymorphic ventricular tachycardias, atrial fibrillation and ventricular fibrillation.[41] Meandering occurs as a consequence of the relationship between wavefront curvature and conduction velocity. When excitability and critical curvature are high, the wavefront will make sharp turns around the functional core, causing it to meet its refractory tail, decreasing excitability as well as the consequent critical curvature. As the critical curvature is decreased, the wavefront detaches from the wavetail, increasing excitability, after which the curvature of the path followed by the tip of the spiral wave (at the core) will again increase. As such, the recurrent changes in critical wavefront curvature will underlie (cycloidal) meandering of the spiral wave. However, if the length of the pivoting trajectory at the core exceeds wavelength, propagation of the wavefront near the core is not affected by the wavetail, precluding meandering. As such, the area circumvented by the spiral wave tip is -in theory- never excited, and the spiral wave contains a fully excitable gap.[34] Thus, at conditions of low excitability, functional reentry circuits can be fixed, giving rise to monomorphic electrograms only.[34, 41] Hence, the stability of spiral waves seems to depend on the currents determining excitability near the core, such as I_{Na} and the inward rectifier K^+ current (I_{K1}).[42] As collision of the spiral wave tip at the core of the spiral wave to anatomical boundaries or a spiral wave tip of an opposite chirality can lead to extinguishing of the spiral wave (as well as the arrhythmic high-frequency activation originating from the spiral wave), altering the stability of the spiral wave core can be very relevant. However, still a lot of controversy exists around the actual state of the spiral wave core (being either unexcitable, inexcitable, continuously excited or never excited),[40] as well as the possible ways to facilitate its destabilization or termination. Moreover, as functional reentrant arrhythmias can become anatomical by pinning to

anatomical obstructions, even the border between anatomical and functional reentry is blurred in practice[41], illustrating the difficulty in dissecting the electrophysiology underlying cardiac arrhythmias.

CURRENT TREATMENT OF CARDIAC ARRHYTHMIAS

Symptomatic treatment

Many of the treatments available for cardiac arrhythmias depend on the alleviation of symptoms or prevention of complications secondary to the arrhythmia. A prime example is oral anticoagulation, to prevent the occurrence of thromboembolic events as a consequence of stasis of blood (and hypercoagulability) through impaired atrial wall movement at excessively high atrial activation frequencies in the treatment of atrial fibrillation.[43] Measures to prevent high ventricular activation rate (rate control) by slowing atrioventricular conduction in patients suffering from atrial fibrillation are another widely used form of symptomatic treatment. Importantly, several studies show superiority with regard to survival of anti-coagulation and rate control strategies over strategies aiming to regain sinus rhythm (rhythm control).[44, 45] However, regaining or preventing any deviations from sinus rhythm can be a reasonable and sometimes imperative goal in the treatment of tachyarrhythmias, especially when hemodynamic instability is involved or expected. Moreover, prevention of the arrhythmia itself can prevent further myocardial remodelling,[46] leading to increased susceptibility to arrhythmias, as well as the associated complications such as thromboembolic events.[43] These rhythm control strategies include anti-arrhythmic drug intake, ablative treatment and device therapy.

Anti-arrhythmic drugs

The least invasive treatment method to attain rhythm control involves the use of pharmacological agents (anti-arrhythmic drugs) to modulate ion channel function. Anti-arrhythmic drugs can be categorized according to the Vaughan Williams classification as being either Na^+ channel blocking (class I), blocking sympathetic activation (class II), K^+ channel blocking (class III) or Ca^{2+} channel blocking (class IV). Anti-arrhythmic drugs acting through other or unknown mechanisms are categorized as class V drugs.[47]

Class I drugs exert their effect through the blockade of Na^+ channels, which decreases excitability and results in conduction slowing. As the stability of tachyarrhythmias based on functional reentry depends on the interplay between I_{K1} and I_{Na}, class I drugs can destabilize spiral waves leading to their termination.[42] In addition, blockade of I_{Na} is implicated in the prevention of triggered activity (EADs) based on late I_{Na}.[48] Moreover, conduction slowing can be anti-arrhythmic in reentrant tachyarrhythmias maintained or initiated by conduction through critical isthmuses. A reduction of Na^+ channel avail-

ability can lead to conduction block at the critical isthmus through enlargement of the source-sink mismatch present at the distal expansion (see also subheading *Source-sink mismatching*),[34] breaking up the reentrant circuit. However, it is the same effect causing the slowing of conduction, that can in theory promote the induction of reentry, by allowing time for repolarization of antegradely conducting tissue before return of the retrograde wavefront (as discussed in subheading *Unidirectional block*).[14]

Class II drugs are mainly used to control ventricular rate (see the subheading *Symptomatic treatment*).

The class III drugs' mode of action involves slowing repolarization by blocking K^+ channels in order to prolong the refractory period. As circus movement reentry exists at the grace of its path length exceeding the wavelength of excitation (preventing blockade of the wavefront on the refractory wavetail), prolonging the area occupied by the wavetail increases the chance of arrhythmia termination (see also subheading *Anatomical and functional reentry*). Moreover, I_{K1} has been implicated in the maintenance of functional reentry. Hence, blockade of this current can induce drift of the spiral wave resulting in its termination.[42] Inversely, also class III drugs come with a pro-arrhythmic downside, as slowing of repolarization can increase the chance of arrhythmia initiation through triggered activity (via EADs, as discussed in subheading *Triggered activity*).[14]

As EADs and DADs largely depends on the deinactivation of Ca^{2+} channels (see subheading *Triggered activity*), class IV drugs are thought to prevent such triggers of tachyarrhythmias. However, the negative effects of Ca^{2+} channel blockers on vascular tone and cardiac inotropy deem its use undesirable in a large number of patients that often suffer from mechanical dysfunction of the heart, coinciding with their pro-arrhythmic substrate, and are hence prone to hemodynamic instability.[49] Moreover, as blockade of the Ca^{2+} channel shortens the action potential plateau, the refractory period is abbreviated. Hence, the use of Ca^{2+} channel blockade also comes with the risk of increased vulnerability to circus movement reentry.[14]

Taken together, theoretically all anti-arrhythmic drugs can have both pro- and anti-arrhythmic effects. The limited efficacy and safety of current anti-arrhythmic drug therapies support this notion. This result, which may be explained by our incomplete understanding, of pro-arrhythmic mechanisms, as well as their interplay, provided the incentive for the development of different anti-arrhythmic interventions such as (cathether) ablation and device therapy.

Ablation-based therapy

Ablation-based therapy involves techniques that aim to alter the substrate or prevent triggers for cardiac arrhythmias, by damaging pro-arrhythmic tissue using radiofrequency energy or cryogenic cooling. Ablation can be performed either surgically (when performed in combination with other procedures which necessitate primary surgical/

open chest access) or catheter-based (*i.e.* transluminal). Targets for ablation include anatomically defined substrates for circus movement reentry, microreentrant circuits, areas of slow conduction (critical isthmuses) or sources of focal activation.[50, 51] Moreover, ablation can prevent atrial arrhythmias through compartmentalization of the functional atrial myocardium below the critical mass (*i.e.* the minimal amount of tissue necessary to allow perpetuation of the arrhythmic wavefronts) rendering the resulting electrically isolated atrial areas too small to maintain the arrhythmia.[50]

As such, ablation-based therapies can be very effective in battling cardiac arrhythmias. Single procedure success rates can be as high as 90% for both atrial fibrillation and ventricular tachycardia.[50-52]

As ablation-based therapy aims to break up the pro-arrhythmic substrate locally, overall electrophysiology is maintained. Hence, ablative treatment can overcome the pro-arrhythmia associated with anti-arrhythmic drugs. However, as the pro-arrhythmic features in the non-ablated tissue remain, new arrhythmias may arise after the procedure requiring repetitive ablation. In addition, while macroreentrant circuits and focal sources are feasible targets for ablation of ventricular arrhythmias, compartmentalization to target smaller or functional circuits is difficult to achieve (due to ventricular wall thickness) and undesirable (due to the consequent impairment of ventricular function). Moreover, little evidence exists for the ablation of functional reentrant circuits (other than achieved by compartmentalization. Of note: triggers of functional reentry cán be prevented). Hence, the efficacy of ablation in ventricular arrhythmias decreases with their complexity. Moreover, ablation techniques comprise highly invasive procedures, which can result in serious complications arising from damage to cardiac structures, thermal or cryogenic injury to adjacent extracardiac structures or thromboembolism.[53]

Device therapy

The most effective direct method for regaining sinus rhythm (*i.e.* to achieve electrical cardioversion or defibrillation) is by the application of a high-energy electric shock. Electric shocks can be delivered by implanted and external devices. Exposure of the cardiomyocytes in the heart to the electric field between the shocking electrodes causes a gradient in extracellular membrane voltage, while the intracellular voltage is thought not to change appreciably, due to the relatively high impedance of the sarcolemma. As a consequence, the transmembrane potential drops in a linear fashion along the extracellular voltage gradient (with hyperpolarization and depolarization at the cells' ends facing the anode and cathode, respectively). If the depolarization at their cathodic ends causes cells to reach threshold membrane voltage, an action potential is initiated. Being applied over the entire heart, the high energy shocks hence serves to depolarize a critical mass of the myocardium simultaneously. As a result, the wavefronts maintaining arrhythmic activity are extinguished through their collision with shock-excited wave-

backs. Subsequently, after synchronized repolarization from the shock, the sinus node is allowed to reestablish normal rhythm.[54]

While implantable and external defibrillators provide very effective rescue therapy, preventing arrhythmic complications (*e.g.* sudden cardiac death in the case of ventricular fibrillation), *electrical shocks* constitute very painful and stressful events. As device therapy does not prevent arrhythmias from occurring, recurring arrhythmias and accompanying shocks remain a problem. Moreover, the electrogram characteristics of some benign rhythms are not readily distinguishable from malignant tachyarrhythmias through programmable algorithms in implantable devices and sensing itself can occur inaccurately (for instance when the repolarization wave or T-wave is recorded as being an extra activation, doubling the sensed activation frequency). As a consequence, inappropriate shocks are known to occur in up to 10-20% of patients.[55-57] Hence, device therapy is associated with a reduced quality of life and even increased mortality rate.[57, 58] In addition, to date, no appropriate device therapy is possible for supraventricular tachycardias, mainly because many of the patients would require multiple painful shocks a day.

Taken together, anti-arrhythmic drug, ablative therapy and device therapy can be effective in the treatment of cardiac arrhythmias. However, all are associated with non-trivial adverse effects. By furthering our understanding of the pro-arrhythmic mechanisms more specific, substrate-oriented therapies may be developed in the future, allowing increased anti-arrhythmic efficacy while decreasing its harmfulness.

AIM AND OUTLINE OF THESIS

To be able to improve anti-arrhythmic treatment efficacy, it is essential to comprehend the electrophysiological mechanisms underlying the initiation (triggers), maintenance (substrate) and termination of cardiac arrhythmias as discussed in **Chapter I.**

Therefore, the aim of this thesis was to develop and utilize *in vitro* and whole heart *ex vivo* models of ventricular tachycardia/fibrillation and atrial fibrillation to investigate their pro-arrhythmic mechanisms and to provide novel rationales for (1) more substrate- or trigger- oriented, (2) more specific and (3) less hazardous treatment strategies.

Cardiac pathological remodelling is a complex agglomerate of multiple processes that aim to compensate for altered biomechanical strain, as occurs after, for example, myocardial infarction and aortic stenosis. There is a clear association between cardiac remodelling and arrhythmias. However, as pathological remodelling constitutes multiple simultaneous processes, including cardiac fibrosis and cardiomyocyte hypertrophy, no distinction can be made between the contribution of these separate processes to the pro-arrhythmic phenotype. Hence, in **Chapter II** the differences between the pro-

arrhythmic triggers and substrates provided by mechanisms specific for pathological cardiomyocyte hypertrophy and cardiac fibrosis are investigated. Moreover, the influence of these specific mechanisms on anti-arrhythmic strategies is evaluated.

Ventricular fibrillation is not compatible with life in part because of the presence of multiple reentrant circuits (constituting a highly complex arrhythmia) within the ventricle(s) which causes dyssynchronous myocardial contractions resulting in insufficient cardiac output. Moreover, highly complex cardiac arrhythmias are associated with decreased defibrillation success rate. Hence, decreasing the number of rotors (*i.e.* the complexity) maintaining ventricular fibrillation can be an important step in improving its treatment. Hence, **Chapter III** describes a study into the electrophysiological characteristics that determine complexity of fibrillation and how they can be utilized to destabilize and ultimately terminate reentrant arrhythmias using a wide range of pharmacological agents.

Pharmocological treatment of atrial fibrillation is hampered by the ventricular pro-arrhythmia associated with the use of anti-arrhythmic drugs. As the atrial ion channel targets of these drugs overlap with the ion channels expressed in the ventricles, these drugs alter ventricular electrophysiology, possibly leading to increased arrhythmia susceptibility. Hence, to improve treatment of atrial fibrillation atrium-specific targets are needed. Moreover, contribution of these targets to atrial pro-arrhythmia needs to be elucidated. Therefore, in **Chapter IV** he effects of blockade or downregulation of the Kir3.x superfamily of K^+ channels, which were found to be expressed in atrial but not ventricular cardiomyocytes, is investigated.

Electroshocks, applied by external and internal defibrillators, are an effective way to terminate reentrant activity underlying both atrial and ventricular fibrillation. However, these shocks are very painful, associated with tissue damage and not always effective. To make better use of electrical shock therapy it seems essential to decrease the energy requirements for successful defibrillation. For atrial fibrillation decreased efficacy of electrical shock therapy is related to the atrial remodelling associated with persistent atrial fibrillation. A constituent of this remodelling is constitutive activation of the acetylcholine-dependent K^+ current (governed by the Kir3.x channels). Therefore, in **Chapter V** the contribution of this current in setting the energy threshold for atrial defibrillation was studied, as well as the mechanisms associated with the interaction between this current and defibrillation threshold.

In **Chapter VI**, a new method of cardioversion/defibrillation that does not rely on the application of electrical shocks is explored. Here, the hypothesis that the depolarizing current, necessary for resynchronizing the atrium during reentrant tachyarrhythmias (in order to regain normal rhythm), could be provided by inserting and (shocklessly) activating light-sensitive ion channels in cardiomyocytes was tested.

In conclusion, **Chapter VII** summarizes the findings of this thesis. Moreover, results are discussed with special emphasis on their translational perspectives.

REFERENCES

1. Herget GW, Neuburger M, Plagwitz R, Adler CP. DNA content, ploidy level and number of nuclei in the human heart after myocardial infarction. *Cardiovascular research*. 1997;36:45-51
2. Buckberg G, Hoffman JI, Mahajan A, Saleh S, Coghlan C. Cardiac mechanics revisited: The relationship of cardiac architecture to ventricular function. *Circulation*. 2008;118:2571-2587
3. Miyasaka Y, Barnes ME, Bailey KR, Cha SS, Gersh BJ, Seward JB, Tsang TS. Mortality trends in patients diagnosed with first atrial fibrillation: A 21-year community-based study. *Journal of the American College of Cardiology*. 2007;49:986-992
4. Zipes DP, Wellens HJ. Sudden cardiac death. *Circulation*. 1998;98:2334-2351
5. Connolly SJ, Camm AJ, Halperin JL, Joyner C, Alings M, Amerena J, Atar D, Avezum A, Blomstrom P, Borggrefe M, Budaj A, Chen SA, Ching CK, Commerford P, Dans A, Davy JM, Delacretaz E, Di Pasquale G, Diaz R, Dorian P, Flaker G, Golitsyn S, Gonzalez-Hermosillo A, Granger CB, Heidbuchel H, Kautzner J, Kim JS, Lanas F, Lewis BS, Merino JL, Morillo C, Murin J, Narasimhan C, Paolasso E, Parkhomenko A, Peters NS, Sim KH, Stiles MK, Tanomsup S, Toivonen L, Tomcsanyi J, Torp-Pedersen C, Tse HF, Vardas P, Vinereanu D, Xavier D, Zhu J, Zhu JR, Baret-Cormel L, Weinling E, Staiger C, Yusuf S, Chrolavicius S, Afzal R, Hohnloser SH, Investigators P. Dronedarone in high-risk permanent atrial fibrillation. *The New England journal of medicine*. 2011;365:2268-2276
6. Echt DS, Liebson PR, Mitchell LB, Peters RW, Obias-Manno D, Barker AH, Arensberg D, Baker A, Friedman L, Greene HL, et al. Mortality and morbidity in patients receiving encainide, flecainide, or placebo. The cardiac arrhythmia suppression trial. *The New England journal of medicine*. 1991;324:781-788
7. Spragg DD, Dalal D, Cheema A, Scherr D, Chilukuri K, Cheng A, Henrikson CA, Marine JE, Berger RD, Dong J, Calkins H. Complications of catheter ablation for atrial fibrillation: Incidence and predictors. *Journal of cardiovascular electrophysiology*. 2008;19:627-631
8. Bohnen M, Stevenson WG, Tedrow UB, Michaud GF, John RM, Epstein LM, Albert CM, Koplan BA. Incidence and predictors of major complications from contemporary catheter ablation to treat cardiac arrhythmias. *Heart rhythm : the official journal of the Heart Rhythm Society*. 2011;8:1661-1666
9. Kamphuis HC, de Leeuw JR, Derksen R, Hauer RN, Winnubst JA. Implantable cardioverter defibrillator recipients: Quality of life in recipients with and without icd shock delivery: A prospective study. *Europace : European pacing, arrhythmias, and cardiac electrophysiology : journal of the working groups on cardiac pacing, arrhythmias, and cardiac cellular electrophysiology of the European Society of Cardiology*. 2003;5:381-389
10. Sanders GD, Hlatky MA, Owens DK. Cost-effectiveness of implantable cardioverter-defibrillators. *The New England journal of medicine*. 2005;353:1471-1480
11. Cabell CH, Heidenreich PA, Chu VH, Moore CM, Stryjewski ME, Corey GR, Fowler VG, Jr. Increasing rates of cardiac device infections among medicare beneficiaries: 1990-1999. *American heart journal*. 2004;147:582-586
12. Kleemann T, Becker T, Doenges K, Vater M, Senges J, Schneider S, Saggau W, Weisse U, Seidl K. Annual rate of transvenous defibrillation lead defects in implantable cardioverter-defibrillators over a period

of >10 years. *Circulation*. 2007;115:2474-2480

13. Hodgkin AL, Huxley AF. Currents carried by sodium and potassium ions through the membrane of the giant axon of loligo. *The Journal of physiology*. 1952;116:449-472
14. Kleber AG, Rudy Y. Basic mechanisms of cardiac impulse propagation and associated arrhythmias. *Physiological reviews*. 2004;84:431-488
15. Roden DM, Balser JR, George AL, Jr., Anderson ME. Cardiac ion channels. *Annual review of physiology*. 2002;64:431-475
16. Berman MF, Camardo JS, Robinson RB, Siegelbaum SA. Single sodium channels from canine ventricular myocytes: Voltage dependence and relative rates of activation and inactivation. *The Journal of physiology*. 1989;415:503-531
17. Fabiato A. Simulated calcium current can both cause calcium loading in and trigger calcium release from the sarcoplasmic reticulum of a skinned canine cardiac purkinje cell. *The Journal of general physiology*. 1985;85:291-320
18. Huxley AF, Niedergerke R. Structural changes in muscle during contraction; interference microscopy of living muscle fibres. *Nature*. 1954;173:971-973
19. Huxley H, Hanson J. Changes in the cross-striations of muscle during contraction and stretch and their structural interpretation. *Nature*. 1954;173:973-976
20. Caspar DL, Goodenough DA, Makowski L, Phillips WC. Gap junction structures. I. Correlated electron microscopy and x-ray diffraction. *The Journal of cell biology*. 1977;74:605-628
21. Makowski L, Caspar DL, Phillips WC, Goodenough DA. Gap junction structures. Ii. Analysis of the x-ray diffraction data. *The Journal of cell biology*. 1977;74:629-645
22. Unwin PN, Zampighi G. Structure of the junction between communicating cells. *Nature*. 1980;283:545-549
23. Davis LM, Kanter HL, Beyer EC, Saffitz JE. Distinct gap junction protein phenotypes in cardiac tissues with disparate conduction properties. *Journal of the American College of Cardiology*. 1994;24:1124-1132
24. Pogwizd SM, Hoyt RH, Saffitz JE, Corr PB, Cox JL, Cain ME. Reentrant and focal mechanisms underlying ventricular tachycardia in the human heart. *Circulation*. 1992;86:1872-1887
25. DiFrancesco D, Ojeda C. Properties of the current if in the sino-atrial node of the rabbit compared with those of the current ik, in purkinje fibres. *The Journal of physiology*. 1980;308:353-367
26. Morel E, Meyronet D, Thivolet-Bejuy F, Chevalier P. Identification and distribution of interstitial cajal cells in human pulmonary veins. *Heart rhythm : the official journal of the Heart Rhythm Society*. 2008;5:1063-1067
27. le Marec H, Dangman KH, Danilo P, Jr., Rosen MR. An evaluation of automaticity and triggered activity in the canine heart one to four days after myocardial infarction. *Circulation*. 1985;71:1224-1236
28. Ming Z, Nordin C, Aronson RS. Role of l-type calcium channel window current in generating current-induced early afterdepolarizations. *Journal of cardiovascular electrophysiology*. 1994;5:323-334
29. Katra RP, Laurita KR. Cellular mechanism of calcium-mediated triggered activity in the heart. *Circulation research*. 2005;96:535-542
30. Bennett PB, Yazawa K, Makita N, George AL, Jr. Molecular mechanism for an inherited cardiac arrhythmia. *Nature*. 1995;376:683-685
31. Attwell D, Cohen I, Eisner D, Ohba M, Ojeda C. The steady state ttx-sensitive ("window") sodium current in cardiac purkinje fibres. *Pflugers Archiv : European journal of physiology*. 1979;379:137-142
32. Wang DW, Yazawa K, George AL, Jr., Bennett PB. Characterization of human cardiac

na+ channel mutations in the congenital long qt syndrome. *Proceedings of the National Academy of Sciences of the United States of America*. 1996;93:13200-13205

33. Clancy CE, Tateyama M, Liu H, Wehrens XH, Kass RS. Non-equilibrium gating in cardiac na+ channels: An original mechanism of arrhythmia. *Circulation*. 2003;107:2233-2237
34. Fast VG, Kleber AG. Role of wavefront curvature in propagation of cardiac impulse. *Cardiovascular research*. 1997;33:258-271
35. Auerbach DS, Grzda KR, Furspan PB, Sato PY, Mironov S, Jalife J. Structural heterogeneity promotes triggered activity, reflection and arrhythmogenesis in cardiomyocyte monolayers. *The Journal of physiology*. 2011;589:2363-2381
36. Waxman MB, Downar E, Wald RW. Unidirectional block in purkinje fibers. *Canadian journal of physiology and pharmacology*. 1980;58:925-933
37. Cabo C, Pertsov AM, Davidenko JM, Baxter WT, Gray RA, Jalife J. Vortex shedding as a precursor of turbulent electrical activity in cardiac muscle. *Biophysical journal*. 1996;70:1105-1111
38. Shaw RM, Rudy Y. The vulnerable window for unidirectional block in cardiac tissue: Characterization and dependence on membrane excitability and intercellular coupling. *Journal of cardiovascular electrophysiology*. 1995;6:115-131
39. Mehra R, Zeiler RH, Gough WB, El-Sherif N. Reentrant ventricular arrhythmias in the late myocardial infarction period. 9. Electrophysiologic-anatomic correlation of reentrant circuits. *Circulation*. 1983;67:11-24
40. Schotten U, Verheule S, Kirchhof P, Goette A. Pathophysiological mechanisms of atrial fibrillation: A translational appraisal. *Physiological reviews*. 2011;91:265-325
41. Ikeda T, Yashima M, Uchida T, Hough D, Fishbein MC, Mandel WJ, Chen PS, Karagueuzian HS. Attachment of meandering reentrant wave fronts to anatomic obstacles in the atrium. Role of the obstacle size. *Circulation research*. 1997;81:753-764
42. Pandit SV, Berenfeld O, Anumonwo JM, Zaritski RM, Kneller J, Nattel S, Jalife J. Ionic determinants of functional reentry in a 2-d model of human atrial cells during simulated chronic atrial fibrillation. *Biophysical journal*. 2005;88:3806-3821
43. Wolf PA, Abbott RD, Kannel WB. Atrial fibrillation as an independent risk factor for stroke: The framingham study. *Stroke; a journal of cerebral circulation*. 1991;22:983-988
44. Roy D, Talajic M, Nattel S, Wyse DG, Dorian P, Lee KL, Bourassa MG, Arnold JM, Buxton AE, Camm AJ, Connolly SJ, Dubuc M, Ducharme A, Guerra PG, Hohnloser SH, Lambert J, Le Heuzey JY, O'Hara G, Pedersen OD, Rouleau JL, Singh BN, Stevenson LW, Stevenson WG, Thibault B, Waldo AL, Atrial F, Congestive Heart Failure I. Rhythm control versus rate control for atrial fibrillation and heart failure. *The New England journal of medicine*. 2008;358:2667-2677
45. Hohnloser SH, Kuck KH, Lilienthal J. Rhythm or rate control in atrial fibrillation--pharmacological intervention in atrial fibrillation (piaf): A randomised trial. *Lancet*. 2000;356:1789-1794
46. Shinbane JS, Wood MA, Jensen DN, Ellenbogen KA, Fitzpatrick AP, Scheinman MM. Tachycardia-induced cardiomyopathy: A review of animal models and clinical studies. *Journal of the American College of Cardiology*. 1997;29:709-715
47. Nattel S. Antiarrhythmic drug classifications. A critical appraisal of their history, present status, and clinical relevance. *Drugs*. 1991;41:672-701
48. Antoons G, Oros A, Beekman JD, Engelen MA, Houtman MJ, Belardinelli L, Stengl M, Vos MA. Late na(+) current inhibition by ranolazine reduces torsades de pointes in the chronic atrioventricular block dog

model. *Journal of the American College of Cardiology*. 2010;55:801-809

49. Epstein SE, Rosing DR. Verapamil: Its potential for causing serious complications in patients with hypertrophic cardiomyopathy. *Circulation*. 1981;64:437-441
50. Lee G, Sanders P, Kalman JM. Catheter ablation of atrial arrhythmias: State of the art. *Lancet*. 2012;380:1509-1519
51. Stevenson WG, Soejima K. Catheter ablation for ventricular tachycardia. *Circulation*. 2007;115:2750-2760
52. Bonanno C, Paccanaro M, La Vecchia L, Ometto R, Fontanelli A. Efficacy and safety of catheter ablation versus antiarrhythmic drugs for atrial fibrillation: A meta-analysis of randomized trials. *Journal of cardiovascular medicine*. 2010;11:408-418
53. Cappato R, Calkins H, Chen SA, Davies W, Iesaka Y, Kalman J, Kim YH, Klein G, Natale A, Packer D, Skanes A, Ambrogi F, Biganzoli E. Updated worldwide survey on the methods, efficacy, and safety of catheter ablation for human atrial fibrillation. *Circulation. Arrhythmia and electrophysiology*. 2010;3:32-38
54. Dosdall DJ, Fast VG, Ideker RE. Mechanisms of defibrillation. *Annual review of biomedical engineering*. 2010;12:233-258
55. Daubert JP, Zareba W, Cannom DS, McNitt S, Rosero SZ, Wang P, Schuger C, Steinberg JS, Higgins SL, Wilber DJ, Klein H, Andrews ML, Hall WJ, Moss AJ, Investigators MI. Inappropriate implantable cardioverter-defibrillator shocks in madit ii: Frequency, mechanisms, predictors, and survival impact. *Journal of the American College of Cardiology*. 2008;51:1357-1365
56. Kreuz J, Balta O, Liliegren N, Mellert F, Esmailzadeh B, Nickenig G, Schwab JO. Incidence and characteristics of appropriate and inappropriate therapies in recipients of icd implanted for primary prevention of sudden cardiac death. *Pacing and clinical electrophysiology : PACE*. 2007;30 Suppl 1:S125-127
57. van Rees JB, Borleffs CJ, de Bie MK, Stijnen T, van Erven L, Bax JJ, Schalij MJ. Inappropriate implantable cardioverter-defibrillator shocks: Incidence, predictors, and impact on mortality. *Journal of the American College of Cardiology*. 2011;57:556-562
58. Borleffs CJ, van Erven L, Schotman M, Boersma E, Kies P, van der Burg AE, Zeppenfeld K, Bootsma M, van der Wall EE, Bax JJ, Schalij MJ. Recurrence of ventricular arrhythmias in ischaemic secondary prevention implantable cardioverter defibrillator recipients: Long-term follow-up of the leiden out-of-hospital cardiac arrest study (lohcat). *European heart journal*. 2009;30:1621-1626

Chapter II

Similar arrhythmicity in hypertrophic and fibrotic cardiac cultures caused by distinct substrate-specific mechanisms

Substrate-specific arrhythmic mechanisms

Saïd F. A. Askar, MSc*; **Brian O. Bingen, MD*;** Martin J. Schalij, MD, PhD; Jim Swildens, Msc; Douwe E. Atsma, MD, PhD; Cindy I. Schutte, BSc; Antoine A. F. de Vries, PhD; Katja Zeppenfeld, MD, PhD; Dirk L. Ypey, PhD; Daniël A. Pijnappels, PhD.

*Equal contribution

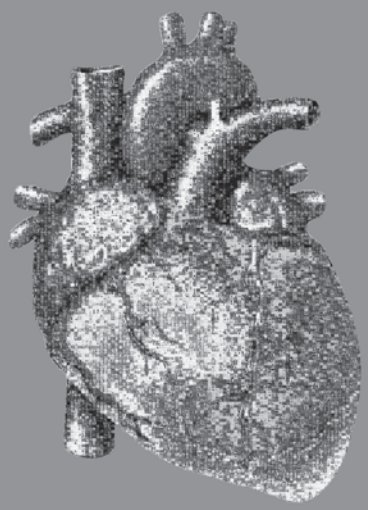

Cardiovasc Res 2013;97:171-181

ABSTRACT

Aims: Cardiac hypertrophy and fibrosis are associated with potentially lethal arrhythmias. As these substrates often occur simultaneously in one patient, distinguishing between pro-arrhythmic mechanisms is difficult. This hampers understanding of underlying pro-arrhythmic mechanisms and optimal treatment. This study investigates and compares arrhythmogeneity and underlying pro-arrhythmic mechanisms of either cardiac hypertrophy or fibrosis in *in vitro* models.

Methods & Results: Fibrosis was mimicked by free myofibroblast (MFB) proliferation in neonatal rat ventricular monolayers. Cultures with inhibited MFB proliferation were used as control or exposed to phenylephrine to induce hypertrophy. At day 9, cultures were studied with patch-clamp and optical-mapping techniques and assessed for protein expression. In hypertrophic (n=111) and fibrotic cultures (n=107), conduction and repolarization were slowed. Triggered activity was commonly found in these substrates and led to high incidences of spontaneous reentrant arrhythmias (67.5% hypertrophic, 78.5% fibrotic vs. 2.9% in controls (n=102)) or focal arrhythmias (39.1% 51.7% vs. 8.8% respectively). Kv4.3 and Cx43 protein expression levels were decreased in hypertrophy but unaffected in fibrosis. Depolarization of cardiomyocytes (CMCs) was only found in fibrotic cultures (-48±7mV vs. -66±7mV in control, $P<0.001$). L-type calcium-channel blockade prevented arrhythmias in hypertrophy, but caused conduction block in fibrosis. Targeting heterocellular coupling by low doses of gap-junction uncouplers prevented arrhythmias by accelerating repolarization only in fibrotic cultures.

Conclusions: Cultured hypertrophic or fibrotic myocardial tissues generated similar focal and reentrant arrhythmias. These models revealed electrical remodeling of CMCs as a pro-arrhythmic mechanism of hypertrophy and MFB-induced depolarization of CMCs as a pro-arrhythmic mechanism of fibrosis. These findings provide novel mechanistic insight into substrate-specific arrhythmicity.

INTRODUCTION

Pathophysiological alterations in myocardial structure as observed in cardiac fibrosis or hypertrophy are associated with the occurrence of lethal cardiac arrhythmias.[1-3] As hypertrophy and fibrosis may occur concomitantly to varying degrees in cardiac remodeling in one patient, it remains unclear how these adaptations independently contribute to the arrhythmogeneity of remodeled tissue. Hence, the mechanisms through which hypertrophy or fibrosis cause arrhythmias remain incompletely understood. Because hypertrophy and fibrosis are characterized by specific modifications at molecular and cellular levels, these alterations could thereby provide a basis for distinct substrate-specific pro-arrhythmic mechanisms. Although treatment of cardiac arrhythmias has improved over recent years, it remains suboptimal in terms of efficacy and safety.[4-6] The notion that pharmacological anti-arrhythmic treatment does not significantly improve survival, and may in fact evoke lethal arrhythmias, could indicate that anti-arrhythmic treatment, without detailed knowledge of the underlying pro-arrhythmic mechanisms, may limit therapeutic efficacy.[7] Therefore, this study aimed to identify and compare independent mechanisms of arrhythmias in hypertrophic or fibrotic myocardial tissue and thereby determine the arrhythmogeneity per substrate. The results revealed a similar occurrence of prolongation of repolarization, triggered activity and reentrant tachyarrhythmias in fibrotic and hypertrophic myocardial cultures. However, the underlying pro-arrhythmic mechanisms in these substrates were distinct, being of intrinsic nature in cardiac hypertrophy and of extrinsic origin in cardiac fibrosis.

MATERIALS AND METHODS

All animal experiments were approved by the Animal Experiments Committee of the Leiden University Medical Center and conform to the Guide for the Care and Use of Laboratory Animals as stated by the US National Institutes of Health.

Cell isolation and culture

Isolation of primary neonatal rat ventricular myocardial cells was performed as described previously.[8] In brief, animals were anaesthetized with 4–5% isoflurane inhalation anaesthesia. Adequate anaesthesia was assured by the absence of reflexes prior to rapid heart excision. After animal sacrifice by rapid heart excision, ventricular tissue was minced and digested with collagenase I (450 units/ml; Worthington, NJ, USA) in two digestion steps of 50 and 40 minutes. After a 75-minute pre-plating step to minimize the amount of fibroblasts in cardiac cell preparation, cells were plated out on fibronectin-coated, round glass coverslips (15 mm) at a cell density of 1-8x10^5 cells/well in 24-well plates

(Corning Life Sciences, Amsterdam, the Netherlands) depending on the experiment. To mimic fibrosis, endogenously present myofibroblasts (MFBs) proliferated freely. As control, proliferation was inhibited by 10 µg/mL Mitomycin-C (Sigma-Aldrich, St. Louis, MO, USA) at day 1.[9] To induce hypertrophy, control cultures were exposed to 100 µM phenylephrine (PE, Sigma) for 24h at day 3 and day 8.

Immunocytological analyses

Cultures were stained for several markers of interest after 20 minute fixation in 1% paraformaldehyde and permeabilization with 0.1% Triton X-100. Primary antibodies (1:200) and corresponding secondary Alexa fluor-conjugated antibodies (1:400, Invitrogen, Carlsbad, CA, USA) were incubated for 2 hours. Counterstaining of nuclei was performed with Hoechst 33342 (Invitrogen). Images of cultures were quantified using dedicated software (Image-Pro Plus, version 4.1.0.0, Media Cybernetics, Silver Spring, MD, USA).

Western Blot

Hypertrophic, fibrotic or control cultures were homogenized in RIPA-buffer containing 50 mmol/L Tris-HCl (pH 8.0), 150 mmol/L NaCl, 1% Triton X-100, 0.5% sodiumdeoxycholate and 0.1% SDS. Then, 10 µg of protein per sample (at least 3 samples per group) were size-fractionated on NuPage 12% gels (Invitrogen) and transferred to Hybond PVDF membranes (GE Healthcare, Diegem, Belgium). Membranes were blocked in TBS-Tween (0.1%) + 5% Bovine Serum Albumin (Sigma) for 1h. Afterwards, these membranes were incubated with primary antibodies directed against Nav1.5 (Abcam, Cambridge, UK), Cav1.2, Kv4.3, Kir2.1, Kv7.1 (all from Alomone Labs, Jerusalem, Israel) for 1h, rinsed three times in TBS-Tween and then incubated with corresponding HRP-conjugated secondary antibodies (Santa Cruz Biotechnlogy, Santa Cruz, CA, USA) for 1h. Chemiluminescence was detected and caught on hyperfilm ECL using ECL Prime detection reagents (GE Healthcare). To check for equal protein loading, GAPDH (Millipore, Billerica, MA, USA) expression was determined. To compare fibrotic and control groups, protein expression was subsequently adjusted for CMC content by normalizing for α-actinin (Sigma).

Optical mapping

Optical mapping in 24-well plates at a density of $8x10^5$ cells/well and subsequent analyses were performed as previously described.[9] At day 9, cultures were incubated with 8 µM Di-4-ANEPPS after which cultures were refreshed with DMEM/Hams F10 (37 °C) and optically mapped immediately using the Ultima-L mapping setup (SciMedia, Costa Mesa, CA, USA). Mapping experiments typically did not exceed 30 minutes per 24-wells plate. Also, cultures were not exposed to excitation light for longer than 50 s to limit possible phototoxic effects. Parameters of interest were determined using Brain Vision Analyze 1108 (Brainvision, Inc., Tokyo, Japan). The incidence of triggered activity was

assessed in all groups after eliminating reentrant conduction by electrical stimulation. Triggered activity was defined as all newly formed optical action potentials independent of initial pacing- or spontaneous frequency, with >10% of the optical amplitude of the initial paced or spontaneous action potential. An early after depolarization (EAD) was defined as a reversal of repolarization during phase 2 or 3 of the action potential of > 10% of optical amplitude. Focal tachyarrhythmias were defined as non-reentrant activation patterns >3 repetitions faster than 2 Hz. Reentrant tachyarrhythmias were defined as repetitive circular activation patterns for >3 rotations at >2 Hz.

Pro-arrhythmic mechanisms studied by pharmacological interventions

Different pharmacological agents were administered during optical mapping for investigation of pro-arrhythmic mechanisms. To reduce the net inward current, L-type Ca^{2+} current was inhibited by administration of a relatively low dose of nitrendipine (3 μM) (Sigma) or verapamil (10 μM) (Centrafarm, Etten-Leur, the Netherlands) directly into the mapping medium. To reduce heterocellular coupling, a relatively low dose of 2-Aminoethoxy diphenyl borate (2-APB, 5 μM) (Tocris Bioscience, Bristol, United Kingdom) or carbenoxolone (100 μM) (Sigma) was incubated for 20 minutes. To investigate effects of Nav1.5 blockade, tetrodotoxin (TTX, 20 μM, Alomone Labs) was directly used. For investigation of the involvement of intracellular calcium handling in arrhythmogeneity, intracellular calcium was buffered using 10-50 μM BAPTA-AM (Sigma) which incubated for 20 minutes. To investigate the effect of action potential duration (APD) prolongation on arrhythmogeneity, 0.5 mM sotalol (Sigma) was used. For reproducibility and comparability between all pharmacological interventions, all cultures were paced with a 1 Hz supra-threshold stimulation protocol during optical mapping recordings.

Whole-cell patch-clamp

Membrane potential recordings were performed with the whole-cell patch-clamp technique in hypertrophic cultures, co-cultures of cardiomyocytes (CMCs) and eGFP labeled MFBs at equal cell quantity and density as fibrotic cultures with freely proliferating MFBs, and control cultures. At day 9, after identification of CMCs by phase contrast and fluorescence microscopy, action potential properties were determined in current-clamp. Whole-cell recordings were performed at 25°C using a L/M-PC patch-clamp amplifier (3kHz filtering) (List-Medical, Darmstadt, Germany). The pipette solution contained (in mmol/L) 10 Na_2ATP, 115 KCl, 1 $MgCl_2$, 5 EGTA, 10 HEPES/KOH (pH 7.4). Tip and seal resistance were 2.0-2.5 MΩ and >1 GΩ, respectively. The bath solution contained (in mmol/L) 137 NaCl, 4 KCl, 1.8 $CaCl_2$, 1 $MgCl_2$, and 10 HEPES (pH 7.4). In a subset of experiments, CMCs were functionally uncoupled by incubation for 20 minutes with 25 μmol/L 2-APB to investigate action potential characteristics in hypertrophic, fibrotic or control cul-

tures. For data acquisition and analysis, pClamp/Clampex8 software (Axon Instruments, Molecular Devices, Sunnyvale, CA, USA) was used.

Statistical analysis

Statistical analyses were performed using SPSS11.0 for Windows (SPSS, Inc., Chicago, IL, USA). Differences were considered statistically significant if $P<0.05$.

RESULTS

Cellular characterization of hypertrophic myocardial cultures

In PE-treated cultures, expression levels of ANP (126.9±8.1 vs. 93.4±5.6 arbitrary units, $P<0.001$) (Supplemental figure 1A and 1B) and α-Skeletal Muscle Actin (131.0±9.0 vs. 116.5±17.0 arbitrary units, $P<0.01$) (Supplemental figure 1C and 1D) were significantly higher compared to control cultures. Furthermore, a significant increase from 1.4±0.7 10^6 pixels to 2.6±0.6x10^6 pixels ($P<0.05$) in cell surface area was observed (Supplemental figure 1F). Non-myocytes expressed α-Smooth-Muscle-Actin and Collagen-I as determined by immunocytological staining and were therefore considered MFBs. Moreover, cellular composition of cultures was analyzed by collagen I/α-actinin double staining, suitable for distinction between MFBs and CMCs.[9] Administration of PE to cardiac cultures did not influence MFB quantities (18.6±2.8% vs. 18.1±2.0% in control cultures, p=ns) (Supplemental figure 1E) or CMC quantities. As MFB quantities were as low as control cultures, PE-treated cultures were considered primarily pathologically hypertrophic with a minimal fibrotic component.

Cellular characterization of fibrotic myocardial cultures

At day 9 of culture, fibrotic cultures contained 61.5±2.6% MFBs whereas control cultures, treated with the antiproliferative agent mitomycin-C, contained 18.9±2.4% MFBs ($P<0.001$) (Supplemental figure 2A and B). Immunocytological staining revealed intercellular Cx43 expression at MFB-MFB, CMC-CMC and CMC-MFB junctions (Supplemental figure 2C). Heterocellular coupling was confirmed by calcein dye transfer between CMCs and MFBs (data not shown). Expression levels of Cx43 at heterocellular CMC-MFB junctions were significantly lower than at homocellular CMC-CMC junctions (35.5±12.3 vs. 7.8±3.1 arbitrary units, $P<0.0001$) (Supplemental figure 2D). Importantly, as fibrotic cultures did not show an increase in cell surface area (1.2±0.46 10^6 pixels in control cultures vs. 1.1±0.35 10^6 pixels in fibrotic cultures) or up regulation of ANP expression (16.8±4.8 vs. 17.3±6.6 arbitrary units in control and fibrotic cultures, respectively, p=ns), absence of a hypertrophic component was confirmed (Supplemental figure 2E and 2F).

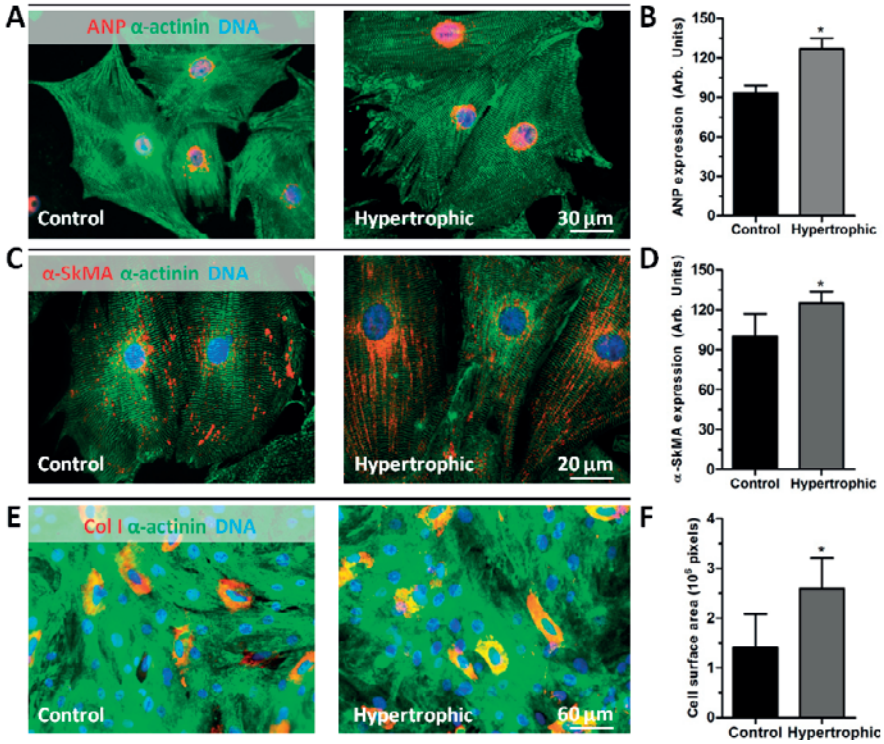

Supplemental Figure 1. *Cellular characterization of hypertrophic myocardial cultures. (A) Typical examples of immunocytological double-staining for ANP (red) and α-actinin (green). (B) Quantification of ANP signal. *:p<0.001 vs control. (C) Immunocytological double-staining for α-skeletal actin (red) and α-actinin (green). (D) Quantification of α-skeletal actin signal. *:p<0.01 vs control. (E) Immunocytological double-staining for collagen type I (red) and α-actinin (green). (F) Quantification of cell surface tracing, *:p<0.05.*

Conduction and repolarization are slowed in fibrotic and in hypertrophic cultures

Optical mapping recordings similarly showed slow conduction in uniformly propagating hypertrophic and fibrotic cultures (12.2±2.5 and 13.2±3.0 cm/s, respectively, vs. 24.5±2.1 cm/s in controls, $P<0.0001$) (Figure 1A). APD_{80} restitution curves from spontaneous optical signals showed prolonged repolarization compared to control cultures, which was most pronounced at activation frequencies ≤1 Hz (238±65 ms in control [range of 157-393 ms] vs. 721±404 ms [range of 396-1842] and 820±681 ms [range of 400-2474 ms], $P<0.001$ and $P<0.05$ respectively) (Supplemental Figure 3 and Figure 1B). Apart from AP prolongation, AP triangulation (APD_{30}-APD_{90}) was significantly increased (140±59 ms in control vs. 303±117 ms and 298±64 ms in hypertrophy and fibrosis, $P<0.05$) (Figure 1C, 1D and 1E). Furthermore, the maximal spatial APD_{80} dispersion was higher in both pathological substrates (240±92ms in hypertrophic and 233±151ms in fibrotic cultures vs. 53±36ms in controls, $P<0.01$) (Figure 1F), suggesting increased heterogeneity of repolarization in hypertrophic or fibrotic cultures.

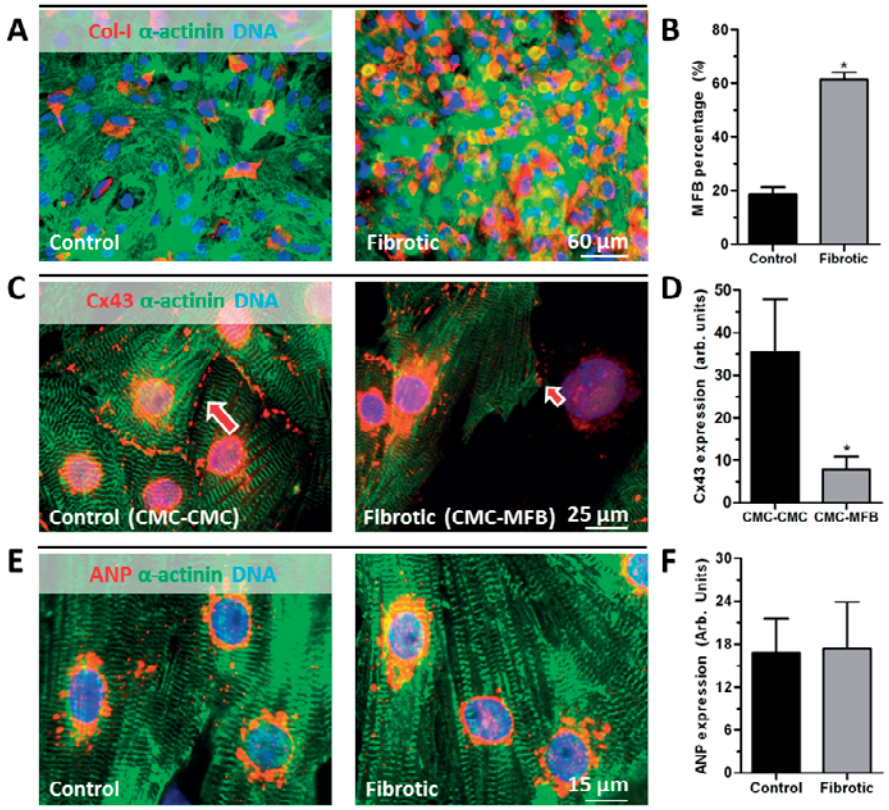

Supplemental Figure 2. *Cellular characterization of fibrotic myocardial cultures. (A) Typical examples of immunocytological double-staining for collagen-I (red) and α-actinin (green) (B) Quantification of MFB count by collagen-I signal *:p<0.0001 vs control (C) Immunocytological double-staining of Cx43 (red) and α-actinin (green) showing homocellular (red arrow) and heterocellular Cx43 expression (indicated by small red arrow) between CMCs (green) and MFBs. (D) Quantification of homocellular (CMC-CMC) and heterocellular (CMC-MFB) Cx43 expression. *:p<0.001 vs control. (E) Typical examples of ANP (red) and α-actinin (green) double-staining. (F) Quantification of ANP signal.*

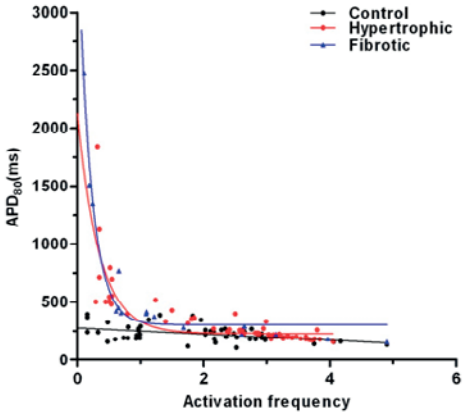

Supplemental Figure 3: *APD_{80} restitution curve shows that the slope of APD_{80} restitution strongly increases at activation frequencies below 1 Hz in hypertrophic or fibrotic cultures.*

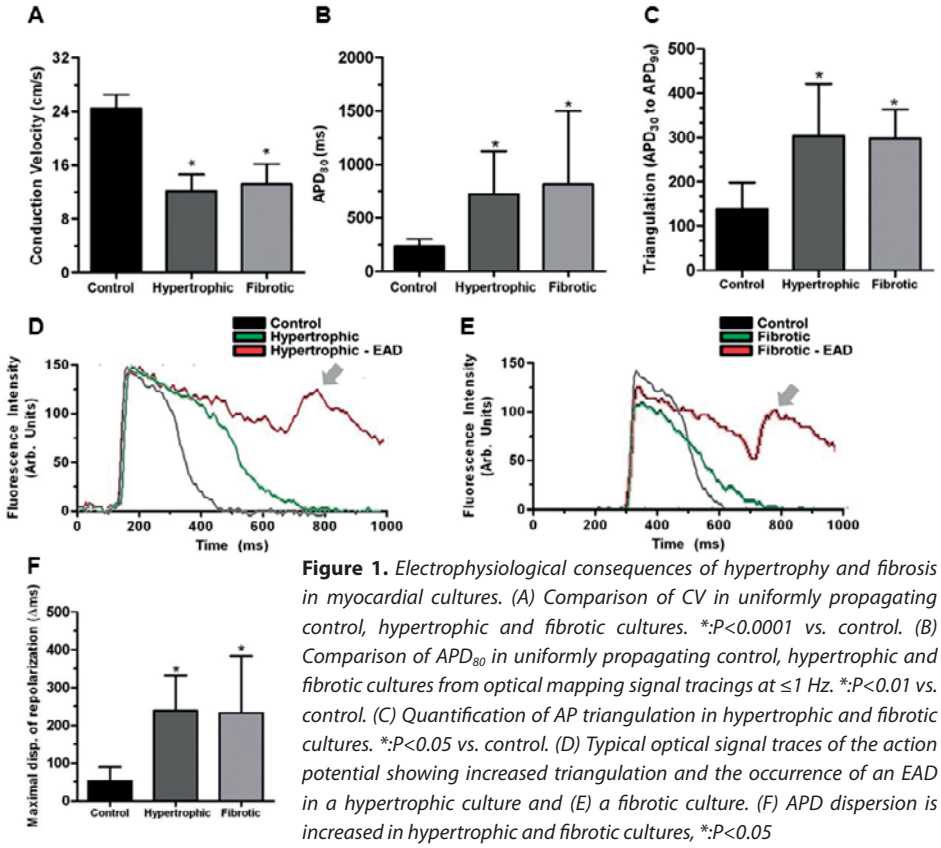

Figure 1. *Electrophysiological consequences of hypertrophy and fibrosis in myocardial cultures. (A) Comparison of CV in uniformly propagating control, hypertrophic and fibrotic cultures. *:P<0.0001 vs. control. (B) Comparison of APD_{80} in uniformly propagating control, hypertrophic and fibrotic cultures from optical mapping signal tracings at ≤1 Hz. *:P<0.01 vs. control. (C) Quantification of AP triangulation in hypertrophic and fibrotic cultures. *:P<0.05 vs. control. (D) Typical optical signal traces of the action potential showing increased triangulation and the occurrence of an EAD in a hypertrophic culture and (E) a fibrotic culture. (F) APD dispersion is increased in hypertrophic and fibrotic cultures, *:P<0.05*

Triggered activity caused by abnormal repolarization gradients underlies focal tachyarrhythmias that occur in fibrotic and hypertrophic cultures

Apart from prolonged repolarization in fibrotic or hypertrophic cultures, triggered activity due to EADs was frequently observed. The incidence of EADs in both hypertrophy (40%, n=25) and fibrosis (65.5%, n=29) was significantly higher compared to control cultures (4.2%, n=24) (Figure 2D). The occurrence of EADs not only lengthened APD_{80}, but also dramatically increased the spatial heterogeneity of repolarization (from 197±78ms during uniform repolarization to 1570±1155ms during EADs, $P<0.05$, Supplemental Figure 4). EADs could be observed spontaneously but were also easily evoked by 1Hz stimulation in both substrates. Additionally, EADs could repeatedly oscillate.

Triggered activity resulted in an increased activation frequency (2.64±0.42 Hz in hypertrophic or 2.99±0.54 Hz for fibrotic cultures vs. 0.82±0.83 Hz in uniformly conducting control cultures, both $P<0.001$ vs. control) (Figure 2F), thereby identifying this activation pattern as a focal tachyarrhythmia. These focal arrhythmias were infrequently observed in controls (8.8%, n=57, Figure 2A), but were prominent in both hypertrophic

(39.1%, n=23) (Figure 2B) and fibrotic cultures (51.7%, n=29, Figure 2C, 2E). During focal tachyarrhythmias, repolarization locally ceased, (Figure 2B and C, point 1) resulting in a sustained depolarized area in both substrates. As a consequence of juxtaposed repolarizing tissue and the resulting repolarization gradient, tissue at the border of the sustained depolarized area (Figure 2B, C point 2) repolarized very slowly. This translated to a diminished maximal repolarizing down stroke velocity in these areas (0.71±0.16 in controls vs. 0.26±0.04 in hypertrophic and 0.251±0.06 arbitrary optical units/ms in fibrotic cultures, $P<0.001$), thereby providing a prolonged time window for reactivation of the depolarizing force, which could lead to EAD formation. As the membrane potential of tissue distal from the constitutively depolarized area lowers again after the triggered action potential, repolarization in proximity of the depolarized area again occurs slowly.

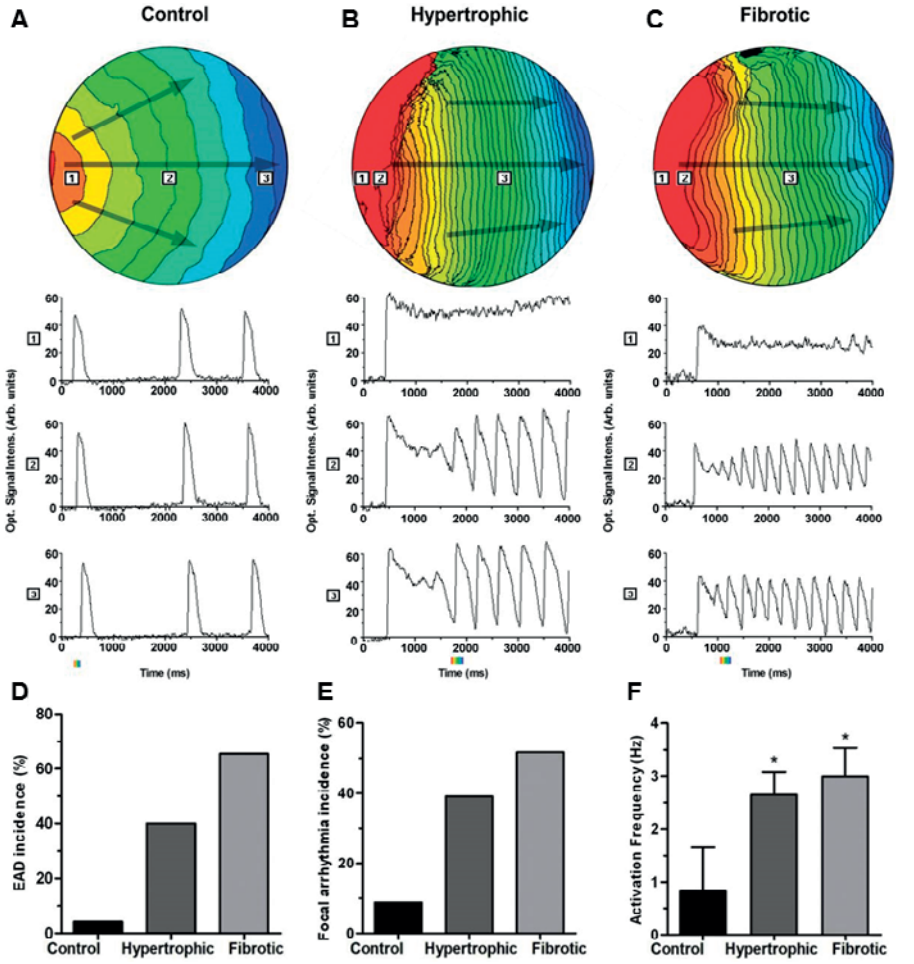

Figure 2. *Spontaneous focal tachyarrhythmias are formed in both hypertrophic and fibrotic myocardial cultures by repetitive EADs.*

This provided an opportunity for subsequent EADs, persistently repeating the previous sequence of events.

Both hypertrophy and fibrosis cause spontaneous reentrant tachyarrhythmias by critically timed EADs

Interestingly, both hypertrophic (n=111) and fibrotic cultures (n=107) showed a high incidence of spontaneous reentrant tachyarrhythmias, whereas control cultures (n=102) exhibited uniform and fast propagation (Figure 3A, 3B and 3C). Spontaneous reentry incidence was 67.5%, 78.5% and 2.9% in hypertrophic, fibrotic and control cultures, respectively (Figure 3D). To investigate the mechanisms behind these high incidences, reentry formation was studied in these cultures. Spontaneous reentry formation in both substrates was found to be a consequence of triggered activity caused by EADs. The common determinant of reentry initiation was the critical timing of EADs, which is described hereafter. During EADs, APD was increased in both hypertrophic and fibrotic cultures compared to controls (Figure 3B and C, point 1) prior to reentrant conduction, as was the case for APD dispersion (Supplemental Figure 4). Consequentially, hypertrophic and fibrotic cultures were vulnerable to conduction block following EADs. These EADs typically formed at the edge of an area with long APD (Figure 3B and C, point 2) where down stroke velocity of repolarization was locally slowed and thus could prolong the time frame for reactivation of depolarizing current (Figure 3B and C, point 2). If an EAD was generated, this newly generated EAD propagates away from the area with the long APD, as the AP will only meet relatively well-repolarized tissue in that direction (Figure 3B and C point 3). Thereby, unidirectional conduction block was formed (Figure 3, indicated by double black lines). If repolarization occurred at the site of EAD origin before return of the wave front, reentry was enabled by such critical timing. This resulted in increased activation frequency (0.82±0.83Hz in uniformly conducting controls vs. 3.22±0.41Hz in hypertrophic or 3.93±0.66Hz in fibrotic cultures showing reentry $P<0.0001$) (Figure 3E, 3F and 3G) identifying this conduction pattern as another type of tachyarrhythmia.

← **Figure 2. (Legend continued)**
*Spontaneous focal tachyarrhythmias are formed in both hypertrophic and fibrotic myocardial cultures by repetitive EADs. (A) Typical example of an activation map of an uniformly propagating control culture (6 ms isochronal spacing). Corresponding non-high-pass filtered and spatially filtered optical signals indicated by numbers 1-3 show short APDs and low activation frequency. Black arrows indicate the diverging direction of AP propagation as a result of the convex waveform. (B) Activation map of focal tachy-arrhythmic activation in a hypertrophic or (C) fibrotic culture (6ms isochrones spacing). Corresponding optical signals show ceased repolarization at point 1, initiation of the first EAD after slow repolarization in point 2 followed by several propagated EADs and propagation of the first and following EADs in point 3 resulting in a high activation frequency. Black arrows indicate converging/planar direction of AP propagation. (D) Incidence of EADs and (E) spontaneous focal arrhythmias. (F) Repetitive focal activation increases activation frequency in both substrates when compared with normal, uniformly propagating control cultures. *:P<0.001 vs. control.*

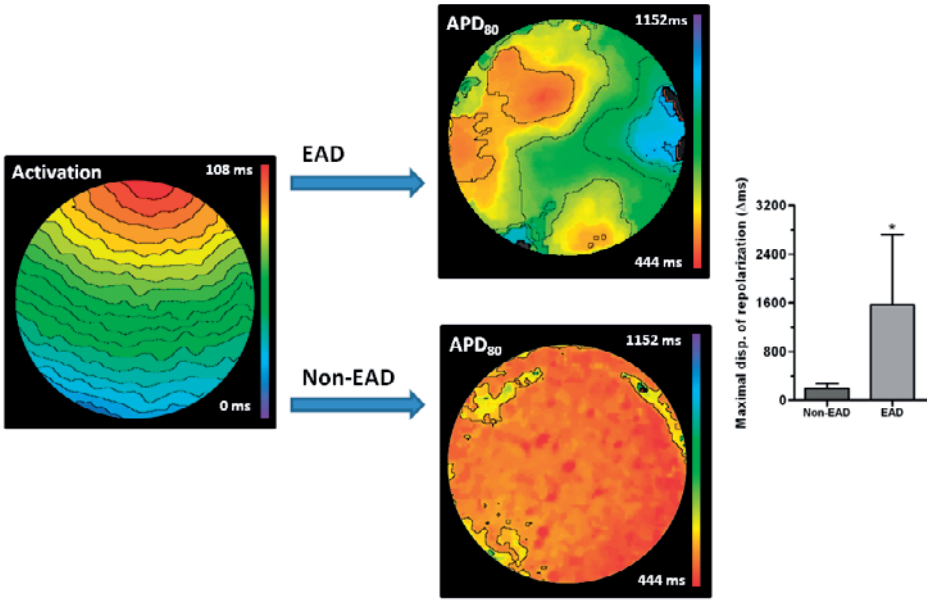

Supplemental Figure 4: *Effect of EADs on APD dispersion. Examples are taken from fibrotic cultures but are also representative for hypertrophic cultures. Uniform activation is shown on the left (6 ms isochrones). After such activation, repolarization occurs throughout the culture (bottom-right repolarization map). However, repolarization can reverse in fibrotic or hypertrophic cultures. The resulting EADs greatly lengthen local APDs (top-right repolarization map), which considerably enhances spatial APD dispersion. This creates a substrate that is vulnerable to reentrant conduction as enhanced differences in refractoriness facilitate formation of unidirectional block. The same observations were made in hypertrophic cultures.*

Figure 3. (Legend continued) →

*Both hypertrophy and fibrosis give rise to spontaneous reentrant tachyarrhythmias by generation of critically timed EADs. (A) Typical example of an activation map of a control myocardial culture showing uniform and rapid propagation (6ms isochrones spacing). Corresponding non-high-pass filtered and spatially filtered optical signals at different places indicated by numbers 1-4. Gray arrow indicates direction of AP propagation. Activation map of a first reentrant wave in a (B) hypertrophic and (C) Fibrotic myocardial culture caused by EADs (6ms isochrones spacing). Corresponding optical signals at places indicated by numbers 1-4. Gray arrow indicates the critically timed EAD. Double black lines indicate unidirectional block, black arrow indicates direction of AP propagation. (D) Incidence of spontaneous reentrant tachyarrhythmias. (E) Activation frequency in normal, uniformly propagating control cultures compared to hypertrophic or fibrotic cultures showing reentrant conduction. *:P<0.0001 vs. control, **:P<0.0001 vs. control and hypertrophic cultures. (F) Typical example of a full AP trace of a hypertrophic and (G) fibrotic culture, showing a critically timed EAD (gray arrow) followed by a reentrant tachyarrhythmia.*

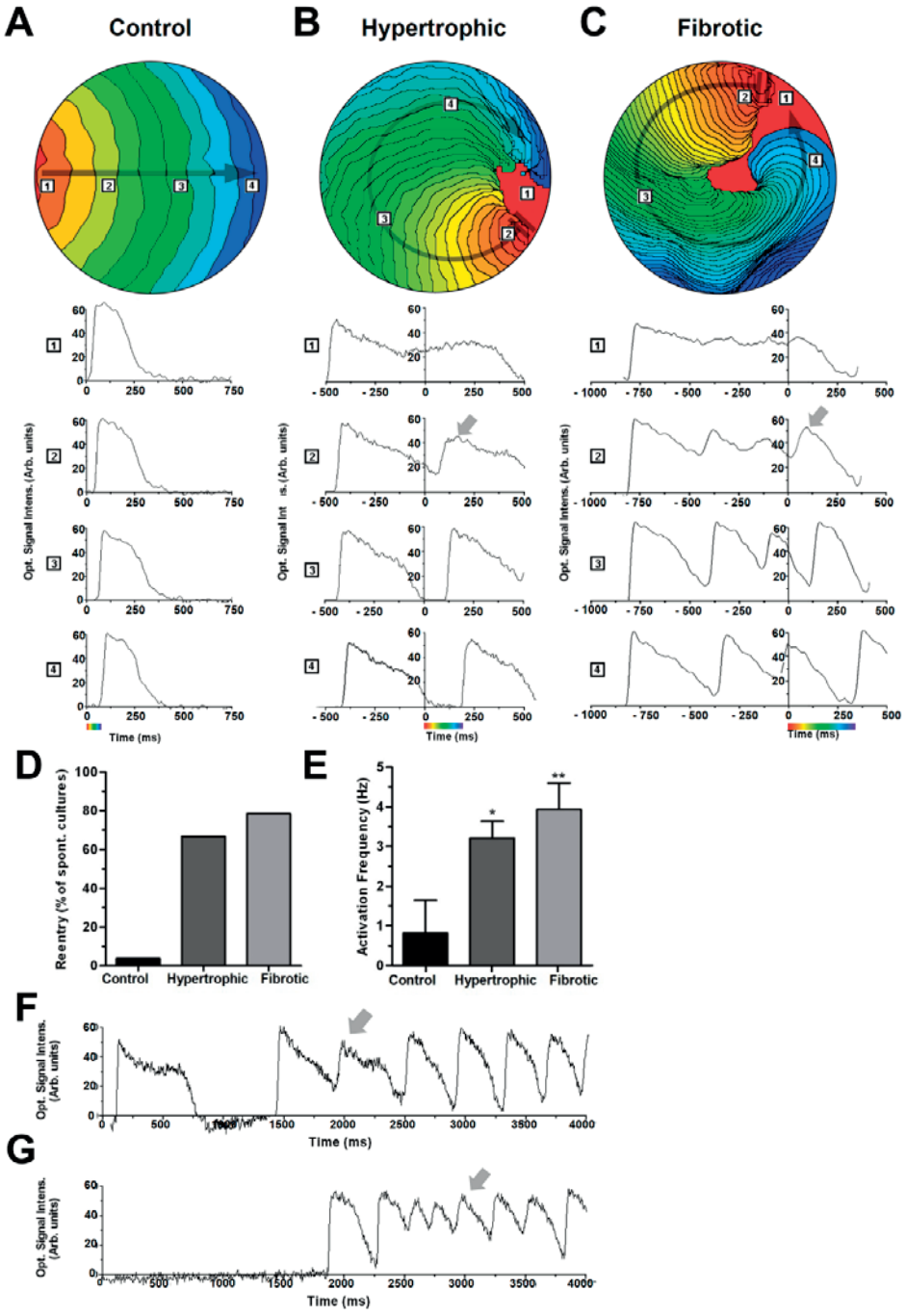

Figure 3. *Both hypertrophy and fibrosis give rise to spontaneous reentrant tachyarrhythmias by generation of critically timed EADs.*

Substrate-specific effects on electrophysiological properties of CMCs

To investigate substrate-specific effects on CMCs, protein expression of several ion channels and Cx43, as well as action potentials were investigated in all groups. Expression of Kv4.3 was decreased by 29%, in hypertrophic CMCs compared to controls (p=0.015). Expression of Nav1.5, Cav1.2, Kir2.1, and Kv7.1 were not significantly altered in hypertrophic cultures (Figure 4A,B). In contrast to hypertrophic cultures, CMCs in fibrotic cultures exhibited significantly higher expression of Kir2.1 only, compared to CMCs in control cultures (p=0.048 vs. control, Figure 4A, C). However, this difference is most likely not attributable to electrical remodeling, but to Kir2.1 expression in myofibroblasts contributing to the overall Kir2.1 expression when corrected for α-actinin.[10] Expression of intercellular Cx43 between CMCs at the protein level was decreased in hypertrophic cultures, while in fibrotic cultures, intercellular protein expression of Cx43 between CMCs was unaltered (12.2±7.1 arbitrary units in hypertrophy vs. 32.8±10.9 and 33.5±10.2 in control and fibrosis, $P<0.01$) (Figure 4D and 4E). Intracellular membrane potential recordings revealed distinctly different action potential morphologies (Figure 4E); with wide action potentials in hypertrophic CMCs and CMCs in fibrotic cultures and narrow action potentials in control CMCs. Furthermore, CMCs in fibrotic cultures were depolarized as maximal diastolic potentials were -48±7 mV (n=12, $P<0.0001$ vs. control) whereas hypertrophic CMCs showed no such alteration (-62±6 mV, n=8, p=ns) compared with control (-66±7 mV, n=8) (Figure 4F and 4G). Importantly, maximal diastolic potential of CMCs in fibrotic cultures became more negative after gap-junctional uncoupling with 25 μM 2-APB (-59±4 mV (n=5) vs. -48±7 mV (n=12) became more negative after gap-junctional uncoupling with 25 μM 2-APB (-59±4 mV (n=5) vs. -48±7 mV (n=12) in untreated fibrotic cultures respectively. In contrast, CMCs in hypertrophic or control cultures showed no significant change after 2-APB in maximal diastolic potential (-62±6 mV without vs. -65±4 mV with 2-APB in hypertrophic cultures, $p>0.05$ n=4 and -66±7 without vs. -68±5 mV with 2-APB in control cultures, $p>0.05$, n=4). Moreover, APD_{80} was strongly reduced in CMCs in fibrotic cultures after uncoupling (608±20ms without vs. 286±32ms with 2-APB, $P<0.05$, n=5) while APD_{80} remained largely unchanged after uncoupling CMCs in hypertrophic (732±26ms without vs. 715±23ms with 2-APB, $p>0.05$, n=4) or CMCs in control cultures (216±11ms without vs. 202±13ms with 2-APB, $p>0.05$). These data imply intrinsic electrical remodeling that decreases repolarization reserve as a pro-arrhythmic mechanism of hypertrophy, as opposed to extrinsic MFB-induced depolarization as a pro-arrhythmic mechanisms of fibrosis.

Substrate-specific effects of pharmacological interventions imply differing pro-arrhythmic mechanisms

To further characterize differences between pro-arrhythmic mechanisms of hypertrophy and fibrosis, *in vitro* effects of several drugs on arrhythmogeneity were compared

between hypertrophic and fibrotic myocardial cultures. Single point 1Hz stimulation for 10 ms evoked focal or reentrant arrhythmias in hypertrophic and fibrotic cultures (Figure 5A, lower records) with incidences of 75% in hypertrophy, 78% in fibrosis and 3% in control. To study the role of reduced repolarization reserve in arrhythmogeneity, 0.5 mmol/L sotalol was administered to control cultures, prolonging APD_{80} to 118% of initial values. Moreover, cultures showed EADs and reentrant arrhythmias after sotalol, which thereby increased arrhythmic incidence from 0% to 50% (n=16). L-type calcium channels were blocked by 3 μM nitrendipine, which is expected to lower net inward current and thereby reduce APD and arrhythmia incidence. In both hypertrophic and fibrotic cultures, no EADs, focal or reentrant arrhythmias could be evoked after nitrendipine (n=25 and n=15 for hypertrophic and fibrotic cultures) (Figure 5B and 5C). Pacing at 1Hz after nitrendipine administration resulted in electrical capture in all hypertrophic cultures (n=24), and shortening of APD_{80} (57.7±7.2% of untreated cultures, $P<0.001$) (Figure 5B), while 9 out of 19 fibrotic cultures were rendered unexcitable (Figure 5B and 5C). In line with these results, 10 μM verapamil treatment fully prevented formation of arrhythmias in both groups, but produced conduction block in fibrotic cultures (11 unexcitable cultures out of 15) (Figure 5B and 5C), while all hypertrophic cultures remained excitable (n=14).

To investigate the effect of blockade of the fast sodium channel in the different substrates, 20 μM TTX was administered to hypertrophic or fibrotic cultures in another set of experiments. Before TTX administration, arrhythmic incidence was 13 out of 22 hypertrophic cultures and 12 out of 19 fibrotic cultures. In 16 controls, no arrhythmias were detected. Following TTX administration, EAD incidence remained largely unchanged, as incidences were 16 out of 22 hypertrophic cultures and 11 out of 19 fibrotic cultures, making nav1.5-dependent mechanisms of EADs unlikely in the tested cultures. To test the contribution of altered intracellular calcium handling to arrhythmogenesis in these models, all intracellular calcium was buffered by treatment with 10-50 μM BAPTA-AM in an optical mapping experiment. Interestingly, BAPTA-AM treatment did not decrease arrhythmia incidence in hypertrophic nor fibrotic cultures (90%, n=40 and 76%, n=39, respectively) compared to non-treated cultures. These findings demonstrate that generation of EADs in these substrates is largely independent of intracellular calcium handling.

As heterocellular coupling is a pro-arrhythmic feature of fibrosis *in vitro*,[11] partial gap junctional uncoupling was performed to further examine differences in arrhythmogeneity of hypertrophic and fibrotic cultures. As MFB-CMC intercellular Cx43 expression is significantly lower than at CMC-CMC junctions (Supplemental Figure 2D), partial uncoupling can lead to inhibition of heterocellular MFB-CMC coupling while preserving sufficient CMC-CMC coupling for propagation. Therefore, cultures were treated with 5 μM 2-APB or 100 μM carbenoxolone. Treatment with 2-APB reduced arrhythmias in

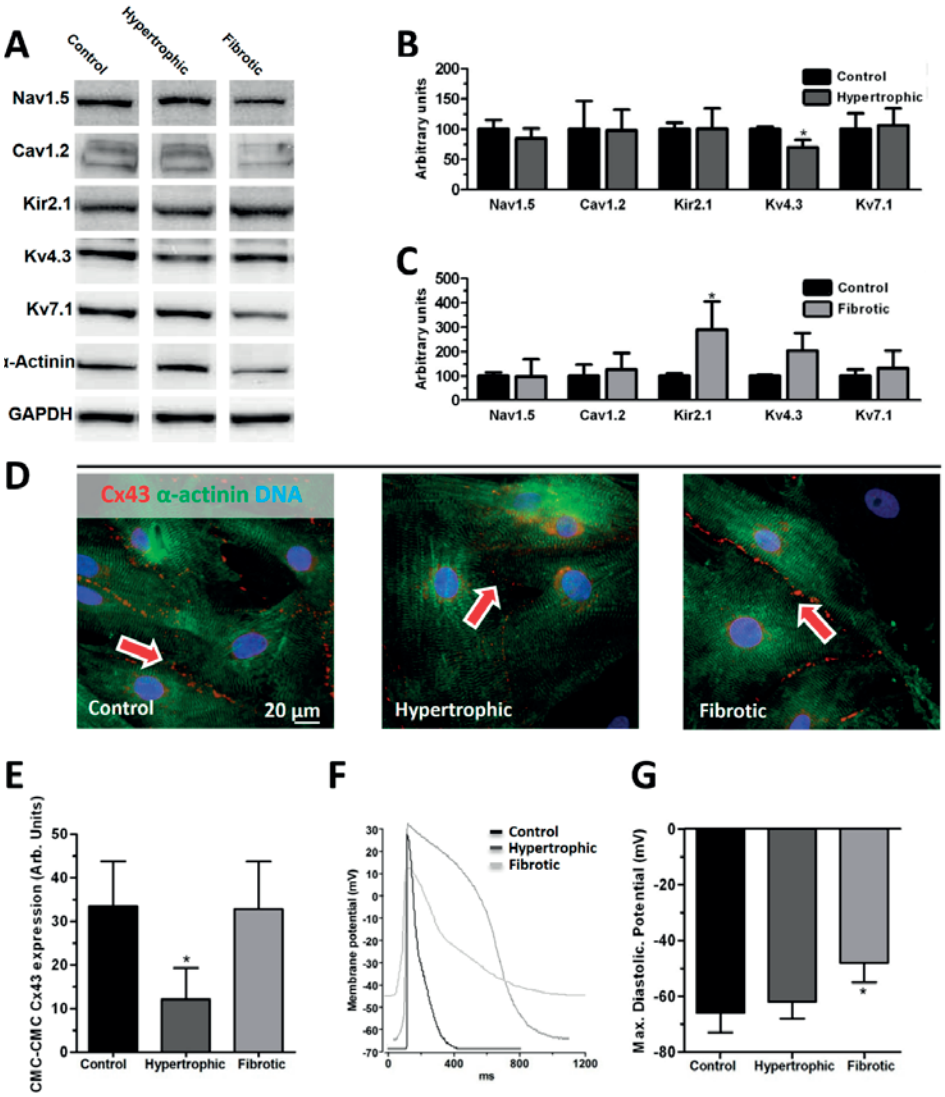

Figure 4. *Conduction slowing and AP triangulation are associated with either ion channel- and gap junctional remodeling or MFB-induced depolarization. (A) Typical examples of protein expression profiles in hypertrophic, fibrotic or control cultures as visualized by Western Blot analysis. (B) Quantification of ion channel protein expression corrected for corresponding GAPDH expression and α-actinin in control and hypertrophic cultures (*:P<0.01) and (C) control and fibrotic cultures. (D) Immunocytological staining of α-actinin (green) and Cx43 (red) in control, hypertrophic or fibrotic cultures. (E) Quantification of intercellular Cx43 signal, *:P<0.01. (F) Current-clamp traces of action potential in control, hypertrophic and fibrotic cultures. (G) Quantification of maximal diastolic potential. *:P<0.001.*

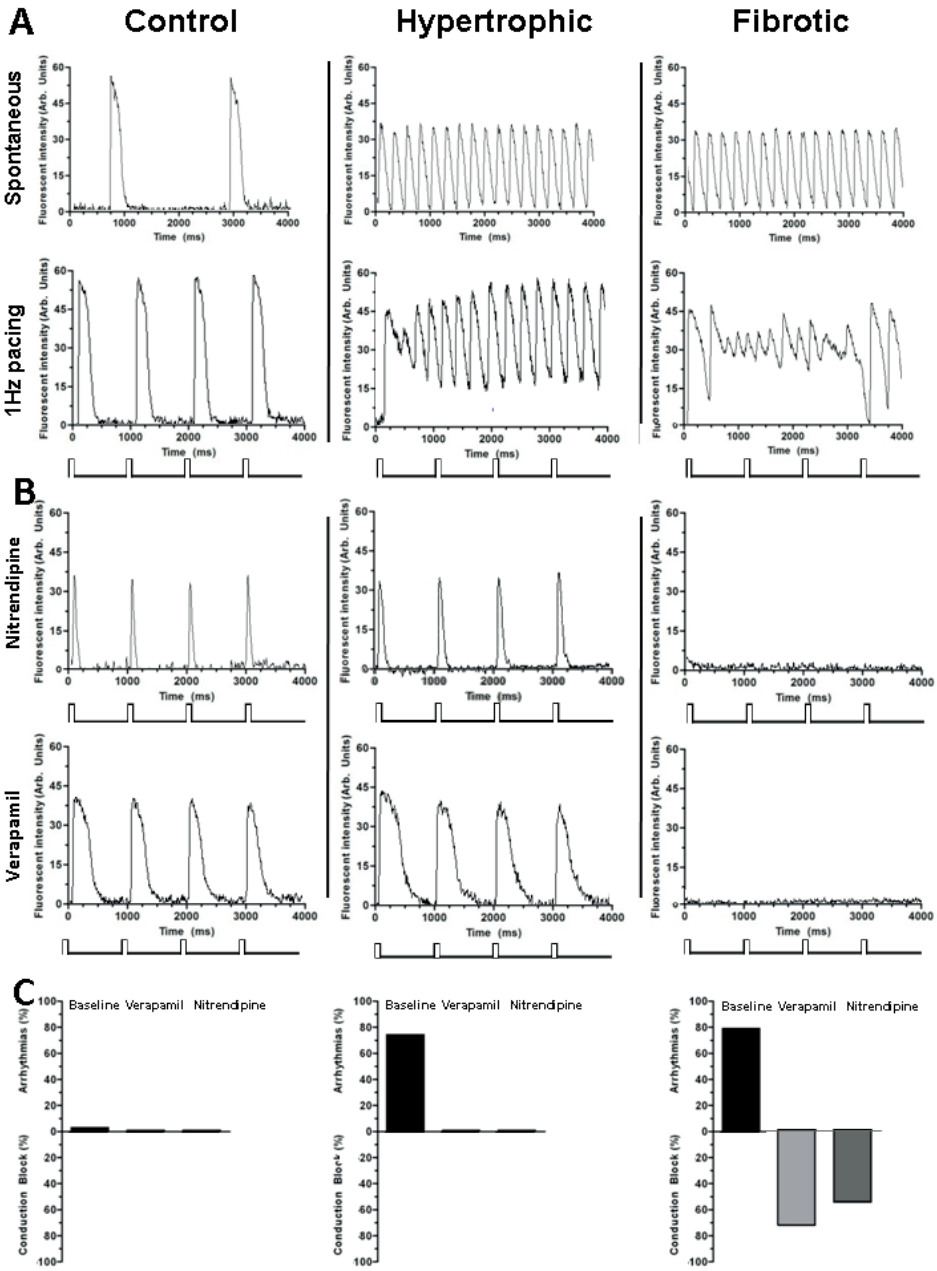

Figure 5. *Substrate-specific effects of L-type calcium channels blockade on arrhythmogeneity. (A) Typical examples of spatially and non-high-pass filtered optical signal traces, occurring spontaneously (above) and during 1Hz pacing (below) in untreated control (left), hypertrophic (middle) and fibrotic (right) cultures. (B) Same traces during 1Hz pacing in control (left), hypertrophic (middle) and fibrotic (right) cultures after treatment with 3 μM nitrendipine (above) and 10 μM verapamil (below). (C) Quantification of the incidence of spontaneous (focal and reentrant) arrhythmias and conduction block in control (left), hypertrophic (middle) and fibrotic (right) cultures after treatment with 10 μM verapamil or 3 μM nitrendipine*

fibrotic cultures (12.5%, n=16 vs. 78%, n=18 in untreated fibrotic cultures, $P<0.05$) (Figure 6A and 6C), and decreased APD_{80} (68.7±31.7% of untreated cultures, $P<0.05$). Such anti-arrhythmic effect was absent in hypertrophic cultures (86% arrhythmias n=14, vs. 75% n=12 in untreated hypertrophic cultures) (Figure 6A and 6C). Carbenoxolone also ameliorated arrhythmogeneity in fibrotic cultures, while arrhythmia incidence remained high in hypertrophic cultures (83% arrhythmias, n=12) (Figure 6B and 6C).

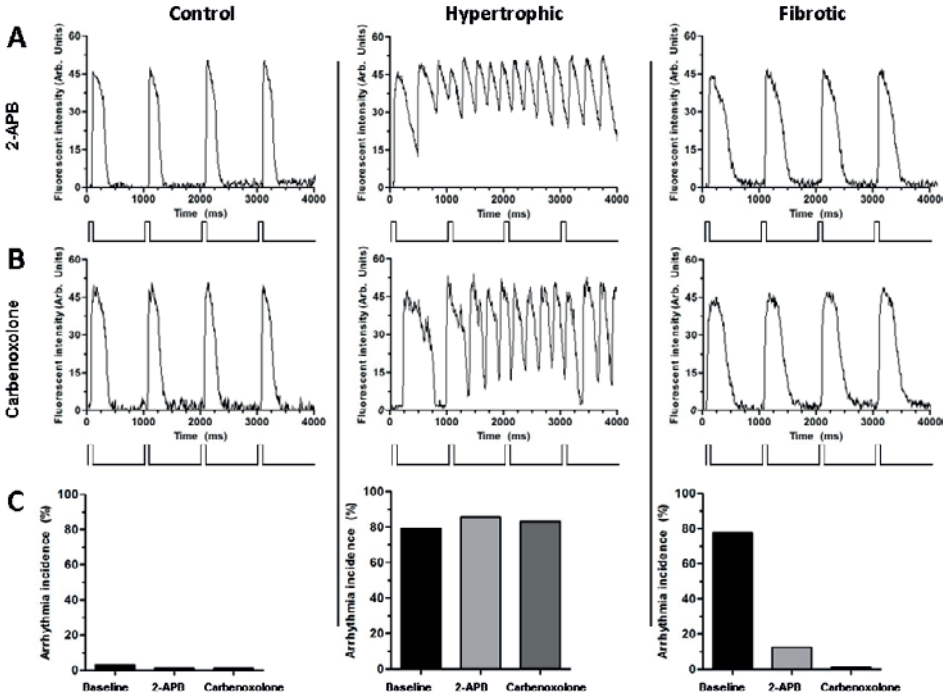

Figure 6. *Effect of gap junctional uncoupling on arrhythmogeneity depends on the arrhythmogenic substrate. (A) Typical examples of spatially filtered and non-high-pass filtered action potential traces during 1Hz pacing in control (left), hypertrophic (middle) and fibrotic (right) cultures after treatment with 5 μM 2-APB or (B) 100 μM carbenoxolone. (C) Quantification of the incidence of spontaneous (focal and reentrant) arrhythmias in control (left), hypertrophic (middle) and fibrotic (right) cultures after treatment with 5 μM 2-APB or 100 μM carbenoxolone.*

DISCUSSION

Key findings of this study are (1) both hypertrophic and fibrotic myocardial cultures give rise to triggered activity causing both focal and reentrant tachyarrhythmias. (2) Underlying pro-arrhythmic mechanisms highly differ between these two pathological conditions; mainly being electrical remodeling of CMCs in hypertrophic cultures or MFB-induced depolarization of CMCs in fibrotic cultures.

Triggered activity, focal and reentrant tachyarrhythmias in experimental models

Cardiac fibrosis and cardiac hypertrophy are both associated with spontaneous tachyarrhythmias.[1-3,12] Traditionally, whole-heart mapping studies suggest either focal or reentrant mechanisms underlying these ventricular tachyarrhythmias.[13,14] However, the complexity of 3-dimensional myocardial tissue hampers complete interpretation of findings and therefore, arrhythmogenesis has also been investigated in experimental 2D and computational models to unequivocally establish the existence of reentrant and focal mechanisms.[15,16] Additionally, despite the spontaneous occurrence of arrhythmias in patients, arrhythmogenesis has been mostly studied by externally applied burst stimulation to force induction of arrhythmias, [17-19] thereby precluding investigation of internal arrhythmic triggers in arrhythmogenesis.

In this study, triggered activity in the form of EADs was found spontaneously and could be evoked by low-frequency stimulation. Moreover, this activity was found to be responsible for the initiation of both focal and reentrant tachyarrhythmias in hypertrophic and fibrotic cultures. It was shown that the onset of focal and reentrant tachyarrhythmias depends on the generation of EADs, which either oscillate during phase 2 or 3 of the AP (focal) or are critically timed to form unidirectional block, slow conduction and thereby facilitate reentry. The importance of EADs in the onset of ventricular tachycardias is in line with previous *in silico*, *in vitro* and *in vivo* studies.[20,21] Traditionally, this correlation of EADs with arrhythmias was studied by inducing EADs by pharmacological or genetic interventions or, in the case of *in silico* studies, by altering ion channel properties to reduce repolarization reserve. While these studies proved useful to implicate EADs as a principal underlying mechanism of arrhythmogeneity**,** it remained unclear how prevalent acquired cardiac diseasessuch as hypertrophy or fibrosis may lead to arrhythmias. For hypertrophy, spontaneous EAD generation has been demonstrated in isolated CMCs.[22,23] The current study shows that EADs in hypertrophy also overcome electrotonic load and propagate in 2-dimensional tissue. Additionally, how predicted source-sink mismatching of propagated EADs is overcome is illustrated by the concave waveform (Figure 2B, C) found during focal tachyarrhythmias. This is in accordance with calculations that show that EAD propagation is favored in concave activation as such waveform morphology helps to overcome the source-sink mismatch that determines the threshold of EAD propagation.[24]

As EADs are reactivations of depolarizing current during repolarization, slowed repolarization is a critical facilitating factor for EAD generation. This was demonstrated in the present study by adding sotalol to control cultures, which prolonged APD and caused focal tachyarrhythmias. In addition, dispersion of repolarization causes steep repolarization gradients, which may provide the depolarizing force necessary for reactivation.[25] This reactivation was mainly calcium-dependent, as Nav1.5 blockade had no pro-

nounced anti-arrhythmic effect in either hypertrophic or fibrotic cultures. Additionally, intracellular calcium buffering was ineffective to prevent EADs and arrhythmias while Cav1.2 blockade ameliorated EADs. Findings of prolonged and dispersed repolarization may readily explain the similar pro-arrhythmogenic findings of triggered activity in hypertrophic or fibrotic tissue. However, the similarities between pro-arrhythmogeneity of hypertrophy and fibrosis end at the cellular level of the mechanisms of repolarization prolongation and dispersion.

Substrate-specific pro-arrhythmic mechanisms in cardiac hypertrophy and fibrosis

During cardiac remodeling, hypertrophy and fibrosis may develop to varying degrees. As a result, the resulting pro-arrhythmic features found in cardiac remodeling remain incompletely understood, as concomitance of these substrates precludes distinction between pro-arrhythmic mechanisms of these substrates and therefore, hamper the development of novel anti-arrhythmic treatment modalities. In this study, cellular and ionic mechanisms of arrhythmogeneity substantially differed between cardiac fibrosis and hypertrophy. In fibrosis, fibroblast proliferation and extracellular matrix deposition are known to extrinsically alter cardiac action potential propagation by forming spatial separations between CMCs, which reduces cell-to-cell contact, favors zigzag conduction and provides anatomic obstacles that increase the propensity towards arrhythmias.[26,27] [17]. However, in recent years, focus has shifted towards the MFB in cardiac fibrosis as a possible key factor in the extrinsic pro-arrhythmic mechanisms of fibrosis.[28-31] In culture, MFBs can inactivate voltage-gated potassium channels by depolarizing CMCs and thereby preclude proper repolarization and facilitate EAD generation.[11,12,32] This study confirms these extrinsic effects on CMCs, as high MFB content in cardiac cultures was associated with depolarized membrane potentials in CMCs, prolonged APD_{80} and an increased incidence of EADs that ultimately led to tachyarrhythmias. Other studies showed that paracrine factors secreted from cardiac fibroblasts were also able to induce a certain degree of ion channel remodeling in CMCs, although no EADs were reported in these CMCs.[33] However, no such effects were detected if cardiac fibroblasts were directly co-cultured with CMCs, as was done in the present study. In our study fibrosis led to an increase in Kir2.1 expression when corrected for alpha actinin. However, this is unlikely the result of a functional overexpression of Kir2.1 in cardiomyocytes. In the hypothetical case of functional kir2.1 overexpression in CMCs the MDP in fibrotic cultures would be more negative after uncoupling compared to non-fibrotic controls, while the opposite is true. This means that either the extra kir2.1 is derived from myofibroblasts or does not lead to an increase in inward rectifier current. Furthermore, Findings of strong anti-arrhythmic effects of partial uncoupling confirm dominance of coupling-based pro-arrhythmic mechanisms over paracrine mechanisms in the currently used model. This

anti-arrhythmic effect is possibly due to the vast functional reserve capacity of CMC-CMC coupling, which is considerably lower in MFB-CMC coupling and thereby allows for heterocellular uncoupling.[34]

In contrast to fibrosis, partial uncoupling had no anti-arrhythmic effects in hypertrophic tissue indicating differing pro-arrhythmic mechanisms. Reduction of total expression and altered distribution of Cx43 are all features of pathologically hypertrophied myocardium that compromise proper intercellular conduction and thereby lead to conduction slowing.[354] In addition, repolarization reserve is diminished by down regulation of voltage-gated potassium channels, which may increase the propensity towards EADs and ultimately towards arrhythmias.[365] In our study, lowered Cx43 expression, increased ANP and altered ion channel protein expression were confirmed in hypertrophic CMCs, and absent in CMCs in fibrotic and control cultures (Supplemental Figures 1, 2 and Figure 4 C, D). The down regulation of Kv4.3, which contributes to the transient outward current (I_{to}) was in accordance with other studies.[37,387] Hoppe et al showed that a reduction in I_{to} leads to a marked increase in APD by an increase in the plateau potential, thereby altering the early trajectory of repolarization.[398]

Due to differences in pro-arrhythmic mechanisms, L-type calcium channel blockade shortened APD and was anti-arrhythmic in hypertrophic cultures but blocked conduction in fibrotic cultures as propagation in such cultures was largely dependent on calcium channels due to MFB-induced depolarization and concomitant inactivation of fast sodium channels. Nevertheless, the arrhythmogenic pathways of hypertrophy and fibrosis converge at the point of prolongation of repolarization, APD dispersion and EAD formation. These results suggest that lowering the incidence of spontaneous arrhythmias by preventing EAD generation may require a different approach in hypertrophic or fibrotic-substrates. Alternatively, common pro-arrhythmic factors should be targeted. Future research is needed to elaborate on the implications these findings may have for the *in vivo* setting.

Study limitations

In our study, fibrosis was mimicked by MFB proliferation in myocardial cultures. However, the deposition of extracellular matrix as another component of fibrosis was not investigated, as *in vitro* deposition of matrix comparable to *in vivo* quality and quantity is difficult to achieve. Although it is well established that MFBs and CMCs functionally couple *in vitro*, strong, undeniable proof of this phenomenon *in vivo* has yet to appear. The implications of changes in expression of Kv4.3 protein found in hypertrophic rat cells cannot be directly extrapolated to human hearts due to differences in expression levels and functions of the associated currents. Consequently, this study establishes an *in vitro* proof-of-principle of cellular pro-arrhythmic mechanisms and recognizes that

more *in vivo* research is necessary before this kind of *in vitro* results can be translated to clinical implications.

CONCLUSIONS

Hypertrophic and fibrotic myocardial tissues are independent, pro-arrhythmic substrates. Both substrates are characterized by slow conduction, APD prolongation, formation of EADs and subsequent focal and reentrant tachyarrhythmias. However, while pathological hypertrophy is characterized by electrical remodeling of CMCs, fibrosis is mainly characterized by MFB-induced depolarization of CMCs. These differences may stress the importance of a substrate-based approach in the treatment of cardiac arrhythmias.

ACKNOWLEDGEMENTS

We wish to thank Dr. W.P.M van Meerwijk for helpful discussions, and Huybert J.F. van der Stadt for excellent technical support.

SOURCES OF FUNDING

This work was supported by the Dutch Heart Foundation (2008/B119) and the Netherlands Organisation for Scientific Research (NWO; VENI grant (91611070), D.A.P).

CONFLICT OF INTEREST

None declared.

SUPPLEMENTAL MATERIAL

MATERIALS AND METHODS

All animal experiments were approved by the Animal Experiments Committee of the Leiden University Medical Center and conform to the Guide for the Care and Use of Laboratory Animals as stated by the US National Institutes of Health.

Experimental protocol

All control cultures were treated with the antiproliferative agent Mitomycin-C (10 µg/ml, Sigma-Aldrich, St. Louis, MO, USA), to prevent proliferation of endogenously present, α-smooth muscle actinin-positive myofibroblasts (MFBs). For this purpose Mitomycin-C dissolved in PBS was diluted in growth medium (Ham's F10 supplemented with 10% fetal bovine serum (FBS, Invitrogen, Carlsbad, CA, USA), 10% horse serum (HS, Invitrogen) and penicillin (100U/ml) and streptomycin (100 µg/ml, P/S; Bio-Whittaker, Carlsbad, CA, USA) and incubated for 2 hours. Subsequently, cultures were rinsed twice in PBS and once in a 1:1 mixture of DMEM/HAMS F10 supplemented with 5% HS and P/S before being kept on this medium throughout the experiment. To induce hypertrophy, Mitomycin-C treated cultures were exposed to 100 µM phenylephrine (PE, Sigma) for 24h at day 3 and day 8[4]. To mimic fibrosis, endogenously present MFBs were allowed to proliferate freely, by treatment with PBS instead of Mitomycin-C. Fibrotic cultures were rinsed identically as control cultures control and hypertrophic cultures after Mitomycin-C/PBS treatment. For reasons of comparability, fibrotic cultures and control cultures received PBS instead of PE.

Immunocytological analyses

Immunocytological stainings were performed as described in earlier studies.[9,40] Cultures were fixed in 1% paraformaldehyde for 20 minutes on ice, after which cultures were rinsed twice with Phosphate Buffered Saline (PBS) and permeabilized with 0.1% Triton X-100. After 2 subsequent wash-steps, cultures were incubated overnight with primary antibodies diluted in PBS with 1% Fetal Bovine Serum. Primary antibodies were directed against α-actinin (Sigma), α-smooth muscle actinin (Sigma), α-skeletal muscle actinin (Abcam, Cambridge, MA, USA), atrial natriuretic peptide (Abcam) or Collagen type I (Abcam) and used at a dilution of 1:200. Double-staining was performed by using primary antibodies that were raised in either mouse or rabbit host species. Corresponding secondary donkey anti-rabbit or donkey anti-mouse Alexa fluor-conjugated antibodies (Invitrogen) were incubated for 2 hours at room temperature at a dilution of 1:400. After rinsing twice, nuclei of these cultures were counterstained for 5 minutes

with Hoechst 33321 (Invitrogen). Following 2 wash steps, stained glass coverslips were mounted in Vectashield mounting medium (Vector Laboratories Inc, Burlingame, CA, USA) to minimize photobleaching. Images of cultures were taken and quantified using dedicated software (Image-Pro Plus, version 4.1.0.0, Media Cybernetics, Silver Spring, MD, USA). Quantification of all staining was performed in at least 6 cultures per group with at least 20 photos taken per culture. Quantification of fluorescent signal intensity was performed in at least 15-fold per photo.

To confirm a pathological hypertrophic phenotype in PE-treated CMCs, cultures were characterized at day 9 for protein expression of the hypertrophic markers atrial natriuretic peptide and α-skeletal muscle actin by immunocytological staining. In addition, cell surface area of CMCs was quantified as another measure of hypertrophy. To confirm fibrosis in cardiac cultures, cultures were stained for collagen-I (Abcam) and positive cells were considered to be MFBs and quantified.[9]

Optical mapping

Propagation of action potentials was investigated on a whole-culture scale in hypertrophic, fibrotic or control cultures using voltage-sensitive dye mapping as described earlier.[9] For reasons of standardization and reproducibility, only cultures without structural inhomogeneities as judged by mapping and light microscopy were included for further analyses. Cardiac cultures were plated out in 24-well plates (Corning) at a cell density of $8x10^5$ cells per well. At day 9, cultures were optically mapped. At least 2 hours after the daily refreshing of culture medium, cultures were incubated with culture medium containing 8 µmol/L di-4-ANEPPS for 15±5 minutes at 37° C in a humidified incubator. Subsequently, cultures were refreshed with serum-free, colorless DMEM/HAMS F10 mixed in a 1:1 ratio. Next, electrical propagation patterns were recorded by optical mapping at 37°C. Mapping experiments typically did not exceed 30 minutes per 24-wells plate. Also, cultures were not exposed to excitation light for longer than 50 s to limit possible phototoxic effects. Excitation light (e_{ex} = 525±25 nm) was delivered by a halogen arc-lamp (MHAB-150W, Moritex Corporation, San Jose, CA, USA) through epi-illumination. Fluorescent emission light passed through a dichroic mirror and a long-pass emission filter (>590 nm) and was focused onto a 100x100 pixels CMOS camera (Ultima-L, SciMedia, Costa Mesa, CA, USA) by a 1.6x converging lens (Leice, Wetzlar, Germany). This resulted in a spatial resolution of 160 µm/pixel and a field of view of 16 by 16 mm. Spontaneous or stimulated electrical activity was recorded for 6-24 seconds at 6ms exposure time per frame. Data analysis was performed with specialized software (Brainvision Analyze 1101, Brainvision Inc, Tokyo, Japan) after pixels signals were averaged with 8 of its nearest neighbors to minimize noise-artifacts. Conduction velocity (CV), maximal optical action potential upstroke (dF/dT_{max}), maximal action potential downstroke velocity (dF/dTmin), action potential duration until 80% repolarization (APD_{80}) were determined at ≤1 Hz at

six different locations equally distributed throughout the culture and averaged before inclusion in further analyses. Spatial dispersion of repolarization was defined as the maximal difference in APD_{80} within a culture and was determined at activation frequencies of ≤1 Hz.

Assessment of EADs and focal tachyarrhythmias

As prevalent reentrant conduction precludes assessment of conduction patterns other than reentry, reentry needed to be eliminated to analyze all possible conduction patterns and spontaneous activity in included cultures. To maintain ion channel properties, reentry had to be eliminated in a non-pharmacological manner. For this purpose, we used a custom-made epoxy-coated platinum electrode and performed unipolar stimulation with 6 V for 4 seconds using an electrical stimulus module with corresponding software (Multichannel Systems), which successfully eliminated reentry in >90% of the cultures. After absence of reentry was confirmed by 2s optical mapping, spontaneous activity was detected by mapping of the cultures for 24 seconds following application of the stimulus. This allowed for detection of EADs and spontaneous focal arrhythmias that otherwise would be overruled by reentrant activation. All cultures included in this analysis, regardless of the presence of reentry, underwent equal stimulation for standardization purposes.

Pharmacological anti-arrhythmic interventions

To investigate the antiarrhythmic potential of pharmacological interventions in different substrates, several pharmacological agents were administered to hypertrophic, fibrotic or control cultures under optical mapping conditions. Inhibition of L-type Ca^{2+} inward current was performed by application of a relatively low dose of verapamil (10 μM) (Centrafarm, Etten-Leur, the Netherlands) or nitrendipine (3 μM) (Sigma) directly into the mapping medium. As this instantly abolished all spontaneous activity in all cultures regardless of composition, cultures were stimulated at 2V (1Hz intervals) for 4 seconds to evaluate capture and propagation parameters. For standardization purposes, arrhythmic activity before verapamil and nitrendipine administration was also investigated following 1Hz stimulation.

To reduce heterocellular coupling between CMCs and MFBs in hypertrophic or fibrotic myocardial cultures, a relatively low dose of the 2-APB (5 μM) (Tocris Bioscience, Bristol, United Kingdom) or carbenoxolone (100 μM) (Sigma) was supplied in the mapping medium and incubated for 20 minutes. To investigate effects of Nav1.5 blockade, tetrodotoxin (TTX, 20 μM, Alomone Labs) was pipetted into the medium and incubated for 10s. For investigation of the involvement of intracellular calcium handling in arrhythmogeneity, intracellular calcium was buffered using 10-50 μM BAPTA-AM (Sigma) which

incubated for 20 minutes. To investigate the effect of action potential duration (APD) prolongation on arrhythmogeneity, 0.5 mM sotalol (Sigma) was used. For reproducibility and comparability between all pharmacological interventions, all cultures were paced with a 1 Hz supra-threshold stimulation protocol during optical mapping recordings.

Whole-cell patch-clamp

Whole-cell current-clamp measurements were performed in spontaneously active (0.2-1 Hz) hypertrophic, fibrotic or control cultures. For fibrotic cultures, MFBs were labeled with eGFP using the vesicular stomatitis virus G protein-pseudotyped self-inactivating lentivirus vector CMVPRES as described previously.[9] Subsequently, these labeled MFBs were plated out with CMCs in equal quantity and density as fibrotic cultures with freely proliferating MFBs at day 9. To maintain the initially plated ratio, cultures were treated with mitomycin-C. Therefore, CMCs were easily identifiable in these fibrotic cultures. At day 9, after identification of CMCs by fluorescence microscopy, current-clamp experiments were performed in these cells. Whole-cell recordings were performed at 25°C using a L/M-PC patch-clamp amplifier (3kHz filtering) (List-Medical, Darmstadt, Germany). The pipette solution contained (in mmol/L) 10 Na_2ATP, 115 KCl, 1 $MgCl_2$, 5 EGTA, 10 HEPES/KOH (pH 7.4). Tip and seal resistance were 2.0-2.5 MΩ and >1 GΩ, respectively. The bath solution contained (in mmol/L) 137 NaCl, 4 KCl, 1.8 $CaCl_2$, 1 $MgCl_2$, and 10 HEPES (pH 7.4). In a subset of experiments, CMCs were functionally uncoupled by incubation for 20 minutes with 25 µmol/L 2-APB to investigate intrinsic action potential morphology in hypertrophic, fibrotic or control cultures. For data acquisition and analysis, pClamp/Clampex8 software (Axon Instruments, Molecular Devices, Sunnyvale, CA, USA) was used.

Statistical analysis

Statistical analyses were performed using SPSS11.0 for Windows (SPSS Inc., Chicago, IL, USA). Comparison between numerical data of groups was performed using the student-t test or paired t-test where appropriate. Values were expressed as mean±SD. Significance of differences in incidences between groups was determined by the Chi-square statistical test. Differences were considered statistically significant if $p<0.05$.

REFERENCES

1. Haider AW, Larson MG, Benjamin EJ, Levy D. Increased left ventricular mass and hypertrophy are associated with increased risk for sudden death. *J Am Coll Cardiol*. 1998;32:1454-1459.
2. McLenachan JM. Ventricular arrhythmias in patients with hypertensive left ventricular hypertrophy. 1987.
3. van der Burg AE, Bax JJ, Boersma E, Pauwels EK, van der Wall EE, Schalij MJ. Impact of viability, ischemia, scar tissue, and revascularization on outcome after aborted sudden death. *Circulation*. 2003;108:1954-1959.
4. Kuck KH, Schaumann A, Eckardt L, Willems S, Ventura R, Delacretaz E, Pitschner HF, Kautzner J, Schumacher B, Hansen PS. Catheter ablation of stable ventricular tachycardia before defibrillator implantation in patients with coronary heart disease (VTACH): a multicentre randomised controlled trial. *Lancet*. 2010;375:31-40.
5. Zeppenfeld K and Stevenson WG. Ablation of ventricular tachycardia in patients with structural heart disease. *Pacing Clin Electrophysiol*. 2008;31:358-374.
6. Borleffs CJ, van EL, Schotman M, Boersma E, Kies P, van der Burg AE, Zeppenfeld K, Bootsma M, van der Wall EE, Bax JJ, Schalij MJ. Recurrence of ventricular arrhythmias in ischaemic secondary prevention implantable cardioverter defibrillator recipients: long-term follow-up of the Leiden out-of-hospital cardiac arrest study (LOHCAT). *Eur Heart J*. 2009;30:1621-1626.
7. Arshad A, Mandava A, Kamath G, Musat D. Sudden cardiac death and the role of medical therapy. *Prog Cardiovasc Dis*. 2008;50:420-438.
8. Pijnappels DA, Schalij MJ, Ramkisoensing AA, van Tuyn J, de Vries AA, van der Laarse A, Ypey DL, Atsma DE. Forced alignment of mesenchymal stem cells undergoing cardiomyogenic differentiation affects functional integration with cardiomyocyte cultures. *Circ Res*. 2008;103:167-176.
9. Askar SF, Ramkisoensing AA, Schalij MJ, Bingen BO, Swildens J, van der Laarse A, Atsma DE, de Vries AA, Ypey DL, Pijnappels DA. Antiproliferative treatment of myofibroblasts prevents arrhythmias in vitro by limiting myofibroblast-induced depolarization. *Cardiovasc Res*. 2011.
10. Walsh KB and Zhang J. Neonatal rat cardiac fibroblasts express three types of voltage-gated K+ channels: regulation of a transient outward current by protein kinase C. *Am J Physiol Heart Circ Physiol*. 2008;294:H1010-H1017.
11. Askar SF, Bingen BO, Swildens J, Ypey DL, van der Laarse A, Atsma DE, Zeppenfeld K, Schalij MJ, de Vries AA, Pijnappels DA. Connexin43 silencing in myofibroblasts prevents arrhythmias in myocardial cultures: Role of maximal diastolic potential. *Cardiovasc Res*. 2011.
12. Kleber AG and Rudy Y. Basic mechanisms of cardiac impulse propagation and associated arrhythmias. *Physiol Rev*. 2004;84:431-488.
13. Pogwizd SM, Hoyt RH, Saffitz JE, Corr PB, Cox JL, Cain ME. Reentrant and focal mechanisms underlying ventricular tachycardia in the human heart. *Circulation*. 1992;86:1872-1887.
14. de Bakker JM, van Capelle FJ, Janse MJ, Wilde AA, Coronel R, Becker AE, Dingemans KP, van Hemel NM, Hauer RN. Reentry as a cause of ventricular tachycardia in patients with chronic ischemic heart disease: electrophysiologic and anatomic correlation. *Circulation*. 1988;77:589-606.
15. Allessie MA, Bonke FI, Schopman FJ. Circus movement in rabbit atrial muscle as a mechanism of tachycardia. III. The "leading circle" concept: a new model of circus movement in cardiac tissue without the

involvement of an anatomical obstacle. *Circ Res*. 1977;41:9-18.

16. Hou L, Deo M, Furspan P, Pandit SV, Mironov S, Auerbach DS, Gong Q, Zhou Z, Berenfeld O, Jalife J. A major role for HERG in determining frequency of reentry in neonatal rat ventricular myocyte monolayer. *Circ Res*. 2010;107:1503-1511.
17. Lim ZY, Maskara B, Aguel F, Emokpae R, Jr., Tung L. Spiral wave attachment to millimeter-sized obstacles. *Circulation*. 2006;114:2113-2121.
18. Baker LC, London B, Choi BR, Koren G, Salama G. Enhanced dispersion of repolarization and refractoriness in transgenic mouse hearts promotes reentrant ventricular tachycardia. *Circ Res*. 2000;86:396-407.
19. Chang MG, Zhang Y, Chang CY, Xu L, Emokpae R, Tung L, Marban E, Abraham MR. Spiral waves and reentry dynamics in an in vitro model of the healed infarct border zone. *Circ Res*. 2009;105:1062-1071.
20. Weiss JN, Garfinkel A, Karagueuzian HS, Chen PS, Qu Z. Early afterdepolarizations and cardiac arrhythmias. *Heart Rhythm*. 2010;7:1891-1899.
21. Sato D, Xie LH, Sovari AA, Tran DX, Morita N, Xie F, Karagueuzian H, Garfinkel A, Weiss JN, Qu Z. Synchronization of chaotic early afterdepolarizations in the genesis of cardiac arrhythmias. *Proc Natl Acad Sci U S A*. 2009;106:2983-2988.
22. Qin D, Zhang ZH, Caref EB, Boutjdir M, Jain P, El-Sherif N. Cellular and ionic basis of arrhythmias in postinfarction remodeled ventricular myocardium. *Circ Res*. 1996;79:461-473.
23. Stengl M, Ramakers C, Donker DW, Nabar A, Rybin AV, Spatjens RL, van der Nagel T, Wodzig WK, Sipido KR, Antoons G, Moorman AF, Vos MA, Volders PG. Temporal patterns of electrical remodeling in canine ventricular hypertrophy: focus on IKs downregulation and blunted beta-adrenergic activation. *Cardiovasc Res*. 2006;72:90-100.
24. Xie Y, Sato D, Garfinkel A, Qu Z, Weiss JN. So little source, so much sink: requirements for afterdepolarizations to propagate in tissue. *Biophys J*. 2010;99:1408-1415.
25. Liu J and Laurita KR. The mechanism of pause-induced torsade de pointes in long QT syndrome. *J Cardiovasc Electrophysiol*. 2005;16:981-987.
26. Spach MS and Dolber PC. Relating extracellular potentials and their derivatives to anisotropic propagation at a microscopic level in human cardiac muscle. Evidence for electrical uncoupling of side-to-side fiber connections with increasing age. *Circ Res*. 1986;58:356-371.
27. de Bakker JM, van Capelle FJ, Janse MJ, Tasseron S, Vermeulen JT, de JN, Lahpor JR. Slow conduction in the infarcted human heart. 'Zigzag' course of activation. *Circulation*. 1993;88:915-926.
28. Vasquez C, Mohandas P, Louie KL, Benamer N, Bapat AC, Morley GE. Enhanced fibroblast-myocyte interactions in response to cardiac injury. *Circ Res*. 2010;107:1011-1020.
29. Miragoli M, Salvarani N, Rohr S. Myofibroblasts induce ectopic activity in cardiac tissue. *Circ Res*. 2007;101:755-758.
30. Miragoli M, Gaudesius G, Rohr S. Electrotonic modulation of cardiac impulse conduction by myofibroblasts. *Circ Res*. 2006;98:801-810.
31. Zlochiver S, Munoz V, Vikstrom KL, Taffet SM, Berenfeld O, Jalife J. Electrotonic myofibroblast-to-myocyte coupling increases propensity to reentrant arrhythmias in two-dimensional cardiac monolayers. *Biophys J*. 2008;95:4469-4480.
32. Askar SF, Bingen BO, Swildens J, Ypey DL, van der Laarse A, Atsma DE, Zeppenfeld K, Schalij MJ, de Vries AA, Pijnappels DA. Connexin43 silencing in myofibroblasts prevents arrhythmias in myocardial cultures: role of maximal diastolic potential. *Cardiovasc Res*. 2012;93:434-444.

33. Pedrotty DM, Klinger RY, Kirkton RD, Bursac N. Cardiac fibroblast paracrine factors alter impulse conduction and ion channel expression of neonatal rat cardiomyocytes. *Cardiovasc Res*. 2009;83:688-697.
34. Danik SB, Liu F, Zhang J, Suk HJ, Morley GE, Fishman GI, Gutstein DE. Modulation of cardiac gap junction expression and arrhythmic susceptibility. *Circ Res*. 2004;95:1035-1041.
35. Peters NS, Green CR, Poole-Wilson PA, Severs NJ. Reduced content of connexin43 gap junctions in ventricular myocardium from hypertrophied and ischemic human hearts. *Circulation*. 1993;88:864-875.
36. Furukawa T and Kurokawa J. Potassium channel remodeling in cardiac hypertrophy. *J Mol Cell Cardiol*. 2006;41:753-761.
37. Zitron E, Gunth M, Scherer D, Kiesecker C, Kulzer M, Bloehs R, Scholz EP, Thomas D, Weidenhammer C, Kathofer S, Bauer A, Katus HA, Karle CA. Kir2.x inward rectifier potassium channels are differentially regulated by adrenergic alpha1A receptors. *J Mol Cell Cardiol*. 2008;44:84-94.
38. Zhang TT, Takimoto K, Stewart AF, Zhu C, Levitan ES. Independent regulation of cardiac Kv4.3 potassium channel expression by angiotensin II and phenylephrine. *Circ Res*. 2001;88:476-482.
39. Hoppe UC, Marban E, Johns DC. Molecular dissection of cardiac repolarization by in vivo Kv4.3 gene transfer. *J Clin Invest*. 2000;105:1077-1084.
40. Pijnappels DA, Schalij MJ, van Tuyn J, Ypey DL, de Vries AA, van der Wall EE, van der Laarse A, Atsma DE. Progressive increase in conduction velocity across human mesenchymal stem cells is mediated by enhanced electrical coupling. *Cardiovasc Res*. 2006;72:282-291.

Chapter III

Prolongation of minimal action potential duration in sustained fibrillation decreases complexity by transient destabilization

Decreasing complexity of ventricular fibrillation

Brian O. Bingen, MD; Saïd F. A. Askar, MSc; Martin J. Schalij, MD, PhD; Ivan V. Kazbanov, Msc; Dirk L. Ypey, PhD; Alexander V. Panfilov, PhD; Daniël A. Pijnappels, PhD.

Cardiovasc Res 2013;97:161-170

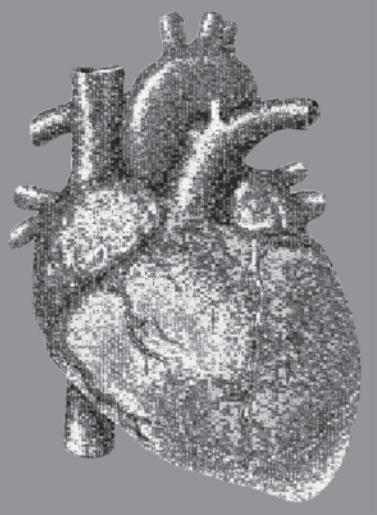

ABSTRACT:

Aims: Sustained ventricular fibrillation (VF) is maintained by multiple stable rotors. Destabilization of sustained VF could be beneficial by affecting VF complexity (defined by the number of rotors). However, underlying mechanisms affecting VF stability are poorly understood. Therefore this study aimed to correlate changes in arrhythmia complexity with changes in specific electrophysiological parameters, allowing to search for novel factors and underlying mechanisms affecting stability of sustained VF.

Methods & Results: Neonatal rat ventricular cardiomyocyte monolayers, and Langendorff-perfused adult rat hearts, were exposed to increasing dosages of the gap junctional uncoupler 2-aminoethoxydiphenyl borate (2-APB) to induce arrhythmias. Ion channel blockers/openers were added to study effects on VF stability. Electrophysiological parameters were assessed by optical-mapping and patch-clamp techniques.

Arrhythmia complexity in cardiomyocyte cultures increased with increasing dosages of 2-APB (n>38), leading to sustained VF: 0.0±0.1 phase singularities/cm^2 in controls vs. 0.0±0.1, 1.0±0.9, 3.3±3.2, 11.0±10.1 and 54.3±21.7 in 5,10,15,20 and 25µmol/L 2-APB, respectively. Arrhythmia complexity inversely correlated with wavelength. Lengthening of wavelength during fibrillation could only be induced by agents ($BaCl_2$/BayK8644) increasing APD at maximal activation frequencies (minimal APD); 123±32%/117±24% of control. Minimal APD prolongation led to transient VF destabilization, shown by critical wave front collision leading to rotor termination, followed by significant decreases in VF complexity and activation frequency (52%/37%). These key findings were reproduced *ex vivo* in rat hearts (n=6 per group).

Conclusions: These results show that stability of sustained fibrillation is regulated by minimal APD. Minimal APD prolongation leads to transient destabilization of fibrillation, ultimately decreasing VF complexity, thereby providing novel insights into anti-fibrillatory mechanisms.

INTRODUCTION

Ventricular fibrillation (VF) is the most common cause of sudden cardiac death.[1] Treatment of VF has vastly improved over the past years, mainly through progress in engineering strategies that resulted in defibrillating devices. However, while defibrillators can have a significant effect on survival, the majority of VF victims are not defibrillator candidates and at least 50% have VF as their first symptom of heart problems.[2] This is indicative of an unabated need to expand the current understanding of mechanisms underlying VF stability and termination.

One of the factors which can underpin the initiation of VF is gap junction remodeling. It is widely accepted that gap junctions are redistributed or down regulated following myocardial infarction, in cardiac hypertrophy and other causes of cardiomyopathy.[3] Such reorganization of gap junctions is associated with the onset of malignant ventricular tachyarrhythmias.[3-5]

After initiation, VF progresses through several distinct activation pattern phases, of which the hindmost are characterized by a reduction in the number of new rotor formations, reduced rotor meandering and increased spatiotemporal periodicity,[6-10] leading to a more organized and stable form of fibrillation. Affecting the stability of sustained VF may lead to a lower complexity of VF (estimated by the number of phase singularities per cm^2), but the underlying mechanisms are poorly understood. Traditionally, the fibrillatory aspect of conduction as well as arrhythmia complexity during fast VF is believed to be determined by conduction velocity (CV), action potential duration (APD), APD restitution slope and wavelength (the product of CV and APD).[11-13] However, considering the distinctive VF activation patterns, the importance of these factors could differ significantly during the different phases of VF. Furthermore, while data on the first phases after VF initiation are abundant,[11,14-16] data on sustained VF are scarce.[5] Therefore, a new *in vitro* and *ex vivo* model of sustained VF was developed that enabled to correlate a systematic and controllable increase in arrhythmia complexity with changes in specific electrophysiological parameters. Subsequent pharmacological modification of key parameters was used to search for novel factors affecting the stability of sustained VF and thereby unravel the underlying anti-fibrillatory mechanisms.

METHODS

All animal experiments were approved by the Animal Experiments Committee of the Leiden University Medical Center and conform to the Guide for the Care and Use of Laboratory Animals as stated by the US National Institutes of Health. A more detailed description can be found in the Supplemental Material.

Cell isolation and culture

Neonatal rat ventricular myocytes were isolated by collagenase digestion as described previously,[17] Animals were anaesthetized with 4–5% isoflurane inhalation anesthesia. Adequate anesthesia was assured by the absence of reflexes prior to rapid heart excision. Ventricles were minced and digested using collagenase (Worthington, Lakewood, NJ, USA) and DNAse (Sigma-Aldrich, St. Louis, MO, USA). After isolation, cells were plated out isotropically on fibronectin-coated, round glass coverslips (15 mm) at a cell density of 2-8x10^5 cells/well in 24-well plates (Corning Life Sciences, Amsterdam, the Netherlands). To prevent overgrowth of remaining cardiac fibroblasts, proliferation was inhibited by Mitomycin-C (Sigma-Aldrich, St. Louis, MO, USA) treatment at day 1, as described previously.[17] All cultures were refreshed daily with DMEM/HAM's F10 in a 1:1 mixture with 5% HS and cultured in a humidified incubator at 37° C and 5% CO_2.

Immunocytological analyses

Cultures were stained for Connexin40 (Sigma), Connexin43 (Santa Cruz Biotechnologies, Santa Cruz, CA, USA) and Connexin45 (Santa Cruz) to assess presence of gap junctional proteins, and for active caspase-3 (Abcam, Cambridge, MA, USA) to assess the number of apoptotic cells. Images of cultures were taken and quantified using dedicated software (ImageJ, National Institutes of Health, USA).

Optical mapping of myocardial cultures

At day 4 of culture, propagation of action potentials was investigated on a whole-culture scale by optical mapping using di-4-anepps (Sigma) as voltage sensitive dye, as described previously.[17] Cells were incubated with 2-APB in 5 different concentrations (5, 10, 15, 20 and 25 μM) for 20±2 minutes, targeting Connexin43, Connexin45 and Connexin40[18,19] to induce arrhythmias of increasing complexity, while vehicle-treated cultures were used as controls. Data analysis, construction of activation maps and stripe analysis (e.g. plotting of optical signal amplitude against time, at the maximal diameter of a culture or short and long axis of whole heart) were performed with specialized software (Brainvision Analyze 1101, Brainvision Inc, Tokyo, Japan) after pixel signals were averaged with 8 of its nearest neighbors, minimizing noise-artifacts. CV in cultures with uniform or reentrant activation patterns was calculated perpendicular to the activation wave front, between two 3 by 3 pixel grids typically spaced 2-8 mm apart. CV, activation frequency, minimal APD (during maximal paced activation frequency) and 1Hz APD were determined at 6 different locations equally distributed throughout the culture and averaged before further analysis. APD was determined at 80% of repolarization (APD_{80}) because of the rat action potential shape. Wavelength was calculated by the product of average CV and an APD_{80} (for uniform propagation) or reentrant cycle length[12]. Arrhythmia complexity was defined as the number of phase singularities per cm^2, determined

by using the phase space method[20] and correlated with CV, APD_{80} and wavelength in order to identify potential targets that can be modified to affect VF stability and thereby reduce VF complexity. As a result of the outcome of this correlation, appropriate drugs (3 µmol/L nitrendipine (Sigma), 1 mmol/L sotalol (Sigma), 0.5 mmol/L $BaCl_2$ (Merck, Darmstadt, Germany) or 1 µmol/L BayK8644 (Sigma)) were administered to 2-APB treated and control cultures to modify these targets and study the effects on arrhythmia complexity.

Assessment of arrhythmia complexity

Arrhythmia complexity in cardiomyocyte cultures was defined as the number of phase singularities per cm^2. To quantify the number of phase singularities the phase space approach was used.[20] Time series analyses using the empirical mode decomposition method and the Hilbert transform were used to determine the phase.[21] Data was smoothed by Gaussian filtering with a spatial size of 5 pixels (approx. 0.75 mm) and a temporal size of 5 frames (30 ms). Subsequently, a discrete Fourier transform was performed for each pixel over the full time series. By using the Fourier spectra the dominant frequency was determined. After that a band-pass filter was applied to each time series removing low and high frequencies. Next, the local extrema for the time series were found using a half of the inverse dominant frequency as the window size. Local maxima (and local minima) were interconnected by a piece-wise linear curve and their mean curve was subtracted from the corresponding time series. Then by using the Hilbert transform of the resulting time series the phase $\varphi_{ij}(t)$ for every pixel (i,j) at the moment of time t was determined as $\varphi_{ij}(t) = \mathrm{atan2}\,(\mathrm{I_{ij}(t)}\,,\,\mathrm{H}\,[\mathrm{I_{ij}(t)}])$

Where $I_{ij}(t)$ is the filtered and detrended intensity of the optical mapping signal for the pixel (i,j) at the moment t and $H[\cdot]$ denotes the Hilbert transform.

The topological charge of the area Ω is determined by

$$n(\Omega) = \frac{1}{2\pi} \oint_{\partial\Omega} \mathrm{grad}\,\varphi \mathrm{d}\boldsymbol{l}$$

where the integral is taken along the oriented boundary of Ω. For each pixel (i,j) we defined Ω_{ij} as a square around it with the side of 3 pixels. Thus the integral was approximated by the sum of 9 finite differences.

$$n(\Omega_{ij}) = \frac{1}{2\pi}\Big((\varphi_{i-1,j-1} - \varphi_{i-1,j}) + (\varphi_{i-1,j} - \varphi_{i-1,j+1}) + \cdots + (\varphi_{i,j-1} - \varphi_{i-1,j-1})\Big)$$

The overall algorithm was implemented in the OCaml programming language using the GTK+ toolkit for visualization.

Meandering of the phase singularities was defined as the maximal straight distance covered by the same phase singularity within 6 s of optical mapping.

Whole-c ell patch-clamp

Whole-cell measurements were performed in spontaneously active cultures plated out in a density of $4x10^5$ cells/well in 24 well plates as described previously.[17] At day 4 of culture, current-clamp experiments were performed in CMCs at 25°C using an L/M-PC patch-clamp amplifier (3 kHz filtering) (List-Medical, Darmstadt, Germany). To study the effects of 2-APB on electrophysiological properties of CMCs, 25 µM 2-APB (Tocris Bioscience, Bristol, United Kingdom) was incubated for 20 min prior to measurements.

Ex vivo experiments

For *ex vivo* experiments, female adult Wistar rats of 6±3 months were anesthetized through inhalation of 3-5% isoflurane and received 400 IE of heparin intraperitoneally. After confirmation of adequate anesthesia by absence of pain reflexes, beating hearts were rapidly excised and immediately submersed in cold Tyrode solution comprised of (in mM) NaCl 130, $CaCl_2$ 1.8, KCl 4.0, $MgCl_2$ 1.0, NaH_2PO_4 1.2, $NaHCO_3$ 24 and glucose 5.5 at pH 7.4. Subsequently, the aorta was canulated and retrogradely perfused with Tyrode that was freshly oxygenated with carbogen (95% O_2, 5% CO_2) and supplemented with 20mM of 2,3-butanedione monoxime (BDM) to reduce motion artifacts, at a constant flow of 15±2 ml/min at 37° C using a modified Langendorff apparatus (AD instruments, Spechbach, Germany). Hearts were stained with 2 µM di-4-anepps by a 10 ml bolus injection into the bubble trap. The optical mapping camera was positioned facing the ventral surface of the heart, viewing equal portions of the left and the right ventricle during mapping. All hearts exhibited spontaneous sinus rhythm during initial acclimatization. Arrhythmia complexity was defined as the as the number of separate wave fronts present at the epicardial surface of the heart. The targets that were shown to affect arrhythmia complexity *in vitro* were modified by administration of 0.5 mM $BaCl_2$ to the perfusate for 10 minutes prior to measurements to confirm their *ex vivo* effects on arrhythmia complexity.

Statistical analysis

Statistical analyses were performed using SPSS11.0 for Windows (SPSS, Inc., Chicago, IL, USA). Data were compared with one-way ANOVA test with Bonferroni post-hoc correction if appropriate and expressed as mean±SD. Comparison between two groups was performed using a student t-test. Before and after comparisons were performed with a paired t-test. Differences were considered statistically significant if $P<0.05$. Non-linear regression curves were constructed by using a robust exponential two phase decay

curve fit. Accuracy of these curves was expressed as the robust standard deviation of the residuals (RSDR).

RESULTS

Cell culture characterization and the effect of gap junctional uncoupling by 2-APB

Immunocytological analysis of cultures by collagen-I and α-actinin double-staining, suitable for distinction between fibroblasts and CMCs,[17] showed that cultures consisted of 17.6±3.1% fibroblasts (n=6) (Supplemental Figure 1A). Fibroblasts were homogeneously spread across the culture. In addition, cultures showed expression of Connexin43 and Connexin45 as well as heterogeneous expression of Connexin40 in between CMCs, which are the targets for 2-APB,[18,19] as judged by immunocytological staining (Supplemental Figure 1B, 1C and 1D).

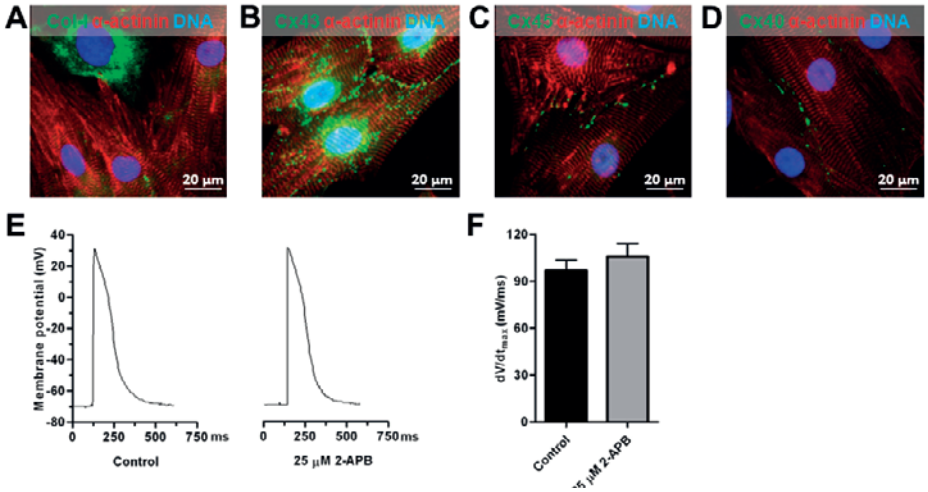

Supplemental Figure 1. *Cell culture characterization, gap junctional protein expression and modulation of gap junctional coupling. (A) Immunocytological double-staining of α-actinin (red) and collagen-I (green), (B) Connexin43 (green), (C) Connexin45 (green) and (D) Connexin40. (E) Typical examples of membrane potential traces in control cultures and cultures treated with 25 µmol/L 2-APB and (F) Assessment of dV/dTmax.*

2-APB causes stable multi-rotor tachyarrhythmias, resembling sustained VF, in a dose-dependent relation

During optical mapping, spontaneously active control cultures typically showed uniform and fast conduction (Figure 1A). However, after incubation with 2-APB, cultures showed a strong increase in the incidence of spontaneous reentrant tachyarrhythmias

(Figure 1A and 1B). Furthermore, we observed a significantincrease in the complexity of tachyarrhythmias, as judged by the number of phase singularities per cm^2 with increasing dosages of 2-APB (Figure 1A, 1C and Supplemental movie 1). As a consequence of the increasing incidence of reentry with increasing 2-APB dosages (activation is higher during reentrant activation when compared to spontaneous uniform activation), average activation frequency was significantly increased after incubation with increasing dosages of 2-APB (Figure 1D). CV was dose-dependently decreased by treatment with 2-APB (Figure 1E). The decrease in CV remained apparent even when determined only during reentrant activation (Figure 1E, hatched subsets). Despite the high complexity of the tachyarrhythmias observed, the arrhythmias showed a high degree of stability that resembled sustained VF. In more detail, after initiation of reentry by treatment with 2-APB cultures showed a minimal extent of rotor meandering, which further decreased significantly with increasing 2-APB dosages (Supplemental Figure 3B). In addition, a relatively low number of fibrillating cultures showed new rotor formations, while all cultures showed minimal dispersion in optical signal amplitude as well as reentrant cycle length (Supplemental Figure 3 C-E), exemplified by stripe analysis of optical mapping recordings (Figure 1F).

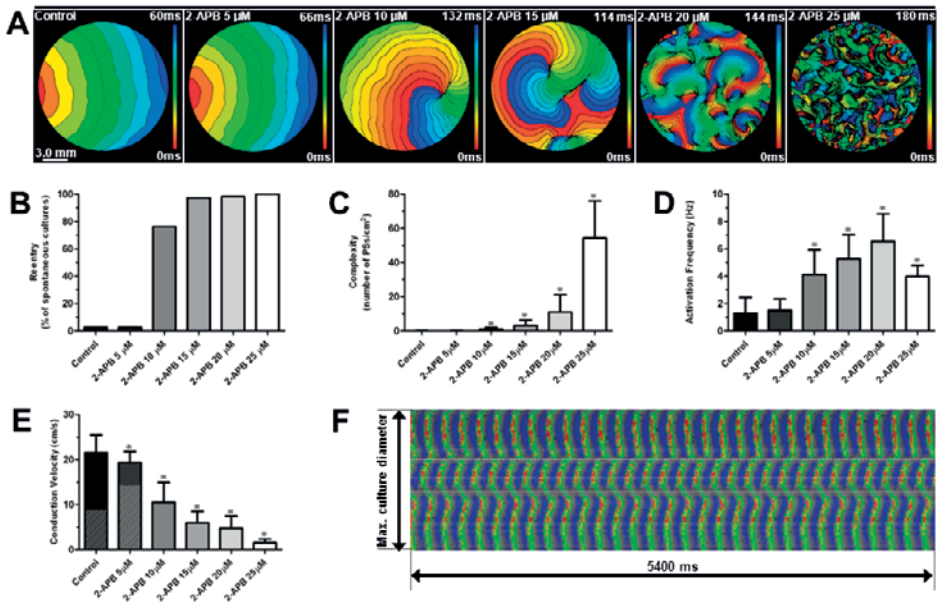

Figure 1. *(A) Activation maps (**6**ms isochronal spacing) of control cultures and 5-25µmol/L 2-APB treated cultures. (B) Quantification of reentry incidence, (C) complexity, (D) average activation frequency (both uniform and reentrant conduction included) and (E) CV in control cultures and 5-25µmol/L 2-APB treated cultures (n=38, n=38, n=39, n=39, n=61 and n=39 respectively). Hatched subsets indicate average CV during reentry in control and 5µmol/L 2-APB treated cultures (n=1 and 1). *: P<0.05 vs. control. (F) Typical line scan analysis across the diameter of a culture treated with 20µmol/L 2-APB (dotted line indicates rotor position).*

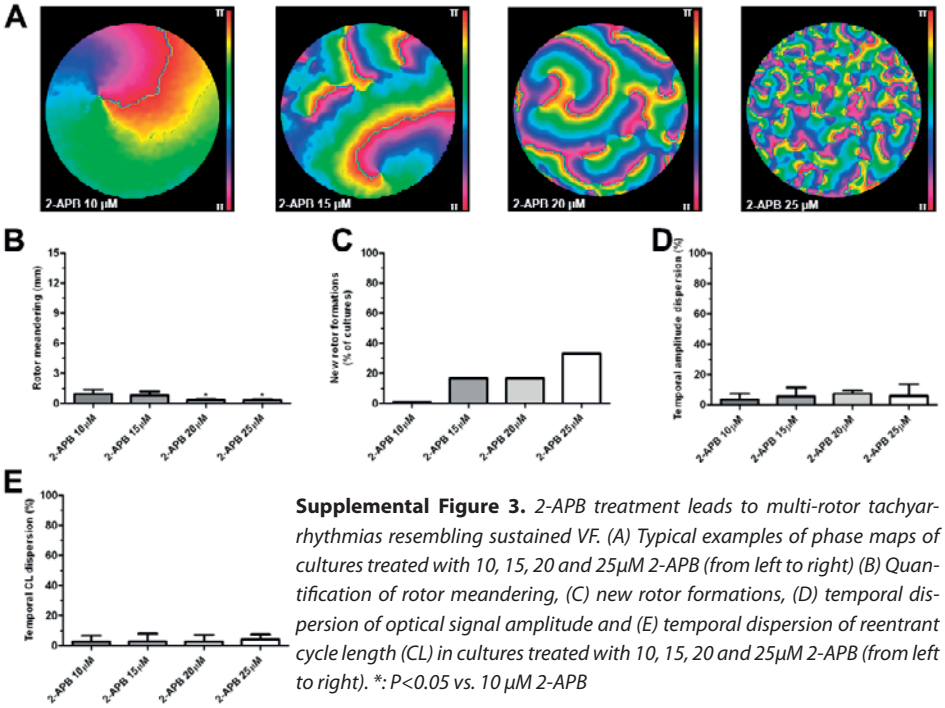

Supplemental Figure 3. *2-APB treatment leads to multi-rotor tachyarrhythmias resembling sustained VF. (A) Typical examples of phase maps of cultures treated with 10, 15, 20 and 25µM 2-APB (from left to right) (B) Quantification of rotor meandering, (C) new rotor formations, (D) temporal dispersion of optical signal amplitude and (E) temporal dispersion of reentrant cycle length (CL) in cultures treated with 10, 15, 20 and 25µM 2-APB (from left to right). *: P<0.05 vs. 10 µM 2-APB*

The effect of gap junctional uncoupling by 2-APB

Treatment by 2-APB did not significantly change the AP morphology (Figure 1E), and dV/dT_{max} (Supplemental Figure 1F). Apoptosis was not increased in 2-APB treated cultures as judged by the expression of active caspase-3 (*P*=ns vs. control) (Supplemental Figure 2). Together these results suggest that the gap junction uncoupling agent 2-APB does not negatively affect cell excitability and viability.

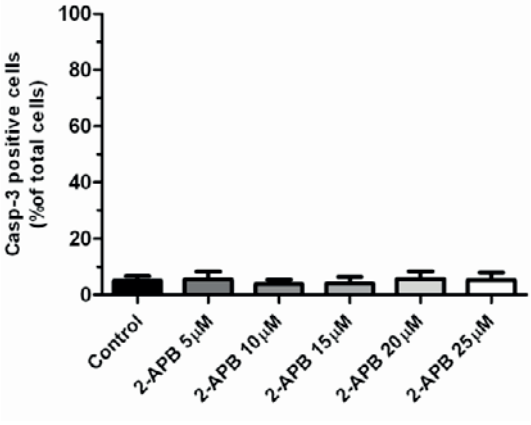

Supplemental Figure 2. *2-APB does not increase apoptosis in myocardial cultures. Quantification of apoptosis as judged by immunocytological staining of caspase-3 positive cells as a percentage of total cells (number of positive nuclei for Hoechst 33342 counterstaining).*

Arrhythmia complexity increase is strongly related to wavelength shortening

To identify factors associated with increased arrhythmia complexity, the relationship between several electrophysiological parameters and complexity were investigated at variable 2-APB concentrations. As increasing 2-APB concentrations dose-dependently increased complexity, while at the same time decreasing CV, expectedly CV showed a strong hyperbolic-like relationship with complexity (RSDR=1.9) (Figure 2A). Furthermore, APD_{80} showed a weak inverse correlation with complexity in the low complexity range (Figure 2B). However, as at the highest 2-APB concentration the beating frequency decreases (Figure 1D), APD increases in cultures treated with 25µmol/L 2-APB. This slightly decreased the negative correlation between APD and complexity, while greatly increasing variation in APD. As wavelength is the product of CV and APD, wavelength shortening strongly related to complexity increases (RSDR=0.4) (Figure 2C). Together, these results support that inversely, complexity may be strongly diminished by increasing wavelength.

Effects of pharmacological ion current modulators on 1Hz and minimal APD

To test whether arrhythmia complexity can be diminished by increasing wavelength, several ion channel modulators were selected, which according to their mechanism of action should have an effect on APD and wavelength. However, as fast activation, during fibrillation, can have an effect on activation and inactivation status of targeted ion channels,[22] the effect of the selected ion channel modulators might differ between fibrillation and normal uniform activation. Therefore, we assessed the effect of pharmacological ion channel modulation on APD at 1Hz electrical activation and at the minimal diastolic interval during 1-10Hz pacing (measuring minimal APD) in absence of reentrant circuits. As expected, nitrendipine, which inhibits I_{CaL}, significantly shortened the 1Hz APD by 28% (to 72±12%, $P<0.05$ vs. control) (Figure 3A and 3I), as well as minimal APD (to 84±14%, $P<0.05$ vs. control) (Figure 3E and 3J). Treatment with sotalol and $BaCl_2$ slowed repolarization and thus prolonged 1Hz APD (to 117±12% $P<0.05$ and 162±25% $P<0.05$ vs. control, respectively) (Figure 3B, 3C and 3I). However, the effect of sotalol on minimal APD was not significant, (Figure 3F and 3J), while $BaCl_2$ still had a significantly prolonging effect on APD during 10Hz pacing (to 145±9%, $P<0.05$ vs. control) (Figure 3G and 3J). Additionally, activation of I_{CaL} by Bayk8644 increased both 1Hz (to 168±13% $P<0.05$ vs. control) (Figure 3D and 3I) and minimal APD (to 133.7±9.6% $P<0.05$ vs. control) (Figure 3H and 3J) significantly.

In line with the previous, electrically stimulated experiments, APD_{80} was significantly decreased by nitrendipine throughout all 2-APB dosages, while APD was increased by both $BaCl_2$ and BayK8644. In contrast, sotalol did not affect APD significantly (Figure 4A, supplemental table 1). Wavelength was decreased significantly by nitrendipine treatment in the lowest concentration of 2-APB, although there was no significant effect in

the other 2-APB dosages. In contrast, wavelength was significantly increased after $BaCl_2$ and BayK8644 treatment while sotalol did not significantly affect wavelength (Figure 4B, Supplemental Table 2). Interestingly, decreasing the APD with nitrendipine increased activation frequency of tachyarrhythmias. Conversely, lengthening of APD decreased activation frequency as seen after treatment with $BaCl_2$ and BayK8644 throughout all 2-APB dosages (Figure 4C, Supplemental Table 3). Sotalol induced a small but significant decrease in activation frequency in 15 and 20µmol/L 2-APB treated cultures only.

The average complexity of conduction did not significantly alter after nitrendipine, while sotalol only had a small but significant effect on complexity in 25µmol/L 2-APB treated cultures. However, in $BaCl_2$ and BayK8644 treated cultures arrhythmia complexity was significantly lowered throughout all 2-APB concentrations except for the less complex arrhythmias after 10µmol/L 2-APB (Figure 4D, Supplemental Table 4). These results are indicative of the importance of minimal APD in decreasing and increasing complexity, through specific ion channel modulation.

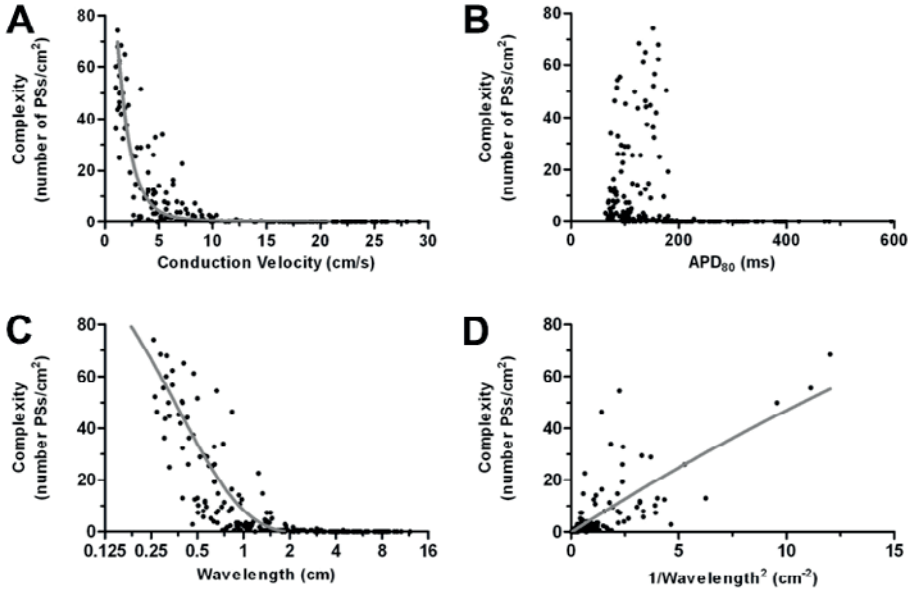

Figure 2. *Relationship between (A) CV and complexity, (B) APD_{80} and complexity, (C) wavelength and complexity (D) 1/[wavelength]^2 and complexity in control and 2-APB treated cultures (5-25µmol/L).*

Mechanism of decrease in arrhythmia complexity by increase in minimal APD

Optical mapping through a permeable membrane during minimal APD prolongation by BayK8644 and $BaCl_2$ again showed that both substances decrease the number of rotors *in vitro* (Figure 5A). Prior to the addition of $BaCl_2$ or BayK8644, optical signal amplitude, spatial rotor distribution and rotor cycle lengths were highly stable (Figure 5B, D left).

During incubation of $BaCl_2$ or BayK8644 transient instability in optical signal amplitude, spatial rotor distribution and rotor cycle length was induced (Figure 5B, D middle and Supplemental Figure 4A,B). Subsequently, a new equilibrium was formed, with increased optical signal amplitude, decreased number of rotors and stable but increased rotor cycle lengths (Figure 5B, D right and Supplemental Figure 4A,B). During incubation of $BaCl_2$ and BayK8644 this transient instability, which was mediated by an increase in wavelength, led to termination of neighboring rotors. Rotor termination resulted from critical collisions of wave fronts propagated from 2 different rotors, after which activation of that particular tissue is taken over by a separate pre-existing rotor, decreasing the total number of rotors (Figure 5C, 5D).

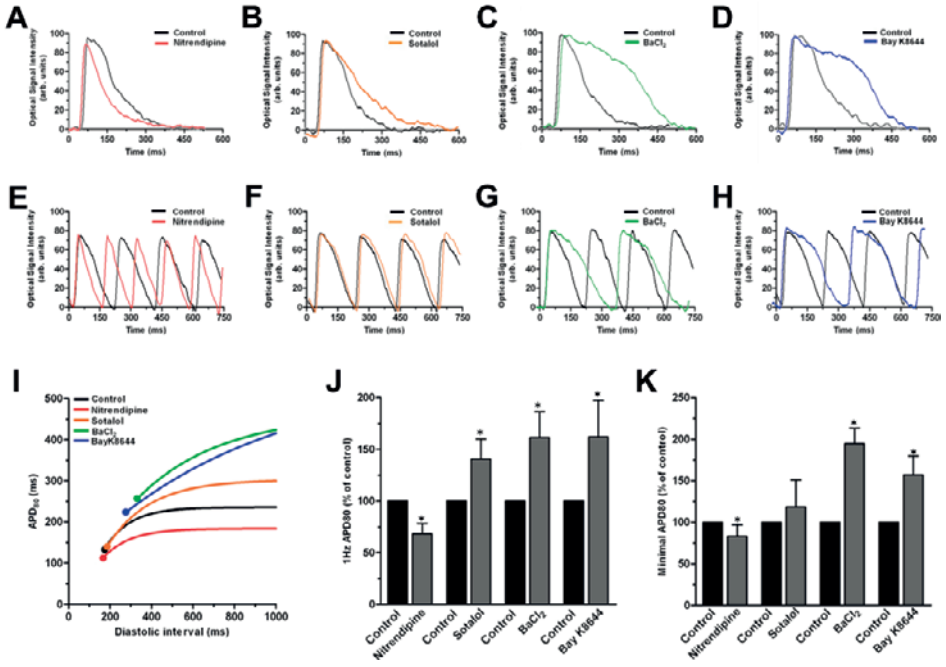

Figure 3. *Typical optical action potential records in control (black) and (A) nitrendipine (red), (B) sotalol (orange), (C) $BaCl_2$ (green) and (D) BayK8644 (blue) treated cultures illustrating treatment effects on 1Hz APD and minimal APD (E-H) and (I) APD restitution. Colored circles indicate the average minimal APD. Quantification of (J) 1Hz APD and (K) minimal APD before and after treatments. *: P<0.05 vs. control.*

2-APB in adult rat heart ventricles

To investigate the functional implications of *in vitro* findings on the intact heart, Langendorff-perfused adult rat hearts were subjected to *ex vivo* optical mapping. Baseline activation frequency before addition of BDM to the oxygenated Tyrode perfusate was 4.50±0.5Hz. After addition of BDM sinus rhythm remained stable for at least 1 hour at an average activation frequency of 2.5±0.4Hz (Supplemental Figure 5A and 5B). Perfu-

sion with oxygenated Tyrode supplemented with 5µmol/L 2-APB for 20 minutes slowed conduction from 54.1±3.2cm/s to 27.8±2.7cm/s (n=6, *P*<0.05).

No arrhythmias developed at this dosage and sinus rhythm was maintained at 2.5±0.5Hz (Supplemental Figure 5A-C, *P*>0.05 vs. control). Perfusion of hearts with 10 µmol/L 2-APB caused VT in all hearts (2.2±0.2 wave fronts at 5.4±3.3Hz, n=6), whereas complexity of arrhythmias increased to fibrillation with 20µmol/L 2-APB (5.0±1.1 wave fronts at 11.0±0.9Hz, n=6) (Supplemental Figure 5A and 5C). Complexity of arrhythmias stabilized within 10 minutes of incubation with 2-APB.

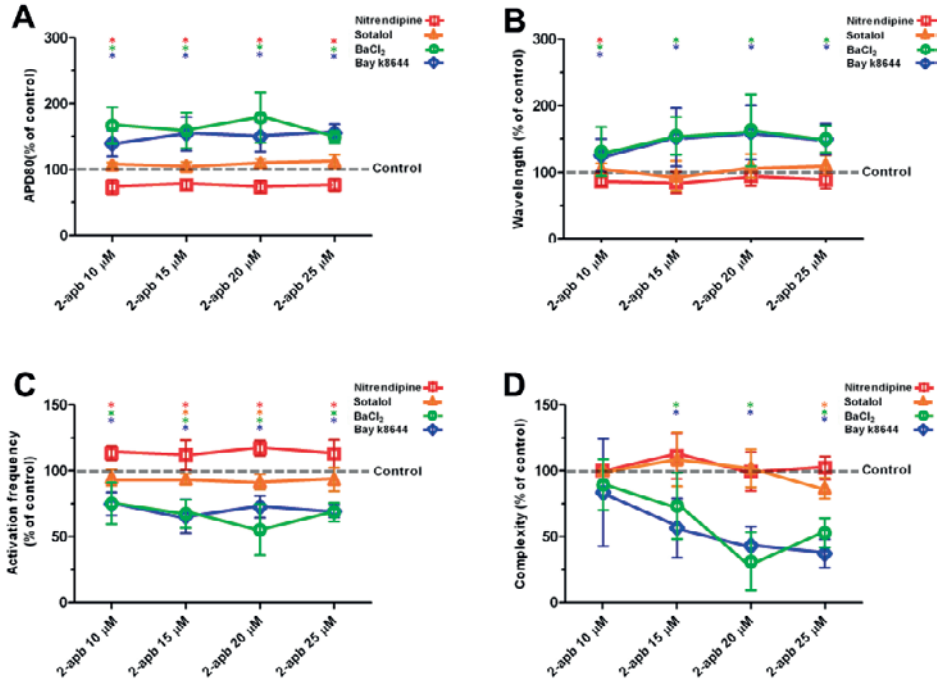

Figure 4. *(A) Quantification of APD, (B) wavelength, (C) activation frequency and (D) complexity after treatment with sotalol (orange), nitrendipine (red), $BaCl_2$ (green) and BayK8644 (blue). Dotted black lines indicate controls (prior to treatment set at 100%). *: P<0.05 vs. control.*

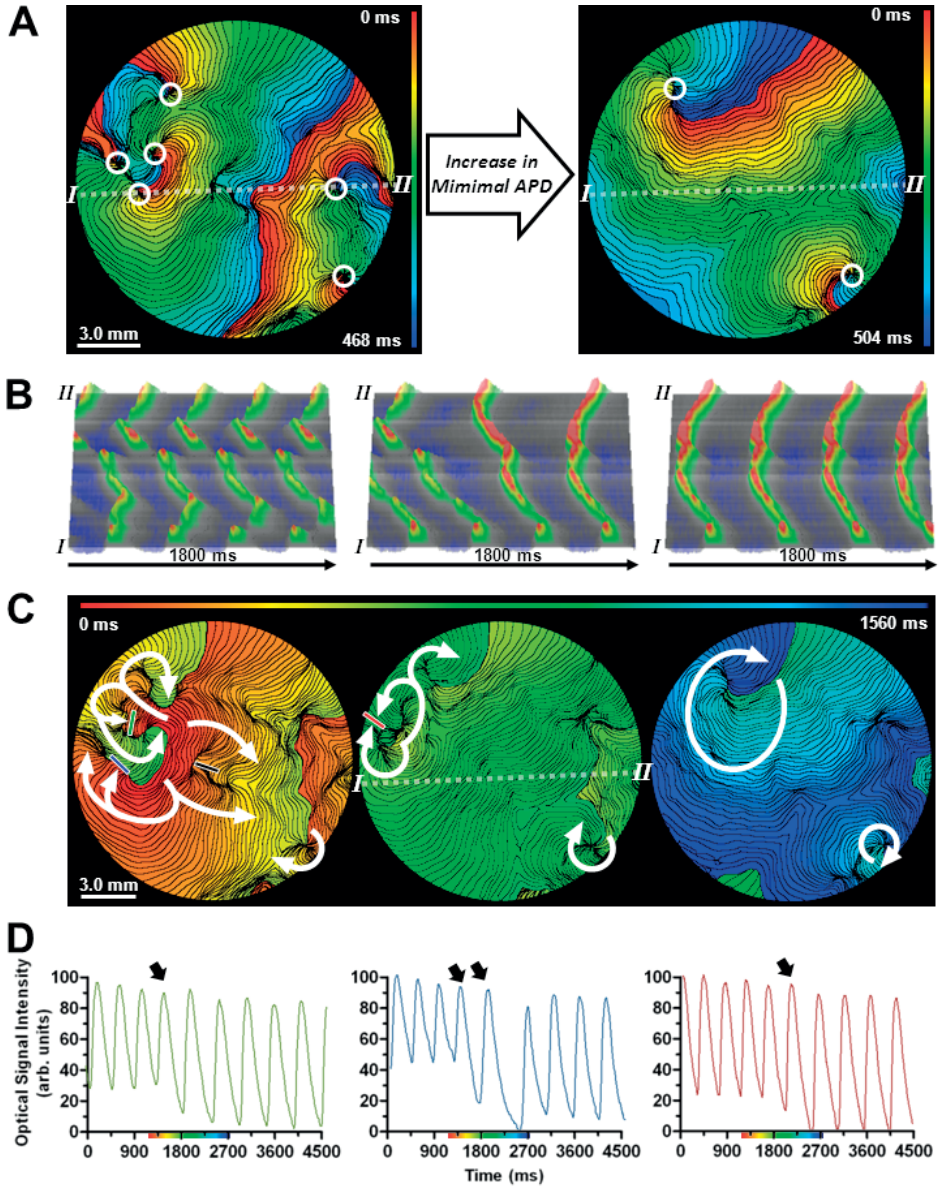

Figure 5. *(A) Activation maps of a culture treated with 20μM 2-APB, before (left) and after (right) minimal APD prolongation. White circles indicate rotor position. (B) Examples of 3 consecutive 3D (rotated 15º) line scan analyses, during 1800 s, from point I to point II in culture shown in A, before (left), during (center) and after (right) minimal APD prolongation. (C) Consecutive activation maps during rotor termination by prolongation. The green, blue, black and red bars indicate the area of critical wave front collision. (D) Optical action potentials at the areas of critical wave front collision of corresponding colors shown in C. Black arrows mark the moment of critical wave front collision.*

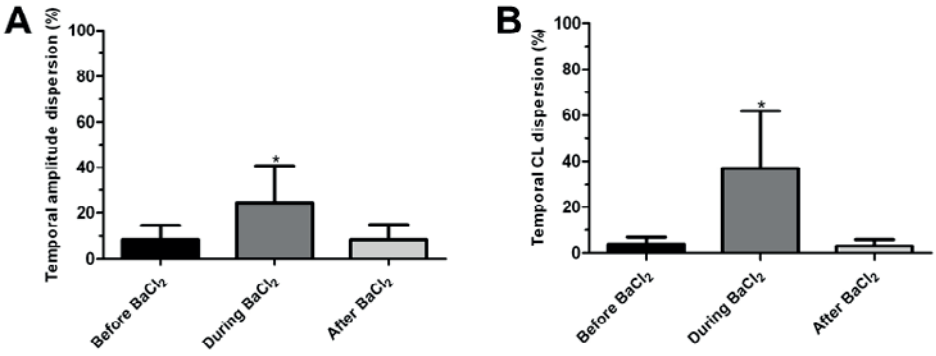

Supplemental Figure 4. *Increasing minimal APD by $BaCl_2$ causes transient instability in optical signal amplitude and rotor cycle length. (A) Quantification of temporal dispersion of optical signal amplitude and (B) temporal dispersion of rotor cycle length, prior to, during and after increasing minimal APD by the incubation with $BaCl_2$. *:P<0.05 vs. before $BaCl_2$.*

Minimal APD determines arrhythmia complexity in adult rat heart ventricles

To investigate whether $BaCl_2$ lowered arrhythmia complexity ex vivo as in vitro, rat hearts were first perfused with 20mmol/L 2-APB until fibrillation was present and stable for at least 5 min. Then, 500 mmol/L of $BaCl_2$ was added to the perfusate consisting of tyrode with 20mmol/L 2-APB. Typically within 5 min, $BaCl_2$ decreased arrhythmia complexity by 71.4% compared with controls (Figure 6A, C, and D, n = 6). Also, activation frequency decreased from 9.98+0.9 to 2.8+0.3 Hz by $BaCl_2$ (Figure 6A and C). Importantly, $BaCl_2$ treatment significantly increased minimal APD80 to 265.4+35.1% of control hearts (Figure 6B, n = 6). Together these results show that, similar to in vitro experiments, arrhythmia complexity can be decreased by increasing minimal APD ex vivo.

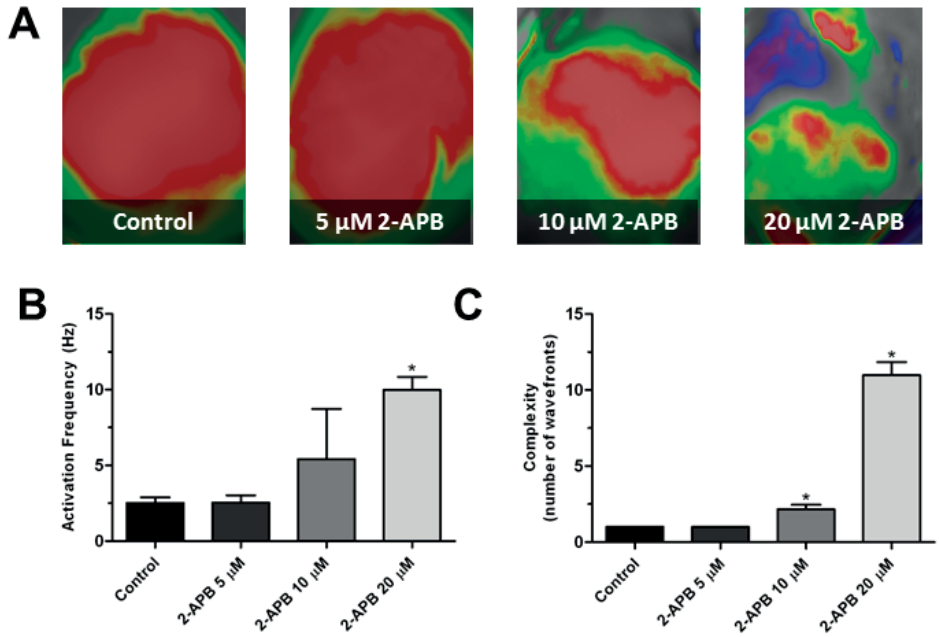

Supplemental Figure 5. *A 2-APB dose-dependent increase in arrhythmia complexity in adult Wistar rat hearts leading to sustained VF. (A) Typical snapshots of ventricular activation during optical mapping of Langendorff-perfused adult rat heart perfused with (from left to right) normal Tyrode solution and tyrode solution supplemented with 5, 10 and 20 µM 2-APB. (B) Quantification of average activation frequency and (C) complexity in control hearts, and hearts treated with 2-APB. *: P<0.05 vs control*

DISCUSSION

The key findings of this study are (1) incubation with 2-APB induces reentrant tachyarrhythmias in myocardial cultures and adult rat hearts, which are maintained by multiple stable and co-existing rotors, resembling sustained VF. (2) The complexity of these arrhythmias increases exponentially with increasing dosages of 2-APB, allowing a systematic study of arrhythmia complexity *in vitro* and *ex vivo*. (3) Increasing arrhythmia complexity during fibrillation is associated with a shortening of the average wavelength and APD. (4) Hence, complexity and activation frequency during fibrillation could be decreased pharmacologically by transient destabilization of sustained VF through prolongation of minimal APD *in vitro* and *ex vivo*, regardless of ionic mechanism.

The importance of wavelength in reentrant tachyarrhythmias

Since the introduction of the circus movement reentry theory[23] and the leading circle concept,[24] it has been established that if the wavelength of a given reentrant circuit exceeds the path-length, reentry cannot be sustained as a consequence of a vanishing

excitable gap. Hence, wavelength prolongation has traditionally been viewed as an important anti-arrhythmic strategy.[12,13] Elaborating on this theory, we now demonstrated that wavelength prolongation affects co-existence of multiple neighboring rotors, although rotor termination by prolongation of wavelength in single rotor tachyarrhythmias appeared to be more complicated (Figure 4D; 10µmol/L 2-APB). The slope in the relationship between wavelength and complexity is steepest in the low complexity range (<2 rotors) (Figure 2D). This implies that in the lower complexity range a greater wavelength prolongation is necessary to facilitate the same decrease in complexity. Also, the absence of boundaries formed by neighboring rotors diminishes the chance of rotor termination in the lower complexity range. Moreover, we show that the effect of a given agent on arrhythmia complexity depends on the activity of the agent at high frequency activation, which can differ from its effect at low frequencies. Sotalol, for instance had a significant effect on 1Hz APD, but not on minimal APD , which may explain the inability of sotalol to terminate rotors during VF. In contrast, increasing minimal APD by $BaCl_2$ and BayK8644, induced a notable reduction in the number of rotors during VF. However,

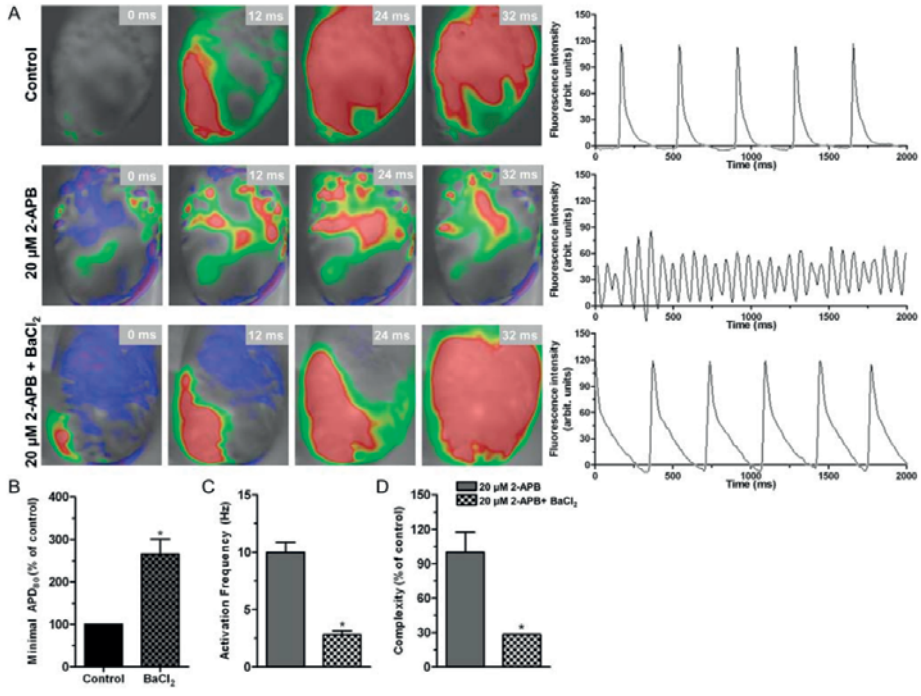

Figure 6. *(A) Typical sequence (12ms between snapshots) of activation in (from top to bottom) Langendorff-perfused control hearts, 20µM 2-APB treated hearts, and 20µM 2-APB treated hearts after introduction of $BaCl_2$ with corresponding optical action potential signals. (B) Quantification of minimal APD in control hearts and hearts perfused with 500µmol/L $BaCl_2$. (C) Assessment of activation frequency and (D) complexity in hearts treated with 20µM 2-APB before and after introduction of $BaCl_2$. *: P<0.05 vs. control.*

decreasing minimal APD by nitrendipine treatment did not increase average arrhythmia complexity. This can be explained by the minute tendency for the formation of new wave breaks during sustained VF, despite an increase in effective size of the culture.

Importantly, in earlier *in silico* work by Ten Tusscher *et al*., minimal APD was shown to be predictive of arrhythmia complexity in animal and human hearts.[25,26] We now showed that minimal APD is not only predictive of arrhythmia complexity, but that prolongation of minimal APD also strongly and effectively reduced arrhythmia complexity.

APD and CV restitution in fibrillation

Other theories involving prevention or termination of VF mostly originate from the 'multiple wavelet' and the 'mother rotor' theory.[16,27] In general, both assume

flattening of APD restitution or narrowing of CV restitution should prevent wave breaks and consequent disorganization of conduction, which should result in termination of VF.[16,27] Indeed, several studies confirmed that flattening of APD restitution by for instance verapamil or bretylium can convert VF to VT.[10,11,14,28]

However, the anti-fibrillatory effects of aforementioned substances are generally confirmed by mapping or *in silico* models during or resembling the first minute after VF induction. Yet, Wiggers *et al*. showed that the heart goes through several stages during VF,[9] by which organization and periodicity increase after the first 2 min.[6-8,10] Hence, therapies aiming to decrease disorganization of conduction could prove to be effective only in this first phases of fibrillation. The findings in the present study partially explain Wiggers' stages III and IV of fibrillation because as ischemia progresses, gap junctional coupling is reduced which may slow VF into a

stable, organized and periodical multi-rotor arrhythmia. Our data on these typical characteristics of sustained VF are consistent with a previous report of sustained (slow) VF in an isolated rabbit heart model of VF.[10] Furthermore, we showed that during these phases of VF, interventions that flatten APD or CV restitution in an attempt to terminate VF may be considered inadequate. This is best exemplified by the effect of the I_{CaL} inhibitor nitrendipine on VF after 2-APB treatment, which according to earlier studies should have flattened APD restitution and terminated VF. However, nitrendipine only caused detrimental effects: increasing activation frequency without affecting complexity. Interestingly, activation of I_{CaL}, by BayK8644 treatment, did decrease complexity during VF, exemplifying the reversal of effects of I_{CaL} targeting in the early phases through the later phases of VF.

IK1 blockade and VF termination

Another approach to revert sustained VF to VT or sinus rhythm could be to destabilize the rotors maintaining VF in an effort to achieve termination of these rotors by collision with a preexisting boundary.[15,29] In several studies rotor stability was demonstrated to

depend on specific ion channel currents, such as I_{K1}.[14,15,29-31] We showed that blockade of I_{K1} during VF decreased rotor frequency and the complexity of conduction, ultimately reverting VF back to VT.[32] However, rotor stability during VF did not seem to be specifically dependent on the I_{K1} current but on the effect blockade of I_{K1} had on the minimal APD. Therefore, the decrease in complexity could be reproduced with Bayk8644, a substance that increases minimal APD by augmenting I_{CaL}, without affecting I_{K1}.[33] By altering the stability of these rotors, collision of rotors with preexisting boundaries, but also novel critical boundaries formed by wave fronts propagated from adjacent rotors are enforced, significantly reducing the complexity of activation patterns during fibrillation.

Patients suffering from sustained VF are still in a timeframe to be resuscitated without cerebral damage.[34] Therefore, the observation that an increase in minimal APD decreases complexity of sustained VF may have important consequences for the treatment of VF, since VF, when driven by a smaller number of rotors, requires less energy for defibrillation.[35]

Study limitations

In our study, 2-APB treatment was used to induce arrhythmias. This agent is known to block gap junctional communication, but also the IP3 receptor and TRP channels, while causing activation of voltage- independent calcium channels.[18,19,36] Of these effects, gap junctional uncoupling has been shown to be related to arrhythmia induction in CMC cultures as a consequence of wave breaks caused by preexistent heterogeneity in gap junctional coupling.[2,37,38] In addition, voltage-independent calcium influx may also cause pro-arrhythmic features in 2-APB treated hearts.[36] As such, the clinical significance of these mechanisms of VF initiation may be very limited. However, as VF can show the same maintenance properties, regardless of the method of initiation[39], this does not hinder the study of VF maintenance and termination as was performed in the present study.

In the *ex vivo* mapping experiments, complexity was determined by the number of epicardial wave fronts, instead of the number of rotors. However, in line with previous research we found that during sustained VF, the number of epicardial rotors is minimal, attenuating the significance of the epicardial number of rotors.[10]

Moreover, this study makes use of a neonatal rat cardiomyocyte culture model as well as adult rat hearts. Rat hearts differ considerably from human hearts in terms of the ion currents determining the action potential morphology. Hence, the conclusions drawn from this study are only conceptual in relation to the mechanisms of ventricular fibrillation maintenance and cannot be readily extrapolated to the human or clinical setting.

Conclusions

Incubation of neonatal rat myocardial cultures or Langendorff-perfused adult rat hearts with increasing dosage of 2-APB allows for the systematic study of arrhythmia complex-

ity, ultimately resembling sustained VF. Arrhythmia complexity and activation frequency during fibrillation can be decreased pharmacologically by transient VF destabilization through prolongation of minimal APD *in vitro* and *ex vivo*, regardless of ionic mechanism. Accordingly, this study could provide a novel conceptual framework for future anti-arrhythmic drug design as well as an extension in the rationale for treatment options of sustained VF.

FUNDING

This work was supported by the Netherlands Organisation for Scientific Research (NWO; VENI grant [91611070 to D.A.P], the Dutch Heart Foundation [2008/B119], the Fund for Scientific Research Flanders (FWO grant [G084811N to I.V.K. and A.V.P.]) and Institut des Hautes Etudes Scientifiques, Bures-sur-Yvette, France, and to the James Simons Foundation [I.V.K.].

ACKNOWLEDGEMENTS

We wish to thank Wilbert P.M van Meerwijk, PhD for helpful discussions, Adriana C. Gittenberger-de Groot, PhD for helpful comments on the manuscript, and Huybert J.F. van der Stadt and Gerry T.M. Wagenaar, PhD for excellent technical and scientific support.

CONFLICT OF INTEREST

None declared.

SUPPLEMENTAL MATERIAL

METHODS

All animal experiments were approved by the Animal Experiments Committee of the Leiden University Medical Center and conform to the Guide for the Care and Use of Laboratory Animals as stated by the US National Institutes of Health.

Cell isolation and culture

Neonatal rat ventricular myocytes were isolated by collagenase digestion as described previously.[17] Briefly, animals were anaesthetized with 4–5% isoflurane inhalation anesthesia.

Adequate anesthesia was assured by the absence of reflexes prior to rapid heart excision.

After animal sacrifice by rapid heart excision, ventricles were minced and digested using collagenase (Worthington, Lakewood, NJ, USA) and DNAse (Sigma-Aldrich, St. Louis, MO, USA). Cell suspensions from a 50 minutes and a subsequent 45 minutes dissociation were pooled, centrifuged and resuspended in HAM's F10 medium supplemented with 10% fetal bovine serum and 10% horse serum (HS) (Invitrogen, Carlsbad, CA, USA). Cells were preplated on Primaria coated culture dishes (BD Biosciences, Franklin Lakes, NJ, USA) to allow preferential attachment of cardiac fibroblasts. Subsequently, cell aggregates and debris were removed by filtering non-adherent cells through a 70 μM cell strainer. Following isolation myocardial cells were plated out on fibronectin-coated, round glass coverslips (15 mm) at a cell density of 2-8x10^5 cells/well in 24-well plates (Corning Life Sciences, Amsterdam, the Netherlands) depending on the experiment. To prevent overgrowth of remaining cardiac fibroblasts, proliferation was inhibited by Mitomycin-C (Sigma) treatment at day 1, as described previously.[17] All cultures were refreshed daily with DMEM/HAM's F10 in a 1:1 mixture with 5% HS and cultured in a humidified incubator at 37° C and 5% CO_2.

Immunocytological analyses

Cultures were stained for Connexin40 (Santa Cruz Biotechnologies, Santa Cruz, CA, USA) connexin43 (Sigma), and connexin45 (Santa Cruz) to assess presence of gap junctional proteins, and for active caspase-3 (Abcam, Cambridge, MA, USA) to assess the number of apoptotic cells. For this purpose, cells were fixated in 1% paraformaldehyde in PBS and permeabilized with 0.1% Triton X-100 in PBS. Primary antibodies and corresponding secondary Alexa fluor-conjugated antibodies (Invitrogen) were used at a 1:200 dilution. Counterstaining of nuclei was performed with Hoechst 33342 (Invitrogen). Images of

cultures were taken and quantified using dedicated software (ImageJ, National Institutes of Health, USA).

Whole-cell patch-clamp

Whole-cell measurements were performed in spontaneously active cultures plated out in a density of $4x10^5$ cells/well in 24 well plates. At day 4 of culture, current-clamp experiments were performed in CMCs at 25° C using an L/M-PC patch-clamp amplifier (3 kHz filtering) (List-Medical, Darmstadt, Germany). The pipette solution contained (in mmol/L) 10 Na_2ATP, 115 KCl, 1 $MgCl_2$, 5 EGTA, 10 HEPES/KOH (pH 7.4). To study the effects of gap junctional uncoupling by 2-APB on electrophysiological properties of CMCs, 25 µM 2-APB (Tocris Bioscience, Bristol, United Kingdom) was incubated for 20 minutes prior to measurements.[17,40]

Tip and seal resistance were 2.0-2.5 MΩ and >1 GΩ, respectively. The bath solution contained (in mmol/L) 137 NaCl, 4 KCl, 1.8 $CaCl_2$, 1 $MgCl_2$, and 10 HEPES (pH 7.4). For data acquisition and analysis, pClamp/Clampex8 software (Axon Instruments, Molecular Devices, Sunnyvale, CA, USA) was used.

Optical mapping

At day 4 of culture, propagation of action potentials was investigated on a whole-culture scale by optical mapping using di-4-anepps as voltage sensitive dye, as described previously.[17] Structurally inhomogeneous cultures, as judged by light microscopy and mapping, were excluded for reasons of reproducibility and standardization (90 out of every 100 cultures were included). CMC cultures were plated out in 24-well plates (Corning) at a cell density of $8x10^5$ cells per well. Cultures underwent daily refreshing of culture medium and >2 hours prior to mapping, after which cultures were incubated with serum-free DMEM and colorless HAM's F10 in a 1:1 mixture (mapping medium), with 8 µmol/L di-4-anepps (Sigma) for 15±5 minutes at 37° C in a humidified incubator. Subsequently, cultures were refreshed with mapping medium. Cells were incubated with 2-APB dissolved in DMSO in 5 different concentrations (5, 10, 15, 20 and 25 µM) for 20±2 min in mapping medium, targeting Connexin43, Connexin45 and Connexin40 to induce gap junctional uncoupling,[18,19] while vehicle treated cultures were used as controls. Next, electrical propagation patterns were recorded by optical mapping at 37° C. Mapping experiments typically did not exceed 20 minutes per 24-wells plate. Also, cultures were not exposed to excitation light for longer than 40 s to limit possible phototoxic effects. Excitation light (e_{ex}=525±25 nm) was delivered by a halogen arc-lamp (MHAB-150W, Moritex Corporation, San Jose, CA, USA) through epi-illumination. Fluorescent emission light passed through a dichroic mirror and a long-pass emission filter (>590 nm) and was focused onto a 100x100 pixels CMOS camera (Ultima-L, SciMedia, Costa Mesa, CA, USA) by a 1.6x converging lens (Leice, Wetzlar, Germany). This resulted

in a spatial resolution of 160 µm/pixel and a field of view of 16 by 16 mm. Spontaneous or stimulated electrical activity was recorded for 6-24 s at 6 ms exposure time per frame. Data analysis, construction of activation maps and stripe analysis (e.g. plotting of optical signal amplitude against time, at the maximal diameter of a culture or short and long axis of whole heart) were performed with specialized software (Brainvision Analyze 1101, Brainvision Inc, Tokyo, Japan) after pixel signals were averaged with 8 of its nearest neighbors, minimizing noise-artifacts. Conduction velocity (CV), action potential duration until 80% repolarization (APD_{80}) and activation frequency were determined at six different locations equally distributed throughout the culture and averaged before further analysis. Wavelength was calculated by the product of average CV and APD_{80} (for uniform propagation) or reentrant cycle length.[12] Temporal dispersion of optical signal amplitude was defined as the difference between the minimal and the maximal optical signal amplitude (in arbitrary units) within 6 s of mapping, expressed as a percentage of the minimal optical signal amplitude. Temporal dispersion of reentrant cycle length was defined as the difference between the minimal and the maximal reentrant cycle length (in ms) within 6 s of mapping, expressed as a percentage of the minimal reentrant cycle length.

Assessment and modification of 1 Hz and minimal APD

As a result of the outcome of correlating changes in APD and wavelength with arrhythmia complexity, the effect of several ion channel modulators on APD was tested during low and high-frequency activation. This was necessary to study the effect of ion channel activation and inactivation dynamics during normal versus rapid activation on the outcome of pharmacological ion channel modulation on APD. For this purpose, we used a custom-made epoxy-coated platinum electrode and performed supra-threshold, 10 ms duration, square, unipolar stimulation using an electrical stimulus module with corresponding software (Multichannel Systems, Reutlingen, Germany). Using this electrode, cultures were paced at 1-10 Hz with 1 Hz increments. Minimal APD was defined as the APD_{80} determined at the pacing frequency (1-10 Hz) resulting in the shortest possible diastolic interval for that specific culture. Ion channel modulation was performed by administering specific ion channel modulators (which according to their mechanism of action should have an effect on APD) directly into the mapping medium and dispersing them by gentle agitation. To reduce the Ca^{2+} influx, L-type Ca^{2+} inward current (I_{CaL}) was inhibited by administration of nitrendipine (3 µmol/L) (Sigma) to reduce APD. Sotalol (1mM) (Sigma), 0.5mM $BaCl_2$ (Merck, Darmstadt, Germany), inhibiting the inward rectifier the current and BayK8644 (1 µmol/L) (Sigma) increasing the I_{CaL}, were used to increase APD. Cultures were optically mapped prior to and after 10s incubation with these pharmacological agents.

During *ex vivo* experiments in adult rat hearts, APD_{80} was measured during 3 s of pacing with a unipolar platinum electrode at 1-10 Hz, to determine minimal APD. To assess the effect of $BaCl_2$ on minimal APD *ex vivo*, 500 µmol/L $BaCl_2$ was added to the perfusate for 5 minutes prior to determination of minimal APD.

Pharmacological interventions during VF

To investigate the effects of APD modifications on VF characteristics, the above mentioned pharmacological agents were also administered to 2-APB treated and control cultures. Cultures were optically mapped before and after 10 s of incubation.

In experiments involving agents that reduced VF complexity, optical signals were recorded through a transparent, permeable membrane (0.4 µm pore size) (Corning) placed in the solution above the culture that allowed for a slow and even distribution of the agents. Using this method the actual process of complexity reduction could be visualized and its underlying mechanisms could be analyzed.

During *ex vivo* experiments, after initiation of VF by 10 minutes perfusion of 20 µmol/L 2-APB, 500 µmol/L $BaCl_2$ was added to the perfusate for 10 minutes prior to measurements to study its effects on arrhythmia complexity. Importantly, the perfusate contained 2-APB prior to and during $BaCl_2$ perfusion to prevent washout of 2-APB.

SUPPLEMENTAL RESULTS

2-APB dosage	APD_{80} (% of control); p value vs control			
	Nitrendipine	**Sotalol**	**$BaCl_2$**	**BayK8644**
10 µM	73±12%; *P*<0.01	107±3%; *P*=ns	167±28%; *P*<0.05	140±19%; *P*<0.05
15 µM	77±8%; *P*<0.001	105±6%; *P*=ns	159±27%; *P*<0.001	154±25%; *P*<0.01
20 µM	73±10%; *P*<0.0001	110±6%; *P*=ns	179±38%; *P*<0.0001	150±20%; *P*<0.001
25 µM	77±10%; *P*<0.01	112±11%; *P*=ns	149±10%; *P*<0.0001	155±13%; *P*<0.0001

Supplemental Table 1. *APD_{80} values after pharmacological ion channel modulation by nitrendipine, sotalol, $BaCl_2$ or BayK8644 during 2-APB (10-25 µM) induced fibrillation. Controls are set at 100%. ns: non-significant.*

2-APB dosage	Wavelength (% of control); p value vs control			
	Nitrendipine	**Sotalol**	**$BaCl_2$**	**BayK8644**
10 µM	87±7%; *P*<0.01	105±9%; *P*=ns	131±37%; *P*<0.05	126±24%; *P*<0.05
15 µM	85±16%; *P*=ns	95±23%; *P*=ns	155±28%; *P*<0.001	153±44%; *P*<0.05
20 µM	94±14%; *P*=ns	110±18%; *P*=ns	163±54%; *P*<0.001	160±40%; *P*<0.01
25 µM	89±13%; *P*=ns	111±15; *P*=ns	150±20%; *P*<0.01	150±23%; *P*<0.001

Supplemental Table 2. *Wavelength values after pharmacological ion channel modulation by nitrendipine, sotalol, $BaCl_2$ or BayK8644 during 2-APB (10-25 µM) induced fibrillation. Controls are set at 100%. ns: non-significant.*

2-APB dosage	Activation frequency (% of control); p value vs control			
	Nitrendipine	Sotalol	$BaCl_2$	BayK8644
10 μM	113±6%; *P*<0.01	95±6%; *P*=ns	75±16%; *P*<0.05	75±9%; *P*<0.01
15 μM	112±11%; *P*<0.05	94±4%; *P*<0.05	67±11%; *P*<0.0001	66±13%; *P*<0.001
20 μM	117±6%; *P*<0.0001	92±6%; *P*<0.05	55±19%; *P*<0.0001	73±8%; *P*<0.0001
25 μM	112±11%; *P*<0.05	93±9%; *P*=ns	69±7%; *P*<0.0001	69±5%; *P*<0.0001

Supplemental Table 3. *Activation frequency values after pharmacological ion channel modulation by nitrendipine, sotalol, $BaCl_2$ or BayK8644 during 2-APB (10-25 μM) induced fibrillation. Controls are set at 100%. ns: non-significant.*

2-APB dosage	Complexity (% of control); p value vs control			
	Nitrendipine	Sotalol	$BaCl_2$	BayK8644
10 μM	100±0%; *P*=ns	100±0%; *P*=ns	89±19%; *P*=ns	83±41%; *P*=ns
15 μM	111±17%; *P*=ns	108±20%; *P*=ns	73±25%; *P*<0.05	56±22%; *P*<0.01
20 μM	99±15%; *P*=ns	102±14; *P*=ns	30±22%; *P*<0.0001	43±15%; *P*<0.0001
25 μM	102±9%; *P*=ns	87±7%; *P*<0.01	52±11%; *P*<0.0001	37±11%; *P*<0.0001

Supplemental Table 4. *Complexity values after pharmacological ion channel modulation by nitrendipine, sotalol, $BaCl_2$ or BayK8644 during 2-APB (10-25 μM) induced fibrillation. Controls are set at 100%. ns: non-significant*

REFERENCES

1. Zipes DP and Wellens HJ. Sudden cardiac death. *Circulation*. 1998;98:2334-2351.
2. Huikuri HV, Castellanos A, Myerburg RJ. Sudden death due to cardiac arrhythmias. *N Engl J Med*. 2001;345:1473-1482.
3. Severs NJ, Bruce AF, Dupont E, Rothery S. Remodelling of gap junctions and connexin expression in diseased myocardium. *Cardiovasc Res*. 2008;80:9-19.
4. Weiss JN, Qu Z, Chen PS, Lin SF, Karagueuzian HS, Hayashi H, Garfinkel A, Karma A. The dynamics of cardiac fibrillation. *Circulation*. 2005;112:1232-1240.
5. Gutstein DE, Morley GE, Tamaddon H, Vaidya D, Schneider MD, Chen J, Chien KR, Stuhlmann H, Fishman GI. Conduction slowing and sudden arrhythmic death in mice with cardiac-restricted inactivation of connexin43. *Circ Res*. 2001;88:333-339.
6. Clayton RH, Nash MP, Bradley CP, Panfilov AV, Paterson DJ, Taggart P. Experiment-model interaction for analysis of epicardial activation during human ventricular fibrillation with global myocardial ischaemia. *Prog Biophys Mol Biol*. 2011;107:101-111.
7. Huang J, Rogers JM, Killingsworth CR, Singh KP, Smith WM, Ideker RE. Evolution of activation patterns during long-duration ventricular fibrillation in dogs. *Am J Physiol Heart Circ Physiol*. 2004;286:H1193-H1200.
8. Kleber AG, Riegger CB, Janse MJ. Electrical uncoupling and increase of extracellular resistance after induction of ischemia in isolated, arterially perfused rabbit papillary muscle. *Circ Res*. 1987;61:271-279.
9. Wiggers CJ, Bell JR, Paine M. Studies of ventricular fibrillation caused by electric shock: II. Cinematographic and electrocardiographic observations of the natural process in the dog's heart. Its inhibition by potassium and the revival of coordinated beats by calcium. *Ann Noninvasive Electrocardiol*. 2003;8:252-261.
10. Wu TJ, Lin SF, Weiss JN, Ting CT, Chen PS. Two types of ventricular fibrillation in isolated rabbit hearts: importance of excitability and action potential duration restitution. *Circulation*. 2002;106:1859-1866.
11. Garfinkel A, Kim YH, Voroshilovsky O, Qu Z, Kil JR, Lee MH, Karagueuzian HS, Weiss JN, Chen PS. Preventing ventricular fibrillation by flattening cardiac restitution. *Proc Natl Acad Sci U S A*. 2000;97:6061-6066.
12. Panfilov AV. Is heart size a factor in ventricular fibrillation? Or how close are rabbit and human hearts? *Heart Rhythm*. 2006;3:862-864.
13. Rensma PL, Allessie MA, Lammers WJ, Bonke FI, Schalij MJ. Length of excitation wave and susceptibility to reentrant atrial arrhythmias in normal conscious dogs. *Circ Res*. 1988;62:395-410.
14. Samie FH, Mandapati R, Gray RA, Watanabe Y, Zuur C, Beaumont J, Jalife J. A mechanism of transition from ventricular fibrillation to tachycardia : effect of calcium channel blockade on the dynamics of rotating waves. *Circ Res*. 2000;86:684-691.
15. Warren M, Guha PK, Berenfeld O, Zaitsev A, Anumonwo JM, Dhamoon AS, Bagwe S, Taffet SM, Jalife J. Blockade of the inward rectifying potassium current terminates ventricular fibrillation in the guinea pig heart. *J Cardiovasc Electrophysiol*. 2003;14:621-631.
16. Zaitsev AV, Berenfeld O, Mironov SF, Jalife J, Pertsov AM. Distribution of excitation frequencies on the epicardial and endocardial surfaces of fibrillating ventricular wall of the sheep heart. *Circ Res*. 2000;86:408-417.
17. Askar SF, Ramkisoensing AA, Schalij MJ, Bingen BO, Swildens J, van der Laarse A, Atsma DE, de Vries AA, Ypey DL, Pijnappels DA. Antiproliferative treatment of myofibroblasts prevents arrhythmias in vitro by

limiting myofibroblast-induced depolarization. *Cardiovasc Res*. 2011;90:295-304.
18. Bai D, del CC, Srinivas M, Spray DC. Block of specific gap junction channel subtypes by 2-aminoethoxydiphenyl borate (2-APB). *J Pharmacol Exp Ther*. 2006;319:1452-1458.
19. Harks EG, Camina JP, Peters PH, Ypey DL, Scheenen WJ, van Zoelen EJ, Theuvenet AP. Besides affecting intracellular calcium signaling, 2-APB reversibly blocks gap junctional coupling in confluent monolayers, thereby allowing measurement of single-cell membrane currents in undissociated cells. *FASEB J*. 2003;17:941-943.
20. Gray RA, Pertsov AM, Jalife J. Spatial and temporal organization during cardiac fibrillation. *Nature*. 1998;392:75-78.
21. Nash MP, Mourad A, Clayton RH, Sutton PM, Bradley CP, Hayward M, Paterson DJ, Taggart P. Evidence for multiple mechanisms in human ventricular fibrillation. *Circulation*. 2006;114:536-542.
22. Kleber AG and Rudy Y. Basic mechanisms of cardiac impulse propagation and associated arrhythmias. *Physiol Rev*. 2004;84:431-488.
23. Mines GR. On dynamic equilibrium in the heart. *J Physiol*. 1913;46:349-383.
24. Allessie MA, Bonke FI, Schopman FJ. Circus movement in rabbit atrial muscle as a mechanism of trachycardia. *Circ Res*. 1973;33:54-62.
25. ten Tusscher KH, Mourad A, Nash MP, Clayton RH, Bradley CP, Paterson DJ, Hren R, Hayward M, Panfilov AV, Taggart P. Organization of ventricular fibrillation in the human heart: experiments and models. *Exp Physiol*. 2009;94:553-562.
26. ten Tusscher KH, Hren R, Panfilov AV. Organization of ventricular fibrillation in the human heart. *Circ Res*. 2007;100:e87-101.
27. Moe GK and ABILDSKOV JA. Atrial fibrillation as a self-sustaining arrhythmia independent of focal discharge. *Am Heart J*. 1959;58:59-70.
28. Riccio ML, Koller ML, Gilmour RF, Jr. Electrical restitution and spatiotemporal organization during ventricular fibrillation. *Circ Res*. 1999;84:955-963.
29. Sekar RB, Kizana E, Cho HC, Molitoris JM, Hesketh GG, Eaton BP, Marban E, Tung L. IK1 heterogeneity affects genesis and stability of spiral waves in cardiac myocyte monolayers. *Circ Res*. 2009;104:355-364.
30. Jalife J. Inward rectifier potassium channels control rotor frequency in ventricular fibrillation. *Heart Rhythm*. 2009;6:S44-S48.
31. Tsuchihashi K and Curtis MJ. Influence of tedisamil on the initiation and maintenance of ventricular fibrillation: chemical defibrillation by Ito blockade? *J Cardiovasc Pharmacol*. 1991;18:445-456.
32. Rees SA and Curtis MJ. Specific IK1 blockade: a new antiarrhythmic mechanism? Effect of RP58866 on ventricular arrhythmias in rat, rabbit, and primate. *Circulation*. 1993;87:1979-1989.
33. Yatani A, Kunze DL, Brown AM. Effects of dihydropyridine calcium channel modulators on cardiac sodium channels. *Am J Physiol*. 1988;254:H140-H147.
34. Safar P. Cerebral resuscitation after cardiac arrest: research initiatives and future directions. *Ann Emerg Med*. 1993;22:324-349.
35. Hillebrenner MG, Eason JC, Trayanova NA. Mechanistic inquiry into decrease in probability of defibrillation success with increase in complexity of preshock reentrant activity. *Am J Physiol Heart Circ Physiol*. 2004;286:H909-H917.
36. Wang P, Umeda PK, Sharifov OF, Halloran BA, Tabengwa E, Grenett HE, Urthaler F, Wolkowicz PE. Evidence that 2-aminoethoxydiphenyl borate provokes fibrillation in perfused rat hearts via voltage-independent calcium channels. *Eur J Pharmacol*. 2012;681:60-67.
37. Nakagami T, Tanaka H, Dai P, Lin SF, Tanabe T, Mani H, Fujiwara K, Matsubara H, Takamatsu T. Generation of reentrant arrhythmias by dominant-negative inhibi-

tion of connexin43 in rat cultured myocyte monolayers. *Cardiovasc Res*. 2008;79:70-79.

38. Bub G, Shrier A, Glass L. Spiral wave generation in heterogeneous excitable media. *Phys Rev Lett*. 2002;88:058101.
39. Curtis MJ and Hearse DJ. Ischaemia-induced and reperfusion-induced arrhythmias differ in their sensitivity to potassium: implications for mechanisms of initiation and maintenance of ventricular fibrillation. *J Mol Cell Cardiol*. 1989;21:21-40.
40. Pijnappels DA, Schalij MJ, Ramkisoensing AA, van Tuyn J, de Vries AA, van der Laarse A, Ypey DL, Atsma DE. Forced alignment of mesenchymal stem cells undergoing cardiomyogenic differentiation affects functional integration with cardiomyocyte cultures. *Circ Res*. 2008;103:167-176.

Chapter III

Appendix I

Prolongation of minimal action potential duration in sustained fibrillation decreases complexity by transient destabilization

Wolkowicz PE, Umeda PK, Sharifov OF, Wang P, Mahtani H, Urthaler F.

Cardiovasc Res. 2013;98:155-6

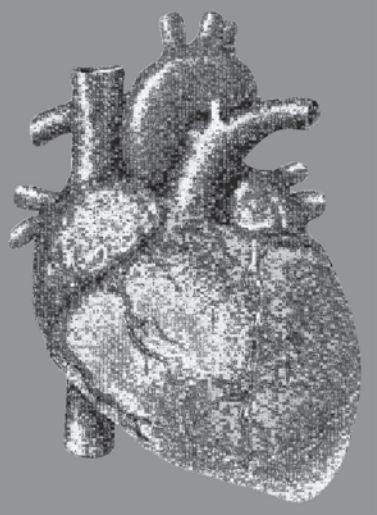

TO THE EDITOR:

We read with great interest the article by Bingen et al.[1] entitled 'Prolongation of minimal action potential duration in sustained fibrillation decreases complexity by transient destabilization'. This paper referred to our report that 2-aminoethoxydiphenyl borate (2APB) induces fibrillation in perfused rat hearts2 (http://youtu.be/pDsm0UKQvt4, http://youtu.be/J0q_YPZyBwk). It also extended our work[3–7] and that of Huo et al.[8] by establishing the arrhythmicity of 2APB in monolayers of neonatal rat ventricular myocytes. Bingen proposed that 2APB provokes electrical instability by inhibiting cardiac connexins which leads to impulse re-entry. They also concluded that prolonging the action potential with Bay K 8644 or barium reduces ectopic complexity to a few re-entrant sources. We would like to highlight four points that are inconsistent with these analyses and suggest an alternate, possibly complementary, explanation for 2APB arrhythmicity.[7]

First, the concentrations of 2APB that initiate sporadic ectopy (10 μM)1,3 do not affect connexin 43 and 45.9 Furthermore, 15–20 μM 2APB which induces tachycardia and fibrillation[1,2] should not appreciably affect connexin 43 while reducing connexin 45 activity about one-half.[9] Transgenesis shows that only large decreases in connexin activity provoke re-entrant arrhythmia.[10] Since arrhythmogenic concentrations of 2APB directly affect connexins to a limited degree, it is not clear how they would so decrease conduction velocity and provoke re-entry.[1] Electromechanical uncouplers and voltage-sensitive dyes themselves decrease impulse conduction.[11,12] This may contribute to the low conduction Bingen reports at doses of 2APB that do not greatly affect connexins.

Secondly, Bingen's voltage-mapping studies expand our data which demonstrated that Bay K 8644 induces organized, high-frequency ectopy in left atria or left ventricular papillary muscles treated with 2APB.[4,5,6] While Bingen concluded that the prolongation of the action potential duration underlies this effect, FPL-64176, isoproterenol, and ouabain also provoke high-frequency ectopy to similar extents.[4] FPL-64176 prolongs the action potential much more than Bay K 8644,[13] isoproterenol increases this variable to a similar degree as Bay K,14 whereas ouabain reduces action potential duration.[15] Thus it would be of interest to test if action potential duration correlates with re-entrant complexity in myocyte cultures treated with 2APB and exposed to this panel of compounds.

Thirdly, small molecules such as SKF-96365 and ML-7 suppress the sporadic ectopy, the high-frequency ectopy, and the fibrillation that 2APB induces in heart muscle.[2,5,6,7] They also interdict voltage-independent calcium signalling.[16] In addition, calmodulin antagonists but not calmodulin-dependent protein kinase II inhibitors suppress 2APB ectopy.[5,6] Our recent data show that bcl-2 inhibitors similarly stifle 2APB ectopy.[7] It would be useful to test if these diverse molecules increase impulse conduction in cultures treated with 2APB or in untreated monolayers, as the restoration of impulse conduction would be required to suppress 2APB ectopy if re-entry were its underlying cause.

Fourthly, 2APB provokes electromechanical ectopy even when it is added to quiescent non-automatic left atria or papillary muscles (e.g. Figure 3B: * and ‡ in ref.6). Since re-entry requires a preceding impulse, how this mechanism for arrhythmia might induce the initial spontaneous depolarization of unpaced muscles treated with 2APB is not apparent to us. Understanding the origin of these primary events which are by definition non-re-entrant will help dissect the molecular mechanism underlying 2APB arrhythmia.

Towards this goal, it is known that 2APB stimulates voltage-independent calcium entry in non-excitable cells through the Orai calcium channels with EC50s identical to those that cause cardiac ectopy.[17] These channels, and the related transient receptor potential proteins, are important regulators of cell calcium signalling. Huo published that 2APB activates calcium entry in isolated myocytes8; we reported that Orai inhibitors suppress 2APB ectopy and that rat left atria and ventricles express Orai1 and Orai3.[2,5,6] Thus the activation of these channels in an excitable cell background may stimulate a novel calcium-linked pathway for automatic arrhythmia, a notion which we have outlined elsewhere in more detail.[5,7]

There are at least three ways that this novel mechanism may be important in arrhythmia. Firstly, intra- and extra-cellular signals including calcium store depletion and inflammatory mediators provoke calcium entry through voltage-independent calcium channels. Thus these channels may provide an unexpected way to couple well-known pathophysiological stimuli to arrhythmia.[18] Secondly, calmodulin-dependent protein kinase II participates in triggered afterdepolarization.[19,20] If our alternate mechanism were to initiate focal atypical automaticity, then calcium signalling could underlie both the triggered and the automatic events that lead to re-entry. Thirdly, the two suggested mechanisms for 2APB ectopy, connexin impairment,1 and aberrant voltage-independent calcium signalling,[2,7] may not be mutually exclusive. That is, calcium entry through voltage-independent calcium channels may offer an unexpected means to suppress connexin activity. Further study of 2APB ectopy may reveal new mechanisms for arrhythmia and identify unforeseen therapeutic targets.

REFERENCES

1. Bingen BO, Askar SFA, Schalij MJ, Kazbanov IV, Ypey DK, Panfilov AV et al. Prolongation of minimal action potential duration in sustained fibrillation decreases complexity by transient destabilization. *Cardiovasc Res* 2013;97:161–170.
2. Wang P, Umeda PK, Sharifov OF, Halloran BA, Tabengwa E, Grenett HE et al. Evidence that 2-aminoethoxydiphenyl borate provokes fibrillation in perfused rat hearts via voltage-independent calcium channels. *Eur J Pharm* 2012;681:60–67.
3. Wolkowicz PE, Wu HC, Urthaler F, Ku DD. 2-APB induces instability in rat left atrial mechanical activity. *J Cardiovasc Pharm* 2007;49:325–335.
4. Wolkowicz PE, Grenett HE, Huang J, Wu HC, Ku DD, Urthaler F. A pharmacological model for calcium overload-induced tachycardia in isolated rat left atria. *Eur J Pharm* 2007;576:122–131.
5. Wolkowicz PE, Huang J, Umeda PK, Tabengwa E, Grenett HE, Urthaler F. A novel mechanism for cardiac abnormal automaticity: Orai-linked calcium signaling. *Circ* 2010;122:A20885 (Abstract).
6. Wolkowicz PE, Huang J, Umeda PK, Sharifov OF, Tabengwa E, Halloran BA et al. Pharmacological evidence for Orai channel activation as a source of cardiac abnormal automaticity. *Eur J Pharm* 2011; 668:208–216.
7. Wolkowicz PE, Umeda PK, Urthaler F, Sharifov OF. Voltage-independent calcium channels, molecular sources of supraventricular arrhythmia. In: Liu T, Li G, Korantzopoulos P, eds. Atrial Fibrillation. Rijeka, Croatia: InTech Publishing; 2013. http://www.intechopen.com/books/atrial-fibrillation-mechanisms-and-treatment/voltage-independent-calcium-channels-molecularsources-of-supraventricular-arrhythmia (28 February 2013).
8. Huo R, Li Z, Lu C, Xie Y, Wang B, Tu YJ et al. Inhibition of 2-aminoethoxydiphenyl borate induced rat atrial ectopic activity by antiarrhythmic drugs. *Cell Physiol Biochem* 2010;25:425–432.
9. Bai D, del Corsso C, Srinivas M, Spray DC. Block of specific gap junction channel subtypes by 2- aminoethoxydiphenyl borate (2-APB). *J Pharm Exp Ther* 2006;319:1452–1458.
10. Gutstein DE, Morley GE, Tamaddon H, Vaidya D, Schneider MD, Chen J et al. Conduction slowing and sudden arrhythmic death in mice with cardiac-restricted inactivation of connexin 43. *Circ Res* 2001; 88:333–339.
11. Larsen AP, Sciuto KJ, Moreno AP, Poelzing S. The voltage-sensitive dye d-4-ANEPPS slows conduction velocity in isolated guinea pig hearts. *Heart Rhythm* 2012;9:1493–1500.
12. Verrecchia F, Herve JC. Reversible blockade of gap junctional communication by 2,3-butanedione monoxime in rat cardiac myocytes. *Am J Physiol* 1997; 272:C875–C885.
13. Rampe D, Anderson B, Rapien-Pryor V, Li T, Dage RC. Comparison of the in vitro and in vivo cardiovascular effects of two structurally distinct calcium channel activators, BAY K 8644 and FPL 64176. *J Pharm Exp Ther* 1993;265:1125–1130.
14. Belardinelli L, Isenberg G. Actions of adenosine and isoproterenol on isolated mammalian ventricular myocytes. *Circ Res* 1983;53:287–297.
15. Ruch SR, Nishio M, Wasserstrom JA. Effect of cardiac glycosides on action potential characteristics and contractility in cat ventricular myocytes: role of calcium overload. *J Pharm Exp Ther* 2003;307:419–428.
16. Ju YK, Chu Y, Chaulet H, Lai D, Gervasio OL, Graham RM et al. Store-operated calcium influx and expression of TRPC

genes in mouse sinoatrial node. *Circ Res* 2007;100:1605–1614.

17. DeHaven WI, Smyth JT, Boyles RR, Bird GS, Putney JW. Complex actions of 2-aminoethydiphenyl borate on store-operated calcium entry. *J Biol Chem* 2008;293:19265–19273.
18. Hirose M, Takeishi Y, Nizeki T, Nakada T, Shimojo H, Kasihara T et al. Diacylglycerol kinase z inhibits ventricular tachyarrhythmias in a mouse model of heart failure: roles of canonical transient receptor potential (TRPC) channels. *Circ J* 2011;75:2333–2342.
19. Yao L, Fan P, Jiang Z, Viatchenko-Karpinski S, Wu Y, Kornyeyev D et al. Nav1.5-dependent persistent sodium influx activates CaMKII in rat ventricular myocytes and N1325S mice. *Am J Physiol* 2011;301: C577–C586.
20. Choi BR, Burton F, Salama G. Cytosolic calcium triggers early afterdepolarizations and Torsade de Pointes in rabbits with type 2 Long QT syndrome. *J Physiol* 2002;543:615–631.

Chapter III

Appendix II

Prolongation of minimal action potential duration in sustained fibrillation decreases complexity by transient destabilization: reply

Wolkowicz PE, Umeda PK, Sharifov OF, Wang P, Mahtani H, Urthaler F.

Cardiovasc Res. 2013;98:155-6

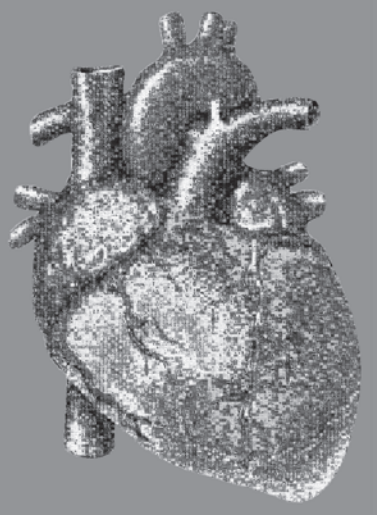

TO THE EDITOR:

In their letter, Wolkowicz *et al*. raise a valid point questioning whether other effects of 2-aminoethoxydiphenyl borate (2-APB) might also have contributed to ventricular fibrillation (VF) initiation, especially its effects on voltage-independent calcium channels, as was also mentioned in the Discussion section of our manuscript recently published in *Cardiovascular Research*.[1]

In this study, we showed that prolonging the minimal action potential duration (APD) can decrease the complexity (e.g. number of rotors) during sustained VF. To induce fibrillation in neonatal rat ventricular cardiomyocyte monolayers and in adult rat hearts, we used 2-APB. We postulated that the re-entrant conduction patterns resembling VF after 2-APB treatment could be partly attributed to the effect of 2-APB on gap junctional coupling.[2]

The main purpose of our study was to study the maintenance properties of VF. Going into length on the mechanism by which 2-APB induces VF would defeat this purpose, as VF can show the same maintenance properties regardless of how it is initiated.[3] Hence, we fully agree with Wolkowicz *et al*. that 2-APB might contribute to VF initiation by other means than only gap junctional uncoupling. Considering that virtually all pharmacological agents are aspecific to some extent it can be expected that different, potentially interacting factors may be responsible for a certain effect.

In our study, we showed a significant decrease in conduction velocity after treatment with 2-APB. Wolkowicz *et al*. suggest that this decrease might have been caused by the use of electromechanical uncouplers[4] and voltage-sensitive dyes[5], and that the effect of 2-APB on gap junctional communication was too little to reach a threshold for arrhythmogenesis.[6] However, in the experiments using cardiomyocyte monolayers we did not use electromechanical uncoupling, while the same concentration of voltage-sensitive dye was used in control and 2-APB-treated cultures or in control and 2-APB-treated hearts. Hence, in our setup the aspecific effects of these pharmacological agents do not seem to provide a plausible explanation for the difference in conduction velocity. Nevertheless, the decrease in gap junctional uncoupling by BDM treatment[4] or the decrease in conduction velocity by di-4-ANEPPS[5] could effectively lower the degree of additional uncoupling needed to reach the arrhythmogenic threshold, which could help explain the tachyarrhythmias found after 2-APB treatment.

Furthermore, we show that in cultures with VF, prolongation of the minimal APD by BayK8644 and $BaCl_2$decreases the activation frequency and complexity of VF. Wolkowicz *et al*.,[7] however, found strongly increased activation frequencies when combining 2-APB with BayK8644 treatment. The differences in results could be attributable to the fact that different models and protocols were used. For example, in our study cells were first incubated with 2-APB for 20 min, after which they were subjected to optical

mapping and BayK8644 treatment.[1] In contrast, Wolkowicz *et al*.[7] used pre-treatment with BayK8644 and direct analysis of activation frequency after the addition of 2-APB. Possibly, the mechanisms causing high activation frequency after short- or long-term 2-APB treatment are different. Wolkowicz *et al*.[7] showed that the increased activation frequency is caused by abnormal automaticity, as a result an increase in APD by BayK8644 pre-treatment does not decrease the frequency. We show that after incubation for 20 min with 2-APB there is a predominant re-entrant activation pattern, in which BayK8644 decreases the frequency.[1] Nevertheless, this does not exclude the possibility that before re-entry initiation there is 2-APB-induced non-re-entrant automaticity in our setup as suggested by Wolkowicz *et al.*, which would strongly increase the chance of re-entry initiation in our cultures.

In conclusion, we acknowledge the issues Wolkowicz *et al*. raised in their letter and support the notion that indeed 2-APB-induced arrhythmias can be initiated by mechanisms other than gap junctional uncoupling. However, based on our data we feel that our model, in which stable re-entrant action patterns are observed after longer 2-APB incubation, allows for studies on sustained VF, despite the incomplete knowledge of its initiation. For more specific and mechanistic studies on the origin of arrhythmias genetic interventions based on viral vector technologies seem more appropriate,[8] especially when such interventions are designed to be cell type-specific and inducible. Nevertheless, additional research is needed to better understand the mechanisms behind 2-APB-induced arrhythmias, as this might contribute to the development of novel anti-arrhythmic strategies focusing on the pro-arrhythmic substrate and its underlying molecular mechanisms.[9]

REFERENCES

1. Bingen BO, Askar SF, Schalij MJ, Kazbanov IV, Ypey DL Panfilov AV et al. Prolongation of minimal action potential duration in sustained fibrillation decreases complexity by transient destabilization. *Cardiovasc Res* 2013;97: 161–170.
2. Bai D, del CC, Srinivas M, Spray DC. Block of specific gap junction channel subtypes by 2-aminoethoxydiphenyl borate (2-APB). *J Pharmacol Exp Ther* 2006;319:1452–1458.
3. Curtis MJ, Hearse DJ. Ischaemia-induced and reperfusion-induced arrhythmias differ in their sensitivity to potassium: implications for mechanisms of initiation and maintenance of ventricular fibrillation. *J Mol Cell Cardiol* 1989;21:21–40.
4. Verrecchia F, Herve JC. Reversible blockade of gap junctional communication by 2,3-butanedione monoxime in rat cardiac myocytes . *Am J Physiol* 1997;272: C875–C885.
5. Larsen AP, Sciuto KJ, Moreno AP, Poelzing S. The voltage-sensitive dye di-4-ANEPPS slows conduction velocity in isolated guinea pig hearts. *Heart Rhythm* 2012;9:1493–1500.
6. Gutstein DE, Morley GE, Tamaddon H, Vaidya D, Schneider MD, Chen J et al. Conduction slowing and sudden arrhythmic death in mice with cardiac-restricted inactivation of connexin43. *Circ Res* 2001;88:333–339.
7. Wolkowicz PE, Grenett HE, Huang J, Wu HC, Ku DD, Urthaler F. A pharmacological model for calcium overload-induced tachycardia in isolated rat left atria. *Eur J Pharmacol* 2007;576:122–131.
8. Askar SF, Bingen BO, Swildens J, Ypey DL, van der Laarse A, Atsma DE et al. Connexin43 silencing in myofibroblasts prevents arrhythmias in myocardial cultures: role of maximal diastolic potential. *Cardiovasc Res* 2012; 93:434–444.
9. Cho HC, Marban E. Biological therapies for cardiac arrhythmias: can genes and cells replace drugs and devices? *Circ Res* 2010;106:674–685.

Chapter IV

Atrium-specific Kir3.x determines inducibility, dynamics and termination of fibrillation by regulating restitution-driven alternans.

Kir3.x in Atrial Fibrillation

Brian O. Bingen, MD; Zeinab Neshati, MSc; Saïd F. A. Askar, MSc; Ivan V. Kazbanov, MSc; Dirk L. Ypey, PhD; Alexander V. Panfilov, PhD; Martin J. Schalij, MD, PhD; Antoine A. F. de Vries, PhD; Daniël A. Pijnappels, PhD.

Circulation. 2013;128:2732-44.

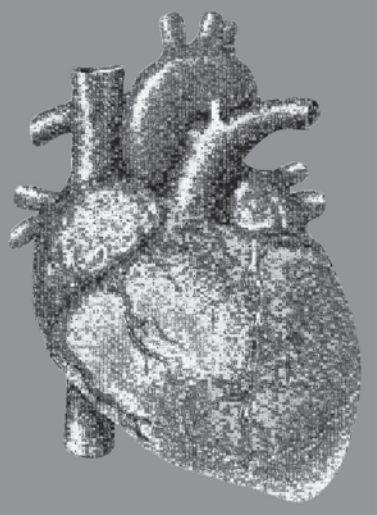

ABSTRACT

Background: Atrial fibrillation (AF) is the most common cardiac arrhythmia. Ventricular pro-arrhythmia hinders pharmacological AF treatment. Modulation of atrium-specific Kir3.x channels, which generate a constitutively active current ($I_{K,ACh-c}$) after atrial remodeling, might circumvent this problem. However, it is unknown whether and how $I_{K,ACh-c}$ contributes to AF induction, dynamics and termination. Therefore we investigated the effects of $I_{K,ACh-c}$ blockade and Kir3.x downregulation on AF.

Methods and Results: Neonatal rat atrial cardiomyocyte cultures and intact atria were burst paced to induce reentry. To study the effects of Kir3.x on action potential characteristics and propagation patterns, cultures were treated with tertiapin or transduced with lentiviral vectors encoding *Kcnj3*- or *Kcnj5*-specific short hairpin RNAs. Kir3.1 and Kir3.4 were expressed in atrial but not in ventricular cardiomyocyte cultures. Tertiapin prolonged action potential duration(APD; 54.7±24.0 to 128.8±16.9ms,$p<0.0001$) in atrial cultures during reentry, indicating the presence of $I_{K,ACh-c}$. Furthermore, tertiapin decreased rotor frequency(14.4±7.4 to 6.6±2.0Hz,$p<0.05$) and complexity(6.6±7.7 to 0.6±0.8 phase singularities,$p<0.0001$). Knockdown of *Kcnj3* or *Kcnj5* gave similar results. Blockade of $I_{K,ACh-c}$ prevented/terminated reentry by prolonging APD and changing APD and conduction velocity (CV) restitution slopes, thereby altering the probability of APD alternans and rotor destabilization. Whole heart mapping experiments confirmed key findings (*e.g.* >50% reduction in AF inducibility after $I_{K,ACh-c}$ blockade).

Conclusions: Atrium-specific Kir3.x controls induction, dynamics and termination of fibrillation by modulating APD and APD/CV restitution slopes in atrial tissue with $I_{K,ACh-c}$. This study provides new molecular and mechanistic insights into atrial tachyarrhythmias and identifies Kir3.x as a promising atrium-specific target for antiarrhythmic strategies.

INTRODUCTION

Atrial fibrillation (AF) is the most common cardiac rhythm disorder in humans, and substantially contributes to morbidity, mortality and health care costs.[1-3] Ablation techniques, breaking up AF circuits or triggers, have improved the outcome of AF in the past decades.[4] While the success rate of AF ablation is relatively high in paroxysmal AF, in permanent AF ablation restores sinus rhythm only in a fraction of patients, due to altering underlying mechanisms and structural changes of the atrial myocardium. Importantly, there is a lack of consensus on the optimal ablation strategy in these patients, while this population is vastly growing.[5,6] In addition, ablation procedures are associated with a risk of complications due to their invasive nature.[7] Furthermore, long-term maintenance of sinus rhythm requires repeated procedures or continuation of anti-arrhythmic drugs in a significant proportion of chronic AF patients.[8] Hence, first line treatment of AF is still performed pharmacologically.[4] However, the use of anti-arrhythmic agents is hampered by potentially lethal ventricular pro-arrhythmia, lack of efficacy and serious side effects.[9-13] Thus, research on AF treatment has focused on finding atrium-selective drugs, with higher efficacy in AF rhythm control but less side effects such as ventricular pro-arrhythmia.

In the heart of most mammals, including humans, the acetylcholine-activated potassium current ($I_{K,ACh}$) is found exclusively in the atrium.[14] Hence, $I_{K,ACh}$ is one of the novel candidates for atrium-specific drug treatment. Activating $I_{K,ACh}$ by acetylcholine has been shown to shorten action potential (AP) duration (APD) in the atria.[15] In patients suffering from persistent AF and atrial remodeling, $I_{K,ACh}$ can become constitutively active.[16,17] Whether this constitutively active acetylcholine-inducible current ($I_{K,ACh\text{-}c}$) affects AF induction, dynamics or termination, the mechanisms by which it could do so, as well as the channels involved in this process remain to be elucidated.

To test whether and how $I_{K,ACh\text{-}c}$ affects fibrillation , a 2D *in vitro* model of atrial tissue and a whole heart model of AF were developed using atrial neonatal rat cardiomyocytes (nrCMCs) and hearts with endogenous $I_{K,ACh\text{-}c}$. Using these models, fibrillation could be systematically and reproducibly studied. Inhibition of Kir3.1 or Kir3.4 activity by the highly specific drug tertiapin or lentiviral vector (LV)-mediated RNA interference (RNAi), was used to study the role of $I_{K,ACh\text{-}c}$ in AF initiation, dynamics and termination.

METHODS

A detailed description of materials and methods can be found in the Supplementary Material online.

All animal experiments were approved by the Animal Experiments Committee of the Leiden University Medical Center and conformed to the Guide for the Care and Use of Laboratory Animals as stated by the US National Institutes of Health.

Cell isolation and culture

After careful separation of the atria and ventricles of neonatal Wistar rat hearts, cardiomyocytes were isolated by collagenase digestion and plated on fibronectin-coated, round glass coverslips (15-mm diameter) at a density of 2-8×10^5 cells/well in 24-well cell culture plates, as described previously.[18] To restrict unwanted expansion of the remaining non-myocytes, cell proliferation was inhibited by incubation with Mitomycin-C (10 µg/ml; Sigma-Aldrich, St. Louis, MO) for 2 h at day 1 of culture.[19]

Western blotting

Cardiomyocytes were lysed in 50 mM Tris–HCl (pH 8.0), 150 mM NaCl, 1% Triton X-100, 0.5% sodium deoxycholate, 0.1% sodium dodecyl sulfate. Three 15-mm wells, each seeded with 8×10^5 cells, were used for each sample, and each experiment consisted of at least 4 samples. The proteins in the lysate were size-fractionated in NuPage Novex 12% Bis-Tris gels (Life Technologies, Bleiswijk, the Netherlands) and transferred to Hybond polyvinylidene difluoride membranes (GE Healthcare, Diegem, Belgium). Membranes were blocked in Tris-based saline, 0.1% Tween-20, 5% bovine serum albumin (Sigma-Aldrich) for 1 h. Next, membranes were incubated with antibodies directed against Kir3.1 (Alomone Labs, Jerusalem, Israel), Kir3.4 (Santa Cruz Biotechnology, Dallas, TX) or glyceraldehyde 3-phosphate dehydrogenase (GAPDH; loading control; Merck Millipore, Billerica, MA) and corresponding horseradish peroxidase-conjugated secondary antibodies (Santa Cruz Biotechnology) for 1 h. Chemiluminescence was detected using ECL Prime Western blot detection reagent (GE Healthcare).-

Optical mapping

At day 9 of culture, investigation of AP propagation on a whole-culture scale by optical mapping (using di-4-ANEPPS [Life Technologies] as voltage-sensitive dye) and subsequent data analyses were performed as described previously.[18] During optical mapping cells were stimulated electrically using a custom-made, epoxy-coated unipolar platinum electrode with square suprathreshold electrical stimuli at 1 and 2-20 Hz (2-Hz increments). Burst pacing with a cycle length of 20-100 ms was used to induce reentry. Complexity was defined as the number of phase singularities (PSs) per cm^2, determined by using the phase space method as described previously.[18] The effect of several drugs (100 nmol/L tertiapin [Alomone Labs], 200 nmol/L atropine [Sigma-Aldrich] and 2 µmol/L carbachol [Sigma-Aldrich])[16] was studied by pipetting them directly into the medium, dispersing them by gentle agitation, immediately followed by optical mapping.

Whole heart mapping was performed by incubating neonatal rat hearts with 2 μM di-4-ANEPPS in a tissue bath containing oxygenated Tyrode's solution (comprising [in mM] NaCl 130, $CaCl_2$ 1.8, KCl 4.0, $MgCl_2$ 1.0, NaH_2PO_4 1.2, $NaHCO_3$ 24 and glucose 5.5 at pH 7.4). Prior to excision of the heart, the left ventricle was injected with Tyrode's solution supplemented with 20 mM 2,3-butanedione monoxime (Sigma-Aldrich) to minimize motion artifacts with or without 200 nM tertiapin to block Kir3.x channels. During whole heart mapping, AF was induced by burst pacing at a cycle length of 20-100 ms using a custom-made bipolar platinum electrode.

RNAi

Kir3.1 and Kir3.4 expression in neonatal rat atrial cell cultures was selectively inhibited using self-inactivating LVs encoding short hairpin (sh) RNAs specific for rat *Kcnj3* (LV-Kir3.1↓) and *Kcnj5* (LV-Kir3.4↓), respectively. The shuttle constructs to generate these LVs are derivatives of plasmid SHC007 from the Mission shRNA library (Sigma-Adrich) in which the *Photinus pyralis luciferase (PpLuc)*-specific shRNA-coding sequence was replaced by a rat *Kcnj3*- or *Kcnj5*-specific shRNA-coding sequence and the marker gene cassette consisting of the human *phosphoglycerate kinase 1* gene promoter and the puromycin-N-acetyltransferase-coding sequence was substituted by the human *eukaryotic translation elongation factor 1 alpha 1* gene promoter and the *Aequorea victoria* enhanced green fluorescent protein-coding sequence. The negative control vector (LV-PpLuc↓) had the same genetic makeup, except that it contained the aforementioned *PpLuc*-specific shRNA-coding sequence.

Statistical analysis

Statistical analyses were performed using SPSS11.0 for Windows (SPSS, Chicago, IL). Comparison between two groups was performed using the Mann-Whitney U test or Wilcoxon signed rank test or Fisher's exact test where appropriate. Kruskall-Wallis testing with Bonferoni *post-hoc* correction was used for multiple groups and comparisons. Data were expressed as mean±standard deviation (SD) for a number (n) of observations. Differences were considered statistically significant if $p<0.05$. Non-linear regression curves were constructed by using a robust exponential one-phase decay curve fit. Accuracy of these curves was expressed as the coefficient of determination (R^2). R^2 was calculated by the formula $R^2= 1-(SS_{reg}/SS_{tot})$ where SS_{reg} is the regression sum of squares (the sum of the square vertical distances of individual points to the regression curve) and SS_{tot} is the total sum of squares (the sum of the square vertical distances to the mean of all Y values).

RESULTS

Cell culture characteristics

A detailed characterization of atrial and ventricular nrCMC cultures by immunocytology and Western blotting can be found in the Supplementary Material online (Supplemental Figure 1).

Activation pattern characteristics in atrial nrCMC cultures

During optical mapping, atrial cultures showed uniform, convex and fast activation originating from the electrode upon 1-Hz stimulation (Figure 1A). After burst pacing, reentry was induced in the vast majority of atrial cultures. In 46 out of 49 of these arrhythmic cultures activation patterns remained stable during each cycle of reentry, while also the number and spatial dispersion of PSs did not change during 6 s of mapping (Figure 1B, Supplemental Movie 1). Return mapping (plotting a peak-to-peak interval [PPI] against the subsequent PPI) and time series of the PPIs showed that through such a fixed activation pattern and PS position these arrhythmias had period-1 (P-1) oscillatory dynamics (*i.e.* all rotor periods had approximately the same length) (Supplemental Figure 2A,C,E). Interestingly, the remaining 6% of cultures showed changes in activation pattern, PS number and PS position for each reentrant cycle (Figure 1C, Supplemental Movie 2). Return mapping and time series of the PPIs in these cultures showed period>1 or aperiodical oscillatory dynamics (*i.e.* the wavefront rotation alternated between >1 different periods or showed a different period during each cycle) (Supplemental Figure 2B,D,F).

During burst pacing-induced reentry (including both the stable and the unstable cases of reentry, n=49), rotor frequency showed a hyperbolic-like relationship with both APD_{80} (R^2=0.91) and wavelength (R^2=0.63). No apparent relation was found between rotor frequency and conduction velocity (CV) (Figure 1D-F). Moreover, the number of rotors negatively correlated with wavelength (R^2=0.73) and APD_{80} (R^2=0.70). Again CV, other than its effects on wavelength did not show a strong individual correlation with the number of PSs during reentry (Figure 1G-I). These results show that fibrillatory activation in this model can be maintained by P-1 or period>1/aperiodical reentry. Furthermore, the correlation analyses suggest that prolongation of atrial APD and wavelength during AF could decrease rotor frequency as well as complexity, possibly leading to prevention or termination of AF.

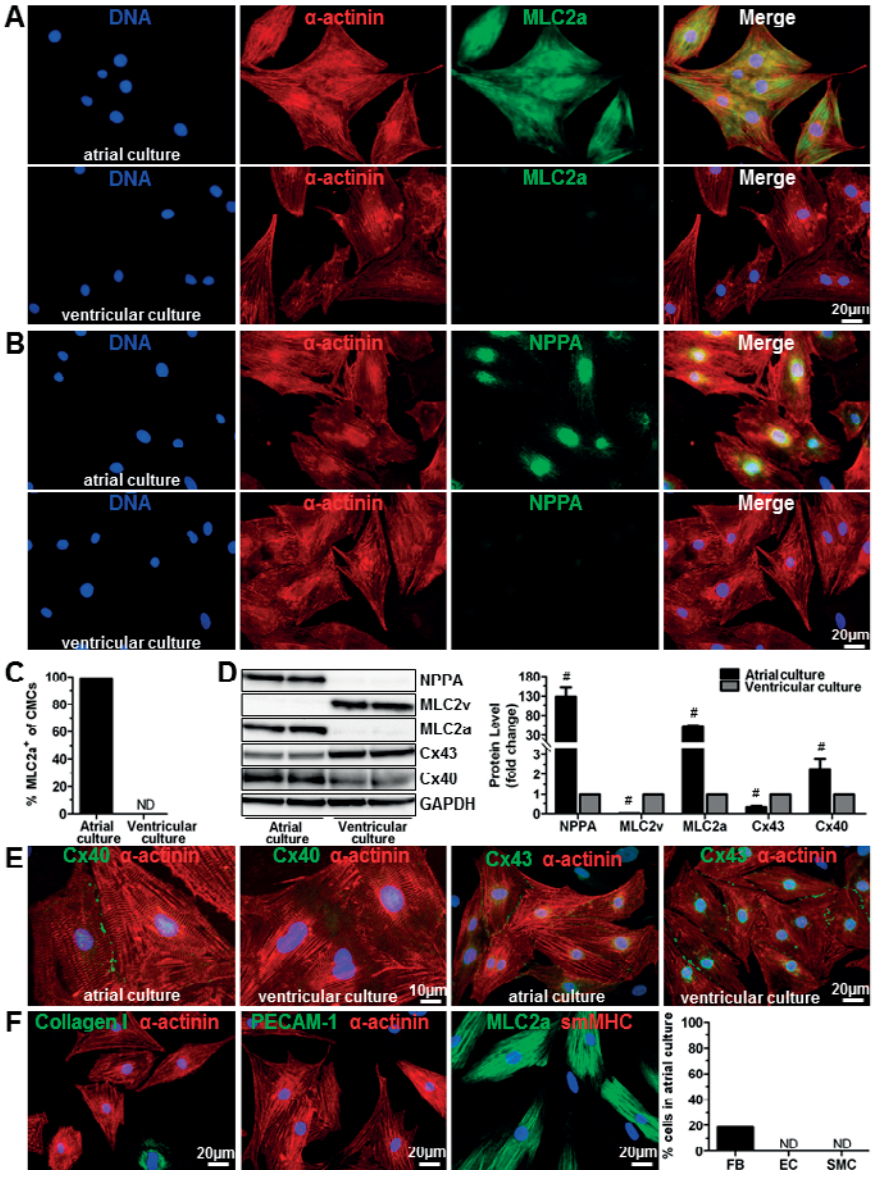

Supplemental Figure I. *Typical examples of immunocytological double staining of (A) MLC2a (green) and α-actinin (red) and (B) NPPA (green) and α-actinin (red) in atrial (upper panels) and ventricular (lower panels) neonatal rat CMC cultures. (C) Quantification of MLC2a and α-actinin double-positive cells in atrial and ventricular neonatal rat CMC cultures. (D) Western blot analysis (left) and quantification (right) of NPPA, MLC2v, MLC2a, Cx43 and Cx40 levels in atrial and ventricular neonatal rat CMC cultures using GAPDH as loading control. (E) Immunocytological double staining of Cx40 (green) and α-actinin (red) and of Cx43 (green) and α-actinin (red) in atrial (1st and 3rd panel from the left, respectively) and ventricular (2nd and 4th panel from the left, respectively) neonatal rat CMC cultures. (F) Immunocytological double staining of collagen type I (green, left) and PECAM-1 (green, middle) with α-actinin (red) and of MLC2a (green, right) with smMHC (red, right). The corresponding quantification of fibroblasts (FB), endothelial cells (EC) and smooth muscle cells (SMC) is depicted on the far right. #: p<0.05 vs ventricular cultures, ND: not detected.*

Blockade of atrium-specific IK,ACh decreases rotor frequency, complexity and inducibility of reentry

Atrial nrCMCs abundantly expressed Kir3.1 and Kir3.4 in comparison to ventricular nrCMCs (100.0±6.3 vs 18.3±0.7 and 100±2.8 vs 7.8±2.0%, respectively, $p<0.05$, n=4 per group) as judged by Western blot analyses (Figure 2A). As such, Kir3.x could be a target for blockade in an attempt to selectively prolong atrial APD, thereby preventing or terminating AF. To test this hypothesis both atrial and ventricular nrCMC cultures were treated with 100 nM tertiapin, a specific blocker of $I_{K,ACh}$.[16] Tertiapin significantly increased APD_{80} in atrial nrCMCs during 1-Hz pacing (from 56.5±12.5 to 145.5±20.6 ms, $p<0.0001$, n=33) (Figure 2B), in the absence of exogenous acetylcholine, showing the presence of $I_{K,ACh-c}$ in these cells (see also Supplemental Results and Supplemental Figure 3). Tertiapin had no significant effect on APD in ventricular nrCMCs (n=12) (Figure 2C). Hence, the increase in APD_{80} induced by tertiapin was significantly larger in atrial nrCMCs (86.7±19.6 vs 9.5±9.9 ms in ventricular nrCMCs) (Figure 2D). Blockade of $I_{K,ACh-c}$ by tertiapin increased APD_{80} during reentry (from 54.7±24.0 to 128.8±16.9 ms, n=42)(Figure 2E-G), which significantly decreased rotor frequency (from 14.1±7.4 to 5.9±1.7 Hz) and complexity (from 6.7±7.7 to 0.58±0.83 PSs) (Figure 2H,I). Interestingly, the inducibility of reentry also decreased (from 89.2 to 27.2%) after tertiapin treatment (Figure 2J). Concomitantly, tertiapin led to complete termination of all rotors in 67.4% of cultures, while rotor termination occurred in only 7.0% of control cultures (Figure 2K).

Figure 1 legend. →

Activation maps (top, 6-ms isochrone spacing) and corresponding phase maps (bottom) of atrial nrCMC cultures during (A) 1-Hz activation showing uniform propagation, (B) three subsequent reentrant cycles after burst pacing showing a stable activation pattern and PS density and localization during each cycle and (C) five subsequent reentrant cycles after burst pacing showing changes in activation pattern and PS density and localization during each cycle. The direction of activation is indicated by the white arrows, PSs are depicted as white circles. Relationship between rotor frequency and (D) APD_{80}, (E) CV and (F) wavelength and between complexity of reentry and (G) APD_{80}, (H) CV and (I) wavelength.

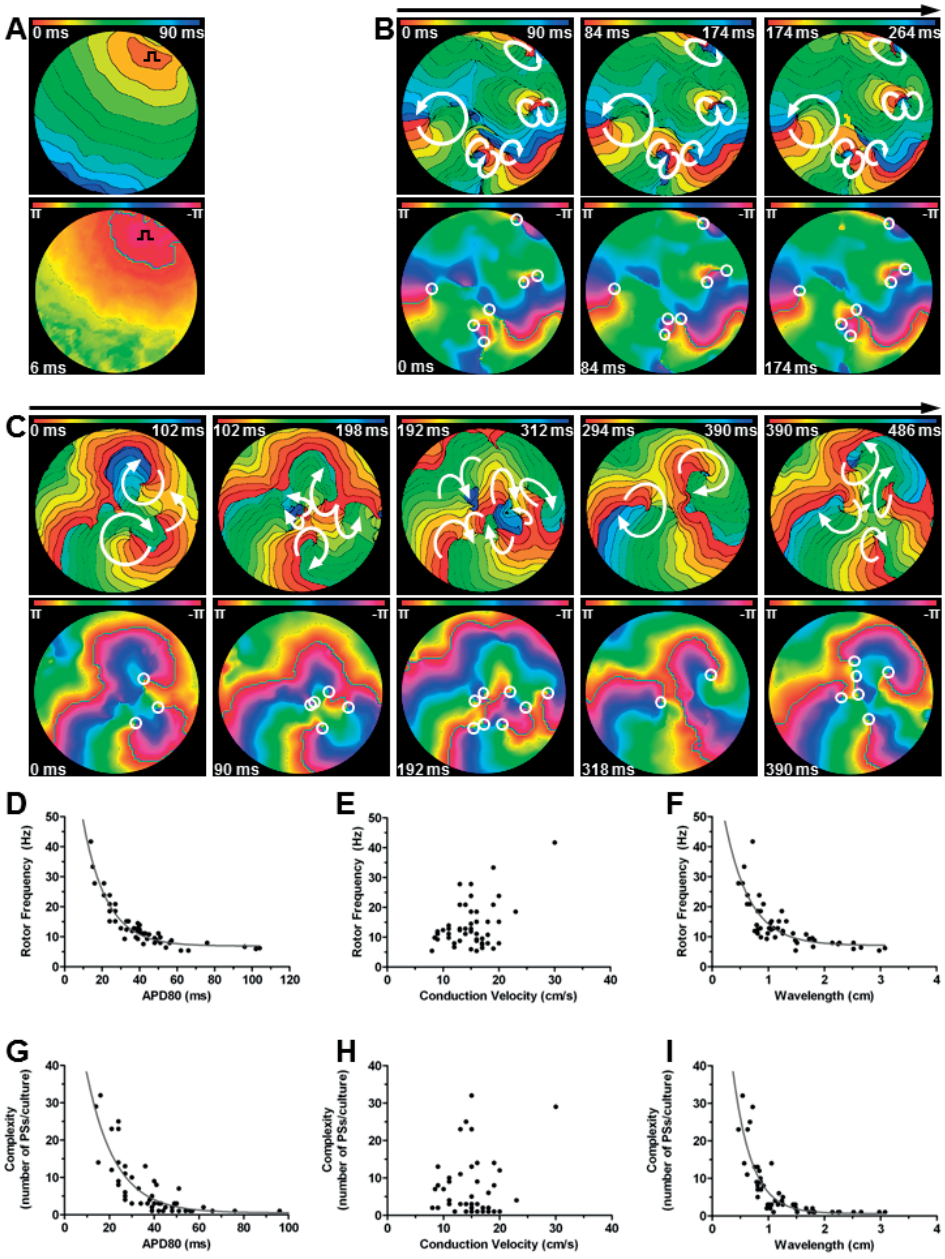
A
0 ms
90 ms
π
-π
6 ms
B
0 ms
90 ms
84 ms
174 ms
174 ms
264 ms
0 ms
84 ms
174 ms
C
0 ms
102 ms
102 ms
198 ms
192 ms
312 ms
294 ms
390 ms
390 ms
486 ms
0 ms
90 ms
192 ms
318 ms
390 ms
D
Rotor Frequency (Hz)
APD80 (ms)
E
Rotor Frequency (Hz)
Conduction Velocity (cm/s)
F
Rotor Frequency (Hz)
Wavelength (cm)
G
Complexity (number of PSs/culture)
APD80 (ms)
H
Complexity (number of PSs/culture)
Conduction Velocity (cm/s)
I
Complexity (number of PSs/culture)
Wavelength (cm)

Figure 1

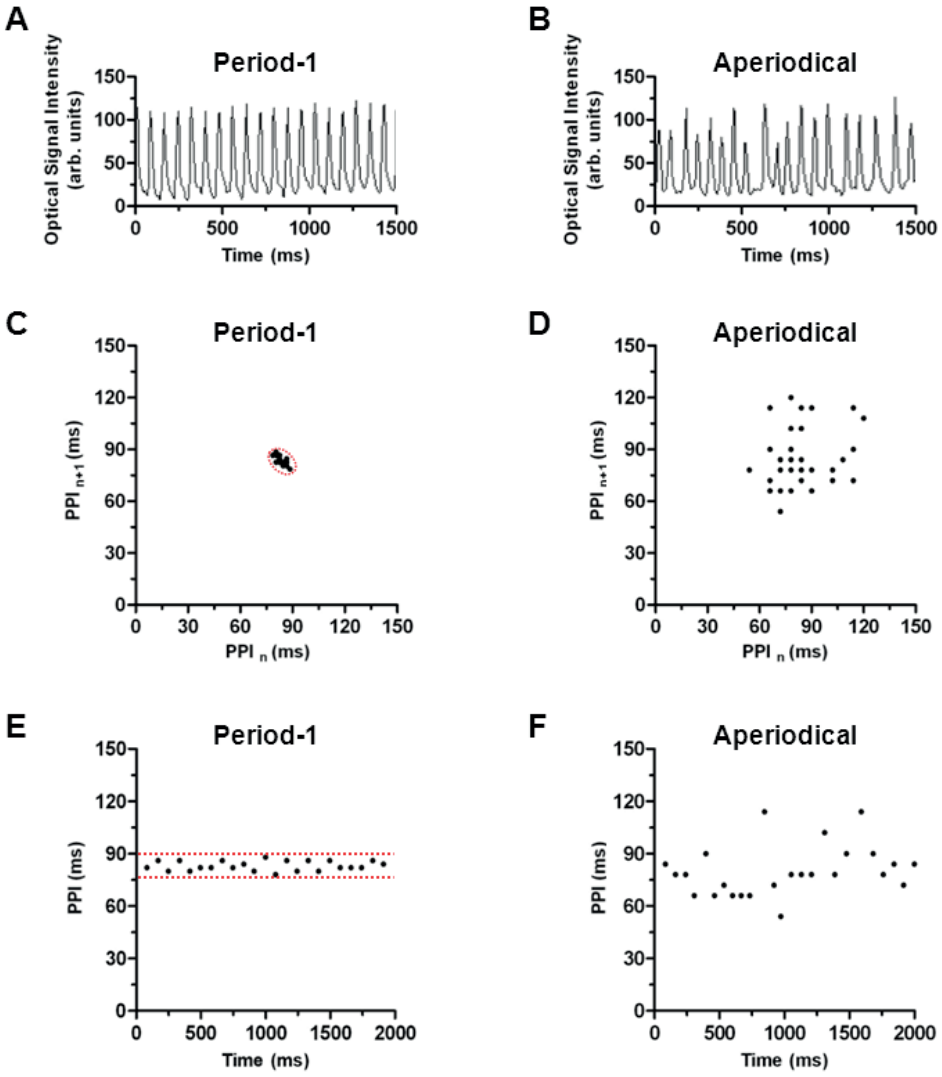

Supplemental Figure II. *Typical examples of the optical signal in neonatal rat atrial CMC cultures with (A) period-1 and (B) aperiodical reentry after burst pacing. Return maps of the peak-to-peak interval (PPI) sequences in an atrial CMC culture after burst pacing with (C) period-1 reentry, characterized by monofocal clustering in the return map and (D) aperiodical reentry, characterized by the absence of clustering in the return map. Time series of the PPIs in an atrial CMC culture with (E) period-1 (corresponding with Supplemental Figure IIA,C and Figure 1B in the main manuscript) and (F) aperiodical reentry (corresponding with Supplemental Figure IIB,D and Figure 1C in the main manuscript). The red dotted lines indicate clustering of PPI sequences and PPIs in the return maps and time series, respectively.*

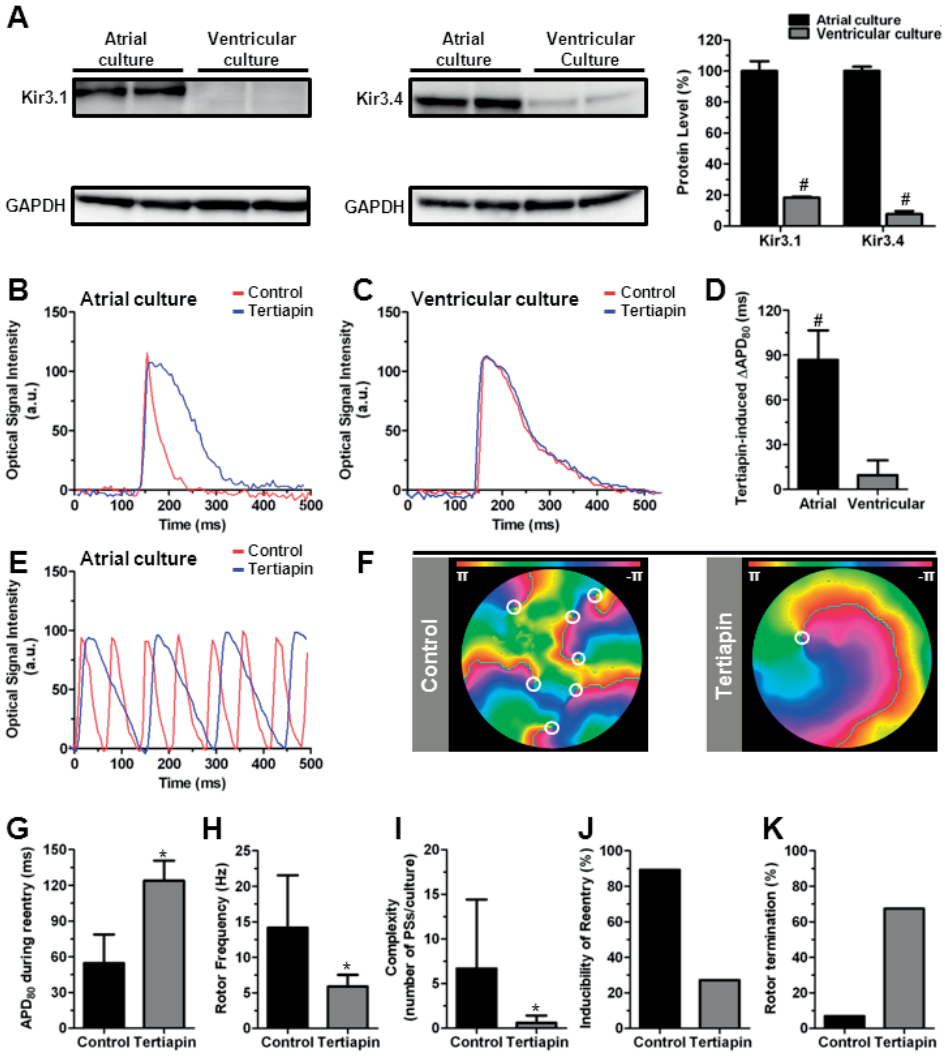

Figure 2 *(A) Western blot analysis of Kir3.1 and Kir3.4 levels in atrial and ventricular nrCMC cultures using GAPDH as loading control. (B,C) Typical optical AP records of untreated (red) and tertiapin-treated (blue) atrial and ventricular nrCMC cultures, respectively. (D) Quantification of ΔAPD_{80} after tertiapin treatment in atrial vs ventricular nrCMC cultures. (E) Typical optical signal records of untreated (red) and tertiapin-treated (blue) atrial nrCMC cultures after induction of AF by burst pacing. (F) Typical phase maps of untreated (left) and tertiapin-treated (right) cultures after burst pacing. White circles indicate PSs. Quantification of (G) APD_{80} during reentry, (H) rotor frequency, (I) complexity of reentry, (J) inducibility of reentry and (K) complete rotor termination in control and tertiapin-treated atrial nrCMC cultures. #: $p<0.05$ vs atrial cultures, *: $p<0.05$ vs control, a.u.: arbitrary units.*

Kcnj3/5 knockdown in atrial nrCMC cultures

To investigate the individual contribution of the molecular determinants of I_{KACh-c} (Kir3.1 and Kir3.4) to the induction and dynamics of AF, expression of *Kcnj3* and *Kcnj5* was specifically downregulated in atrial nrCMC cultures by means of lentiviral, shRNA-mediated RNAi. Kir3.1 and Kir3.4 protein levels were significantly lowered in cultures transduced with LV-Kir3.1↓ and LV-Kir3.4↓, respectively, when compared to those in LV-PpLuc↓-treated control cultures (20.2±1.7 vs 100.0±2.4 and 34.6±3.5 vs 100.0±34.6%, respectively, n=4 per group) (Figure 3A-C). As expected, transduction with LV-Kir3.1↓ (n=11) and LV-Kir3.4↓ (n=20) resulted in significant APD prolongation when compared to PpLuc↓-treated control cultures (n=11) (Figure 3D). APD_{80} was significantly increased throughout all pacing cycle lengths (PCLs) (Figure 3E). Also, CV was lowered significantly by both *Kcnj3* and *Kcnj5* knockdown (Figure 3F), possibly caused by a depolarizing effect of long-term $I_{K,ACh}$ downregulation on the resting membrane potential.

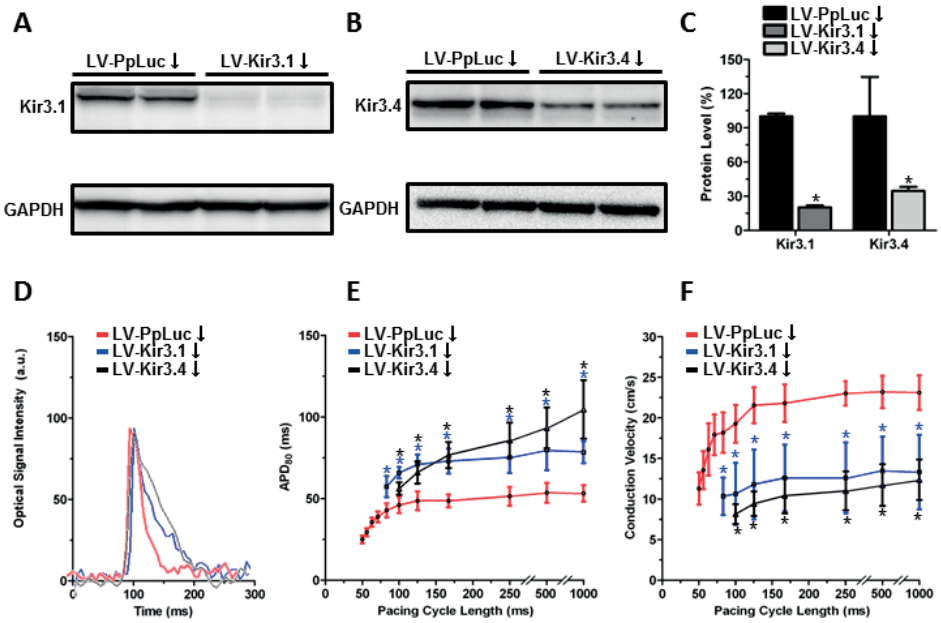

Figure 3. *Western blot of (A) Kir3.1 levels in LV-PpLuc↓ (i.e. control vector)- and LV-Kir3.1↓-transduced atrial nrCMC cultures and (B) Kir3.4 levels in LV-PpLuc↓- and LV-Kir3.4↓-transduced atrial nrCMC cultures using GAPDH as loading control and (C) their quantification. (D) Typical optical signal in atrial nrCMC cultures transduced with the control vector LV-PpLuc↓ or with LV-Kir3.1↓ or LV-Kir3.4↓. Quantification of (E) APD and (F) CV restitution in atrial nrCMC cultures transduced with the control vector LV-PpLuc↓ or with LV-Kir3.1↓ or LV-Kir3.4↓. *: p<0.05 vs LV-PpLuc↓, a.u.: arbitrary units.*

Effect of Kcnj3/5 knockdown on reentry in atrial nrCMC cultures

Next, reentry was induced in cultures transduced with LV-Kir3.1↓(n=14), LV-Kir3.4↓ (n=12) or the control LV (n=19) to investigate the effect of Kir3.x-dependent APD prolongation on spiral waves. As expected, reentrant cycle length was significantly increased after knockdown of either *Kcnj3* or *Kcnj5* (Figure 4A-D,F) consistent with prolongation of APD_{80} during reentry (Figure 4E). Similarly, activation frequency and complexity were significantly decreased (Figure 4G,I, Supplemental Movie 3). In addition, inducibility of reentry was clearly reduced by *Kcnj3* or *Kcnj5* knockdown (Figure 4H). Together, these results show that the effect of tertiapin on reentry induction and dynamics can be reproduced by RNAi-mediated reduction of Kir3.1 or Kir3.4 protein levels.

$I_{K,ACh-c}$ blockade prevents APD alternans by decreasing APD and CV restitution slope

To investigate how $I_{K,ACh-c}$ blockade or downregulation prevents reentry induction we studied the effect of tertiapin on APD and CV restitution. During pacing at 1-20 Hz Kir3.x blockade by tertiapin increased the APD_{80} throughout all PCLs when compared to control cultures (n=8 per group) (Figure 5A). CV was unaltered following 1-2 Hz pacing after tertiapin treatment. However, at higher pacing frequencies, CV was significantly lower in cultures treated with tertiapin (Figure 5B). This was possibly attributable to a change in the maximal diastolic potential, which gets more depolarized at higher pacing frequencies if the APD is prolonged by $I_{K,ACh-c}$ blockade.[20] Furthermore, wavelength was significantly increased by tertiapin at all activation frequencies (Figure 5C). Interestingly, the slope of the APD and CV restitution curves were strongly flattened by tertiapin treatment as a consequence of significantly increased minimal APD_{80} and decreased maximal activation frequency (Figure 5D,E). As the restitution curves naturally become steeper at shorter diastolic intervals (Figure 5A-C), prolonging minimal APD (and thereby decreasing maximal activation frequency) prevents steepening in APD and also CV restitution. Tertiapin treatment decreased the maximal APD restitution slope from 1.0±0.4 to 0.3±0.2 (Supplemental Figure 4A,B), while the percentage of cultures with a maximal APD restitution slope above the critical value of 1[21] decreased from 71.4% to 0% (Supplemental Figure 4C).

As a consequence of restitution moderation, spatial (21.7±8.0 vs 56.5±4.4% in control) and temporal (7.8±6.5 vs 38.1±8.0% in control) dispersion in APD were significantly decreased by Kir3.x blockade (Figure 5F-I). Since steepening in APD and CV restitution causes small PCL changes to result in large APD and CV changes, APD alternans occurred in control but not in tertiapin-treated cultures. During APD alternans at stable PCL in a control culture, as a consequence of the relationship between APD and diastolic interval (see also Figure 5A) a long APD is repeatedly followed by a short APD, because the diastolic interval is shortened after the long APD (Figure 5G). Because the short APD follows

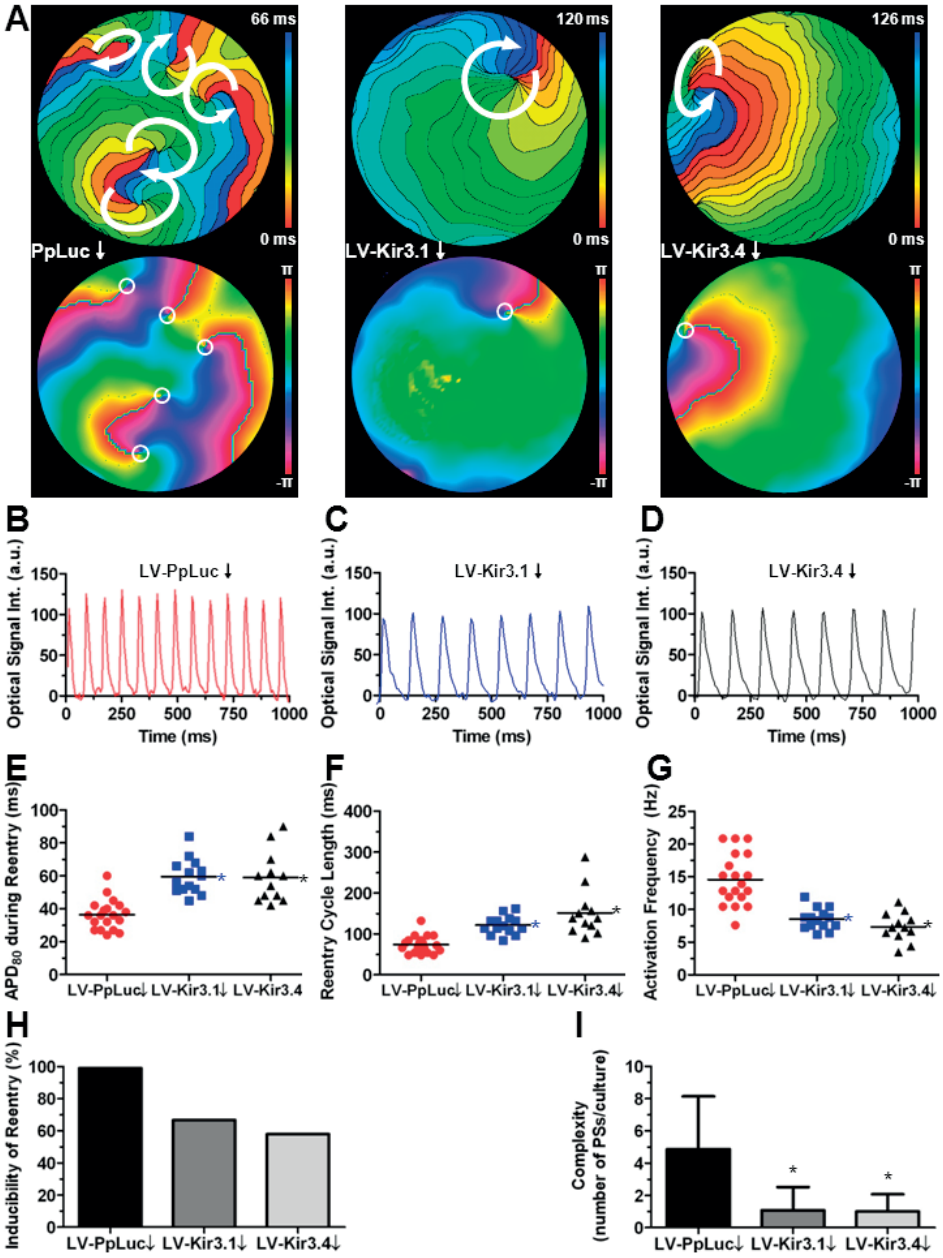

Figure 4. *(A) Activation maps and corresponding phase maps during reentry in atrial nrCMC cultures transduced with the control vector LV-PpLuc↓ or with LV-Kir3.1↓ or LV-Kir3.4↓. White arrows indicate the direction of AP propagation, white circles depict PS position. Optical signal traces during reentry in atrial nrCMC cultures transduced with (B) LV-PpLuc↓, (C) LV-Kir3.1↓ or (D) LV-Kir3.4↓. Quantification of (E) APD, (F) cycle length, (G) activation frequency, (H) inducibility of reentry and (I) complexity of reentry after burst pacing in control (red), LV-Kir3.1↓-transduced (blue) and LV-Kir3.4↓-treated (black) atrial nrCMC cultures. *: p<0.05 vs LV-PpLuc↓, a.u.: arbitrary units.*

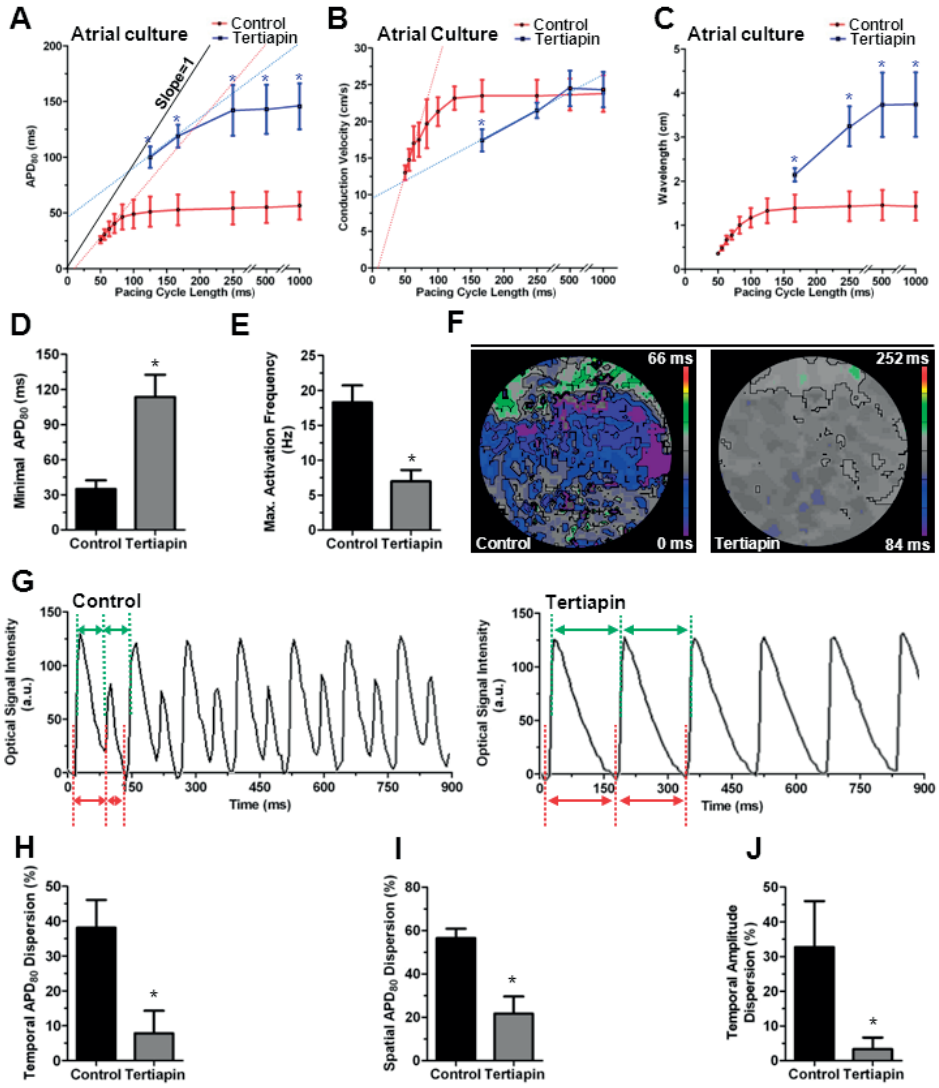

Figure 5. *Restitution of (A) APD_{80}, (B) CV and (C) wavelength during 1-20 Hz pacing in control (red) and tertiapin-treated (blue) atrial nrCMC cultures. Red and blue dotted lines indicate the maximal slopes in the restitution curves, the solid black line indicates slope=1. Quantification of (D) minimal APD and (E) maximal activation frequency in control and tertiapin-treated atrial nrCMC cultures. (F) APD_{80} maps of untreated (left) and tertiapin-treated (right) atrial nrCMC cultures. (G) Typical optical signal traces during pacing at maximal activation frequency in control cultures (left) showing alternating APDs (red double arrows) on equal PCLs (green double arrows) and tertiapin-treated cultures showing stable APDs (red double arrows) on equal PCLs (green double arrows). Quantification of (H) temporal APD_{80} dispersion, (I) spatial APD_{80} dispersion and (J) temporal amplitude dispersion. *: $p<0.05$ vs control, a.u.: arbitrary units.*

after incomplete repolarization during the long AP, amplitude alternans occurs (likely due to inactivation of Na^+ channels as a result of incomplete repolarization). Therefore blockade of $I_{K,ACh-c}$ leads to a significant decrease in temporal amplitude dispersion (Figure 5G,J). Altogether, these findings suggest that I_{KACh-c}-dependent alternans is linked to restitution kinetics (see also Supplemental Results, Supplemental Figure 5).

Role of APD alternans in reentry

In control atrial cultures, reentry initiation after burst pacing was found to be a consequence of highly incident APD alternans, during which a long AP was repeatedly followed by a short AP (Figure 6, left panel). Typically, the long AP was uniformly propagated throughout the culture (Figure 6, right panel, long AP). However, because of the spatial heterogeneity in APD, the short AP frequently underwent conduction block when propagated from an area with short-long APD to an area with long-long APD. This caused PSs to arise adjacent to the area of conduction block (Figure 6, left and right panel, short AP). The AP was subsequently propagated around the PS. This could lead to reentry if the area

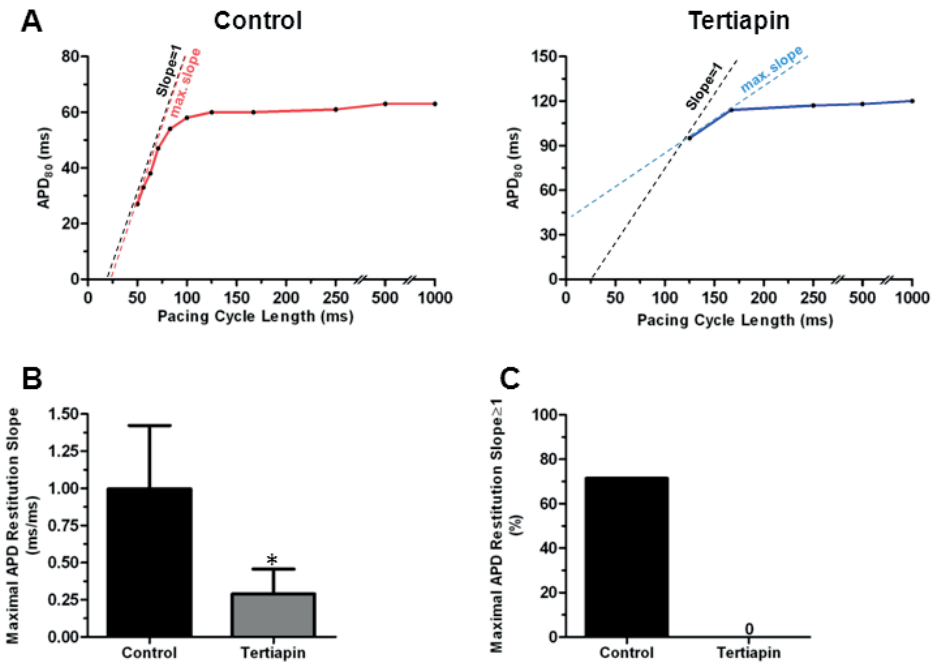

Supplemental Figure IV. *(A) Typical examples of APD restitution curves of a single control (left) and a single tertiapin-treated (right)culture of neonatal rat atrial CMCs, showing that the maximal slope of the curve in the control culture exceeds 1, while the slope in the tertiapin-treated culture remains well below 1. Black dotted lines indicate slope=1. Colored dotted lines indicate the maximal slope in control (red) and tertiapin-treated (blue) cultures. (B) Quantification of the maximal slope in the APD restitution curve of control and tertiapin-treated cultures. (C) Quantification of the percentage of cultures with a maximal slope in the APD restitution curve ≥1.*

in which the conduction block occurred repolarized before return of the wavefront, which then circled the PS in a retrograde fashion (Figure 6, right panel, short AP). These results show that APD alternans, which can be prevented by blockade of $I_{K,ACh-c}$, is a major factor in reentry initiation.

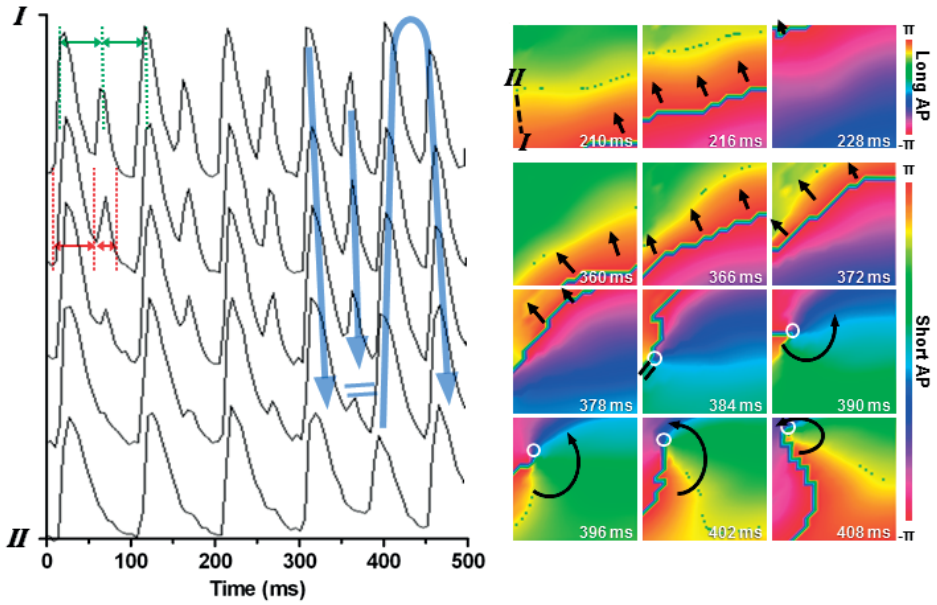

Figure 6. *Typical optical signal traces (graph at left side) in a 9-mm² square in a control atrial nrCMC culture during APD alternans leading to reentry. Green and red dotted lines indicate PCL and alternating APD, respectively. Corresponding phase maps (panels at right side) during uniform propagation of the long AP (top panel) and conduction block followed by circular propagation of the short AP (lower panel). Arrows, double lines (blue in the optical signal traces and black in the phase maps) and white circles indicate the direction of AP propagation, conduction block and the PS position, respectively. The positions of points I and II in the culture are indicated in the upper left phase map.*

Mechanism of rotor termination after IK,ACh blockade

In addition to preventing reentry induction, blockade of $I_{K,ACh}$ terminated a large portion of rotors initiated by burst pacing. Atrial cultures were mapped during addition of tertiapin, to study how $I_{K,ACh}$ blockade led to rotor termination. Interestingly, during tertiapin incubation rotors with P-1 oscillatory dynamics destabilized into period-2 (P-2) and aperiodical reentry before termination (Figure 7 and Supplemental Figure 6). As shown in Figure 5A, incubation of atrial cultures with tertiapin led to an increase in minimal APD and a decrease in the maximal slope of the APD restitution curve. The higher steepness of the restitution slope at-long PCLs in the tertiapin-treated cultures suggests that this slope becomes critically steep before tertiapin has completely increased minimal APD. This caused APD alternans in vulnerable spots during reentry, leading to P-2 oscillatory dynam-

ics (Figure 7, middle panel and Supplemental Figure 6B,D). Subsequently, APD prolonged further and refractory periods around the PSs increased. Consequently, if the refractory period got critically long the reentrant wave had to alter its path from the previous cycle in order to sustain. Therefore, PSs tended to shift position after incubation with tertiapin, leading to aperiodical reentry dynamics (Figure 7, lower panel, Supplemental Figure 6C,D), which simultaneously increased the chance of these PSs to meet a boundary, followed by rotor termination (Figure 7, lower panel, Supplemental Figure 6C,D). As tertiapin increased wavelength and decreased the incidence of APD alternans after full incubation, new rotors are not formed, resulting in a net decrease in complexity of conduction patterns after tertiapin treatment, ultimately leading to termination of AF (Supplemental Movie 4). These results show that apart from affecting reentry initiation and global reentry characteristics, I_{KACh-c} also determines the period dynamics and propensity towards termination by controlling the onset of APD alternans and PS drift during reentry.

Kir3.x blockade in whole heart mapping

Our novel 2D model of atrial tissue appeared to be crucial for a mechanistic understanding of the role of I_{KACh-c} in rotor formation, dynamics and termination, as these events are likely to occur subepicardially in the intact atria, which precludes their direct read-out and interpretation. However, whole heart data are needed to show the effects of I_{KACh-c} on actual AF in a more complex and relevant setting. We thus studied the effects of tertiapin in a whole heart model of AF using neonatal rat hearts. In these hearts, immunocytological analyses confirmed the expression of myosin light chain 2a (MLC2a) in the atria only (Supplemental Figure 7A). The atria consisted of 37.9±12.1% non-myocytes, which were predominantly fibroblasts as judged by α-actinin/collagen-I double staining (Supplemental Figure 7B,C). Consistent with the *in vitro* results, Western blot analyses showed a significantly higher expression of Kir3.1 and Kir3.4 in the atrium when compared to the ventricle (100.0±21.3 vs 13.7±6.0 % $p<0.05$ and 100.0±24.2 vs 22.4±5.2 % $p<0.05$ respectively) (Supplemental Figure 7D). During optical mapping of whole neonatal rat hearts blockade of Kir3.x channels by tertiapin significantly increased atrial APD (62.8±20.9 vs 111.0±32.9 ms, $p<0.05$) in sinus rhythm while the APD in the ventricles was not significantly altered (219.7±57.6 vs 211.8±42.7 ms, $p<0.05$) (n=10 per group) (Figure 8A-C). Atropine treatment had no significant effect on atrial APD (54.7±13.9 vs 62.8±20.9 ms in control hearts) (Supplemental Figure 8 A-C), confirming the M2-receptor independent, constitutive activation of I_{KACh} in neonatal rat atria. After burst pacing, AF was maintained by period-1 oscillatory dynamics in both control and tertiapin-treated hearts. In hearts treated with tertiapin, APD during AF was significantly longer when compared to control hearts (54.8±14.2 ms vs 38.8±7.9, $p<0.05$) (Figure 8D,E). As a consequence, AF cycle length was significantly increased (106.5±10.3 vs 81.3±11.3 ms, $p<0.05$) (Figure 8F), while the inducibility of AF showed a significant decrease after tertiapin incubation

(90% vs 40%, p<0.05) (Figure 8G). Together, these results support the notion that Kir3.x determines the initiation and maintenance of AF in the whole heart.

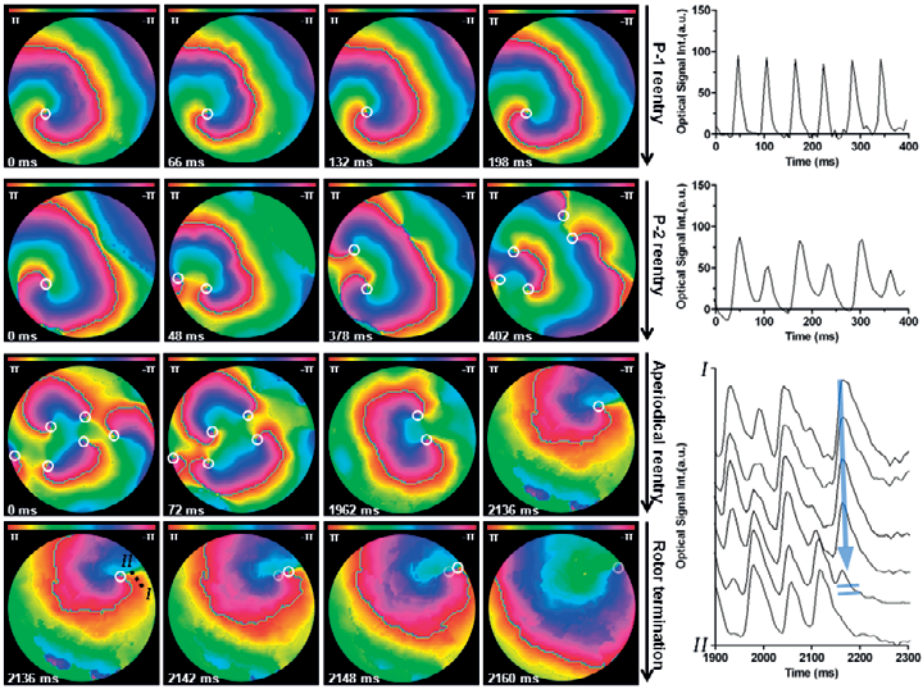

Figure 7. *Phase map sequence of an atrial nrCMC culture during tertiapin incubation. The upper row shows the initial P-1 reentrant arrhythmia rotating around a single stable PS and its corresponding optical signals. The second row shows the change into a P-2 reentry (approximately 4 s after tertiapin addition), with meandering, disappearing and reappearing PSs and its corresponding optical signals showing APD alternans in critical areas. The lower 2 rows show the shift in aperiodical reentry (approximately 9 s after tertiapin addition) followed by the termination of rotors as a consequence of PS drift towards the edge of the culture as the wavefront increasingly meets refractory tissue. The white circles indicate PSs, the translucent white circles indicate the PS position in the previous frame. The lower right graph shows the corresponding AP between point I and II in the culture, where the blue arrow indicates the propagation of the final AP leading to conduction block. a.u.: arbitrary units.*

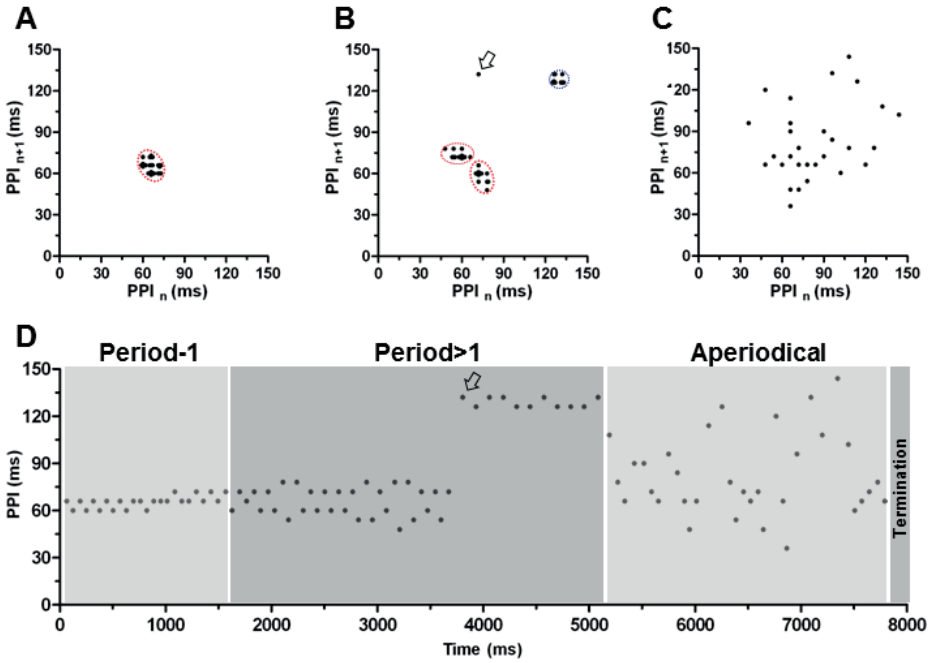

Supplemental Figure VI. *Return maps of the PPI sequences in an atrial CMC culture during (A) typical period-1 reentry showing a single cluster in the return map, (B) the early phase of tertiapin incubation leading to a change into period-2 reentry showing two clusters (red) as a result of APD alternans (See Figure 7 in the main manuscript, second row) and a third cluster (blue) corresponding to the subsequent prolonged reentrant cycle length (temporary 2:1 conduction) starting at the arrow in both subfigures B and D, (C) the late phase of tertiapin incubation leading to aperiodical reentry lacking any clustering in the return map. Dotted red circles indicate clustering of PPI sequences. (D) Time series of the PPIs during the incubation with tertiapin, showing the progression of period-1, to period>1, to aperiodical reentry and eventually termination. The return maps in A-C are each based on a part of the time series separated by the gray rectangles.*

Figure 8 legend. →

*(A) Typical examples of a control neonatal rat heart during optical mapping, showing the real image (left panel; left atrium, right atrium ventricles are indicated by the letters LA, RA and V, respectively), a map of atrial activation sequence during sinus rhythm (middle panel, 6-ms isochrone spacing) and a map of the atrial activation sequence during AF induced by burst pacing (right panel, 6-ms isochrone spacing) showing circular activation in the atrial epicardium (white arrow). The white squares indicate the areas from which typical optical signals were derived. (B) Examples of the optical signal traces in the atrium (red) and ventricle (black) in control (left) and tertiapin-treated hearts (right). Quantification of (C) the APD_{80} in atria and ventricles of control and tertiapin-treated hearts during sinus rhythm and (D) of the atrial APD_{80} during AF. (E) Examples of the optical signal traces during AF after burst pacing in the atrium (red) and ventricle (black) in control and tertiapin-treated hearts. Irregularly appearing ventricular traces are indicative of AF. Quantification of (F) AF cycle length and (G) inducibility of AF by burst pacing in control and tertiapin-treated neonatal rat hearts. *: $p<0.05$ vs control NS: non significant*

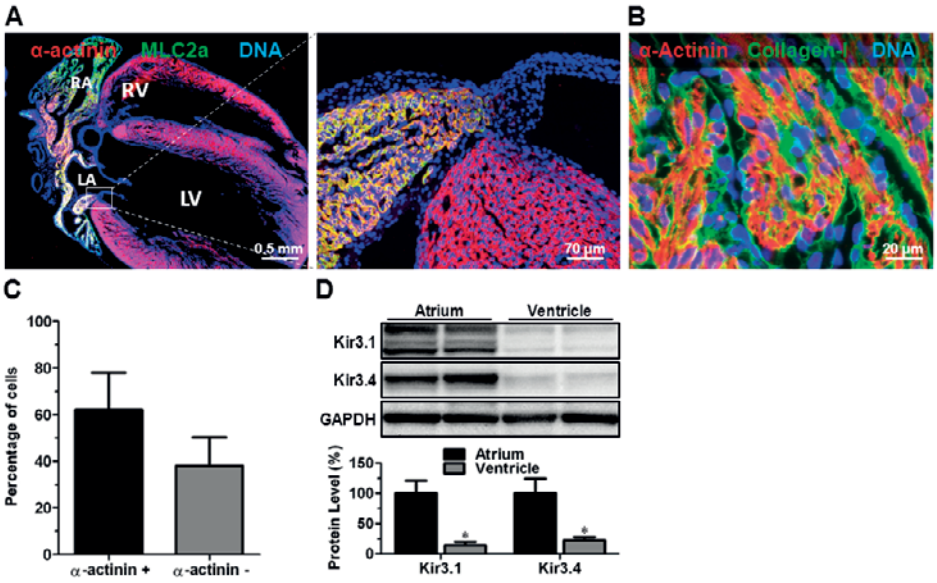

Supplemental Figure VII. *Immunohistological double staining of whole neonatal rat hearts for (A) MLC2a (green) and α-actinin (red) and (B) collagen type I (green) and α-actinin (red). (C) Quantification of the number of α-actinin-positive (i.e. CMCs) and -negative cells (i.e. non-myocytes) as judged by immunohistology. (D) Western blot analysis and quantification of Kir3.1 and Kir3.4 levels in the neonatal rat atrium and ventricle using GAPDH as loading control. LA: left atrium, RA: right atrium, LV: left ventricle, RV: right ventricle, *: p<0.05 vs control.*

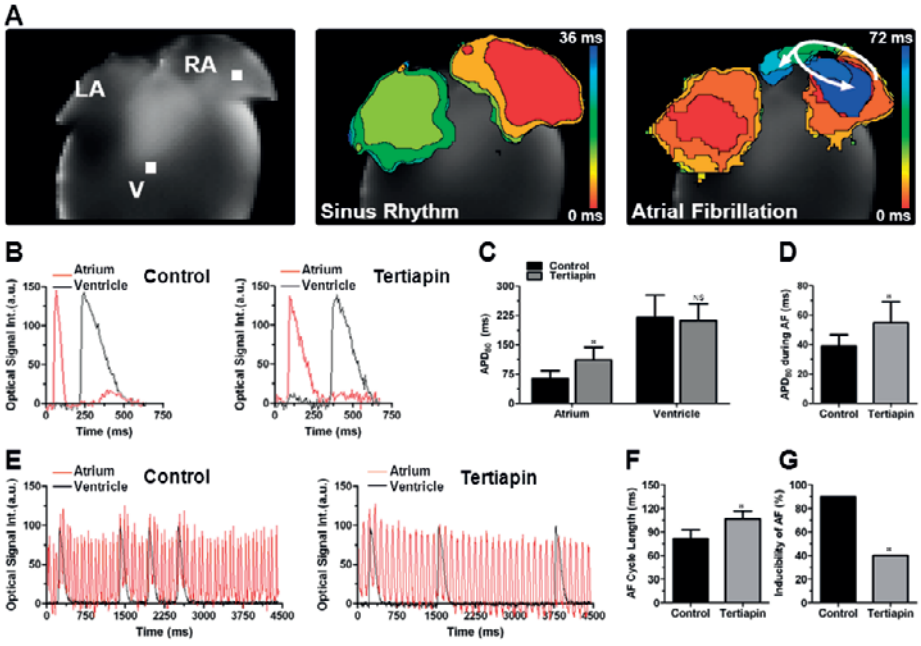

Figure 8.

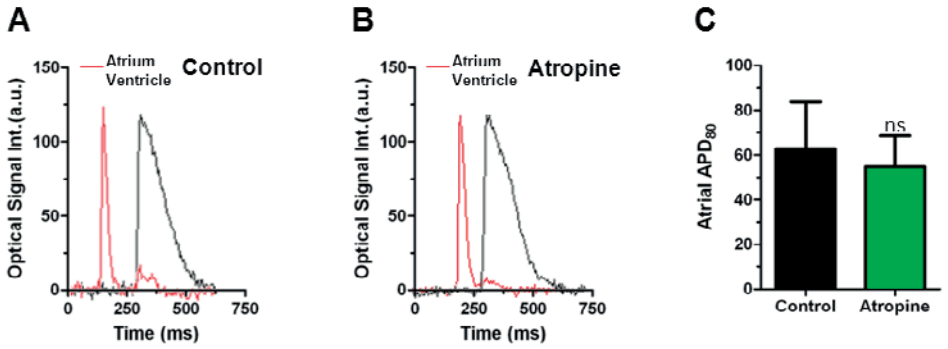

Supplemental Figure VIII. *Typical optical signal traces in the atria (red trace) and ventricles (black trace) of (A) control and (B) atropine-treated neonatal rat hearts. (C) Quantification of APD_{80} in the atria of control and atropine-treated neonatal rat hearts. NS: non-significant vs control,. a.u.: arbitrary units.*

DISCUSSION

The key findings of this study are, (1) the acetylcholine-inducible potassium current (I_{KACh}), mediated by Kir3.x, is highly atrium-specific and constitutively active in neonatal rat atrial cell monolayers and intact atria. (2) In the presence of this current, sustained re-entry can be easily induced electrically (~90% incidence), while the incidence decreases strongly after I_{KACh} blockade. (3) After induction, tachyarrhythmias in atrial cultures are maintained by stable period-1, shifting period>1 or aperiodical rotors, and result from restitution-driven alternans, whereas they are terminated by alternans-mediated PS drift. (4) Mechanistically it is shown by pharmacological and genetic interventions that Kir3.x is a key regulator of these processes of rotor induction, dynamics and termination by controlling APD and APD alternans through APD restitution steepening. (5) Kir3.x represents a promising atrium-specific target for anti-arrhythmic strategies.

Kir3.x in models of AF

Previous studies showed that $I_{K,ACh}$ may play an important role in the onset of AF, as acetylcholine activates $I_{K,ACh}$ during parasympathetic stimulation and thereby shortens APD.[15] However, after atrial remodeling, which occurs for instance during permanent AF, APD is shortened independently of parasympathetic activation, partly because $I_{K,ACh}$ has become constitutively active.[16] While alteration of atrial electrophysiology after atrial remodeling has been established, most of the insights into the electrophysiological mechanisms and complex dynamics of wave propagation in AF have come from detailed investigations in computer and animal models of AF, which did not take into account the molecular consequences of atrial remodeling.[22] Hence, these results may be applicable to paroxysmal AF, but translation to persistent AF and AF after atrial remodeling remains difficult. In the current study, models have been used that include one of these molecular consequences, being constitutive activation of $I_{K,ACh}$. As such, the present models

might provide a novel means to link the molecular biology of (persistent) AF to its basic electrophysiological mechanisms.[22]

We found that the detrimental effects of $I_{K,ACh-c}$ are strongly dependent on Kir3.x expression, as is the case when $I_{K,ACh}$ is activated by increased parasympathetic tone.[14,15] As Kir3.1 homomers do not to form a functional channel,[23,24] the preventive effect of *Kcnj3* knockdown is likely attributable to diminished density of Kir3.1/Kir3.4 heteromers at the sarcolemma, while Kir3.4 downregulation affects both Kir3.4 homomers and Kir3.1/Kir3.4 heteromers. This might explain why a 3-fold reduction in Kir3.4 level produced similar results as a 5-fold decrease in Kir3.1 abundance. While earlier studies show that there is very little contribution of Kir3.4 homomers to $I_{K,ACh}$,[25] our results suggest that after *Kcnj3* knockdown there is still residual $I_{K,ACh-c}$, most likely provided by Kir3.4 homomers, the formation of which is inhibited after *Kcnj5* knockdown. This could imply that the contribution of Kir3.x subunits to $I_{K,ACh}$ and to its constitutively active counterpart differs.

Nevertheless, the effects of tertiapin on APD, rotor frequency, arrhythmia complexity and inducibility were found to be larger than those of Kir3.1 and Kir3.4 downregulation. As the atrial nrCMCs have a higher tolerability for short-term $I_{K,Ach-c}$ blockade by tertiapin as opposed to long-term $I_{K,ACh-c}$ blockade by LV-mediated RNAi, tertiapin treatment could provide a somewhat more efficient blockade of $I_{K,Ach-c}$ at the moment of electrophysiological analysis. Furthermore, long-term downregulation of Kir3.1 or Kir3.4 seemed to induce a depolarization of the cardiomyocyte membrane potential, decreasing CV even at long PCLs. The conduction-slowing effect of *Kcnj3/5* knockdown by shRNAs strongly diminishes its wavelength-prolonging effect. Therefore, we used tertiapin as an alternative means to study the role of $I_{K,Ach-c}$ in AF in whole hearts. The fact that Kir3.1 and Kir3.4 downregulation still strongly decreased inducibility of reentry in atrial cell cultures shows that the effects of $I_{K,ACh-c}$ inhibition on the slopes in the restitution curves prevails over its effects on wavelength.

Mechanisms of AF maintenance

For years there has been an ongoing discussion on whether AF is the consequence of single or multiple ectopic focal discharges, the result of reentrant waves or of randomly appearing and disappearing wavelets.[22] Isolating the pulmonary veins (PV) can be successful in preventing paroxysmal AF, which could be interpreted as evidence for the focal discharge theory.[26] Nevertheless, reentrant sources generating fibrillatory conduction as a consequence of a dominant frequency gradient have been demonstrated in chronic AF.[27] Importantly, in patients with a long history of AF, PV isolation has a low success rate.[5,6] Therefore, at least in permanent AF, reentry seems to play an important role. The presence of a dominant frequency gradient also makes the multiple wavelet hypothesis less plausible, as a hierarchy in frequencies defies randomness as postulated in this theory.[28]

As demonstrated in our models, constitutive activation of $I_{K,ACh}$ may be one of the determinants of the seemingly increasing role of reentry in the maintenance of AF over time. We show that the constitutively active $I_{K,ACh}$ causes APD alternans, making the atrial tissue prone to wavebreak and reentry initiation. In most cases, after reentry is initiated, multiple stable rotors maintain fibrillation. Without ongoing electrical remodeling, emergence of such rotors in the left atrium would lead to fibrillatory conduction to the right atrium. However, in several cultures we observed AF maintained by shifting aperiodical rotors. As the APD and CV restitution can become critically steep if the $I_{K,ACh}$ is constitutively active, causing both spatial and temporal heterogeneity in repolarization, rotors can meander and break up. Therefore, in the remodeled atrium (*c.q.* with constitutively active $I_{K,ACh}$) random wavelets (*i.e.* random rotors of which the propagated wavefront appear as wavelets at the atrial surface) could maintain AF. This could also explain the possibility of AF originating from a rotor in the right atrium with fibrillatory conduction to the left atrium (for instance after left atrium ablation and permanent AF)[28], even though the refractory period is shorter in the left atrium. The fibrillatory aspect of conduction could here be provided by the seemingly random breakup, appearance and disappearance of rotors in the right atrium as opposed to an APD gradient.

APD alternans and AF

Disturbed repolarization is thought to play an important role in producing spatial heterogeneity causing fibrillation in the ventricles. In theory, if fast ectopic firing occurs, for instance from the PVs, spatial heterogeneity in repolarization would also favor reentry initiation in the atria. Hence, it has recently been proposed that repolarization alternans could also play an important role in AF. Indeed, it has been shown that atrial repolarization alternans occurs frequently before initiation of AF.[29-31] In the diseased atrium changes in calcium handling have been shown to cause the APD to alternate as a consequence of calcium instabilities.[32] During calcium-dependent APD alternans, APD restitution is not necessarily altered. We show here for the first time that APD alternans underlying reentry can be caused by constitutive activation of $I_{K,ACh}$ which steepens APD restitution. Hence, we confirm that disturbed atrial repolarization is associated with the onset of AF. In addition to this association we show experimentally that wavebreak and resultant reentry are the direct consequence of APD alternans. Earlier *in silico* work predicted that discordant APD alternans leads to wavebreak if the short AP in a long-short sequence reaches the refractory tail of a long AP in a short-long sequence. In accordance with these predictions, we found that propagation of a short AP of an alternating long-short sequence halts when it meets the refractory tail of a long AP. However, in our model the long AP was usually not the consequence of discordant APD alternans, *e.g.* a short-long sequence. Instead, it was the result of a large APD dispersion causing areas with APD alternans to border areas with solely long APDs. Thus, in our model, we provide

an extension to the aforementioned theory by showing that spatial APD dispersion in combination with APD alternans (while not being classically discordant) can cause AF in cells with constitutively active $I_{K,ACh}$.

Atrial fibrosis in AF

Atrial fibrosis is thought to be an important component of AF substrates.[33] In this study, atrial cell cultures consisted of approximately 17% cardiac fibroblasts as deduced by collagen type I immunostaining. Previous studies showed that atrial conduction abnormalities as a consequence of fibrosis strongly depend on the pattern of fibrosis.[34] It was found that long fibrotic strands of tissue could cause significant conduction abnormalities, and thereby contribute to AF, while diffuse fibrosis only marginally affected conduction. In our *in vitro* model, fibroblasts are diffusely spread. Also, the percentage of fibroblasts in this model is lower than in intact neonatal rat atria (see also Supplemental figures 1F and 7B,C). In spite of this difference in fibroblast content the atrial cell culture and whole heart models yielded very similar results in terms of the inducibility of AF and the ability to suppress AF by $I_{K,Ach-c}$ blockade. Furthermore, in both our *in vitro* and whole heart model, pathological conditions that promote fibrosis are absent. It thus appears that in our models a possible contribution of fibroblast to AF induction is overshadowed by the strong pro-arrhythmic effects of $I_{K,Ach-c}$.

Study limitations

The present study made use of nrCMCs and neonatal rat hearts, which differ electrophysiologically from the more clinically relevant adult human cardiomyocytes and hearts. Use of cardiomyocytes from human adults is hampered by the difficulties to (i) obtain human cardiac tissue of sufficient quality for the isolation of cardiomyocytes and (ii) maintain human cardiomyocytes in a differentiated state during culture. In addition, healthy atrial nrCMCs were used to facilitate the study of Kir3.x and $I_{K,ACh-c}$. It should be noted, however, that constitutive activation of $I_{K,ACh}$ in human atrial myocytes is usually preceded by significant atrial remodeling and hence may have a different origin than in our model. Hence, our study focused on a proof-of principle, investigating the role of $I_{K,ACh}$ on APD alternans, AF prevention and termination irrespective of its onset. As such, the results may not be directly extrapolatable to the clinical setting.

CONCLUSIONS

In neonatal rat atrial cell monolayers and intact atria, the acetylcholine-inducible potassium current is constitutively active and plays a crucial role in the initiation of sustained tachyarrhythmias. Mechanistically it is shown in atrial cell monolayers that I_{KACh-c} is

mediated by Kir3.x and not only regulates the initiation but also the maintenance and termination of these arrhythmias by controlling APD and APD alternans through APD restitution steepening. Accordingly, this study provides insights into the molecular basis of atrium-specific I_{KACh-c} and revealed the crucial role it could play in pro- and anti-arrhythmic mechanisms in atrial tissue. These novel insights could contribute to the development of mechanistically driven and atrium-specific, anti-arrhythmic strategies.

FUNDING

This work was supported by the Dutch Heart Foundation (E. Dekker grant [2012/T023 to B.O.B.]) and the Netherlands Organisation for Scientific Research (NWO; VENI grant [91611070 to D.A.P].

ACKNOWLEDGEMENTS

We wish to thank Huybert J.F. van der Stadt for excellent technical support.

CONFLICT OF INTEREST DISCLOSURES

None.

SUPPLEMENTAL MATERIAL

METHODS

All animal experiments were approved by the Animal Experiments Committee of the Leiden University Medical Center and conformed to the Guide for the Care and Use of Laboratory Animals as stated by the US National Institutes of Health.

Cell isolation and culture

Ventricular and atrial cardiomyocytes (CMCs) were isolated from 2-3 old neonatal Wistar rats by collagenase digestion as described previously.[35] Isoflurane inhalation (4-5%) was used to anaesthetize animals. After adequate anesthesia had been confirmed by the absence of pain reflexes, hearts were excised. Subsequently, large vessels were removed and atria were separated from ventricles. Atrial and ventricular tissue was gently minced and digested using collagenase type 1 (450 U/ml; Worthington, Lakewood, NJ) and DNase I (18,75 Kunitz/ml; Sigma-Aldrich, St. Louis, MO) during 2 subsequent 30-min digestion steps with agitation in a water bath at 37°C. Cell suspensions were pre-plated on Primaria-coated culture dishes (Becton Dickinson, Breda, the Netherlands) for 120 min to allow for preferential attachment of non-myocytes. Next, the unattached cells (mainly CMCs) were passed through a nylon cell strainer with a mesh pore size of 70 µm (Becton Dickinson) to remove cell aggregates and, after counting, the cells were plated isotropically on fibronectin (Sigma-Aldrich)-coated, round glass coverslips (15-mm diameter) in 24-well plates (Corning Life Sciences, Amsterdam, the Netherlands). Cell densities of 2-8×10^5 cells/well were used depending on the experiment. To restrict unwanted expansion of the remaining non-myocytes, cell proliferation was inhibited by incubation with Mitomycin-C (10 µg/ml; Sigma-Aldrich) for 2 h at day 1 of culture as described previously.[35,36] All cultures were refreshed daily with Dulbecco's modified Eagle's medium (DMEM)/HAM's F10 (1:1, v/v; both from Life Technologies, Bleiswijk, the Netherlands) supplemented with 5% horse serum (Life Technologies) and cultured in a humidified incubator at 37°C and 5% CO_2.

Immunocytology

Cells were stained for the markers of interest after several rinses with ice-cold phosphate-buffered saline (PBS) to wash out the culture medium, fixation with 1% formaldehyde in PBS and permeabilization with 0.1% Triton X-100 in PBS. Primary antibodies (1:200 dilution in PBS+5% fetal bovine serum [FBS; Life Technologies]) and corresponding Alexa Fluor 488/568-conjugated secondary antibodies (1:400 dilution in PBS+5% FBS; Life Technologies) were left on the cells for 16 and 2 h, respectively, at 4°C. Cultures were stained using antibodies directed against α-actinin (Sigma-Aldrich) as CMC marker,

myosin light chain 2a (MLC2a; a gift from Dr. S.W. Kubalak, Charleston, SC) and natriuretic peptide precursor A (NPPA, Merck Millipore, Billerica, MA) as markers for atrial CMCs and myosin light chain 2v (MLC2v; Synaptic Systems, Goettingen, Germany) to identify ventricular CMCs. Non-myocytes were characterized immunostaining using antibodies specific for collagen type I (fibroblasts; Abcam, Cambridge, MA), platelet endothelial cell adhesion molecule-1 (PECAM-1; endothelial cells; Abcam) and smooth muscle myosin heavy chain (smMHC; smooth muscle cells; Abcam). Primary antibodies specific for connexin40 (Cx40; Santa Cruz Biotechnology, Dallas, TX) and connexin43 (Cx43; Sigma-Aldrich) were used to determine expression of gap junction proteins. Counterstaining of the nuclei was performed by a 5-min incubation at room temperature with 10 µg/ml Hoechst 33342 (Life Technologies) in PBS+5% FBS. Cells were rinsed twice with PBS+5% FBS after incubation with primary antibodies, secondary antibodies and Hoechst 33342. Coverslips were mounted in Vectashield mounting medium (Vector Laboratories, Burlingame, CA) to minimize photobleaching. Images were taken at equal exposure times between compared groups using a fluorescence microscope equipped with a digital color camera (Nikon Eclipse 80i; Nikon Instruments Europe, Amstelveen, the Netherlands). Dedicated software (NIS Elements [Nikon Instruments Europe] and ImageJ [version 1.43; National Institutes of Health, Bethesda, MD]) were used to store and quantify immunofluorescence signals, respectively. All proteins of interest were studied in at least 3 different cultures per experimental group, from which at least 15 representative images were taken.

Immunohistology

Neonatal rat hearts were rinsed with PBS, fixed overnight using 4% formaldehyde in PBS and dehydrated by immersion in 70% ethanol (3 h), 96% ethanol (3 h), 100% ethanol (3 h) and 1-butanol (overnight), respectively. Hearts were embedded in paraffin, cut in 5-µm-thick sections and mounted on StarFrost adhesive microscope slides (Knittel Glass, Braunschweig, Germany). Next, sections were deparaffinized in xylene and rehydrated by the subsequent immersion in 100% ethanol, 96% ethanol, 70% ethanol and PBS for 5 min each. Antigen retrieval was performed by incubating the slides with 0.05% trypsin and 0.1% $CaCl_2$ in dimineralized water at pH 7.8 for 15 min at 37°C and 15 min at 20°C, respectively. Sections were immunostained overnight with the aforementioned primary antibodies directed against MLC2a, α-actinin and collagen type I diluted 1:100 in PBS with 1% bovine serum albumin (BSA; Sigma-Aldrich) and 1% Tween-20 (PBSBT). Corresponding secondary antibodies (Alexa Fluor 488/568-conjugated antibodies, Life Technologies) diluted in PBSBT were incubated for 2 hours, after which the nuclei were counterstained with 10 µg/ml Hoechst 33342 in PBSBT. Image acquisition, processing and analysis were done using the fluorescence microscope and software described above.

Western blotting

CMC cultures were rinsed twice with ice-cold PBS to wash out the culture medium. Next, the cells were lysed in RIPA buffer (50 mM Tris–HCl [pH 8.0], 150 mM NaCl, 1% Triton X-100, 0.5% sodium deoxycholate, 0.1% sodium dodecyl sulfate supplemented with protease inhibitors [cOmplete, Mini Protease Inhibitor Cocktail Tablet; Roche Applied Science, Penzberg, Germany]). Lysates were subsequently flash frozen in liquid nitrogen, thawed and centrifuged at 4ºC and 21,130×*g* for 15 min to get rid of undissolved material. The protein concentration in the supernatant was determined using BCA Protein Assay Reagent (Thermo Fisher Scientific, Etten-Leur, the Netherlands). Proteins (10 µg per sample; ≥3 samples per group) were then size-fractionated in NuPage Novex 12% Bis-Tris gels (Life Technologies) and transferred to Hybond polyvinylidene difluoride membranes (GE Healthcare, Diegem, Belgium) by wet electroblotting. Membranes were blocked in Tris-based saline, 0.1% Tween-20 (TBST) supplemented with 5% BSA for 1 h at room temperature. Next, the blots were incubated with primary antibodies directed against Cx40 (1:1,000), Cx43 (1:100,000), Kir3.1 (1;1,000; Alomone Labs, Jerusalem, Israel), Kir3.4 (1; 1,000; Santa Cruz Biotechnology), MLC2a (1:200,000), MLC2v (1:5,000), NPPA (1:5,000) and glyceraldehyde 3-phosphate dehydrogenase (1:120,000; loading control; Merck Millipore) for 1 h at room temperature in TBST+5% BSA. Following 3 rinses with TBST, the blots were incubated with appropriate horseradish peroxidase-conjugated secondary antibodies (Santa Cruz Biotechnology) diluted 1:1,000 in TBST+5% BSA for 1 h at room temperature. After another 3 rinses with TBST, membranes were immersed in ECL Prime Western blot detection reagent (GE Healthcare) and chemiluminescence was captured using the ChemiDoc XRS imaging system (Bio-Rad Laboratories, Veenendaal, the Netherlands).

For Western blotting of whole hearts, hearts were excised, atria and ventricles were carefully separated and rinsed in ice-cold PBS before lysis in RIPA buffer using a TissueLyser LT (QIAGEN, Benelux, Venlo, the Netherlands). The whole heart lysates were subsequently processed in the same manner as the lysates of cultured cells.

Construction of self-inactivating lentivirus (SIN-LV) shuttle plasmids

To repress rat *Kcnj3* expression, a SIN-LV shuttle construct encoding a short hairpin (sh) RNA targeting mouse *Kcnj3*, and matching perfectly with the coding sequence of the rat *Kcnj3* gene, was obtained from the MISSION shRNA library (Sigma-Aldrich; clone TRCN0000069736). To knock down rat *Kcnj5* expression, the hybridization product of oligodeoxyribonucleotides 5′ CCGGGACCACAAGAAGATCCCCAAACTCGAGTTTGGGGATCTTCTTGTGGTCTTTTTG 3′ and 5′ AATTCAAAAAGACCACAAGAAGATCCCCAAACTCGAGTTTGGGGATCTTCTTGTGGTC 3′ was inserted in between the unique SgrAI and EcoRI recognition sites of SHC007 (MISSION shRNA library; Sigma-Aldrich) to replace its *Photinus pyralis luciferase (PpLuc)*-specific shRNA-coding sequence. Next, the marker gene cassette in these constructs and in SHC007, which

consisted of the human *phosphoglycerate kinase 1* gene promoter and the puromycin-N-acetyltransferase-coding sequence was replaced by the human *eukaryotic translation elongation factor 1 alpha 1* gene promoter and the *Aequorea victoria* enhanced green fluorescent protein (eGFP)-coding sequence. This yielded the SIN-LV shuttle plasmids pLKO.1-mKcnj3-shRNA.hEEF1a1.eGFP, pLKO.1-rKcnj5-shRNA.hEEF1a1.eGFP and pLKO.1-PpLuc-shRNA.hEEF1a1.eGFP, which were used to generate LV-Kir3.1↓, LV-Kir3.4↓ and LV-PpLuc↓ particles, respectively.

SIN-LV production

Vesicular stomatitis virus G protein-pseudotyped SIN-LV particles were generated by transfecting subconfluent monolayers of 293T cells with the packaging plasmids psPAX2 (Addgene, Cambridge, MA; plasmid number: 12260) and pLP/VSVG (Life Technologies) and one of the 3 aforementioned SIN-LV shuttle constructs at a molar ratio of 2:1:1. The 293T cells were cultured in high-glucose DMEMcontaining 10% FBS. The transfection mixture, which consisted of 40 µg of plasmid DNA and 120 µg of polyethyleneimine (Polysciences Europe, Eppelheim, Germany) in 2 ml of 150 mM NaCl per 175-cm^2 cell culture flask (Greiner Bio-One, Alphen aan den Rijn, the Netherlands) was directly added to the culture medium. Sixteen hours later, the transfection medium in each flask was replaced by 15 ml of DMEM supplemented with 5% FBS and 25 mM HEPES-NaOH (pH 7.4). At 40-48 h after the start of the transfection procedure, the culture medium was harvested and cleared from cellular debris by centrifugation for 10 min at 3,000×*g* and filtration through a 33-mm diameter, 0.45-µm pore size polyethersulfone syringe filter (Millex Express; Merck Millipore). To concentrate and purify the SIN-LV particles, 30 ml of vector suspension were layered onto a 5-ml cushion of 20% (wt/vol) sucrose in PBS and centrifuged at 15,000 rotations per min for 2 h at 4ºC in an SW32 rotor (Beckman Coulter, Fullerton, CA). Next, the supernatant was discarded and the pellet containing the SIN-LV particles was suspended in 500 µl of PBS-1% BSA by gentle rocking overnight at 4ºC. The concentrated vector suspension was divided in 50-100 µl aliquots and stored at -80ºC until use. The 3 SIN-LVs were applied to the atrial CMC cultures at doses that resulted in transduction of essentially all cells in the cultures. The transduction level was assessed using a Zeiss Axiovert 200M inverse fluorescence microscopy to visualize eGFP fluorescence.

In vitro optical mapping

At day 9 of culture, action potential (AP) propagation was investigated on a whole-culture scale by optical mapping using the voltage-sensitive dye di-4-ANEPPS (Life Technologies) as described previously.[35,36] During optical mapping cells were stimulated electrically using a custom-made, epoxy-coated unipolar platinum electrode with square suprathreshold electrical stimuli at 1 and 2-20 Hz (2-Hz increments). Fibrillation was induced by burst pacing with a cycle length of 20-100 ms. A specialized electri-

cal stimulus module with corresponding software (Multichannel Systems, Reutlingen, Germany) was used to perform electrical stimulation. Data analysis and construction of activation maps were performed with specialized software (BrainVision Analyzer 1101; Brainvision, Tokyo, Japan) after pixel signals were averaged with 8 of its nearest neighbors, to minimize noise artifacts. Conduction velocity (CV) in cultures with uniform or reentrant activation patterns was calculated perpendicular to the activation wavefront, between two 3 by 3 pixel grids typically spaced 2-8 mm apart. CV, activation frequency, APD during maximal paced activation frequency (*i.e.* minimal APD) and APD during 1 Hz pacing were determined at 6 different locations equally distributed throughout the culture and averaged before further analysis. APD was determined at 80% of repolarization (APD_{80}) because of the rat AP shape. Wavelength was calculated by multiplying average CV with APD_{80} (for uniform propagation) or reentrant cycle length.[35] Complexity was defined as the number of phase singularities (PSs) per culture, determined by using the phase space method as described previously.[35]The effect of several drugs (100 nmol/L tertiapin [Alomone Labs], 200 nmol/L atropine (Sigma-Aldrich) and 2 µmol/L carbachol (Sigma-Aldrich)[16] was studied by pipetting them directly into the medium, dispersing them by gentle agitation, immediately followed by optical mapping.

Whole heart mapping

Neonatal (2-3 days old) Wistar rats were anesthetized by isoflurane inhalation (4-5%) and adequate anesthesia was confirmed by the absence of pain reflexes. Subsequently, the thoracic wall was cut and lifted to expose the heart. Oxygenated Tyrode's solution (comprising [in mM] NaCl 130, $CaCl_2$ 1.8, KCl 4.0, $MgCl_2$ 1.0, NaH_2PO_4 1.2, $NaHCO_3$ 24 and glucose 5.5 at pH 7.4) supplemented with 20 mM 2,3-butanedione monoxime (Sigma-Aldrich, BDM) with or without 200 nM tertiapin to minimize motion artifacts and to block Kir3.x channels, respectively, was carefully injected in a 200 uL bolus into the left ventricle using a 30-G needle. The heart was excised just prior to absence of visible contractions, and submersed in Tyrode's solution with BDM and tertiapin to remove remaining blood. Next, hearts were incubated in Tyrode's solution with BDM and tertiapin containing 2 µM di-4-ANEPPS for 2 min at 37°C, after which the heart was rinsed and submersed in Tyrode's solution with BDM and tertiapin and placed on top of a 37°C heating plate under the optical mapping camera. AF was induced by burst pacing at a cycle length of 20-100 ms using a custom-made bipolar platinum electrode. Control hearts were treated in an identical manner except that tertiapin was left out during the entire procedure. Typical optical mapping experiments were performed within 6 min after excision of the heart.

RESULTS

Cell culture characterization

Immunocytological analysis at day 9 of culture showed that 100% of the CMCs (*i.e.* α-actinin-positive cells) in the atrial cell cultures were MLC2a-positive (*i.e.* of atrial origin) while in the ventricular cell cultures no MLC2a-positive CMCs were detected (Supplemental Figure IA,C). In addition, NPPA levels were much higher in the atrial than in the ventricular CMC cultures (Supplemental Figure IB). Western blot analyses confirmed these results and showed that MLC2v was exclusively present in the ventricular cell cultures. (Supplemental Figure ID). Atrial CMC cultures contained more Cx40 than the ventricular CMC cultures, while Cx43 levels were higher in ventricular CMCs as judged by both Western blotting (Supplemental Figure ID) and immunocytology (Supplemental Figure IE). Atrial cell cultures were also analyzed by collagen type I, PECAM-1 and smMHC staining. While none of the cells contained detectable amounts of PECAM-1 or smMHC, 17.0±2.5% of the cells stained positive for collagen-I (Supplemental Figure IF) suggesting that the non-myocytes in atrial cell cultures consisted mainly, if not exclusively, of fibroblasts.

Constitutive activation of IKACh in neonatal rat atrial CMC cultures

During constitutive activation I_{KACh} becomes activated independently of acetylcholine or the acetylcholine receptor. Therefore, to confirm constitutive I_{KACh} ($I_{KACh\text{-}c}$) activity in our neonatal rat atrial CMC cultures, atropine (a non-selective muscarinergic receptor antagonist) was used to block the acetylcholine receptor during optical mapping to study the dependence of APD on acetylcholine receptor activation. Atropine had no significant effect on the APD_{80} (38.5±3.9 vs 38.6±3.9 ms in control cultures, p=ns), whereas subsequent treatment with tertiapin significantly increased APD_{80} (to 110.9±13.1 ms, p<0.0001) (Supplemental Figure IIIA,C). This illustrates that after blockade of the acetylcholine receptor there is still current flowing through Kir3.x channels shortening APD. Thus, our cultures of neonatal rat atrial CMCs indeed possess $I_{KACh\text{-}c}$ activity. Nonetheless, treatment of neonatal rat atrial CMCs with carbachol (a non-selective muscarinergic receptor agonist) induced a significant shortening of APD_{80} (from 39.6±4.2 to 29.3±3.9 ms, p<0.0001). After subsequent atropine treatment APD_{80} rose to 45.6±6.9 ms, (p<0.0001 vs carbachol-treated cells) abolishing the carbachol-induced APD shortening, while addition of tertiapin to the carbachol- and atropine-treated CMCs again greatly increased APD_{80} (to 119.8±18.5, p<0.0001 vs [carbachol- and] atropine-treated cells) (Supplemental Figure IIIB,D). Together, these results show that the short AP in neonatal rat atrial CMC cultures is caused by a tertiapin-sensitive current which is independent of ligand-induced muscarinergic receptor activation and therefore constitutively active. The cells, however, also still possess muscarinergic receptor stimulation-dependent Kir3.x activity given the APD shortening-effect of carbachol treatment and its inhibition by atropine.

APD alternans in neonatal rat atrial CMCs is independent of intracellular [Ca2+]

To confirm the restitution-based nature of APD alternans, neonatal rat atrial CMC cultures were treated with the cell-permeable Ca^{2+} chelator BAPTA-AM (10-100 µmol/L; Life Technologies) to rule out the contribution of intracellular Ca^{2+} to APD alternans and reentry induction. Successful buffering of intracellular Ca^{2+} was confirmed by phase contrast microscopy, showing absence of visible contractions after incubation with 10 µmol/L BAPTA-AM during 1-Hz pacing (data not shown).

Treatment with BAPTA-AM did not prevent APD alternans (Supplemental Figure VA), while the frequency of reentry induction after burst pacing remained equal for all tested concentrations of BAPTA-AM (84.6% in controls vs 91.7%, 83.3% and 83.3% after treatment of the cells with 10, 50 or 100 µmol/L BAPTA-AM, respectively) (Supplemental Figure VB). This suggests that APD alternans and consequential reentry induction in our model are driven by the I_{KACh-c}-induced steepness in the APD/CV restitution curve.

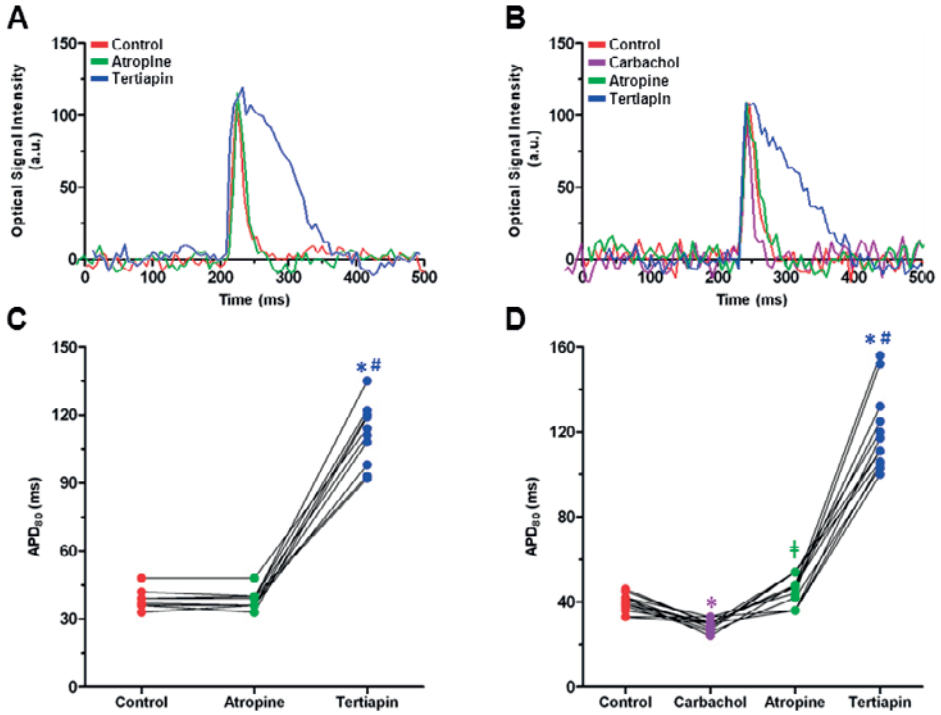

Supplemental Figure III. *(A) Typical examples of optical signal traces in a neonatal rat atrial CMC culture before (control) and after the cumulative treatment with 200 nmol/L atropine and 100 nmol/L tertiapin during 1-Hz pacing. (B) Typical examples of optical signal traces in a neonatal rat atrial CMC culture before (control) and after the cumulative treatment with 2 µmol/L carbachol, 200 nmol/L atropine and 100 nmol/L tertiapin during 1-Hz pacing. (C) Quantification of APD_{80} at a 1-Hz pacing frequency in untreated atrial CMC cultures and in atrial CMC cultures treated with atropine and tertiapin, respectively. (D) Quantification of APD_{80} at a 1-Hz pacing frequency in untreated atrial CMC cultures and in atrial CMC cultures treated with carbachol, atropine and tertiapin, respectively. *: p<0.05 vs control, #: p<0.05 vs atropine, ǂ: p<0.05 vs carbachol.*

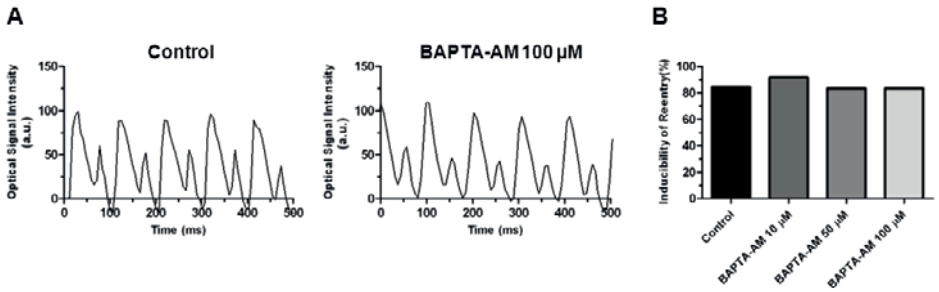

Supplemental Figure V. *(A) Typical examples of optical signal traces of control (left) and BAPTA-AM-treated (right) neonatal rat atrial CMC cultures at maximal activation frequency in areas showing APD alternans (B) Quantification of reentry inducibility in control cultures and in cultures treated with 10 µmol/L, 50 µmol/L or 100 µmol/L BAPTA-AM showing no difference in the induction of reentry by burst pacing during buffering of intracellular Ca^{2+}.*

Movie 1: *Typical example from an optical mapping experiment in a neonatal rat atrial CMC culture after burst pacing showing period-1 reentry dynamics. The first part shows the high-pass-filtered optical signal exemplifying the repeating activation pattern during period-1 reentry. The second part displays the phase map progression of the same optical mapping experiment, showing the wave propagation around multiple PSs with fixed positioning throughout the experiment.*

Movie 2: *Typical example from an optical mapping experiment in a neonatal rat atrial CMC culture after burst pacing showing aperiodical reentry dynamics. The first part shows the high-pass-filtered optical signal exemplifying the transient activation pattern during aperiodical reentry. The second part displays the phase map progression of the same optical mapping experiment, showing multiple instances of PS formation and disappearance leading to aperiodical dynamics.*

Movie 3: *Typical example from an optical mapping experiment in neonatal rat atrial cultures investigating the effect of treatment with LV-Kir3.1↓, LV-Kir3.4↓ or the control vector LV-PpLuc↓ after reentry induction by burst pacing. The high-pass-filtered optical signal shows less complex conduction patternsand a lower activation frequency in cell cultures that had been transduced with the Kcnj3- or Kcnj5-specific shRNA-coding SIN-LV than in those exposed to the control vector.*

Movie 4: *Typical movie from optical mapping experiment investigating the effect of tertiapin on reentry dynamics and termination. Part 1 shows the high-pass-filtered optical signal in an atrial culture after burst pacing during the first 500 ms after tertiapin incubation, which is characterized by persisting rotors and period-1 dynamics. The second part shows the high-pass-filtered optical signal in an atrial culture after a few seconds of tertiapin incubation, characterized by drifting rotors and aperiodical dynamics, which is followed by termination (part 3) when the last rotor collides with the culture boundary.*

REFERENCE LIST

1. Lloyd-Jones DM, Wang TJ, Leip EP, Larson MG, Levy D, Vasan RS, D'Agostino RB, Massaro JM, Beiser A, Wolf PA, Benjamin EJ. Lifetime risk for development of atrial fibrillation: the Framingham Heart Study. *Circulation*. 2004;110:1042-1046.
2. Miyasaka Y, Barnes ME, Bailey KR, Cha SS, Gersh BJ, Seward JB, Tsang TS. Mortality trends in patients diagnosed with first atrial fibrillation: a 21-year community-based study. *J Am Coll Cardiol*. 2007;49:986-992.
3. Wolowacz SE, Samuel M, Brennan VK, Jasso-Mosqueda JG, Van Gelder IC. The cost of illness of atrial fibrillation: a systematic review of the recent literature. *Europace*. 2011;13:1375-1385.
4. Calkins H, Kuck KH, Cappato R, Brugada J, Camm AJ, Chen SA, Crijns HJ, Damiano RJ, Jr., Davies DW, DiMarco J, Edgerton J, Ellenbogen K, Ezekowitz MD, Haines DE, Haissaguerre M, Hindricks G, Iesaka Y, Jackman W, Jalife J, Jais P, Kalman J, Keane D, Kim YH, Kirchhof P, Klein G, Kottkamp H, Kumagai K, Lindsay BD, Mansour M, Marchlinski FE, McCarthy PM, Mont JL, Morady F, Nademanee K, Nakagawa H, Natale A, Nattel S, Packer DL, Pappone C, Prystowsky E, Raviele A, Reddy V, Ruskin JN, Shemin RJ, Tsao HM, Wilber D. 2012 HRS/EHRA/ECAS Expert Consensus Statement on Catheter and Surgical Ablation of Atrial Fibrillation: recommendations for patient selection, procedural techniques, patient management and follow-up, definitions, endpoints, and research trial design. *Europace*. 2012;14:528-606.
5. Oral H, Knight BP, Tada H, Ozaydin M, Chugh A, Hassan S, Scharf C, Lai SW, Greenstein R, Pelosi F, Jr., Strickberger SA, Morady F. Pulmonary vein isolation for paroxysmal and persistent atrial fibrillation. *Circulation*. 2002;105:1077-1081.
6. Brooks AG, Stiles MK, Laborderie J, Lau DH, Kuklik P, Shipp NJ, Hsu LF, Sanders P. Outcomes of long-standing persistent atrial fibrillation ablation: a systematic review. *Heart Rhythm*. 2010;7:835-846.
7. Cappato R, Calkins H, Chen SA, Davies W, Iesaka Y, Kalman J, Kim YH, Klein G, Packer D, Skanes A. Worldwide survey on the methods, efficacy, and safety of catheter ablation for human atrial fibrillation. *Circulation*. 2005;111:1100-1105.
8. Weerasooriya R, Khairy P, Litalien J, Macle L, Hocini M, Sacher F, Lellouche N, Knecht S, Wright M, Nault I, Miyazaki S, Scavee C, Clementy J, Haissaguerre M, Jais P. Catheter ablation for atrial fibrillation: are results maintained at 5 years of follow-up? *J Am Coll Cardiol*. 2011;57:160-166.
9. Coplen SE, Antman EM, Berlin JA, Hewitt P, Chalmers TC. Efficacy and safety of quinidine therapy for maintenance of sinus rhythm after cardioversion. A meta-analysis of randomized control trials. *Circulation*. 1990;82:1106-1116.
10. Echt DS, Liebson PR, Mitchell LB, Peters RW, Obias-Manno D, Barker AH, Arensberg D, Baker A, Friedman L, Greene HL, . Mortality and morbidity in patients receiving encainide, flecainide, or placebo. The Cardiac Arrhythmia Suppression Trial. *N Engl J Med*. 1991;324:781-788.
11. Ehrlich JR and Nattel S. Novel approaches for pharmacological management of atrial fibrillation. *Drugs*. 2009;69:757-774.
12. Hohnloser SH and Singh BN. Proarrhythmia with class III antiarrhythmic drugs: definition, electrophysiologic mechanisms, incidence, predisposing factors, and clinical implications. *J Cardiovasc Electrophysiol*. 1995;6:920-936.
13. Waldo AL, Camm AJ, deRuyter H, Friedman PL, MacNeil DJ, Pauls JF, Pitt B, Pratt CM, Schwartz PJ, Veltri EP. Effect of d-sotalol on mortality in patients with left ventricular dysfunction after recent and remote myocardial infarction. The SWORD

Investigators. Survival With Oral d-Sotalol. *Lancet*. 1996;348:7-12.

14. Dobrzynski H, Marples DD, Musa H, Yamanushi TT, Henderson Z, Takagishi Y, Honjo H, Kodama I, Boyett MR. Distribution of the muscarinic K+ channel proteins Kir3.1 and Kir3.4 in the ventricle, atrium, and sinoatrial node of heart. *J Histochem Cytochem*. 2001;49:1221-1234.
15. Liu L and Nattel S. Differing sympathetic and vagal effects on atrial fibrillation in dogs: role of refractoriness heterogeneity. *Am J Physiol*. 1997;273:H805-H816.
16. Dobrev D, Friedrich A, Voigt N, Jost N, Wettwer E, Christ T, Knaut M, Ravens U. The G protein-gated potassium current I(K,ACh) is constitutively active in patients with chronic atrial fibrillation. *Circulation*. 2005;112:3697-3706.
17. Ehrlich JR, Cha TJ, Zhang L, Chartier D, Villeneuve L, Hebert TE, Nattel S. Characterization of a hyperpolarization-activated time-dependent potassium current in canine cardiomyocytes from pulmonary vein myocardial sleeves and left atrium. *J Physiol*. 2004;557:583-597.
18. Bingen BO, Askar SF, Schalij MJ, Kazbanov IV, Ypey DL, Panfilov AV, Pijnappels DA. Prolongation of Minimal Action Potential Duration in Sustained Fibrillation Decreases Complexity by Transient Destabilization. *Cardiovasc Res*. 2012;97:161-170
19. Askar SF, Ramkisoensing AA, Schalij MJ, Bingen BO, Swildens J, van der Laarse A, Atsma DE, de Vries AA, Ypey DL, Pijnappels DA. Antiproliferative treatment of myofibroblasts prevents arrhythmias in vitro by limiting myofibroblast-induced depolarization. *Cardiovasc Res*. 2011;90:295-304.
20. Kleber AG and Rudy Y. Basic mechanisms of cardiac impulse propagation and associated arrhythmias. *Physiol Rev*. 2004;84:431-488.
21. Nolasco JB and Dahlen RW. A graphic method for the study of alternation in cardiac action potentials. *J Appl Physiol*. 1968;25:191-196.
22. Jalife J. Deja vu in the theories of atrial fibrillation dynamics. *Cardiovasc Res*. 2011;89:766-775.
23. Hedin KE, Lim NF, Clapham DE. Cloning of a Xenopus laevis inwardly rectifying K+ channel subunit that permits GIRK1 expression of IKACh currents in oocytes. *Neuron*. 1996;16:423-429.
24. Krapivinsky G, Gordon EA, Wickman K, Velimirovic B, Krapivinsky L, Clapham DE. The G-protein-gated atrial K+ channel IKACh is a heteromultimer of two inwardly rectifying K(+)-channel proteins. *Nature*. 1995;374:135-141.
25. Bettahi I, Marker CL, Roman MI, Wickman K. Contribution of the Kir3.1 subunit to the muscarinic-gated atrial potassium channel IKACh. *J Biol Chem*. 2002;277:48282-48288.
26. Medi C, Sparks PB, Morton JB, Kistler PM, Halloran K, Rosso R, Vohra JK, Kumar S, Kalman JM. Pulmonary vein antral isolation for paroxysmal atrial fibrillation: results from long-term follow-up. *J Cardiovasc Electrophysiol*. 2011;22:137-141.
27. Kalifa J, Jalife J, Zaitsev AV, Bagwe S, Warren M, Moreno J, Berenfeld O, Nattel S. Intra-atrial pressure increases rate and organization of waves emanating from the superior pulmonary veins during atrial fibrillation. *Circulation*. 2003;108:668-671.
28. Hocini M, Nault I, Wright M, Veenhuyzen G, Narayan SM, Jais P, Lim KT, Knecht S, Matsuo S, Forclaz A, Miyazaki S, Jadidi A, O'Neill MD, Sacher F, Clementy J, Haissaguerre M. Disparate evolution of right and left atrial rate during ablation of long-lasting persistent atrial fibrillation. *J Am Coll Cardiol*. 2010;55:1007-1016.
29. Narayan SM, Bode F, Karasik PL, Franz MR. Alternans of atrial action potentials during atrial flutter as a precursor to atrial fibrillation. *Circulation*. 2002;106:1968-1973.
30. Gong Y, Xie F, Stein KM, Garfinkel A, Culianu CA, Lerman BB, Christini DJ.

Mechanism underlying initiation of paroxysmal atrial flutter/atrial fibrillation by ectopic foci: a simulation study. *Circulation*. 2007;115:2094-2102.

31. Hiromoto K, Shimizu H, Furukawa Y, Kanemori T, Mine T, Masuyama T, Ohyanagi M. Discordant repolarization alternans-induced atrial fibrillation is suppressed by verapamil. *Circ J*. 2005;69:1368-1373.
32. Tsai CT, Chiang FT, Tseng CD, Yu CC, Wang YC, Lai LP, Hwang JJ, Lin JL. Mechanical stretch of atrial myocyte monolayer decreases sarcoplasmic reticulum calcium adenosine triphosphatase expression and increases susceptibility to repolarization alternans. *J Am Coll Cardiol*. 2011;58:2106-2115.
33. Schotten U, Verheule S, Kirchhof P, Goette A. Pathophysiological mechanisms of atrial fibrillation: a translational appraisal. *Physiol Rev*. 2011;91:265-325.
34. Kawara T, Derksen R, de Groot JR, Coronel R, Tasseron S, Linnenbank AC, Hauer RN, Kirkels H, Janse MJ, de Bakker JM. Activation delay after premature stimulation in chronically diseased human myocardium relates to the architecture of interstitial fibrosis. *Circulation*. 2001;104:3069-3075.
35. Bingen BO, Askar SF, Schalij MJ, Kazbanov IV, Ypey DL, Panfilov AV, Pijnappels DA. Prolongation of minimal action potential duration in sustained fibrillation decreases complexity by transient destabilization. *Cardiovasc Res*. 2013;97:161-170.
36. Askar SF, Ramkisoensing AA, Schalij MJ, Bingen BO, Swildens J, van der Laarse A, Atsma DE, de Vries AA, Ypey DL, Pijnappels DA. Antiproliferative treatment of myofibroblasts prevents arrhythmias in vitro by limiting myofibroblast-induced depolarization. *Cardiovasc Res*. 2011;90:295-304.

Chapter V

Constitutively Active Acetylcholine-Dependent Potassium Current Increases Atrial Defibrillation Threshold by Favoring Post-Shock Re-Initiation.

Role of I_{KACh-c} in Atrial Defibrillation Threshold

Brian O. Bingen, MD; Saïd F. A. Askar, PhD; Zeinab Neshati, MSc; Iolanda Feola, MSc; Alexander V. Panfilov, PhD; Martin J. Schalij, MD, PhD; Antoine A. F. de Vries, PhD; Daniël A. Pijnappels, PhD.

Sci Rep 2015;5:15187

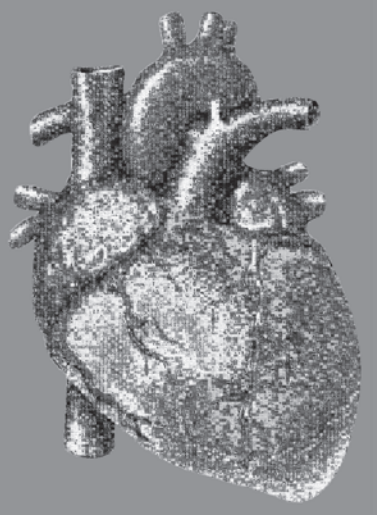

ABSTRACT

Electrical cardioversion (ECV), a mainstay in atrial fibrillation (AF) treatment, is unsuccessful in up to 10-20% of patients. An important aspect of the remodeling process caused by AF is the constitutive activition of the atrium-specific acetylcholine-dependent potassium current (IK,ACh→IK,ACh-c), which is associated with ECV failure. This study investigated the role of IK,ACh-c in ECV failure and setting the atrial defibrillation threshold (aDFT) in optically mapped neonatal rat cardiomyocyte monolayers. AF was induced by burst pacing followed by application of biphasic shocks of 25-100V to determine aDFT. Blocking IK,ACh-c by tertiapin significantly decreased DFT, which correlated with a significant increase in wavelength during reentry. Genetic knockdown experiments, using lentiviral vectors encoding a Kcnj5-specific shRNA to modulate IK,ACh-c, yielded similar results.

Mechanistically, failed ECV was attributed to incomplete phase singularity (PS) removal or reemergence of PSs (i.e. re-initiation) through unidirectional propagation of shock-induced action potentials. Re-initiation occurred at significantly higher voltages than incomplete synchronization and was inhibited by IK,ACh-c blockade. Whole-heart mapping confirmed our findings showing a 60% increase in ECV success rate after IK,ACh-c blockade.

This study provides new mechanistic insight into failing ECV of AF and identifies IK,ACh-c as possible atrium-specific target to increase ECV effectiveness, while decreasing its harmfulness.

INTRODUCTION

Atrial fibrillation (AF) is the most common cardiac arrhythmia in humans.1 Over time, AF usually progresses from paroxysmal, to persistent and finally to permanent AF, partly due to the effect of AF on the arrhythmogenic substrate and/or progression of underlying structural heart disease.2,3 While short self-terminating episodes of AF may remain asymptomatic, the occurrence of longer episodes is associated with morbidity and mortality.2,4-6 Hence, it is important to quickly convert AF to sinus rhythm in order to ameliorate symptoms and to prevent complications, but also to reduce AF-induced atrial remodeling leading to further AF progression. Consequently, termination of AF by electrical cardioversion (ECV) remains the mainstay of acute AF treatment.7,8

While progression of AF increases the need for ECV, it is also an independent predictor of ECV failure.9,10 ECV may fail to convert AF to sinus rhythm in as much as 10-20% of patients, although the rate of success also depends on the energy applied.9,11 However, perpetually increasing the energy of ECV in case of failure is undesirable, as this is associated with a progressive tendency for adverse events.12,13 To improve acute AF treatment it is essential to increase the effectiveness of ECV and decrease the energy required for successful cardioversion, i.e. the atrial defibrillation threshold (aDFT).

A major aspect of the electrophysiological remodeling process associated with AF progression is the shortening of repolarization caused by (among other factors such as decreased L-type calcium current and increased inward rectifier potassium current) constitutive activity of the acetylcholine-dependent potassium current (IK,ACh→IK,ACh-c).14-17 Remodeling of IK,ACh-c may therefore play a pivotal role in the diminishing success of ECV with AF progression. IK,ACh is mediated by the Kir3.x family of potassium channels, which are expressed in the atria, but not in the ventricles.18, As anti-arrhythmic drugs targeting ion channels shared between atria and ventricles have been shown to increase the burden of ventricular arrhythmias,19,20 modulation of IK,ACh-c (as a consequence of its atrial specificity) might provide the advantage of decreasing aDFT without risking alteration of ventricular electrophysiology. However, whether IK,ACh-c affects the ECV success rate and, if so, by which mechanism, remains to be elucidated. Therefore the effects of IK,ACh-c on ECV success rate in a 2D model of reentrant atrial tachyarrhythmias were investigated. Complementary experiments were performed in a whole-heart AF model. Selective inhibition of Kir3.x activity was accomplished using tertiapin or by lentiviral vector (LV)-mediated RNA interference (RNAi).

RESULTS

IK,ACh-c blockade decreases aDFT

To test the hypothesis that IK,ACh-c affects the atrial defibrillation success rate or the aDFT, fibrillating atrial cardiomyocyte (aCMC) cultures were treated with tertiapin (a blocker of IK,ACh-c) before being subjected to electric shocks of 25-100 V in order to determine the DFT. Tertiapin treatment notably increased the success rate of defibrillation compared to untreated controls (from 36.3 to 80.0% at 50 V and from 91.0 to 100.0% at 100 V, Figure 1D). The increase in success rate was accompanied by a significant decrease in DFT from 60.0±25.1 V in control aCMC cultures (n=33) to 35.5±10.9 V in tertiapin-treated aCMC cultures (n=10; $p<0.05$) (Figure 1E).

IK,ACh-c blockade decreases aDFT by increasing wavelength

To elucidate the mechanisms by which IK,ACh-c blockade decreased the DFT, we first investigated the effects of tertiapin on several electrophysiological parameters (i.e. conduction velocity [CV], action potential [AP] duration at 80% repolarization [APD80], wavelength, reentry cycle length and complexity). Tertiapin (n=10) significantly increased APD80 in aCMCs during reentry (54.0±20.7 vs 25.8±4.6 ms in control cultures [n=33]) (Supplemental Figure 2A,B), in the absence of acetylcholine, confirming the presence of constitutively active IK,ACh in the aCMC cultures.18 The CV during reentry was not significantly affected (9.5±2.8 vs 11.7±2.9 cm/s in control cultures) (Supplemental Figure 2A,C). Hence, the wavelength (determined by the product of APD and CV) was significantly increased by tertiapin treatment (0.48±0.15 vs 0.30±0.10 cm in control cultures) (Supplemental Figure 2A,D). Through this increase in wavelength, IK,ACh-c blockade both caused a significant increase in reentry cycle length (106.2±28.5 vs 61.9±18.1 ms in control cultures) (Supplemental Figure 2A,E) and decrease in arrhythmia complexity (2.5±3.5 vs 5.06±5.06 PSs in control cultures) (Supplemental Figure 2A,F).

Subsequently, DFT was plotted as a function of CV, APD80, wavelength, reentry cycle length or complexity. As shown in Supplemental Figure 3A, CV did not show any apparent relationship with DFT (R2=0.12). Furthermore, both reentry cycle length and APD80 displayed a weak inverse (hyperbolic-like) relationship with DFT (R2=0.24 and 0.34, respectively) (Supplemental Figure 3B,C). DFT seemed to increase concordantly with the complexity of the arrhythmia, although this correlation was not very strong (R2=0.51, Supplemental Figure 3D). In contrast, a more apparent relationship was found between wavelength and DFT, which showed an increase in DFT with decreasing wavelengths (R2=0.65, Supplemental Figure 3E). Together, these results suggest that a blockade of IK,ACh-c decreases DFT through the resulting increase of the wavelength during reentrant tachyarrhythmias.

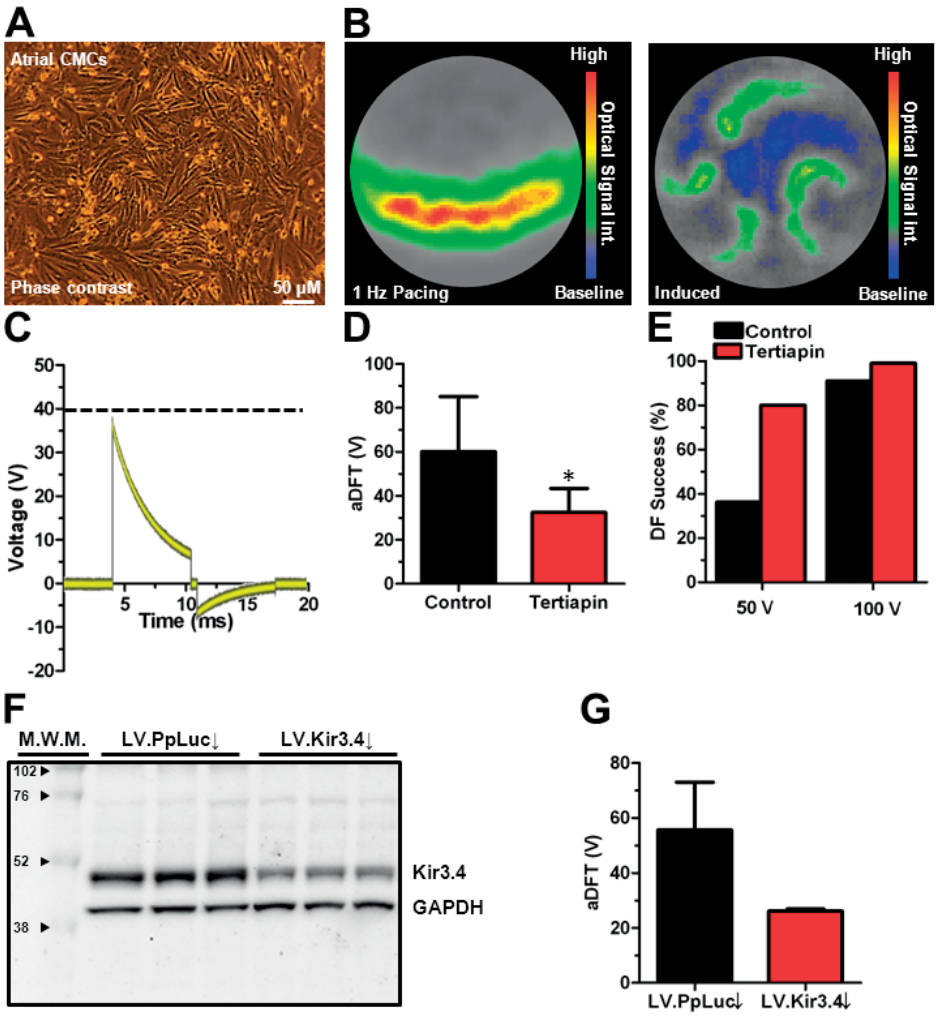

Figure 1. *Model characterization and effect of IK,ACh-c modulation on aDFT. (A) Typical phase-contrast image of a confluent aCMC monolayer. (B) Snapshot of the spatial- and high-pass-filtered optical signal in an aCMC monolayer during 1-Hz pacing (left panel) showing a normal uniformly propagated convex wavefront, and after burst pacing displaying complex spiral wave reentry as a 2D model of AF (right panel). (C) Typical example of an oscilloscope output during a 40-V biphasic truncated exponential shock. Dashed line indicates the peak voltage of the first phase used in further analyses. Quantification of (D) percentage of successful defibrillation (DF) at 50 and 100 V and (E) atrial DF threshold (aDFT) in control and tertiapin-treated cultures. (F) Western blot of Kir3.4 expression in LV.Kir3.4↓-transduced aCMC cultures and in LV-PpLuc↓-transduced control aCMC cultures using glyceraldehyde 3-phosphate dehydrogenase as loading control. M.W.M: molecular weight marker (numbers are in kDa). (G) Quantification of aDFT in aCMC cultures transduced with LV.PpLuc↓ or LV-Kir3.4↓. *: p<0.05 vs control; #:p<0.05 vs LV.PpLuc↓.*

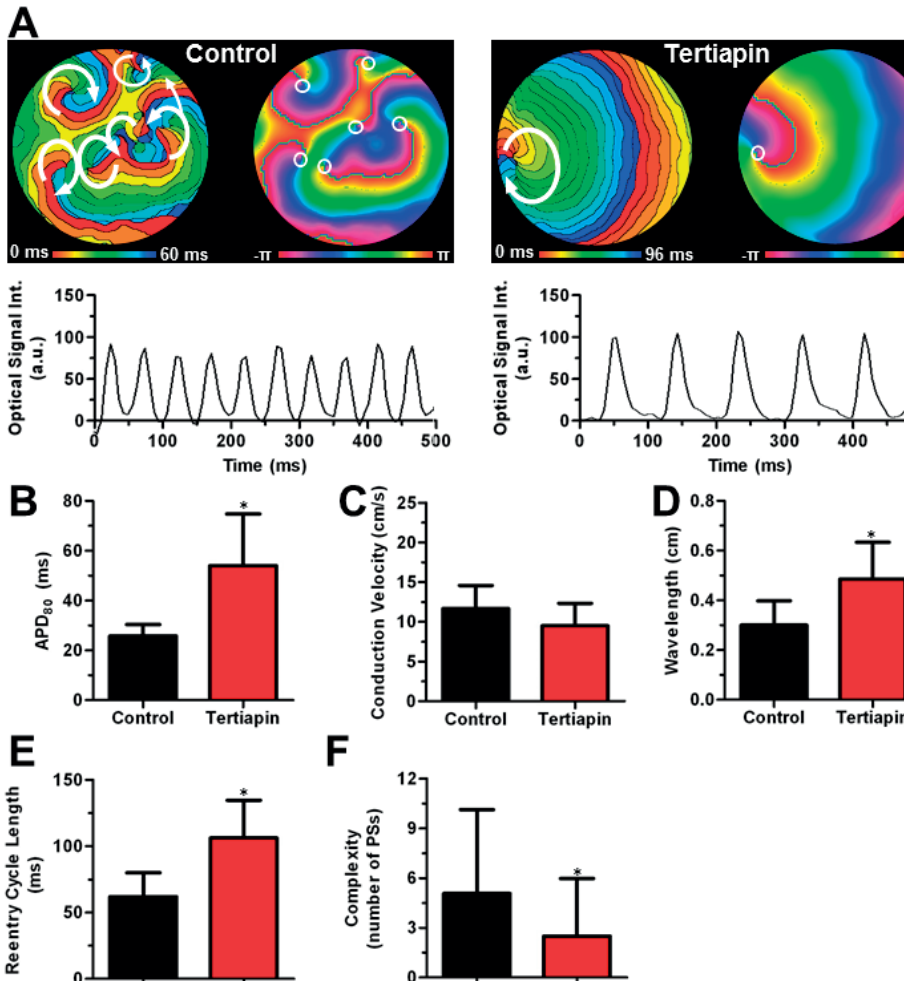

Supplemental Figure 2. *Effect of IK,ACh blockade on electrophysiological characteristics during reentry. (A) Typical examples of activation maps, phase maps and optical signal during fibrillation induced by burst pacing in control (left), and tertiapin-treated (right) aCMC monolayers. Quantification of (B) APD80, (C) conduction velocity, (D) wavelength, (E) reentry cycle length, and (F) complexity. *:p<0.05 vs control.*

Effect of Kcnj5 knockdown on electrophysiological parameters and aDFT

To exclude the possibility that the DFT-lowering effect of tertiapin was caused by another mode of action than by its ability to block IK,ACh-c, Kcnj5 expression in aCMC cultures was specifically downregulated by RNAi using LV.Kir3.4↓. After transduction with LV.Kir3.4↓, Kir3.4 levels decreased to 36.5±3.6 % of those in LV.PpLuc↓-transduced control cultures), as judged by Western blot analyses (Figure 1F). Optical mapping of these cultures during reentry yielded similar results as obtained following tertiapin treatment, being a significant increase in APD80 (Supplemental Figure 4A,B), a non-significant decrease in

CV (Supplemental Figure 4A,C) and a significant increase in wavelength (Supplemental Figure 4A,D) and reentry cycle length (Supplemental Figure 4A,E), while arrhythmia complexity significantly decreased (Supplemental Figure 4A,F). Importantly, also the DFT was significantly decreased by Kcnj5 knockdown (25.0±3.5 [n=14] vs 50.7±19.4 V in LV.PpLuc↓-transduced cultures [n=13]) (Figure 1G). Trends in the relationship between aDFT and CV, APD80, wavelength, reentry cycle length or complexity were similar to those found in the tertiapin experiments described in Supplemental Figure 3 (data not shown).

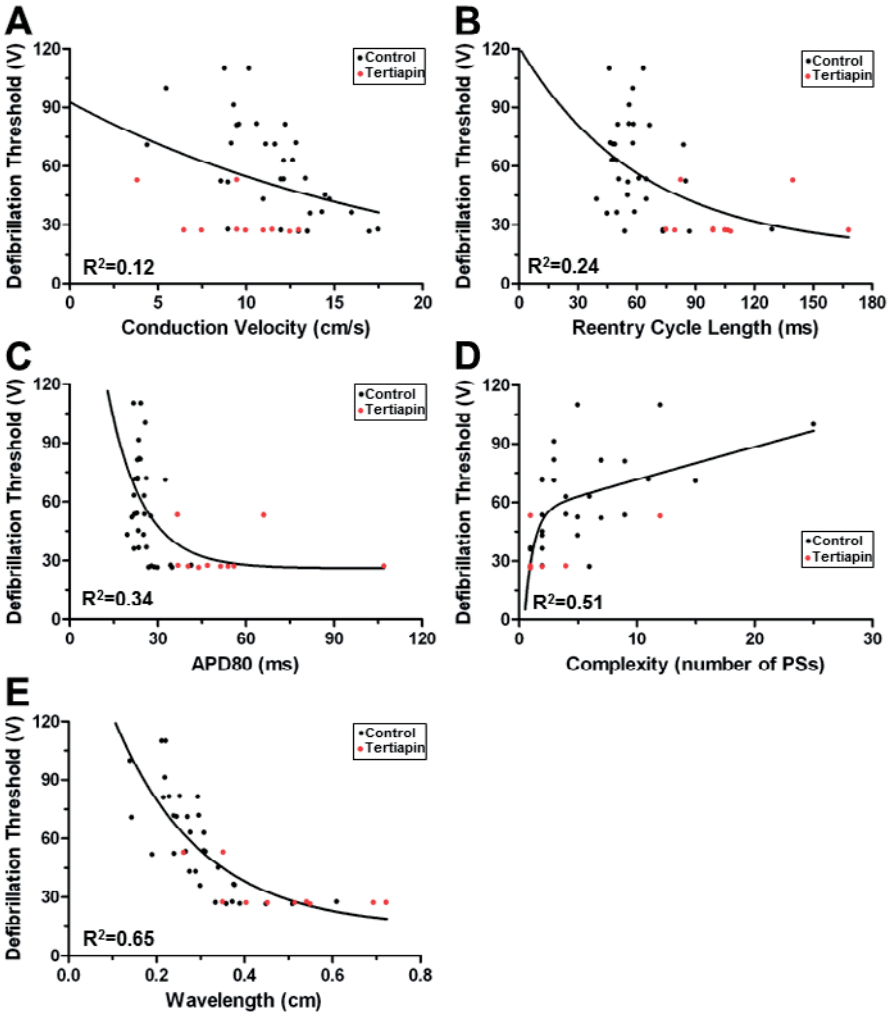

Supplemental Figure 3. *Relationship between electrophysiological parameters and defibrillation threshold. Plots of the correlation between defibrillation threshold and (A) conduction velocity, (B) reentry cycle length, (C) APD80, (D) complexity and (E) wavelength using control and tertiapin-treated aCMC monolayers.*

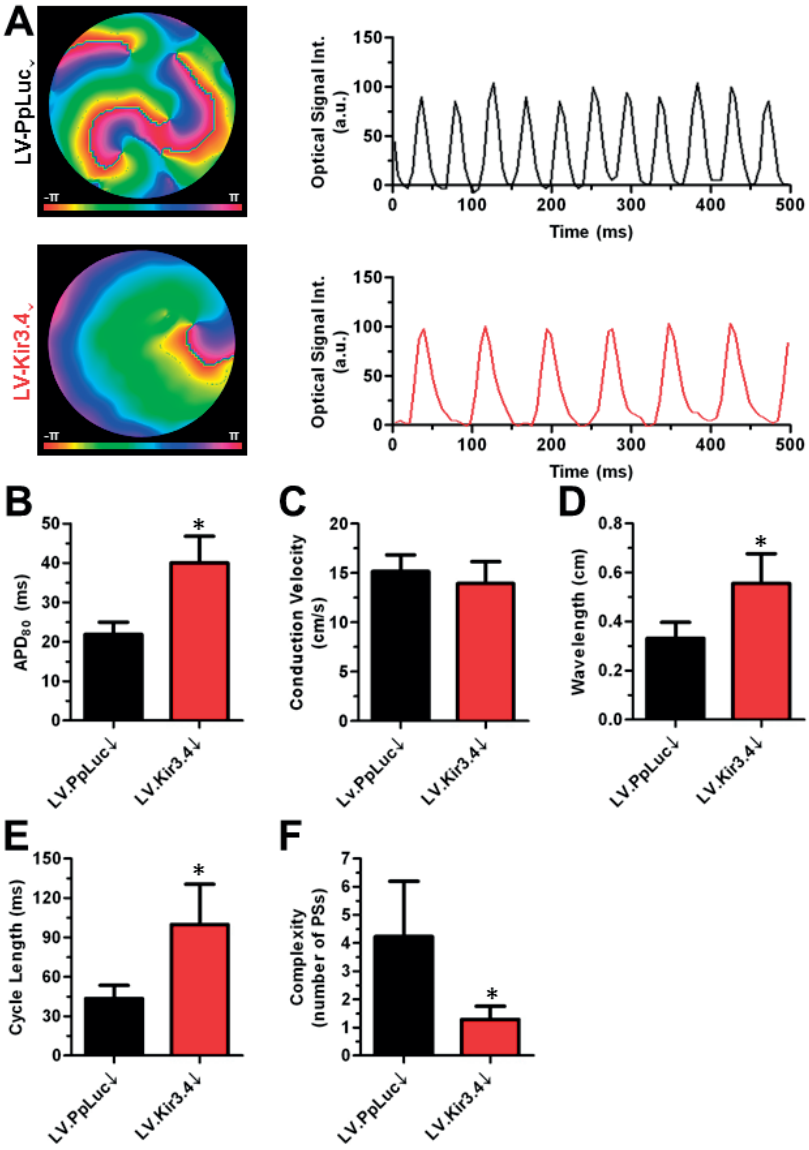

Supplemental Figure 4. *Effect of KCNJ5/2 knockdown on electrophysiological parameters. (A) Typical phase-maps and corresponding single pixel recordings in aCMC monolayers transduced with LV.PpLuc↓ (upper panel) or LV-Kir3.1↓ (lower panel). Quantification of (B) APD80, (C) conduction velocity, (D) wavelength, (E) cylcle length, (F) and complexity in aCMC monolayers transduced with LV.PpLuc↓ or LV-Kir3.1↓.*

Successful defibrillation depends on forced PS removal

To investigate how an increase in wavelength by IK,ACh-c blockade or Kcnj5 knockdown decreases aDFT, mechanisms of successful and failed defibrillation were studied.

During reentry, a continuous spatial progression of activation and phase around a PS (the point surrounded by a complete cycle of phase [2π])21 (Figure 2A,B, left pictures) was observed, perpetuating both the PS and its consequent reentrant tachyarrhythmia. Following exposure of such a culture to a high-energy electric shock, this continuous spatial progression of activation was disturbed, through simultaneous depolarization of large areas of the culture (Figure 2A, right picture; Figure 2C, red arrow). As a consequence, the electrical shock forced all cells to the same phase of the AP (Figure 2B, middle picture; Figure 2D, red and green arrow), breaking the 2π phase convergence necessary for PS maintenance. Hence, after synchronous repolarization (Figure 2B, right picture; Figure 2C) reentry was fully terminated (Supplemental Movie 1).

Concordantly, following exposure of a culture to a shock below the DFT, termination of the arrhythmia failed as a consequence of incomplete synchronization of phases around a PS preventing its definitive removal. In these cases, the electrical shock still elicited simultaneous activation of large areas of the cultures (Figure 3A,C), perturbing the continuous spatial (Figure 3A,B) and temporal (Figure 3D) progression of activation and phase around the PS. However, tracking of the spatial and temporal phase progression showed incomplete synchronization of phase (point B in Figure 3B,D) after the low-energy shock, causing PS persistence and failure of defibrillation (Supplemental Movie 2).

Interestingly, application of electrical shocks to aCMC cultures during fibrillation at voltages that eliminated all PSs present prior to the shock did not necessarily lead to successful defibrillation. In such instances, the gradual spatial progression of activation and phase present prior to shock (Figure 4A-B, left pictures) was again interrupted by simultaneous activation of large areas of the culture, leading to phase synchronization and elimination of the existing PSs (Figure 4B, middle picture; Figure 4C,D, green arrows and Figure 5A). However, if the shock strength was below DFT, new PSs formed in the culture prior to its full repolarization. The newly formed PSs again gave rise to reentrant activation, reestablishing fibrillation in a different activation pattern (re-initiation), causing a failed defibrillation attempt (Figure 4A,B, right pictures; Figure 4C,D; Supplemental Movie 3).

Importantly, failure of defibrillation as a consequence of re-initiation was found to occur at significantly higher voltages (e.g. closer to the DFT) than failure of defibrillation caused by failed PS removal (58.6±21.6 vs 34.5±8.2 V) (Figure 5B). This indicates that of the mechanisms responsible for failed defibrillation, re-initiation is more important in setting the DFT. Together these results suggest that an increase in wavelength by IK,ACh-c blockade might decrease DFT by suppressing the occurrence of post-shock PS formation.

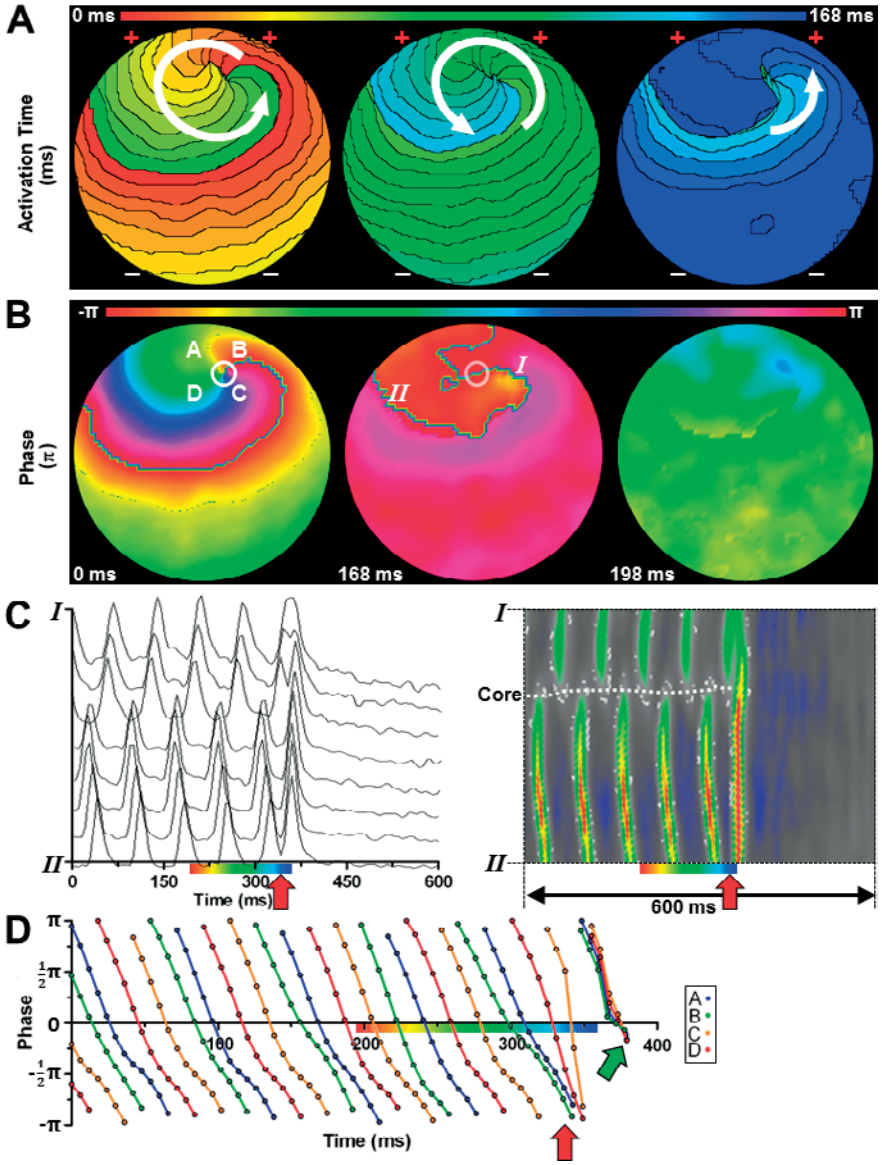

Figure 2. *Successful defibrillation. (A,B) Typical activation (A) and phase (B) map sequence of an atrial culture exhibiting a single-rotor tachyarrhythmia prior to (left), during (middle) and after (right) exposure to an electric shock above the DFT. To simplify interpretation of the results, an example of limited complexity was chosen. The white arrows and circles indicate the direction of AP propagation and the location of the PS, respectively. +: side of first-phase cathode. –: side of first-phase anode. (C) Line analysis of "optical APs" (left) and filtered optical signals (right) (between points I and II in subfigure B) showing synchronization of depolarization after electrical shock application (indicated by the red arrow). Dashed white line indicates the position of the functional core of reentry. Color bar below the X-axis corresponds to that in subfigure A. (D) Plot of the phase at four points equally spaced around the PS (points A, B, C and D in subfigure B) prior to, during and after application of an electrical shock (indicated by the red arrow), showing completely asynchronous phase progression before but full synchronization of all phases (green arrow) after delivery of the electrical shock.*

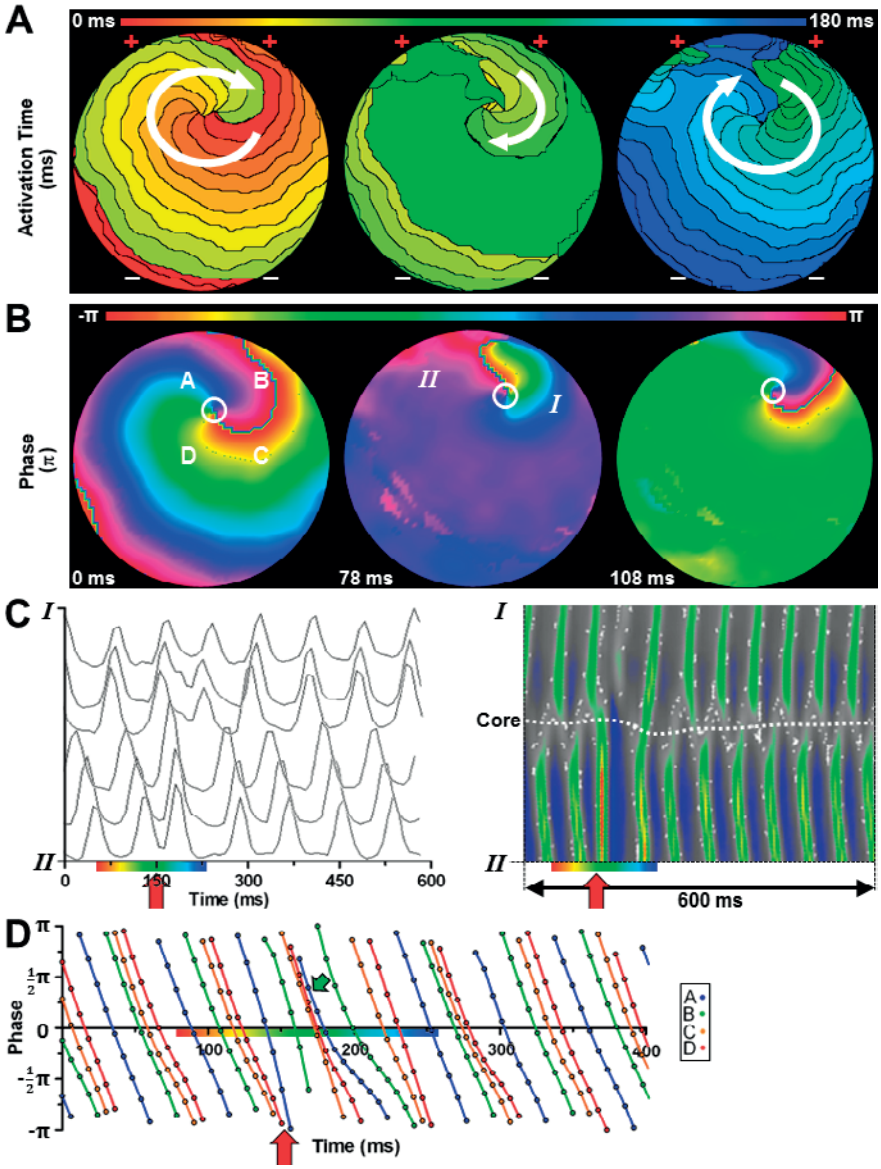

Figure 3. *Failed defibrillation caused by incomplete PS removal. (A,B) Typical activation (A) and phase (B) map sequence of an atrial culture exhibiting a single rotor tachyarrhythmia prior to (left), during (middle) and after (right) exposure to an electrical shock below the DFT. To simplify interpretation of the results, an example of limited complexity was chosen. (C) Line analysis of "optical APs" and filtered optical signals (between points I and II in subfigure B) showing synchronization of depolarization during application of an electrical shock (indicated by the red arrow). (D) Plot of the phase at four points equally spaced around the PS (points A, B, C and D in subfigure B) prior to, during and after application of an electrical shock (indicated by the red arrow), showing asynchronous phase progression before and incomplete synchronization of all phases (green arrow), mainly at point B, after delivery of the electrical shock resulting in continued asynchronous phase progression. Symbols are equal to those in Figure 2.*

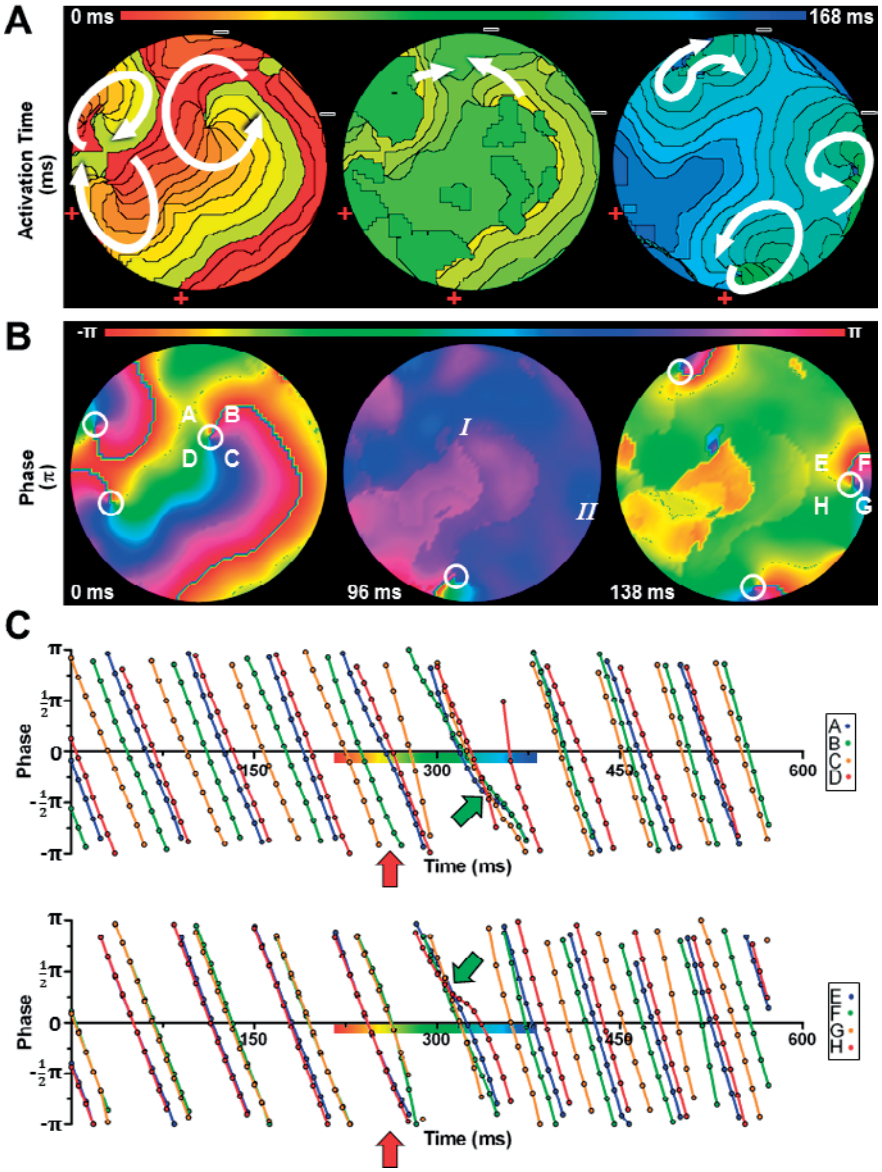

Figure 4. *Failed defibrillation caused by re-initiation. (A,B) Typical activation (A) and phase (B) map sequence of an atrial culture prior to (left), during (middle) and after (right) exposure to an electrical shock below DFT. (C) Plot of the phase at four points (A, B, C and D in subfigure B) equally spaced around a PS that is eliminated by the electrical shock and at four points (E, F, G and H in subfigure B) around a PS that emerges after electrical shock application (indicated by the red arrow). Points A, B, C and D showed asynchronous phase progression before and complete synchronization of all phases after delivery of the electrical shock (green arrow), followed by phase progression synchronized at points A and D and B and C due to AP propagation from a different PS. Before application of an electrical shock, points E, F, G and H showed phase progression synchronized at points E and H and F and G as a consequence of AP propagation from a nearby PS. Electrical shock delivery resulted in complete synchronization of all phases (green arrow) after which phase progression proceeded asynchronously as a consequence of a PS arising between these points. Symbols are equal to those in Figure 2.*

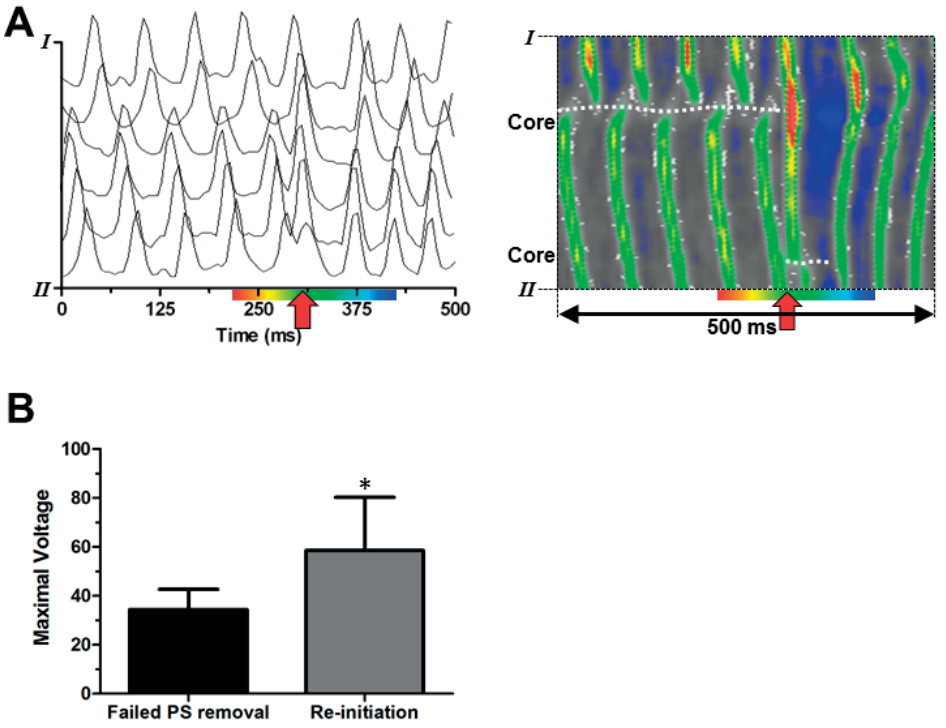

Figure 5. *The relative role of re-initiation in failed defibrillation. (A) Line analysis of "optical APs" (left) and filtered optical signals (right) showing synchronization of depolarization during application of an electrical shock (indicated by the red arrow). Points I and II correspond to points I and II in Figure 4B. Dashed white lines indicate the positions of the functional cores of reentry. Color bar below the X-axis corresponds to that in Figure 5A. (B) Quantification of the maximal voltage during a 25-100 V incremental shock protocol at which defibrillation failed because of failed phase singularity (PS) removal or post-shock PS formation leading to re-initiation of reentry. *: p<0.05 vs failed synchronization.*

Mechanism of post-shock re-initiation

To elucidate the mechanism underlying post-shock formation of PSs ,we first subjected control atrial cultures (n=10) to 25-100 V shocks without prior induction of reentry or electrical stimulation. In none of these cultures post-shock emergence of PSs was observed (Supplemental Figure 5A,B), ruling out the shock protocol or configuration as a cause of post-shock re-initiation of reentry.

Next, we studied the repolarization of fibrillating control or tertiapin-treated cultures after applying shocks with a magnitude below the DFT established for control conditions (i.e. 30 V). This showed that the position of newly formed PSs co-localized with the steepest gradients in APD after the shock, with the post-shock reentrant wavefront moving from the area of latest towards to area of earliest repolarization (Figure 6A). Dispersion in duration of the shock-induced AP was found to be significantly higher at the shortest pre-shock peak-to-post-shock peak intervals (PPIs) (Figure 6B,D). IK,ACh-c

blockade by tertiapin, did not prevent dispersion in repolarization of such shock-induced APs (Figure 6 C,D). In fact, post-shock APD dispersion in the tertiapin-treated cultures was significantly higher at diastolic intervals from 18-42 ms (Figure 7D). Still, the maximal post-shock APD dispersion (i.e. at the shortest diastolic interval) did not significantly differ between control and tertiapin-treated cultures. Therefore, to actively assess the contribution of APD dispersion to re-initiation, we created permanent repolarization heterogeneities in aCMC cultures, by transducing the left half of the cultures with LV.Kir3.4↓ (or LV.PpLuc↓ as control), while leaving the right half of the cultures untransduced as described in the Supplemental Material online (Supplemental Figure 6,7). Interestingly, such spatially-defined downregulation of Kir3.4 significantly lowered the defibrillation threshold (29.2±4.6 vs 41.1±13.5 V in heterogeneously PpLuc↓-transduced control cultures) (Supplemental Figure 7F). Moreover, analysis of the area of first activation after applying shocks below the DFT showed that these sites were only found in the untransduced part (area I) of LV.Kir3.4↓-transduced aCMC cultures(n=10) (Supplemental Figure 7G). In comparison, in LV.PpLuc↓-treated cultures, no clear preference in re-initiation site was found, i.e. 40% of the first post-shock APs originated in the untransduced area (area I) vs 10% and 20% in the border area (area II) and transduced area (area III), respectively; n=10) (Supplemental Figure 7G). Together these results suggest that re-initiation and prevention of re-initiation by IK,ACh-c inhibition are not driven by repolarization heterogeneities in our model.

Subsequently, to actively assess the role of shock-induced depolarization in re-initiation, we quantified the effect of the PPI on the amplitude of the shock-induced APs at 30 V (i.e. below the average DFT) and at 90 V (i.e. above the average DFT) during fibrillation. Shock-induced AP amplitudes were significantly higher at 90 V than at 30 V (Supplemental Figure 8A). The shock-induced AP amplitude diminished significantly with decreasing PPIs at both voltages (Supplemental Figure 8A). Interestingly, 90-V shocks flattened the curve of the relationship between PPI and amplitude in comparison to 30-V shocks (n=6 cultures per group), attributable to its increased effect on relative refractory tissue at short PPIs. Concordantly, in the absence of reentry or prior to electrical stimulation there was no difference in the AP amplitude induced by a 30 or 90 V shock (Supplemental Figure 8B, n=6 cultures per group), while the functional core of the reentrant spiral waves did not affect shock-induced depolarization (as judged by the effect of distance to the PS on the local shock-induced AP amplitude, Supplemental Figure 8C, n=6 cultures per group).

Importantly, the areas of PS emergence after the electrical shock also co-localized with the (borders of) areas of lowest shock-induced AP amplitude (i.e. at the areas with the shortest PPIs) (Figure 7A), with conduction of the shock-induced AP wavefront directed from highly depolarized towards the incompletely depolarized regions (Figure 7A,D). Tertiapin did not significantly affect the shock-induced AP amplitude (Figure 7C).

However, similar to high voltage shocks, tertiapin treatment showed a trend to flatten the curve of the relationship between PPI and shock-induced AP amplitude (Figure 7C). Moreover, at areas of heterogeneous shock-induced depolarization in tertiapin-treated cultures, the shock-induced AP wavefront blocked on the refractory tail of the pre-shock activation, as a consequence of the tertiapin-dependent increase in wavelength (Figure 7E).

Taken together, these results suggest that failed defibrillation through re-initiation is caused by heterogeneous depolarization as a consequence of impaired tissue depolarization at short PPIs. This causes steep post-shock membrane potential gradients, which allow unidirectional propagation of the shock-induced AP in these critical areas. IK,ACh-c blockade blunts the heterogeneity in depolarization induced by low-voltage shocks and inhibits the unidirectional propagation of shock-induced APs by increasing wavelength, which prevents re-initiation and lowers DFT.

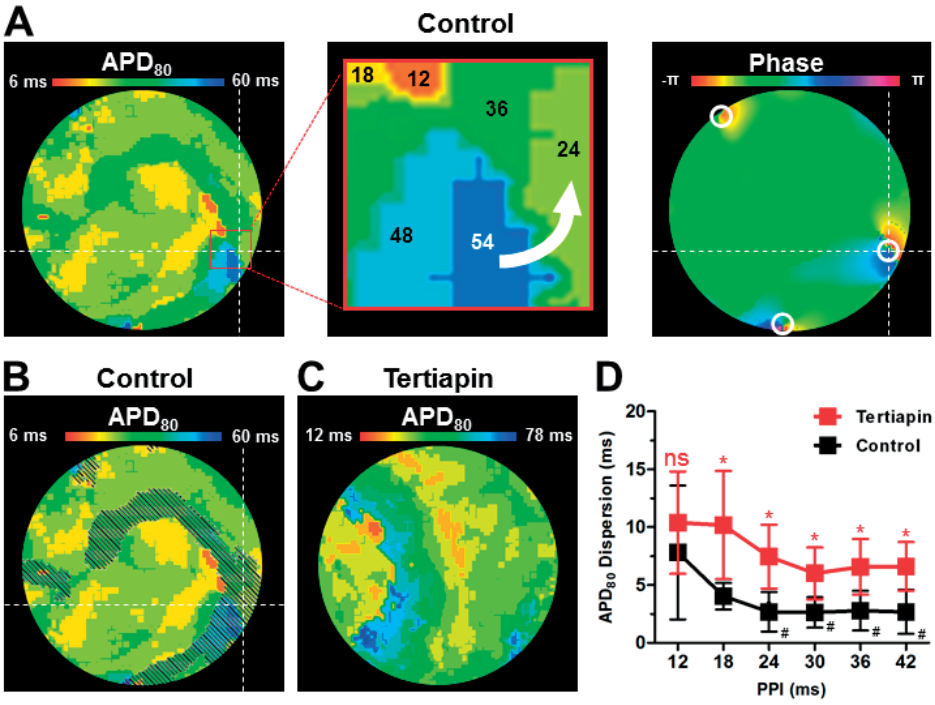

Supplemental Figure 5. *Shock application without prior reentry induction. (A) Typical activation map of a control culture subjected to a 60V shock without previous induction of reentry, showing near-simultaneous activation of the entire culture. (B) Typical single pixel recording in a culture subjected to a 60V shock without previous induction of reentry, showing a single action potential without any post-shock activity. Red arrow indicated the moment of shock application.*

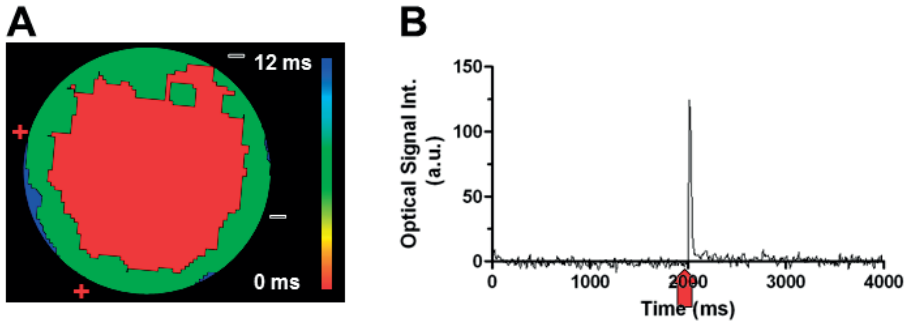

Figure 6. *Repolarization heterogeneities and failed defibrillation. (A) Map of AP duration until 80% repolarization (APD80) (left panel) of the shock-induced AP and phase map (right panel) of a control culture directly after electrical shock delivery, showing that the locations of the steepest APD/repolarization gradients co-localize with the areas of PS formation directly after the shock. The magnified area (red square) of the repolarization map (upper right panel) indicates the APDs and the direction of AP propagation going from the area of latest repolarization towards the area of earliest repolarization (white arrow). (B) Overlay of the areas with 6- to12-ms PPIs (grey hatching) and the APD80 map, showing that areas of steep APD gradients fall in the areas with the shortest PPIs. (C) Repolarization map (left panel) of the shock-induced AP in a tertiapin-treated culture. (D) Quantification of APD80 dispersion of APs induced by 30-V electrical shocks in tertiapin-treated and control cultures at PPIs of 12 to 42 ms.*

Effect of IK,ACh-c blockade in whole-heart electrical cardioversion

As many of the events investigated in the present study may occur subepicardially in the whole heart, our 2D AF model allowed us to obtain unique insights into the mechanisms determining aDFT. However, to confirm the aDFT lowering effect of IK,ACh-c blockade in the more complex and clinically relevant 3D setting, we studied the effect of IK,ACh-c blockade by tertiapin during whole-heart mapping (Figure 8A). Indeed, using the lowest defibrillation energy (30 V), failed defibrillation was observed in control hearts. Re-initiation of fibrillation was a major mechanism of failed defibrillation, because a notable change in cycle length could be observed after the electrical shock, suggesting that a different reentrant pathway maintained subsequent fibrillation (Figure 8B). Following tertiapin treatment, hearts displayed a strong increase in atrial APD and cycle length after AF induction (Figure 8C), and showed termination of AF by ECV at the lowest voltage (30 V). As expected from the in vitro experiments, tertiapin evidently decreased the ECV threshold (36.1±11.3 vs 27.2±0.66 V in untreated control hearts) (Figure 8D), while the success rate of ECV at 30 V shocks was increased by 60% (100% vs 40% in control hearts) (Figure 8E). Together, these results support the notion that IK,ACh-c increases ECV threshold and decreases success rate of atrial defibrillation in the whole heart.

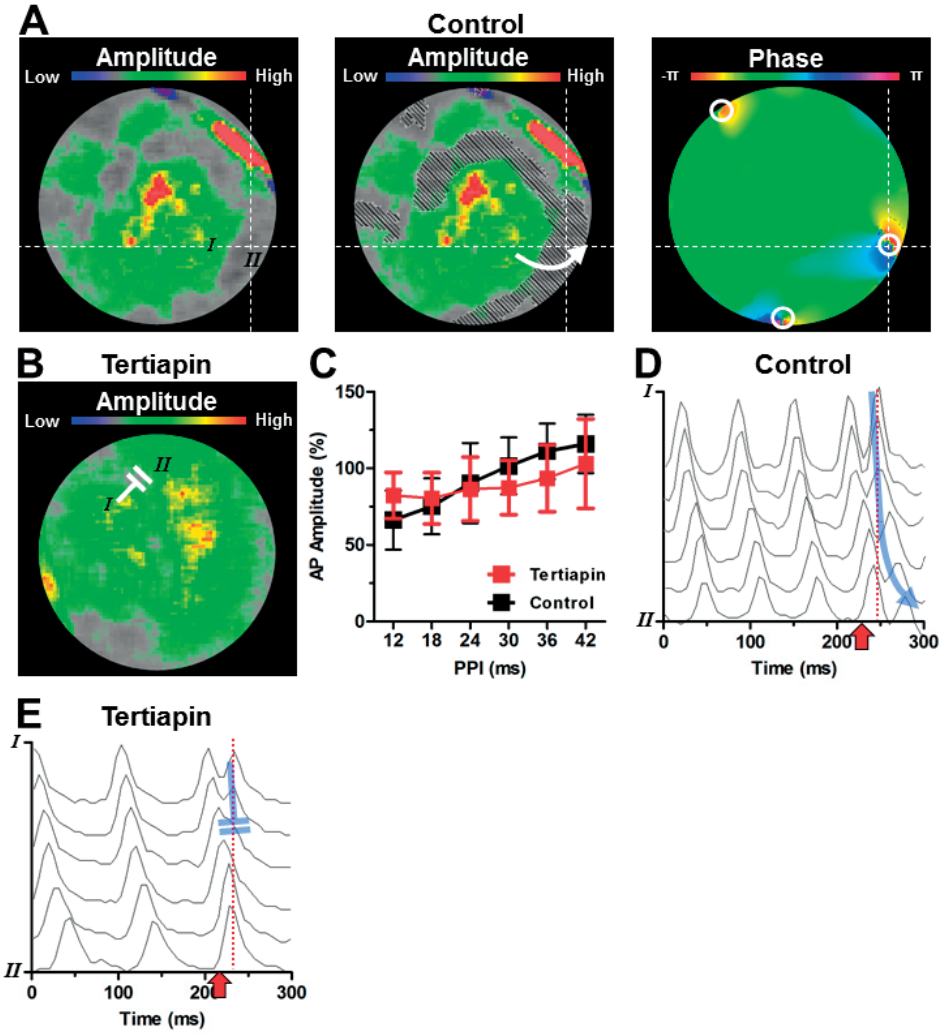

Figure 7. *Depolarization heterogeneities and failed defibrillation. (A) Map of the amplitude of the shock-induced AP without (left panel) or with an overlay of the areas with 6- to 12-ms PPIs (grey hatching; middle panel) and the phase map of a control culture directly after delivery of a 30-V electrical shock, showing co-localization of short PPIs, low shock-induced AP amplitudes and sites of post-shock PS emergence. (B) Map of the amplitude of the shock-induced AP of a tertiapin-treated culture. (C) Quantification of the shock-induced AP amplitude in control and tertiapin-treated cultures at PPIs between 12 and 42 ms. (D) Filtered optical signals between points I and II depicted in subfigure A, showing impaired shock-induced depolarization near point II, leading to propagation of the shock-induced AP wavefront towards point II (direction indicated by blue arrow and white arrow in A). (E) Filtered optical signals between points I and II depicted in subfigure B, showing block of conduction (indicated by double blue lines and double white lines in A) of the shock-induced AP wavefront on the repolarizing waveback of the pre-shock activation between areas of large and impaired shock-induced depolarization..*

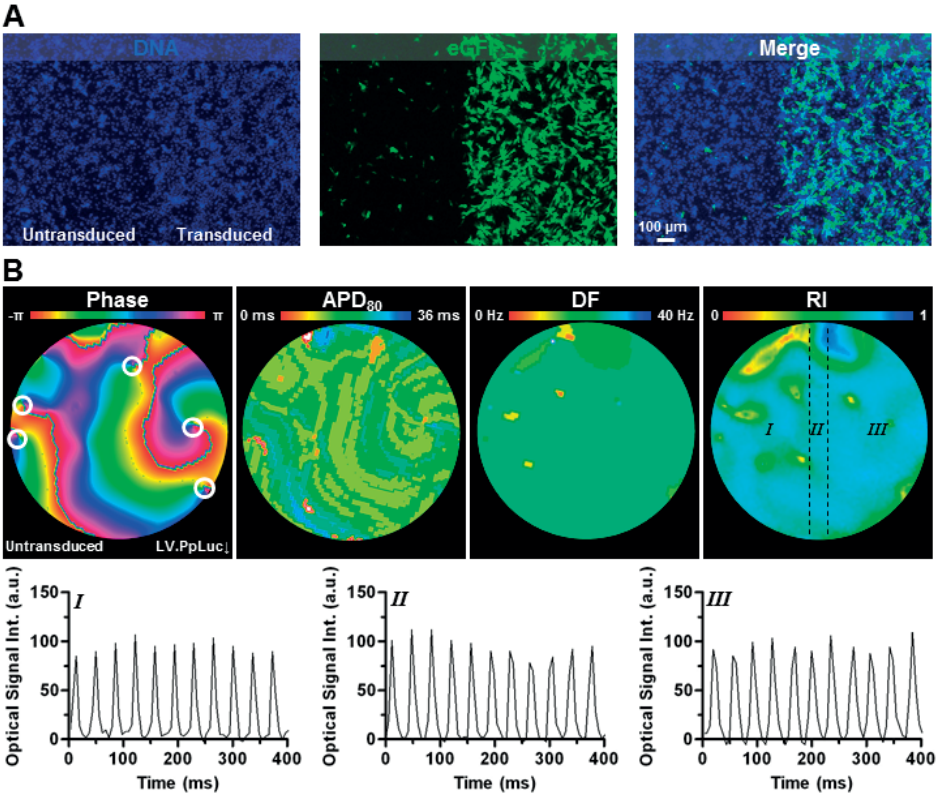

Supplemental Figure 6. *Baseline electrophysiological characteristics in locally transduced aCMC cultures. (A) Example of a fluorescent staining in a culture with the left half transduced with a control eGFP vector, and the right half left untransduced using patterned attachment showing abundant eGFP expression localized to the transduced half. (B) Typical phase, APD80, dominant frequency an regularity index map and corresponding optical signal in the untransduced area (I), the border area (II) and the transduced area (III).*

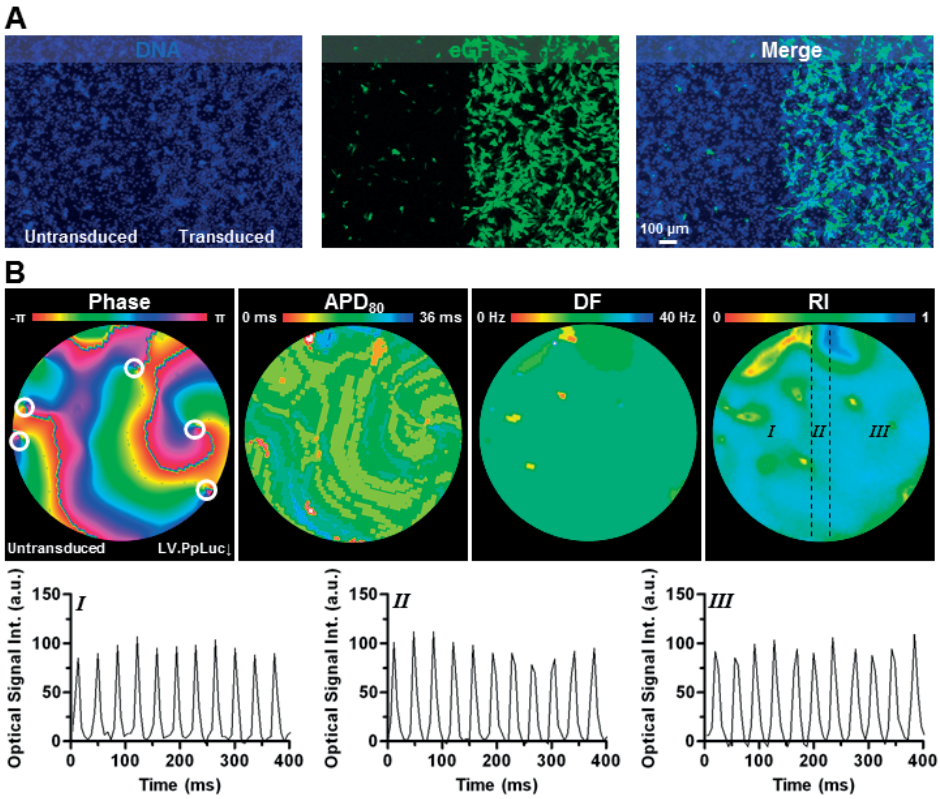

Supplemental Figure 7. *Role of repolarization and $I_{K,ACh-c}$-heterogeneity in post shock PS formation. (A) Typical phase, APD80, dominant frequency an regularity index map and corresponding optical signal in the untransduced area (I), the border area (II) and the transduced area (III), showing wavebreak and APD alternans in the border area and a large APD with 2:1 conduction in the area transduced with LV.Kir3.4↓. Quantification of the difference in (B) APD_{80} (C) conduction velocity (D) wavelength and (E) activation frequency between the transduced and untransduced area in aCMC cultures locally transduced with LV.PpLuc↓ or LV.Kir3.4↓. Quantification of the difference in (F) DFT and (G) site of first activation after application of shock during fibrillation in aCMC cultures locally transduced with LV.PpLuc↓ or LV.Kir3.4↓. I: untransduced area, II: border area, III:transduced area corresponding to the areas depicted in subfigure A (upper right panel).*

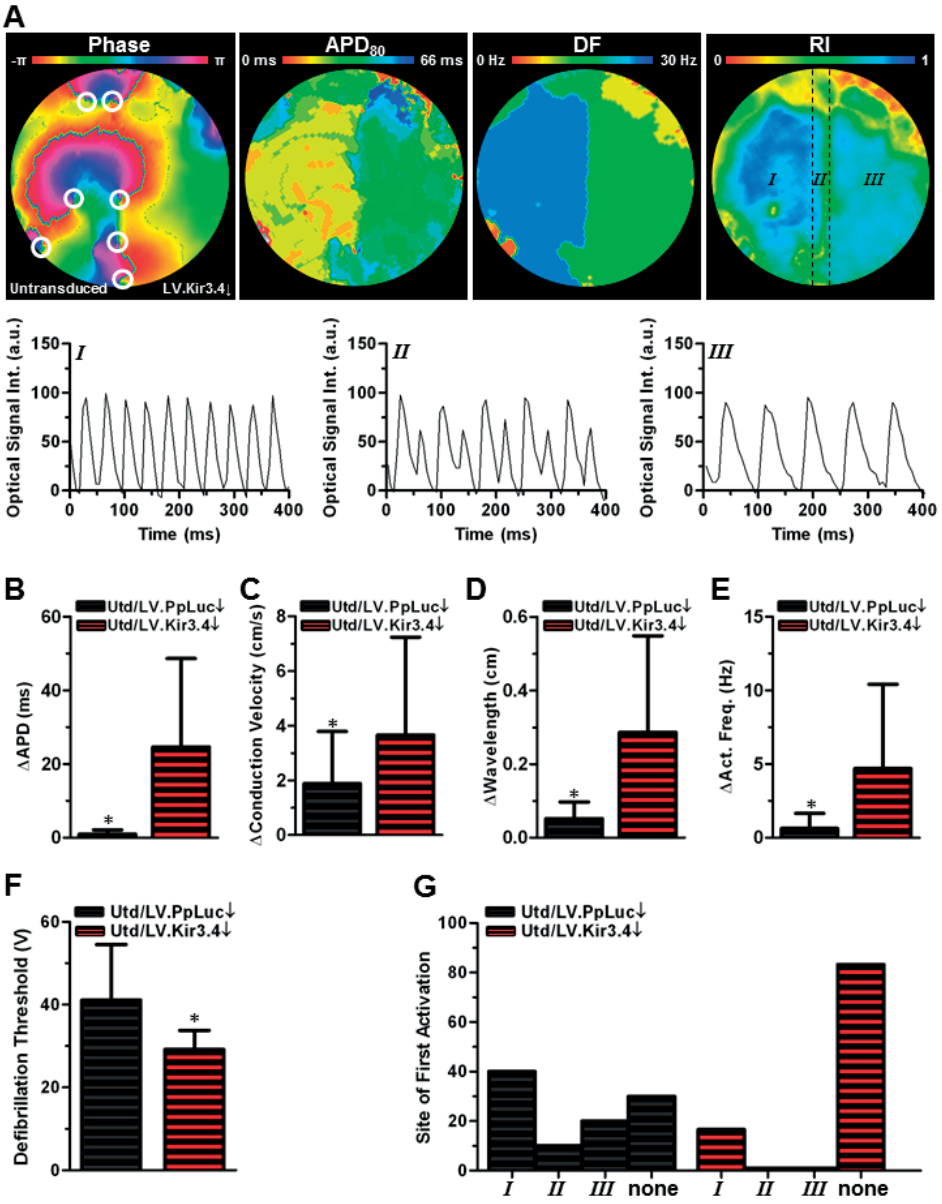

Supplemental Figure 8. *Effect of shock strength on depolarization* **.** *(A) Typical examples of "optical APs" during 3-4 cycles of reentrant activity followed by an electrical shock of 30 (blue) or 90 (orange) V. The timing of the electrical shocks caused a shock-induced*

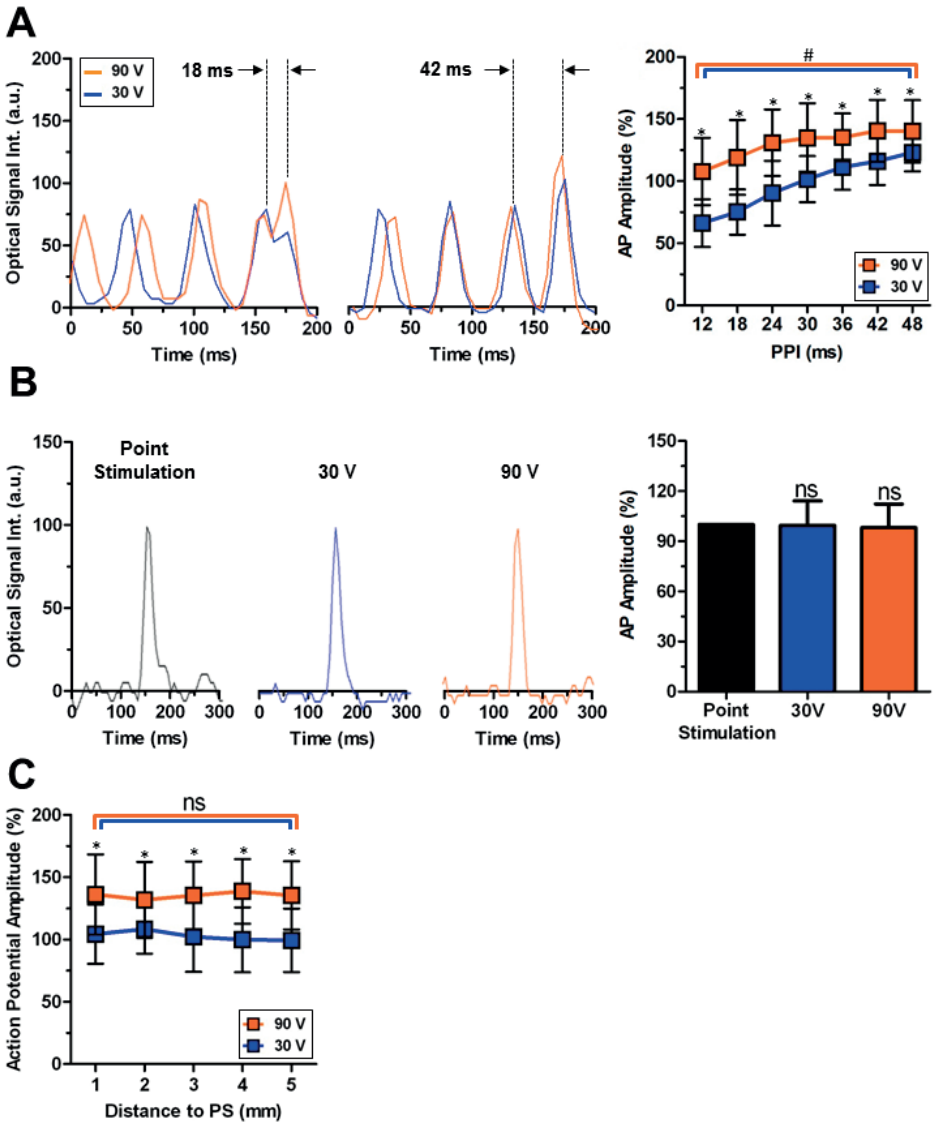

Figure 8. *Ex vivo confirmation of the role of IK,ACh-c in determining aDFT. (A) Example of a neonatal rat heart in the ex vivo mapping setup, prior to commencing the AF induction protocol. Typical ventricular (V) and atrial(B) single-pixel recordings of (B) a control (n=6, 16.7% non-inducible) and (C) a tertiapin-treated (n=7, 57.1% non-inducible) heart. Red arrows indicate the moment of electrical shock application. Notice the increase in atrial activation frequency following electrical shock application in the control heart. Quantification of (D) atrial defibrillation threshold (aDFT) and (E) electrical cardioversion (ECV) success rate following delivery of a 30-V electrical shock in control and tertiapin-treated hearts. a.u.: arbitrary units.*

DISCUSSION

Key findings of this study are : (1) Pharmacological blockade of $I_{K,ACh-c}$ in neonatal rat aCMC cultures or intact atria exhibiting persistent spiral waves of electrical activity, results in a significant increase in the wavelength of reentry and decrease in the energy required for electrical defibrillation (*i.e.* a decreases in aDFT). Similar results were obtained after RNAi-mediated downregulation of one of the molecular correlates of $I_{K,ACh-c,}$ Kir 3.4. (2) $I_{K,ACh-c}$ inhibition lowers aDFT by preventing post-shock arrhythmia re-initiation following defibrillation attempts with low voltage shocks. (3) Mechanistically, blockade of $I_{K,ACh-c}$ moderates the spatial shock-induced differences in depolarization and prevents propagation of the shock-induced AP wavefront, through the increase in wavelength. (4) Finally, $I_{K,ACh-c}$ may serve as a target for lowering the energy requirements for ECV and increasing its effectiveness, without altering ventricular electrophysiology, thereby limiting the harmfulness of (pharmacologically assisted) ECV.

AF is known to be a progressive disease; patients with paroxysmal AF therefore often develop persistent or even permanent AF.[2,3] The underlying principle of AF begetting AF, is one of the reasons for applying cardioversion in AF patients. Moreover, with disease progression, increasing amounts of energy may be required for successful ECV and patients with permanent AF may ultimately become refractory to cardioversion.[9,10,22] As the success rate of ECV already decreases after 24 h of AF,[22] this decrease is likely (at least partially) attributable to electrical remodeling (as opposed to its structural counterpart). In this study, we have elaborated on the effect of electrical remodeling on ECV success rate. We show that $I_{K,ACh-c,}$ as a constituent of this remodeling, is a sufficient cause for an increase in aDFT and a decrease in ECV success rate. Since the molecular components of $I_{K,ACh-c}$ are absent in the ventricles, blockade of $I_{K,ACh-c}$ might provide an atrium-specific target to facilitate successful ECV of AF without increasing the risk of ventricular pro-arrhythmia, thereby adding to the significance of our results.

According to present theories, defibrillation will fail if the portion of the myocardium that is excited or rendered refractory by the electrical shock is too small to effectively cause termination of all reentrant conduction.[23,24] Indeed, the present study confirms that exciting a critical portion of the myocardium is essential for successful defibrillation. If the shock strength is too low to meet this requirement, the consequent incomplete synchronization of the gradual progression of phase around the PS will lead to its continued existence and thereby to ineffective defibrillation. However, we show that close to the DFT, failure of electrical shocks to defibrillate may occur even if their strength is enough to cause elimination of all pre-existing PSs.[25-27] Here, post-shock formation of PSs is the underlying cause of defibrillation failure. Hence, extinguishing the wavefronts that perpetuate fibrillation through synchronous depolarization is necessary but not sufficient for successful defibrillation.

While other studies, mostly focusing on ventricular fibrillation, have postulated re-initiation of fibrillation as an important mechanism of defibrillation failure of electrical shocks near the DFT, controversy remains regarding the origin of post-shock re-initiation. The presence of an isoelectric window after a failed defibrillation shock (*i.e.* the temporal gap between the application of a shock and the observation of first epicardial activation) was the first clue that led to the introduction of the theories postulating re-initiation of reentry to underlie defibrillation failure.[27] Because of this gap it has been hypothesized that the re-initiation of (ventricular) fibrillation could be caused by triggered activity resulting from early (EADs) or delayed afterdepolarizations (DADs).[28] In the present study post-shock EADs and DADs were not observed. Moreover, APD prolongation was shown to prevent post-shock re-initiation of reentrant activity. If in our case formation of the first PS after the electrical shock would depend on phase-2 EADs, APD prolongation would increase the chance for re-initiation as well as the DFT. However, APD prolongation does decrease the susceptibility for post shock late phase-3 EADs and DADs.[27] Still, in contrast to our findings, these phenomena are associated with long isoelectric windows or immediate recurrence of AF (IRAF) after primary ECV success.[29] Our results therefore suggest that afterdepolarizations are an unlikely cause of defibrillation failure in AF. Given the rapid reappearance of fibrillatory electrical activity after unsuccessful ECV (Figure 5,8), the isoelectric window in whole hearts could be attributable to intramural reentry occurring before activation becomes measurable at the epicardium.

In theory, the origin of re-initiation could also be the electrical shock itself. Several studies showed that when exposed to external field stimulation, areas of cardiac tissue can be either excited (*i.e.* the virtual cathode) or de-excited (*i.e*. the virtual anode).[30,31] The latter causes AP shortening, which restores excitability in the de-excited area.[26,32] As a consequence of electrotonic interaction between the depolarized and the hyperpolarized area (*i.e*. break excitation).[33] new wavefronts can be formed and propagated in the direction of the excitable de-excited area after the shock, potentially creating new reentrant circuits that cause shock failure.[26,34]

In the present study, de-excitation was far less apparent (although small areas of APD shortening were observed, analogous to virtual anodes). As tissue heterogeneity may be a determinant of the occurrence of virtual electrode polarization,[35,36] this difference may, in part, be attributed to the homogeneous nature of our cell culture model. More importantly, virtual electrode polarization may be prevented by the use of a biphasic shock, as utilized in our study. The second phase of a biphasic shock is thought to quickly re-excite the de-excited area, while only partially de-exciting the excited area, homogenizing post-shock polarization.[26] As such, the effectiveness of the biphasic shock in preventing virtual electrode formation depends on the amplitude of the second phase relative to that of the first phase. In the present study, the peak voltage of the second phase was 20% of the maximum voltage in the first phase, which has been previously shown to

cause effective asymmetric reversal of the polarity in the first phase, thereby preventing virtual electrode formation.[26]

Moreover, according to the virtual electrode hypothesis of defibrillation strong shocks can prevent virtual electrode polarization and re-initiation by enlarging the areas of complete de-excitation. If a wavefront is formed by break excitation, this wavefront will promptly excite the de-excited area as a consequence of its local shock-induced gain in excitability. As this fast excitation does not allow for recovery of the virtual cathode area, new reentrant circuits are prevented.[32] In our model, strong shocks do not increase de-excitation (again as a consequence of its biphasic nature), but increase the amount of excited tissue (that would have been refractory to low shock voltages). As a consequence post-shock polarization is homogenized, which prevents re-initiation. Similarly, tertiapin decreases the steepness in the relationship between the shock-induced AP amplitude and the PPI, which also homogenized post-shock polarization. Simultaneously, tertiapin increases refractoriness in incompletely depolarized areas and hence prevents propagation of wavefronts initiated at depolarized areas, which together decrease DFT. Hence, our paper shows that DFT can be decreased through other means than by increasing de-excitation, in the context of a biphasic shock. Still, mechanisms of re-initiation found in our study are largely analogous to the virtual electrode hypothesis being dependent heterogeneous polarization.

Finally, the critical point hypothesis of defibrillation states that reentry can initiate at critical junctions between the shock-induced extracellular potential gradient and the refractoriness gradient caused by the last pre-shock activation.[37] The present study confirms that re-initiation of AF depends on local tissue refractoriness. It should be noted, however, that the critical point hypothesis stems from experiments in which a monophasic S2 shock was given during phase 2 or 3 of the AP from a plane perpendicular to that of the S1 shocks, causing potential and refractoriness gradients to cross each other.[28,37] Applying biphasic shocks during fibrillation, should partly resolve the potential gradient, and cause the refractoriness to be dispersed. At variance with the critical point hypothesis, in our model formation of critical points (*i.e.* post-shock PSs) occurred in the area of highest refractoriness (*i.e*. the shortest PPI), instead of remote from this area.

The fact that most of the current theories about cardiac fibrillation and defibrillation mechanisms come from the field of ventricular fibrillation and can only partly explain our findings, may also indicate that different mechanisms might be responsible for defibrillation failure in ventricular fibrillation and AF, underlining the novelty of our results.

In this study, we utilized models of AF in which tachyarrhythmic activation after burst pacing relies on reentrant activity. As focal mechanisms may also underlie fast activation during AF,[38] the energy necessary to eliminate AF of focal origin, as well as the effect of diminishing $I_{K,ACh\text{-}c,}$ on the efficiency with which such an arrhythmia can be terminated

may be different from what was found in the present study. Still, it should be noted that reentrant re-initiation at critical PPIs can also occur after eliminating a focal source by electrical shock. Hence, in this case a protective effect of $I_{K,ACh-c}$ might be expected. Further studies will be necessary to explore this possibility.

In addition, ECV in the clinical setting not only fails because of true shock failure but also by IRAF in which, after the electrical shock, one or more sinus beats are followed by re-initiation of AF.[39] Only the true shock failure aspect of ECV failure has been investigated in the present manuscript. Since the mechanisms for true shock failure and IRAF may differ, blockade of $I_{K,ACh-c}$ might not prevent ECV failure due to IRAF. Nonetheless, we and others have shown that $I_{K,ACh-c}$ blockade can also prevent the initiation of AF.[18,40]

The use of neonatal rat aCMC monolayers allowed us to systematically study the mechanisms of AF in the context of $I_{K,ACh-c}$ inhibition in a controllable environment. These monolayers are, however, inherently different from intact human atria because of their 2D nature and the electrophysiological differences between human and rat aCMCs. Nonetheless, results obtained in our 2D model were reproduced in intact hearts, confirming its relevance. Due to the minute dimensions of the intact neonatal rat heart, crosstalk between the ventricular and atrial optical signal was observed during optical mapping. Still, presence or absence of AF is easily derived from the obtained atrial signal. As a consequence of this crosstalk, no analyses on post-shock reinitiation mechanisms were performed in the whole heart. Hence, we concur that the results of this study are conceptual with respect to ECV in humans and therefore cannot be readily extrapolated to the clinical setting.

CONCLUSIONS

This is the first study to systematically study the role of the $I_{K,ACh-c}$ in atrial defibrillation. The results indicate that remodeling of this current, as occurs during AF, can contribute to an increase in aDFT and failure of ECV. Hence, $I_{K,ACh-c}$ may serve as an interesting target for lowering the energy requirements for ECV and increasing its effectiveness, without altering ventricular electrophysiology, limiting the harmfulness of (pharmacologically assisted) ECV.

METHODS

A detailed description of materials and methods can be found in the Supplementary Material online.

All animal experiments were approved by the Animal Experiments Committee of the Leiden University Medical Center and conformed to the Guide for the Care and Use of Laboratory Animals as stated by the US National Institutes of Health.

Preparation of aCMC monolayers

Neonatal rat aCMCs were isolated by collagenase digestion and cultured on 15-mm-diameter fibronectin-coated coverslips as described previously.[18] A cell density of 8×10^5 cells/well in 24-well culture plates was maintained throughout the experiments by restricting proliferation (of non-myocytes) through treatment with Mitomycin-C (Sigma-Aldrich, St. Louis, MO) at day 1 of culture.

RNAi

Self-inactivating lentiviral vectors encoding enhanced green fluorescent protein (eGFP) and a shRNA specific for rat *Kcnj5* (LV-Kir3.4↓) or for *Photinus pyralis luciferase* (LV-PpLuc↓, negative control vector) were generated as described in detail in the Supplementary Material online. Transduction was performed at day 4 of culture. Knockdown of Kir3.4 after transduction with LV-Kir3.4↓ was confirmed using Western blot.

Optical mapping

High resolution optical mapping was performed at day 9 of culture using di-4-ANEPPS (Life Technologies) as a voltage-sensitive dye and a MiCAM ULTIMA-L imaging system (SciMedia, Costa Mesa, CA) as described previously.[18] For 1-Hz or burst pacing of confluent aCMC cultures (Figure 1A), a custom epoxy-coated bipolar electrode was used, resulting in normal convex waves (Figure 1B, left picture) or reentrant spiral waves (Figure 1B, right picture), respectively. Defibrillation was performed using a custom electroshock module (Supplemental Figure 1A), which was coupled to two platinum electrodes fixed in a plastic ring that was readily mountable to the top of a 24-well culture plate. Electrodes were 9-mm in length, placed parallel 11-mm apart, and 2 mm above the surface of the culture (Supplemental Figure 1B-D). This setup produced biphasic truncated exponential shocks of adjustable voltages (≈25-105 V) with the second-phase peak voltage being 20% of the first-phase peak voltage (Figure 1C). DFT was defined as the voltage used during the first shock (starting from ≈25 V and progressively increasing with 10-V increments) leading to full elimination of arrhythmic activity.

To assess the effect of $I_{K,ACh-c}$ blockade on defibrillation, tertiapin (100 nM) was pipetted in the medium and dispersed by gentle agitation, directly followed by optical mapping.

Whole heart di-4-ANEPPS-mapping was performed on neonatal rat hearts suspended in a 16-mm diameter tissue bath. Hearts were perfused with oxygenated Tyrode's solution (comprising [in mM] NaCl 130, $CaCl_2$ 1.8, KCl 4.0, $MgCl_2$ 1.0, NaH_2PO_4 1.2, $NaHCO_3$ 24 and glucose 5.5 at pH 7.4) supplemented with 20 mM 2,3-butanedione monoxime

(Sigma-Aldrich) to minimize motion artifacts. The burst pacing, electrical shock protocol and electrode setup (mounted to the tissue bath) used to determine the aDFT were equal to those used in the *in vitro* experiments.

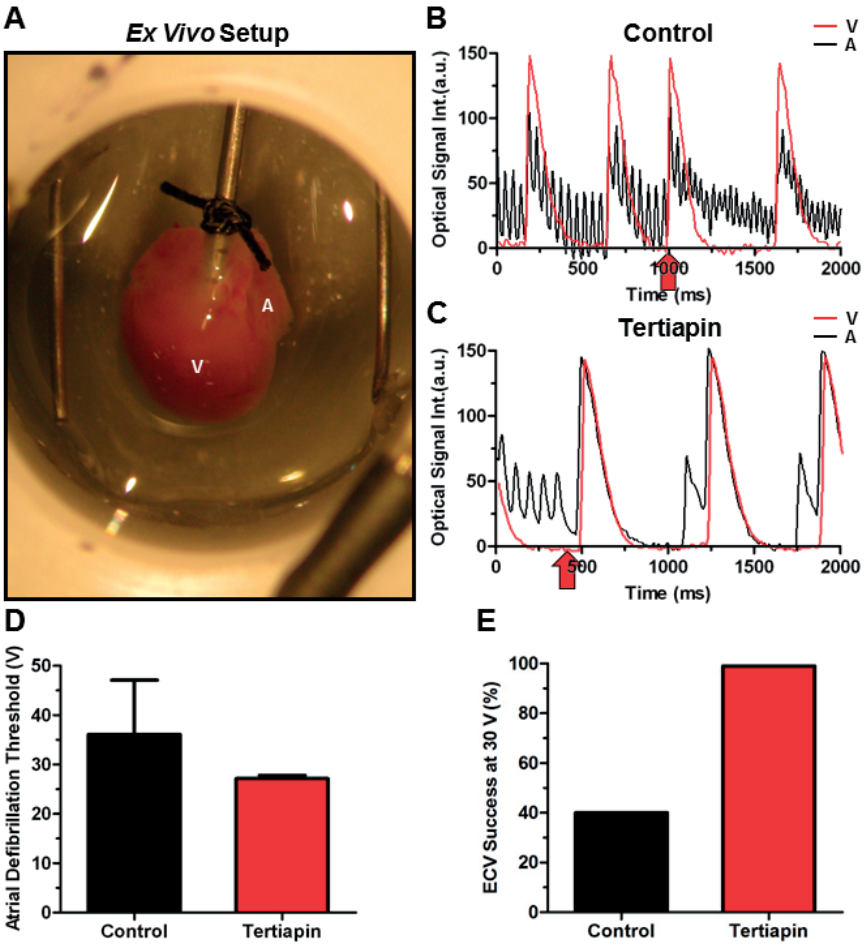

Supplemental Figure 1. *Characterization of experimental setup. (A) In vitro electroshock device consisting of a module capable of generating biphasic truncated exponential shocks at adjustable voltages, coupled to 2 platinum perpendicular electrodes fixed to a plastic rim (dotted square) that is readily mountable to the top of a 24-wells culture plate. (B) Schematic 3D representation, (C) top view (right panel) and (D) lateral view (lower panel) of the used electrodes mounted on a fibrillating atrial culture.*

Statistics

Statistical analyses and construction of corresponding graphs were performed using Graphpad Prism 6.0 (Graphpad Software, San Diego, CA). Comparison between two groups was performed using the non-parametric Mann-Whitney U test (for unpaired

measurements) or Wilcoxon signed rank (for paired measurements) test. Kruskall-Wallis testing with Bonferoni *post-hoc* correction was used for multiple groups and comparisons. Data were expressed as mean±standard deviation (SD) for a number (n) of observations. Differences were considered statistically significant if $p<0.05$. Non-linear regression curves were constructed by using a robust exponential two-phase decay curve fit. Accuracy of these curves was expressed as the coefficient of determination (R^2).

ACKNOWLEDGEMENTS

We thank Sander van Berloo and Huybert van der Stadt for excellent technical support and Dirk Ypey for instructive discussions. We thank Martin Schalij for commenting on the manuscript.

SOURCES OF FUNCING

This study was supported by the Dutch Heart Foundation (E. Dekker grant [2012/T023 to B.O.B.]) and the Netherlands Organization for Scientific Research (Veni grant [91611070 to D.A.P.]).

COMPETING FINANCIAL INTERESTS

None.

AUTHOR CONTRIBUTIONS

B.O.B. conceived and designed the study, performed experiments, analyzed and interpreted data and prepared the manuscript and figures. S.F.A. analyzed data, supervised experiments and prepared the manuscript. Z.N. and I.F. constructed the SIN-LV shuttle plasmids and produced LV vectors. A.P analyzed and interpreted data and prepared the manuscript. A.A.F.d.V. designed LV vectors, supervised LV vector production and designed the study. D.A.P supervised design, experiments, analyses, and preparation of manuscript and figures. All authors commented on and approved the final version of the manuscript.

SUPPLEMENTAL MATERIAL

RESULTS

Optical mapping of cultures with local transduction of LV.PpLuc↓ or LV.Kir3.4↓

To assess the contribution of structural repolarization heterogeneities to post-shock PS formation, aCMC monolayers were locally transduced with LV.Kir3.4↓ or LV.PpLuc↓ using patterned attachment, prior to inducing fibrillation and attempting defibrillation. Fluorescence microscopy showed that patterned attachment indeed led to locally increased expression of eGFP in the transduced area (Supplemental Figure 6A). Expectedly, optical mapping of aCMC cultures locally transduced with LV.PpLuc↓ showed similar electrophysiological characteristic in the transduced, the border and untransduced area (depicted as I, II and III in Supplemental Figure 6B respectively, Supplemental Figure 7B-E). In contrast, in cultures with local transduction of LV.Kir3.4↓ a notable increase in the APD was observed in the transduced area during reentry. As a consequence (given the presence of a rotor in the untransduced area) wavebreak occurred in the border (Supplemental Figure 7A, PSs in area depicted as II), with APD alternans occurring in this zone with 2:1 conduction to the transduced area. Hence the difference in APD_{80} (24.7±24.0 vs 1.0±1.1 ms), wavelength (0.05±0.04 vs 0.29±0.26 cm) and activation frequency (4.7±5.7 vs 0.6±1.0 Hz) between the transduced and untransduced area, was significantly higher in the LV.Kir3.4↓ group as compared to controls. The difference in conduction velocity did not show any significant differences (1.9±1.9 vs 3.7±3.6 cm/s) (Supplemental Figure 7B-E). These result confirmed the possibility to establish APD/repolarization heterogeneities in aCMC cultures by patterned attachment.

MOVIE 1:

Typical example from an optical mapping experiment in a neonatal rat atrial CMC culture exhibiting a single rotor tachyarrhythmia after burst pacing, during exposure to a high voltage shock leading to successful defibrillation (corresponding to Figure 2 in the Main Manuscript). The left panel displays the high-pass-filtered optical signal, the right panel shows the corresponding phase map progression.

MOVIE 2:

Typical example from an optical mapping experiment in a neonatal rat atrial CMC culture exhibiting a single rotor tachyarrhythmia after burst pacing, during exposure to an electric shock below DFT leading to failed defibrillation as a consequence of incomplete PS removal (corresponding to Figure 3 in the Main Manuscript). The left panel displays the high-pass-filtered optical signal, the right panel shows the corresponding phase map progression.

MOVIE 3:

Typical example from an optical mapping experiment in a neonatal rat atrial CMC culture exhibiting a single rotor tachyarrhythmia after burst pacing, during exposure to an electric shock below DFT leading to failed defibrillation as a consequence reinitiation (corresponding to Figure 4 in the Main Manuscript). The left panel displays the high-pass-filtered optical signal, the right panel shows the corresponding phase map progression.

METHODS

All animal experiments were approved by the Animal Experiments Committee of the Leiden University Medical Center and conformed to the Guide for the Care and Use of Laboratory Animals as stated by the US National Institutes of Health.

Preparation of aCMC monolayers

The isolation and culture of neonatal rat aCMCs was performed essentially as described elsewhere.[18] Two-Day-old Wistar rats were anesthetized using 5% isoflurane inhalation. Anesthesia was considered adequate if pain reflexes were absent. Subsequently, hearts were excised aseptically, remaining large vessels were removed and atria were separated from the ventricles. Next, atria were gently minced and rinsed in solution A (0.02% phenol red, 137 mM NaCl, 5.4 mM KCl, 0.34 mM Na2HPO4, 0.44 mM KH2PO4, 5.6 mM D-glucose and 20 mM HEPES, pH 7.3) to remove remaining blood. Atrial tissue was dissociated using collagenase (200 U/ml in solution A, Worthington Biochemical Corporation, Lakewood, NJ) and DNAse (6U/ml in solution A, Sigma-Aldrich, St. Louis, MO) in a shaking water bath at 37°C for 2×30 minutes, after which cells were spun down and suspended in Ham's F10 medium (ICN Biomedicals, Irvine, CA, USA) with 10% horse serum (HS, Invitrogen, Carlsbad, CA, USA) and 10% fetal bovine serum (FBS, Invitrogen).

Cell suspensions were pre-plated on primaria-coated culture dishes (Becton Dickinson, Franklin Lakes, NJ, USA) to allow preferential attachment of non-myocytes. The suspension of non-adherent cells (mainly aCMCs) was run through a 70-µm cell strainer (Beckton Dickinson) to remove incompletely digested tissue and cell aggregrates, and plated on fibronectin-coated glass coverslips (15-mm diameter) in 24-wells cell culture plates. A cell density of 8×10^5 cells/well was maintained throughout the experiments by restricting proliferation (of non-myocytes) by treatment with Mitomycin-C (10µg/ml, Sigma-Aldrich, St. Louis, MO) at day 1 of culture. Cultures were kept in a humidified incubator at 37 °C and 5% CO_2 and refreshed daily with culture medium consisting of a 1:1 mixture of DMEM (Invitrogen) and Ham's F10 supplemented with 5% HS, penicillin (100 U/ml, Life Technologies, Bleiswijk, the Netherlands) and streptomycin (100 µg/ml, Life Technologies).

Western blotting

Cultures of aCMCs were lysed in radioimmunoprecipitation-assay buffer comprised of 50 mM Tris–HCl (pH 8.0), 150 mM NaCl, 1% Triton X-100, 0.5% sodium deoxycholate, 0.1% sodium dodecyl sulfate. The proteins in the lysate were size fractionated in Bolt 10% Bis-Tris gels (Life Technologies) and blotted on Hybond polyvinylidene difluoride membranes (GE Healthcare, Diegem, Belgium). Membranes were first incubated with antibodies directed against Kir3.4 (Santa Cruz Biotechnology, Dallas, TX) or glyceraldehyde 3-phosphate dehydrogenase (GAPDH; Merck Millipore, Billerica, MA) as a loading control, followed by incubation with corresponding horseradish peroxidase-conjugated secondary antibodies (Santa Cruz Biotechnology) after blocking in in Tris-based saline, 0.1% Tween-20, 5% bovine serum albumin (Sigma-Aldrich). Chemiluminescence was detected by a ChemiDoc XRS imaging system (Bio-Rad Laboratories, Veenendaal, the Netherlands) using SuperSignal West Femto chemiluminescent substrate (Thermo Scientific, Rockford, IL).

Fluorescence microscopy

After a double rinsing step with ice-cold PBS, 10 min fixation in 1% formaldehyde in PBS and 5 min permeabilization with 0.1% Triton X-100 in PBS, cells were stained for nuclei by incubating Hoechst 33342 for 5 min on ice. After double rinsing with PBS, coverslips were mounted in Vectashield mounting medium (Vector Laboratories, Burlingame, CA) to minimize photobleaching. Images were captured using a fluorescence microscope equipped with a digital color camera (Nikon Eclipse 80i; Nikon Instruments Europe, Amstelveen, the Netherlands). Dedicated software (NIS Elements [Nikon Instruments Europe] was used to store immunofluorescence signals.

RNAi

Knockdown of Kir3.4 expression in aCMC cultures was performed by transduction with self-inactivating lentiviral vectors (LVs) encoding short hairpin (sh) RNAs specific for rat *Kcnj5* (LV-Kir3.5↓). The *Photinus pyralis luciferase (PpLuc)*-specific shRNA-coding sequence and the marker gene cassette consisting of the human *phosphoglycerate kinase 1* gene promoter and the puromycin-N-acetyltransferase-coding sequence in the plasmid SHC007 from the Mission shRNA library (Sigma-Aldrich) were replaced by a rat *Kcnj5*-specific shRNA-coding sequence and the human *eukaryotic translation elongation factor 1 alpha 1* gene promoter and the *Aequorea victoria* enhanced green fluorescent protein-coding sequence, respectively, to acquire the shuttleplasmid constructs to produce aforementioned LVs. The shuttle construct for negative control vector (LV-Ppluc↓) was obtained by omitting the substitution of the *Ppluc*-specific shRNA-coding sequence.

LV particles from the resulting SIN-LV shuttle plasmids, pLKO.1-mKcnj5-shRNA.hEEF1a1.eGFP and pLKO.1-PpLuc-shRNA.hEEF1a1.eGFP were produced as described previously.[18]

Transduction of aCMCs was performed at day 4 of culture by pipetting LV suspension in the culture medium and incubating for 18 hours at a multiplicity of infection that resulted in transduction of essentially all aCMCs.

Patterned attachment

To study the effect of Kir3.4 heterogeneity in atrial defibrillation, regional differences in Kir3.4 expression were created using patterned attachment of cardiomyocytes transduced with LV-Kir3.4↓ or LV-PpLuc↓ (as a negative control) and untransduced cells. Directly after aCMC isolation, lentiviral vector suspension was pipetted in half of the aCMC suspension. Custom-made UV-treated Plexiglas inserts were used to occupy the exact upper half (down to 0.5mm from the bottom of the culture to prevent damaging of the fibronectin coating and attached cells later on) of the culture during plating of the transduced cells (4×10^5 cells/well). After allowing the transduced aCMCs to attach to the bottom half of the culture for 4 hours, medium was removed and cells were rinsed 3 times with PBS to remove unattached cells and remaining lentiviral vector particles. The Plexiglas inserts were moved to the bottom half of the dish after which untransduced cells (4×10^5) were plated on the upper half of the culture. Plexiglass inserts were removed after 4 hours followed by rinsing with PBS and refreshing of the Ham's F10 medium. Mitomycin-C treatment was performed at day 1 of culture to prevent unwanted proliferation of the non-myocyte fraction. Culturing of confluent monolayers with patterned expression of Kir3.4 and controls followed the standard protocol described above. Analyses were performed at day 9 of culture.

Optical mapping

Optical mapping of the action potential propagation using di-4-ANEPPS (Life Technologies) as a voltage sensitive dye and its corresponding analyses were performed essentially using methods described previously.[18,41] Briefly, aCMC monolayers were incubated with DMEM/HamsF12 containing 8μM di-4-ANEPPS for 15 minutes in the humidified CO_2 incubator at 37ºC. Following incubation, cells were refreshed with DMEM/HamsF12 and optical images were immediately captured with a MiCAM ULTIMA-L high resolution (100x100 pixels, 160μm/pixel) imaging system (SciMedia, Costa Mesa, CA) at 6ms/frame. Conduction velocity, APD to 80% repolarization APD_{80}, reentry cycle length and wavelength (defined as the conduction velocity×APD_{80} during reentry) were calculated using BrainVision Analyzer 1304 (BrainVision, Tokyo, Japan). Pre-shock peak-to-peak interval (PPI) was defined as the time between the peaks of the last pre-shock action potential and shock-induced action potential. Activation maps and line analyses were constructed after high-pass filtering. APD maps, PPI maps and single pixel recordings were non-high-pass and spatially filtered in a 3x3 pixel grid. Complexity was defined as the number of phase singularities (PSs) per culture, determined by using the phase space method as described previously.[18,41] Defibrillation was performed using a custom electroshock module, capable of producing biphasic truncated exponential shocks of adjustable voltages (Supplemental Figure 1A) coupled to two platinum electrodes fixed in a plastic ring that is readily mountable to the top of a 24-well culture plate. Electrodes were 9-mm in length, placed parallel 11-mm apart, 2 mm above the surface of the culture (Supplemental Figure 1B-D). Peak voltage of the first phase was documented and used in further analyses (Figure 1C). Settings of the electroshock module were calibrated using a DLM4000 digital oscilloscope (Yokogawa, Tokyo, Japan). Successful defibrillation was defined elimination of all reentrant conduction without reinitiation of reentrant conduction after termination. Reinitiation of fibrillation was defined as the occurrence of new PSs and consequent reentrant conduction after elimination of the PS giving rise to the activation wavefront in the respective area within 1000 ms after application after the shock.

To assess the effect of $I_{K,ACh-c}$ blockade on defibrillation, tertiapin (100 nM) was pipetted in the medium en dispersed by gentle agitation, directly followed by optical mapping.

Ex vivo mapping

Two-Day-old Wistar rats were anesthetized by isoflurane inhalation (5%). After confirmation of adequate anesthesia by absence of pain reflexes, the hearts were excised and submersed in ice cold Tyrode's solution (comprising [in mM] NaCl 130, $CaCl_2$ 1.8, KCl 4.0, $MgCl_2$ 1.0, NaH_2PO_4 1.2, $NaHCO_3$ 24 and glucose 5.5 at pH 7.4). Subsequently, the aorta was canulated and retrogradely perfused with oxygenated Tyrode's solution supplemented with 20 mM 2,3-butanedione monoxime (Sigma-Aldrich) to minimize motion artifacts

using a modified Langendorff apparatus (AD instruments, Spechbach, Germany). The heart was submersed in a 16-mm diameter tissue bath containing Tyrode's solution to allow usage of the same electroshock module as in the aCMC monolayer experiments for defibrillation (see Supplemental Figure 1 and Figure 8A). Hearts were stained with 2 µM di-4-anepps by a 5 ml bolus injection. AF was induced by burst pacing at a cycle length of 20-100 ms using a concentric bipolar platinum/iridium electrode (FHC inc. Bowdoin, ME). To assess the effect of $I_{K,ACh}$ blockade on defibrillation, tertiapin (100 nM) was added to the perfusate as well as the tissue bath.

Statistics

Statistical analyses and construction of corresponding graphs were performed using Graphpad Prism version 6.0 software (Graphpad Software, San Diego, CA). Comparison between two groups was performed using the Mann-Whitney U test or Wilcoxon signed rank test where appropriate. Kruskall-Wallis testing with Bonferoni *post-hoc* correction was used for multiple groups and comparisons. Data were expressed as mean±standard deviation (SD) for a number (n) of observations. Differences were considered statistically significant at $p<0.05$. Non-linear regression curves were constructed by using a robust exponential two-phase decay curve fit. Accuracy of these curves was expressed as the coefficient of determination (R^2).

REFERENCE LIST

1. Lloyd-Jones, D.M. et al. Lifetime risk for development of atrial fibrillation: the Framingham Heart Study. *Circulation*. **110**, 1042-1046 (2004).
2. Nieuwlaat, R. et al. Prognosis, disease progression, and treatment of atrial fibrillation patients during 1 year: follow-up of the Euro Heart Survey on atrial fibrillation. *Eur Heart J*. **29**, 1181-1189 (2008).
3. Wijffels, M.C., Kirchhof, C.J., Dorland, R. & Allessie, M.A. Atrial fibrillation begets atrial fibrillation. A study in awake chronically instrumented goats. *Circulation*. **92**. 1954-1968 (1995).
4. Benjamin, E.J. et al. Impact of atrial fibrillation on the risk of death: the Framingham Heart Study. *Circulation*. **98**, 946-952 (1998).
5. Shinbane, J.S. et al. Tachycardia-induced cardiomyopathy: a review of animal models and clinical studies. *J Am Coll Cardiol*. **29**, 709-715 (1997).
6. Wolf, P.A., Abbott, R.D. & Kannel, W.B. Atrial fibrillation as an independent risk factor for stroke: the Framingham Study. *Stroke*. **22**, 983-988 (1991).
7. Anderson, J.L. et al. Management of patients with atrial fibrillation (compilation of 2006 ACCF/AHA/ESC and 2011 ACCF/AHA/HRS recommendations): a report of the American College of Cardiology/American Heart Association Task Force on Practice Guidelines. *J Am Coll Cardiol*. **61**, 1935-1944 (2013).
8. Chugh, S.S., Blackshear, J.L., Shen, W.K., Hammill, S.C. & Gersh, B.J. Epidemiology and natural history of atrial fibrillation: clinical implications. *J Am Coll Cardiol*. **37**, 371-378 (2001).
9. Mittal, S. et al. Transthoracic cardioversion of atrial fibrillation: comparison of rectilinear biphasic versus damped sine wave monophasic shocks. *Circulation*. **101**, 1282-1287 (2000).
10. van Gelder, I.C., Crijns, H.J., van Gilst, W.H., Verwer, R. & Lie, K.I. Prediction of uneventful cardioversion and maintenance of sinus rhythm from direct-current electrical cardioversion of chronic atrial fibrillation and flutter. *Am J Cardiol*. **68**, 41-46 (1991).
11. Blich, M. & Edoute, Y. Electrical cardioversion for persistent or chronic atrial fibrillation: outcome and clinical factors predicting short and long term success rate. *Int J Cardiol*. **107**, 389-394 (2006).
12. Ambler, J.J. & Deakin, C.D. A randomised controlled trial of the effect of biphasic or monophasic waveform on the incidence and severity of cutaneous burns following external direct current cardioversion. *Resuscitation*. **71**, 293-300 (2006).
13. Page, R.L. et al. Biphasic versus monophasic shock waveform for conversion of atrial fibrillation: the results of an international randomized, double-blind multicenter trial. *J Am Coll Cardiol*. **39**, 1956-1963 (2002).
14. Cha, T.J. et al. Kir3-based inward rectifier potassium current: potential role in atrial tachycardia remodeling effects on atrial repolarization and arrhythmias. *Circulation*. **113**, 1730-1737 (2006).
15. Dobrev, D. et al. Human inward rectifier potassium channels in chronic and postoperative atrial fibrillation. *Cardiovasc Res*. **54**, 397-404 (2000).
16. Dobrev, D. et al. The G protein-gated potassium current I(K,ACh) is constitutively active in patients with chronic atrial fibrillation. *Circulation*. **112**, 3697-3706 (2005).
17. Ehrlich, J.R. et al. Characterization of a hyperpolarization-activated time-dependent potassium current in canine cardiomyocytes from pulmonary vein myocardial sleeves and left atrium. *J Physiol*. **557**, 583-597 (2004).
18. Bingen, B.O. et al. Atrium-Specific Kir3.x Determines Inducibility, Dynamics, and

Termination of Fibrillation by Regulating Restitution-Driven Alternans. *Circulation*. **128**, 2732-2744 (2013).

19. Echt, D.S. et al. Mortality and morbidity in patients receiving encainide, flecainide, or placebo. The Cardiac Arrhythmia Suppression Trial. *N Engl J Med*. **324**, 781-788 (1991).
20. Hohnloser, S.H., & Singh, B.N. Proarrhythmia with class III antiarrhythmic drugs: definition, electrophysiologic mechanisms, incidence, predisposing factors, and clinical implications. *J Cardiovasc Electrophysiol*. **6**, 920-936 (1995).
21. Clayton, R.H., Zhuchkova, E.A. & Panfilov, A.V. Phase singularities and filaments: simplifying complexity in computational models of ventricular fibrillation. *Prog Biophys Mol Biol*. **90**, 378-398 (2006).
22. Ricard, P. et al. Prospective assessment of the minimum energy needed for external electrical cardioversion of atrial fibrillation. *Am J Cardiol*. **79**, 815-816 (1997).
23. Dosdall, D.J., Fast, V.G. & Ideker, R.E. Mechanisms of defibrillation. *Annu Rev Biomed Eng*. **12**, 233-258 (2010).
24. Zipes, D.P., Fischer, J., King, R.M., Nicoll, A.D. & Jolly, W.W. Termination of ventricular fibrillation in dogs by depolarizing a critical amount of myocardium. *Am J Cardiol*. **36**, 37-44 (1975).
25. Chen, P.S. et al. Activation during ventricular defibrillation in open-chest dogs. Evidence of complete cessation and regeneration of ventricular fibrillation after unsuccessful shocks. *J Clin Invest*. **77**, 810-823 (1986).
26. Efimov, I.R., Cheng, Y., Van Wagoner, D.R., Mazgalev, T. & Tchou, P.J. Virtual electrode-induced phase singularity: a basic mechanism of defibrillation failure. *Circ Res*. **82**, 918-925 (1998).
27. Wang, N.C. et al. Optical mapping of ventricular defibrillation in isolated swine right ventricles: demonstration of a postshock isoelectric window after near-threshold defibrillation shocks. *Circulation*. **104**, 227-233 (2001).
28. Chattipakorn, N. & Ideker, R.E. Delayed afterdepolarization inhibitor: a potential pharmacologic intervention to improve defibrillation efficacy. *J Cardiovasc Electrophysiol*. **14**, 72-75 (2003).
29. Burashnikov, A. & Antzelevitch, C. Reinduction of atrial fibrillation immediately after termination of the arrhythmia is mediated by late phase 3 early afterdepolarization-induced triggered activity. *Circulation*. **107**, 2355-2360 (2003).
30. Sobie, A., Susil, R.C., & Tung, L. A generalized activating function for predicting virtual electrodes in cardiac tissue. *Biophys J*. **73,** 1410-1423 (1997).
31. Wikswo, J.P., Lin, S.F. & Abbas, R.A. Virtual electrodes in cardiac tissue: a common mechanism for anodal and cathodal stimulation. *Biophys J*. **69**, 2195-2210 (1995).
32. Cheng, Y., Mowrey, K.A., Van Wagoner, D.R., Tchou, P.J. & Efimov, I.R. Virtual electrode-induced reexcitation: A mechanism of defibrillation. *Circ Res*. **85**, 1056-1066 (1999).
33. Skouibine, K.B., Trayanova, N.A. & Moore, P.K. Anode/cathode make and break phenomena in a model of defibrillation. *IEEE Trans Biomed Eng* **46**, 769-777 (1999).
34. Hillebrenner, M.G., Eason, J.C. & Trayanova, N.A. Mechanistic inquiry into decrease in probability of defibrillation success with increase in complexity of preshock reentrant activity. *Am J Physiol Heart Circ Physiol*. **286**, H909-H917 (2004).
35. Fast, V.G., Rohr, S., Gillis, A.M. & Kleber, A.G. Activation of cardiac tissue by extracellular electrical shocks: formation of 'secondary sources' at intercellular clefts in monolayers of cultured myocytes. *Circ Res*. **82**, 375-385 (1998).
36. Trayanova, N., Skouibine, K. & Aguel, F. The role of cardiac tissue structure in defibrillation. *Chaos*. **8**, 221-233 (1998).
37. Frazier, D.W. et al. Stimulus-induced critical point. Mechanism for electrical initiation

of reentry in normal canine myocardium. *J Clin Invest*. **83**, 1039-1052 (1989).

38. Jalife, J. Deja vu in the theories of atrial fibrillation dynamics. *Cardiovasc Res*. **89**, 766-775 (2011).
39. Rossi, M., & Lown, B. The use of quinidine in cardioversion. *Am J Cardiol*. **19**, 234-238 (1967).
40. Yamamoto, W. Effects of the selective KACh channel blocker NTC-801 on atrial fibrillation in a canine model of atrial tachypacing: comparison with class Ic and III drugs. *J Cardiovasc Pharmacol*. **63**, 421-427 (2014).
41. Bingen, B.O. et al. Prolongation of minimal action potential duration in sustained fibrillation decreases complexity by transient destabilization. *Cardiovasc Res*. **97**, 161-170 (2013).

Chapter VI

Light-induced termination of spiral wave arrhythmias by optogenetic engineering of atrial cardiomyocytes.

Light-induced arrhythmia termination

Brian O. Bingen, MD,*; Marc C. Engels, MD,*; Martin J. Schalij, MD, PhD; Wanchana Jangsangthong, PhD; Zeinab Neshati, MSc; Iolanda Feola, MSc; Dirk L. Ypey, PhD; Saïd F.A. Askar, PhD; Alexander V. Panfilov, PhD; Daniël A. Pijnappels, PhD,*; Antoine A.F. de Vries, PhD,*

Cardiovasc Res. 2014;104:194-205

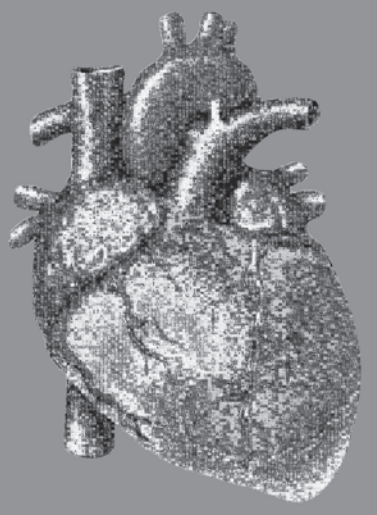

ABSTRACT

Aims: Atrial fibrillation (AF) is the most common cardiac arrhythmia and often involves reentrant electrical activation (e.g. spiral waves). Drug therapy for AF can have serious side effects, while electrical shock therapy is associated with discomfort and tissue damage. Hypothetically, forced expression and subsequent activation of light-gated cation channels in cardiomyocytes might deliver a depolarizing force sufficient for defibrillation, thereby circumventing the aforementioned drawbacks. Therefore, we investigated the feasibility of light-induced spiral wave termination through cardiac optogenetics.

Methods and Results: Neonatal rat atrial cardiomyocyte monolayers were transduced with lentiviral vectors encoding light-activated Ca2+-translocating channelrhodopsin (CatCh; LV.CatCh~eYFP↑) or eYFP (LV.eYFP↑) as control, and burst-paced to induce spiral waves rotating around functional cores. Effects of CatCh activation on reentry were investigated by optical and multi-electrode array (MEA) mapping. Western blot analyses and immunocytology confirmed transgene expression. Brief blue light pulses (10ms/470nm) triggered action potentials only in LV.CatCh~eYFP↑-transduced cultures, confirming functional CatCh-mediated current. Prolonged light pulses (500ms) resulted in reentry termination in 100% of LV.CatCh~eYFP↑-transduced cultures (n=31) vs 0% of LV.eYFP↑-transduced cultures (n=11). Here, CatCh activation caused uniform depolarization, thereby decreasing overall excitability (MEA peak-to-peak amplitude decreased 251.3±217.1 vs 9.2±9.5μV in controls). Consequently, functional coresize increased and phase singularities (PSs) drifted, leading to reentry termination by PS-PS or PS-boundary collisions.

Conclusions: This study shows that spiral waves in atrial cardiomyocyte monolayers can be terminated effectively by a light-induced depolarizing current, produced by the arrhythmogenic substrate itself, upon optogenetic engineering. These results provide a new rationale for the design of shockless defibrillation strategies.

INTRODUCTION

Atrial Fibrillation (AF) is the most common cardiac rhythm disorder in clinical practice, substantially contributing to morbidity and mortality, especially in the elderly.[1] Yet, knowledge about its underlying mechanisms remains far from complete, although reentrant conduction is widely accepted to play a prominent role in AF. Still, current treatment of AF is suboptimal.[1-3] To convert AF to normal cardiac rhythm, drug treatment and/or electrical cardioversion are being employed. Drug treatment is rather ineffective and may have dangerous side effects such as the occurrence of ventricular arrhythmias, while electrical cardioversion is associated with tissue damage and serious discomfort. This makes the use of external or implantable cardioverter/defibrillator devices in AF treatment undesirable, as most patients would require multiple shocks per day causing electrical cardioversion to serve as a last resort treatment modality only.[4] Hence, a search for an effective, but less painful and shockless method of cardioversion is warranted.

Electrical cardioversion relies on synchronous depolarization of large areas of the atrial myocardium, in order to terminate the reentrant conduction underlying fibrillation.[5] In theory, shockfree cardioversion might be elicited by genetically modifying the atrial cardiomyocytes to express depolarizing cation channels that can be activated through other means than electroshock, granted that the endogenous electrochemical gradients provide sufficient depolarizing force. Recently, optogenetics has been introduced as a method combining genetic engineering with light stimulation to control, with very high spatial and temporal resolution, specific cellular properties,[6] including the membrane potential of excitable cells.[7-9] To this end, light-gated ion channels from the microbial opsin family are expressed in target cells like cardiomyocytes or neurons, and subsequently activated by light of defined wavelengths to generate a controllable ioncurrent. This strategy has previously been proven to be effective for light-induced pacing of ventricular cardiomyocytes following the forced expression of depolarizing light-gated channels in these cells.[8] Hence, optogenetics might provide a feasible combination of cation channels and mode of activation to achieve shockfree cardioversion. Still, it is unknown whether optogenetic engineering of atrial cardiomyocytes (aCMCs) allows for light-induced termination of fibrillation maintained by reentrant spiral waves.

Therefore, we investigated whether by optogenetic modification of aCMCs, a depolarizing photocurrent (*i.e.* an ion current elicited by light) could be generated sufficiently strong to terminate reentrant conduction in monolayer cultures of these cells. To this purpose, we employed Ca^{2+}-translocating channelrhodopsin (CatCh),[10] an ultra-sensitive light-gated cation channel, and a blue (470 nm) light-emitting diode (LED)-based light source for its activation. The effects of CatCh activation on reentrant conduction were investigated by voltage-sensitive dye and multi-electrode array (MEA) mapping in a 2D monolayer model of spiral wave reentry using neonatal rat aCMCs.[11]

METHODS

Animal studies

All animal experiments were approved by the Animal Experiments Committee of the Leiden University Medical Center and conformed to the Guide for the Care and Use of Laboratory Animals as stated by the US National Institutes of Health.

Cell isolation and culture

Neonatal rat aCMCs were isolated as described previously.[11] Briefly, 2-day-old Wistar rats were anaesthetized by 5% isoflurane inhalation and adequate anaesthesia was confirmed by the absence of reflexes. Hearts were rapidly excised and atria were carefully separated from the ventricles. Next, atrial tissue was minced and dissociated with collagenase type 1 (450 U/ml; Worthington, Lakewood, NJ) and DNase I (18,75 Kunitz/ml; Sigma-Aldrich, St. Louis, MO) and pre-plated on Primaria-coated cell culture dishes (Becton Dickinson, Breda, the Netherlands) for 120 minutes to allow selective attachment of non-myocytes (mainly cardiac fibroblasts). Unattached cells (mainly aCMCs) were seeded in 24-well cell culture plates (Corning Life Sciences, Amsterdam, the Netherlands) containing fibronectin (Sigma-Aldrich)-coated, round glass coverslips (15-mm diameter). Cell densities of $0.5\text{-}8\times10^5$ cells/well were used depending on the assay. At day 1 of culture, cells were incubated with Mitomycin-C (10 µg/ml; Sigma-Aldrich) for 2 hours, as described previously.[12] The culture medium, which consisted of Dulbecco's modified Eagle's medium/HAM's F10 (1:1, v/v; Life Technologies, Bleiswijk, the Netherlands) supplemented with 5% horse serum (Life Technologies), was refreshed daily and cells were cultured in a humidified incubator at 37°C and 5% CO_2.

Construction of self-inactivating lentiviral vector (SIN-LV) shuttle plasmids

The CatCh-encoding SIN-LV shuttle plasmid pLV-CaMKIIa-hChR2(L132C)-eYFP.WPRE was kindly provided by the Stanford Optogenetics Resource Center (http://www.stanford.edu/group/dlab/optogenetics). To allow generation of SIN-LVs directing high-level *CatCh* expression in aCMCs, the murine *calcium/calmodulin-dependent protein kinase II alpha* promotor in pLV-CaMKIIa-hChR2(L132C)-eYFP.WPRE was replaced by a polymerase chain reaction (PCR) fragment encoding the striated muscle-specific MHCK7 promotor.[13] The MHCK7 promoter was amplified with VELOCITY DNA polymerase (GC Biotech, Alphen aan den Rijn, the Netherlands) from a derivative of plasmid LV.ΔPRE.pA+.MHCK7.Luc[14] using deoxyribonucleotides A117 (5' CCTTAATTAACCCTTCAGATTAAAAATAACTGA 3') and A118 (5' TTACCGGTGCTGGCTGGCTCCTGA 3'; Sigma-Aldrich) as forward and reverse primer, respectively. Subcloning was done using the restriction enzymes PacI and AgeI-HF (both from New England Biolabs, Ipswich, MA), recognition sequences of which were introduced at both ends of the MHCK7 promoter fragment

by the PCR procedure. This yielded the SIN-LV shuttle plasmid pLV.MHCK7.CatCh~eYFP.WHVPRE. For making a negative control vector, pLV.MHCK7.CatCh~eYFP.WHVPRE was incubated with AgeI-HF and BoxI (Thermo Fisher Scientific, Waltman, MA), treated with Klenow polymerase (Thermo Fisher Scientific) and the resulting 10.0-kb DNA fragment was self-ligated yielding pLV.MHCK7.eYFP.WHVPRE. The correctness of the SIN-LV shuttle constructs was verified by restriction mapping with 5 different enzymes and by partial nucleotide sequence analysis using the Quick Shot sequencing services of BaseClear (Leiden, the Netherlands). For large-scale purification of the SIN-LV shuttle and packaging plasmids the JETSTAR 2.0 Plasmid Maxiprep kit (Genomed, Löhne, Germany) was used following the instructions of the manufacturer.

SIN-LV production

LV.CatCh~eYFP↑ and LV.eYFP↑ particles were produced from the SIN-LV shuttle plasmids pLV.MHCK7.CatCh~eYFP.WHVPRE and pLV.MHCK7.eYFP.WHVPRE, respectively, using a previously described method.[11] The concentrated vector suspensions were aliquoted in 100 µL portions and stored at -80ºC until use. aCMCs were transduced at day 4 of culture by adding vector suspension directly to the culture medium. After 18 hours, cells were washed once with phosphate-buffered saline (PBS) and given fresh culture medium. The SIN-LVs were applied at doses that resulted in the transduction of essentially all aCMCs. Transduction level was assessed by eYFP visualization with an Axiovert 200M inverse fluorescence microscope (Carl Zeiss, Sliedrecht, the Netherlands).

Immunocytology

Cultures were stained with antibodies directed against α-actinin (mouse IgG1, clone EA-53; Sigma-Aldrich), collagen type 1 (rabbit IgG; Abcam, Cambridge, MA, ab292), Cx43 (rabbit Ig; Sigma-Aldrich, C6219) and MLC2a (a gift from Dr. S.W. Kubalak, Charleston, SC)[15] after fixation in PBS/4% formaldehyde and permeabilization with PBS/0.1% Triton X-100. Incubation with primary antibodies (1:200 dilution in PBS+5% fetal bovine serum [FBS; Life Technologies]) and corresponding Alexa Fluor 488/568-conjugated secondary antibodies (Life Technologies; 1:400 dilution in PBS+5% FBS) was done at 4ºC. Nuclear counterstaining was performed at room temperature with 10 µg/ml Hoechst 33342 (Life Technologies) in PBS/5% FBS. Coverslips were mounted in Vectashield mounting medium (Vector Laboratories, Burlingame, CA). Images were acquired with a digital color camera-equipped fluorescence microscope (Nikon Eclipse 80i; Nikon Instruments Europe, Amstelveen, the Netherlands). Storage and quantification of immunofluorescence signals was done using dedicated software (NIS Elements [Nikon Instruments Europe] and ImageJ [version 1.43; National Institutes of Health, Bethesda, MD]). Each immunostaining was performed on ≥3 independent aCMC cultures.

Western blotting

Cells were lysed in RIPA buffer (50 mM Tris–HCl [pH 8.0], 150 mM NaCl, 1% Triton X-100, 0.5% sodium deoxycholate, 0.1% sodium dodecyl sulfate supplemented with protease inhibitors [cOmplete, Mini Protease Inhibitor Cocktail Tablet; Roche Applied Science, Penzberg, Germany]). Protein concentration was determined with the BCA Protein Assay Reagent (Thermo Fisher Scientific). Proteins were size-fractionated in NuPage Novex 12% Bis-Tris gels (Life Technologies) and transferred to Hybond polyvinylidene difluoride membranes (GE Healthcare, Diegem, Belgium) by wet electroblotting. After blocking for 1 hour in Tris-based saline/0.1% Tween-20 (TBS-T)/5% bovine serum albumin (BSA; Sigma-Aldrich), membranes were incubated for 1 hour with primary antibodies directed against green fluorescent protein (rabbit IgG; 1:1,000; Life Technologies, A-11122;) to detect eYFP or the CatCh~eYFP fusion protein or against glyceraldehyde 3-phosphate dehydrogenase (GAPDH; mouse IgG1, clone 6C5; 1:100,000; Merck Millipore, Billerica, MA) as loading control. Next, blots were incubated with corresponding horseradish peroxidase-conjugated secondary antibodies (1:1,000 in TBST/5% BSA; Santa Cruz Biotechnology, Dallas, TX) again for 1 hour. Blots were then immersed in ECL Prime Western blot detection reagent (GE Healthcare) and chemiluminescence was measured with the ChemiDoc XRS imaging system (Bio-Rad Laboratories, Veenendaal, the Netherlands).

Optical mapping

To analyze the electrophysiological effect of CatCh-generated photocurrents on aCMC cultures, cells were assayed by optical mapping on day 7 or 8 of culture. Action potential (AP) propagation was visualized using the voltage-sensitive dye di-4-ANEPPS (Life Technologies). Cells were stimulated either electrically with an epoxy-coated bipolar platinum electrode with square suprathreshold electrical stimuli at 1-2 Hz or optically with light pulses from a 470-nm light-emitting diode (LED; SR-01-B0040 Rebel Star LED assembly; 70 lm at 700 mA; Luxeonstar, Brantford, Ontario, Canada) mounted 10 mm below the center of the wells of a 24-well cell culture plate. A specialized stimulus generator (STG 2004) with corresponding software (MC Stimulus II; both from Multichannel Systems, Reutlingen, Germany) was used to perform both electrical and optical stimulation (see also Supplementary material online, *Figure S1*). Irradiance was measured using a PM100D optical power meter (Thorlabs, Munich, Germany) equipped with a S130C slim dual range sensor with the range set at 5 nW-5 mW and the wavelength set at 470 nm. Optical images were captured using a MiCAM ULTIMA-L imaging system (SciMedia, Costa Mesa, CA). Optical pacing was performed by exposure for 10 milliseconds (ms) to blue LED light at the maximal irradiance achievable with our setup (0.038 mW/mm^2). Strength-duration curves of optical pacing threshold were constructed by varying pulse duration (5-25 ms) and irradiance (0.0050 -0.038 mW/mm^2. Reentry was induced by electrical burst pacing with a cycle length of 20-100 ms. After confirmation of the presence of reentrant arrhyth-

mias, cultures were exposed to blue LED light for 500 ms (at 0.038 mW/mm^2). Specialized software was used for data analysis and construction of activation maps (BrainVision Analyzer 1101; Brainvision, Tokyo, Japan). For baseline shift adjustment during blue LED light exposure, several filters were applied allowing data interpretation during the LED-on period (see Supplementary material online, *Figure S1*). The phase space method was used to identify and track phase singularities (PSs) of spiral waves as described previously.[16] As measure of wavefront curvature the straight distance between the spiral wave tip and the point of the first (or second) half winding of the wavefront was determined.[17] To this purpose, a tangent line was drawn along the wavefront in the direct vicinity of the PS (*Supplemental Figure S3, dashed white lines*). Next, the length of the normal line from its intersection with the tangent line to its intersection with the wavefront at half of the spiral wave's full winding was measured (*Supplemental Figure S3*).

MEA mapping

To provide additional mechanistic insight into CatCh-mediated effects on spiral waves and to avoid potential complexities associated with the combined application of light-activated potentiometric dyes and ion channels (see also Supplementary material online, *Figure S1*), MEA mapping of extracellular potentials was performed in parallel to optical mapping as a matching non-optical control. For MEA mapping, aCMCs were cultured in fibronectin-coated MEA culture dishes containing sixty 30 µm-diameter electrodes with an interelectrode spacing of 200 µm (Multi Channel Systems). Next, reentry was induced by electrical burst pacing as described above. During recording, cultures were exposed to blue LED light pulses (10 ms for optical pacing or 500 ms for reentry termination). Electrograms were analyzed using MC-Rack software (Multi Channel Systems).[18]

Whole-cell patch-clamp recordings

Voltage-clamp recordings in single LV.CatCh~eYFP↑-transduced aCMCs were carried out in parallel to optical mapping experiments. Transduced cells (identified by their green-yellow fluorescence) were exposed to 10- or 500-ms blue LED light pulses to study CatCh-mediated currents, after reaching GΩ seal, establishing whole-cell configuration and setting holding potential at -45 mV. Experiments were performed at 19-23°C using a MultiClamp 700B amplifier, a Digidata 1440A A/D converter, Clampex 10.3 software (all from Axon CNS, Molecular Devices, Sunnyvale, CA), the STG 2004 pulse generator with corresponding computer software and an Axiovert 35 inverted phase contrast and fluorescence microscope (Carl Zeiss). Cells were bathed in an extracellular solution composed of (in mmol/L) 137 NaCl, 5 KCl, 1 $MgCl_2$, 1.8 $CaCl_2$, 10 HEPES, and 11 glucose (pH 7.4 adjusted with NaOH). Patch pipettes manufactured from borosilicate glass with capillary 1.5 mm outer diameter and 1.17 mm inner diameter (Harvard Apparatus, Kent, United Kingdom) were pulled by a model P-30 vertical micropipette puller (Sutter Instrument Company,

Novato, CA). The internal pipette solution contained (in mmol/L) 20 NaCl, 120 KCl, 1 $MgCl_2$, 5 EGTA, and 10 HEPES (pH 7.4 adjusted with KOH). Pipettes showed a typical resistance of 2-3 MΩ and liquid junction potentials (~5 mV) were corrected. Data were digitized at 10 kHz, filtered at 10 kHz, -3 decibel (dB), 4 pole Bessel and analyzed off-line using pClamp 10 electrophysiology data acquisition and analysis software (Axon CNS, Molecular Devices).

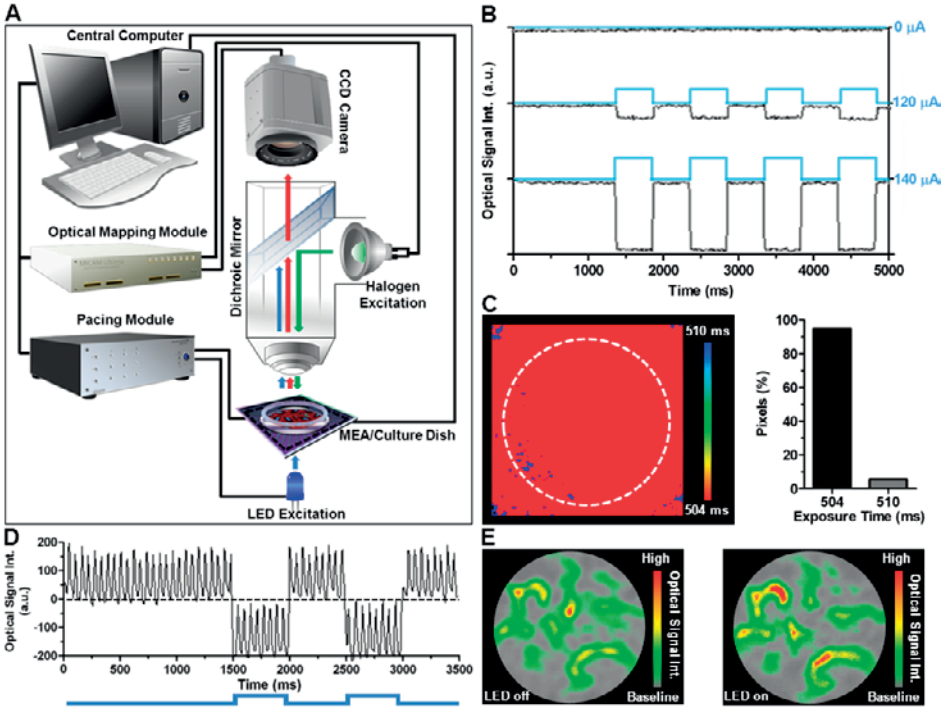

Supplementary Figure S1. *Mapping setup and LED-induced shift in optical signal baseline. (A) Schematic representation of the mapping setup. (B) Examples of optical signal traces during exposure of an atrial culture to 500-ms blue LED light pulses of different intensities by changing the current input generated by the pacing module from 0 (upper lines) to 120 (middle lines) and 140 (lower lines) µA, showing that the magnitude of the decrease in baseline optical signal depends on the intensity of the blue light. (C) Exposure map and quantification of the exposure time per pixel of the CCD camera measured at 6-ms intervals, showing exposure times of 504 and 510 ms for 94 and 4% of the pixels, respectively. (D) Typical example of an optical signal trace of an atrial culture during reentry induced by electrical burst pacing followed by exposure to two subsequent 500-ms blue LED light pulses, demonstrating that the drop in the baseline of the optical signal coincides with the exposure to blue light. The signal morphology remains unchanged, enabling direct read-out of the LED-on period in the optical mapping trace. (E) Snap shots of the optical signal in an atrial culture during reentry without exposure to blue light (left panel), and during exposure to blue light after correction of the baseline-drop artifact (right panel), showing similar optical signal distributions immediately before and 250 ms after the LED was turned on. MEA, multi-electrode array; a.u., arbitrary units.*

Statistical analysis

Statistical analyses were performed using SPSS11.0 for Windows (SPSS, Chicago, IL). The Mann-Whitney U test or the Wilcoxon signed rank test was used for comparison

between groups. Data were expressed as mean±standard deviation (SD) for a number (n) of observations. Differences were considered statistically significant at $p<0.05$.

RESULTS

Characterization of 2D AF model

Immunocytological analysis at day 8 showed that 100% of the α-actinin$^+$ cells in monolayer cultures of neonatal rat atrial cells were positive for myosin light chain 2a (MLC2a), *i.e.* no MLC2a$^-$/α-actinin$^+$ cells were detected, confirming that all cardiomyocytes in these cultures were of atrial origin (*Figure 1A*). Cultures contained 18.3±4.8% fibroblasts as judged by collagen type 1 immunostaining (*Figure 1B*). At day 8 of culture, cells showed abundant connexin 43 (Cx43) expression at intercellular junctions (*Figure 1C*) forming a dense "syncytial" monolayer (*Figure 1D*), which could be assessed for conduction patterns by optical mapping and by MEA analysis. Typically, no spontaneous activity was observed in the atrial cell cultures. Upon 1-Hz electrical stimulation cultures showed 1:1 uniform convex activation originating from the bipolar pacing electrode, while no PSs were observed (*Figure 1E,G*), resembling normal atrial activation as occurs during sinus rhythm. However, after burst pacing, multiple spiral wave reentry circuits and corresponding PSs arose maintaining high frequency activation (mean 13.8±7.0 Hz) independent of any subsequent electrical stimulation (*Figure 1F,H*), resembling activation patterns found in AF.

Confirmation of functional CatCh expression

Atrial cell cultures were transduced with either the lentiviral vector LV.CatCh~eYFP↑ encoding a fusion protein between CatCh and enhanced yellow fluorescent protein (eYFP), or the eYFP-encoding lentiviral vector LV.eYFP as a control, to study the effects of CatCh activation on spiral waves (for vector maps, see *Figure 2A*).

Because transgene expression is driven by a striated muscle-specific promoter, lentiviral vector-transduced atrial cultures showed eYFP signals almost exclusively in the α-actinin$^+$ cells (100±38.6 vs 8.7.±1.7 arbitrary units in non-myocytes and 100±37.0 vs 4.2±1.6 arbitrary units in non-myocytes for the LV.eYFP↑- and LV.CatCh~eYFP↑-transduced cultures, respectively; $p<0.05$). As expected, in the LV.eYFP↑-transduced aCMCs, eYFP localized to the cytoplasm, while in the LV.CatCh~eYFP↑-transduced cells, eYFP fluorescence was membrane-associated (*Figure 2B-D*). Western blot analysis confirmed eYFP expression in atrial cell cultures after transduction with both LV.eYFP↑ and LV.CatCh~eYFP↑, showing immunoreactive protein species of ~27 kDa (the predicted molecular weight of eYFP) and of around 60 kDa (due to fusion of CatCh to the N terminus of eYFP), respectively (*Figure 2E*). Optical and MEA mapping experiments showed

that APs could be elicited by optical pacing through exposure to 10-ms light pulses (at 0.038 mW/mm^2) in LV.CatCh~eYFP↑- but not in LV.eYFP↑-transduced cultures (see also Supplementary material online, *Figure S2* for a strength-duration analysis of the pacing threshold in LV.CatCh~eYFP↑-transduced cultures), while both culture types could be paced electrically (*Figure 3A,B*; n=12 and n=9, respectively). The maximum change in fluorescence intensity occurred within 12.0±8.5 ms (n=5) throughout the culture (*Figure 3C*), indicating synchronous depolarization of the monolayer by CatCh activation. The functionality of the generated photocurrent was further confirmed in patch-clamp experiments on single aCMCs (*Figure 3D*), which revealed inward currents with a peak current density of5.31±1.13 pA/pF upon exposure to 10-ms blue light pulses (n=6).

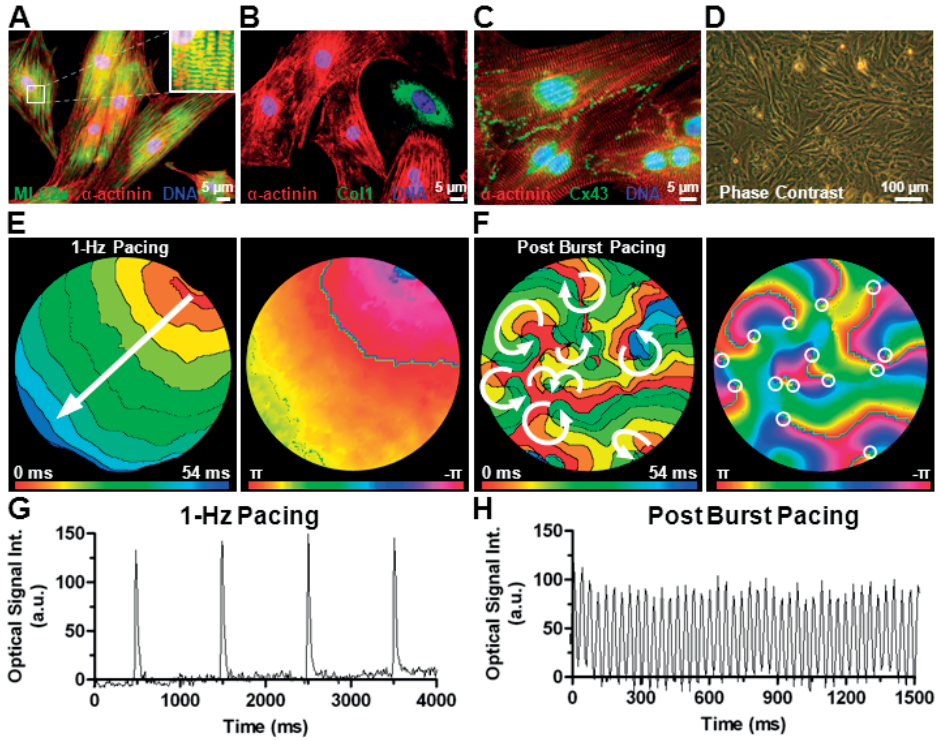

Figure 1. *Characterization of 2D AF model. Typical examples of immunocytological double stainings for (A) MLC2a (aCMCs, green) and α-actinin (cardiomyocytes, red), (B) α-actinin (cardiomyocytes, red) and collagen type 1 (Col1, fibroblasts, green) and (C) α-actinin (cardiomyocytes, red) and Cx43 (gap junctions, green) in atrial cell cultures. The white inset in panel A (top right) shows a magnification of the boxed area (left). (D) Phase contrast image of a confluent atrial cell monolayer. (E) Typical activation map (6-ms isochrone spacing) and corresponding phase map of an atrial culture during 1-Hz electrical pacing, showing uniform convex propagation originating from the electrode (in the direction of the white arrow; left panel) and absence of PSs (right panel). (F) Typical activation map (6-ms isochrone spacing) and corresponding phase map of an atrial culture after electrical burst pacing. Multiple reentrant circuits are evident in the activation map, following the directions of the white arrows. The phase map shows multiple PSs indicated by white circles. Typical spatially filtered optical (i.e. di-4-ANEPPS-derived) signal traces in an atrial culture (G) during 1-Hz pacing and (H) after fibrillation is established by electrical burst pacing. a.u., arbitrary units.*

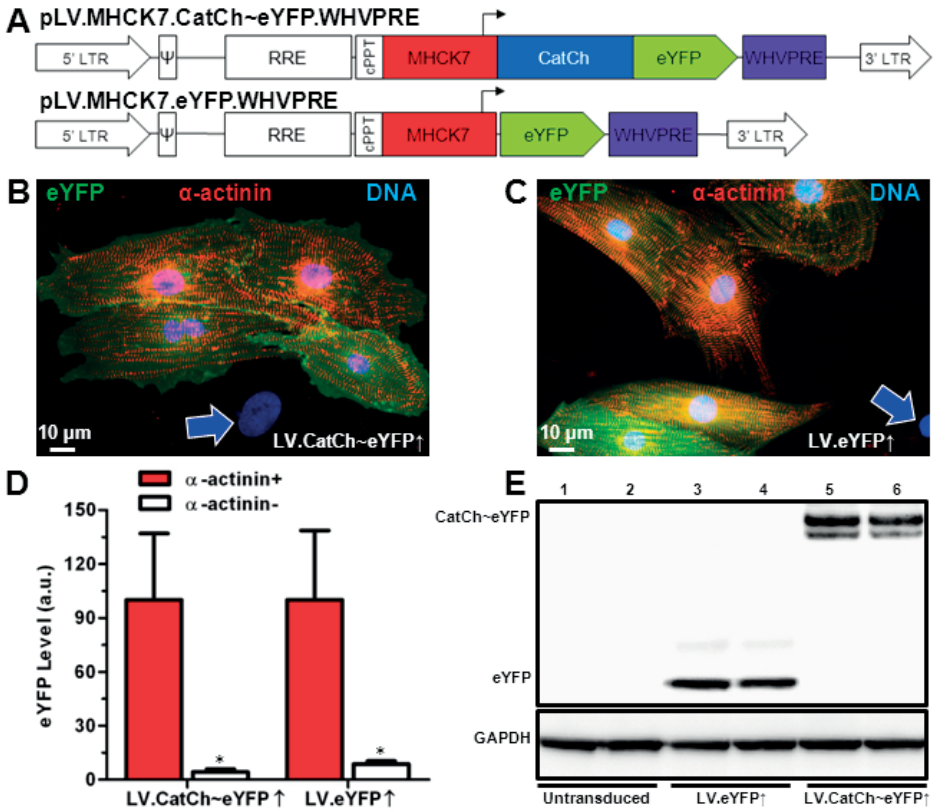

Figure 2. *Immunocytological and Western blot confirmation of forced CatCh expression. (A) Structure of the lentiviral vector DNA in plasmids pLV.MHCK7.CatCh~eYFP.WHVPRE (for generating LV.CatCh~eYFP↑) and pLV.MHCK7.eYFP.WHVPRE (to produce LV.eYFP↑). 5' LTR: chimeric 5' long terminal repeat containing enhancer and promoter elements of the human cytomegalovirus immediate-early gene and the human immunodeficiency virus type 1 (HIV1) R and U5 regions. Ψ: HIV1 packaging signal. RRE: HIV1 Rev-responsive element. cPPT: HIV1 central polypurine tract and termination site. MHCK7: chimeric striated muscle-specific promoter.[13] CatCh: coding sequence of an ultra-light-sensitive and highly Ca^{2+}-permeable mutant of the Chlamydomonas reinhardtii chlamyopsin 4 light-gated ion channel, also known as ChR2.[10] eYFP: Aequorea victoria enhanced yellow fluorescent protein-coding sequence. WHVPRE: woodchuck hepatitis virus posttranscriptional regulatory element. 3' LTR: wild type 3' HIV1 LTR. (B,C) Immunocytological staining of (B) LV.CatCh~eYFP↑- and (C) LV.eYFP↑-transduced atrial cultures for α-actinin (red; cardiomyocyte marker), showing membrane-associated and cytoplasmic eYFP signals (green), respectively. Blue arrows indicate nuclei of $eYFP^-$/α-$actinin^-$ cells (mainly cardiac fibroblasts). (D) Quantification of the eYFP signal in α-$actinin^+$ (red bars) and α-$actinin^-$ (white bars) cells in atrial cultures after transduction with LV.CatCh~eYFP↑ or with LV.eYFP↑. (E) Western blot analysis of eYFP/CatCh~eYFP levels in untransduced (lanes 1 and 2) atrial cultures and cultures transduced with LV.eYFP↑ (lanes 3 and 4) or LV.CatCh~eYFP↑ (lanes 5 and 6) using GAPDH as loading control. *:$p<0.05$ vs α-$actinin^+$ using the Mann-Whitney U test. a.u., arbitrary units.*

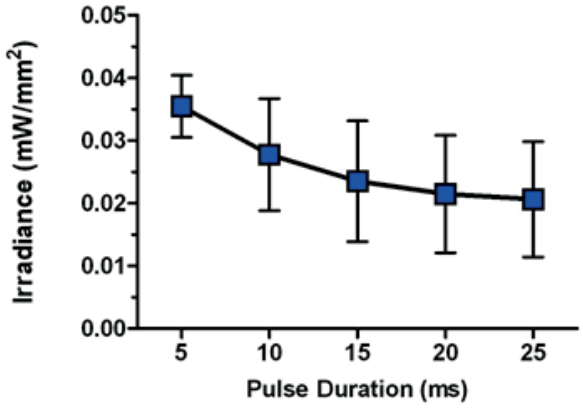

Supplementary Figure S2. *Strength-duration analysis of optical pacing threshold. Quantification of the average minimal irradiance necessary to elicit an AP at pulse durations of 5, 10, 15, 20 and 25 ms in aCMC cultures transduced with LV.CatCh~eYFP↑ (n=8).*

LIGHT-INDUCED SPIRAL WAVE TERMINATION

Exposure to prolonged light pulses (500 ms at 0.038 mW/mm^2), producing a sustained current with a peak density of 12.01±2.54 pA/pF in single aCMCs (n=6; *Figure 3D*), led to spiral wave termination in all of the LV.CatCh~eYFP↑- (31 out of 31), but none of the LV.eYFP↑-transduced (0 out of 11) cultures, as judged by optical mapping analyses and confirmed by MEA recordings (*Figure 4A-F*). Importantly, LV.CatCh~eYFP↑-transduced cultures that had been subjected to repeated optogenetic spiral wave termination displayed normal uniform conduction upon subsequent electrical activation implying retained excitability (*Figure 4E*). No significant persisting electrophysiological or pro-arrhythmic changes were observed in LV.CatCh.eYFP↑-transduced cultures following prolonged exposure (*i.e.* 500 ms) to blue light (see Supplementary material online, *Figure S4*). Also, contractility, as judged by phase-contrast microscopy, was retained after expression of CatCh~eYFP and its subsequent activation by a 500-ms blue light pulse. During exposure to a 500-ms light pulse reentry was terminated within 163.1±105.8 ms (range 36-444 ms, n=22) suggesting that reentry could be terminated using pulses shorter than 500 ms. Hence, to find the pulse duration necessary for termination we induced reentry in LV.CatCh.eYFP↑-transduced cultures and attempted spiral wave termination by exposure to subsequent blue light pulses of 10, 20, 50, 100, 200 and 500 ms at 0.038 mW/mm^2. This showed that the average pulse duration necessary for arrhythmia termination was 133.3±180.7 ms (n=6).

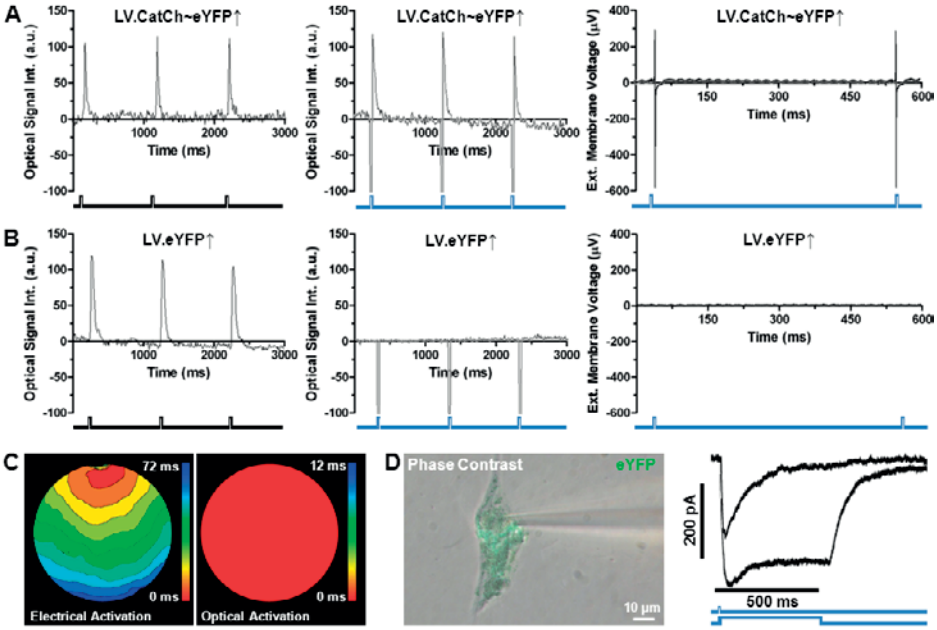

Figure 3. *Confirmation of functional CatCh expression. (A,B) Typical optical signal traces (left and middle panels) and MEA recordings (right panels) in aCMC cultures transduced with (A) LV.CatCh~eYFP↑ or (B) LV.eYFP↑ during 1-Hz electrical activation (left panels) or exposure to 10-ms blue light pulses at 1 Hz (middle panels) and 2 Hz (right panels). (C) Activation map of LV.CatCh~eYFP↑-transduced atrial cultures during 1-Hz electrical pacing (left) and exposure to 10-ms blue light pulses of 1 Hz (right). (D) Typical example of a CatCh~eYFP-expressing aCMC used for patch-clamping (left) and two superimposed records of whole-cell inward currents from the same aCMC evoked at a holding potential of -45 mV by a 10- and 500-ms blue light pulse of equal intensity (see bottom traces) (right). As expected, non-transduced aCMCs did not show light-dependent currents. a.u., arbitrary units.*

Next, we investigated the anti-arrhythmic mechanism underlying arrhythmia termination by CatCh activation. During reentry, a gradient in conduction velocity and AP amplitude was observed. Both parameters decreased near the spiral wave core (*Figure 5A*) while wavefront curvature was significantly higher near the core than in the periphery (the second vs the doubled first half winding distance of the wavefront were 7.2±1.9 vs 4.1±1.1 mm; $p<0.05$, n=6) (*Figure 5B*).

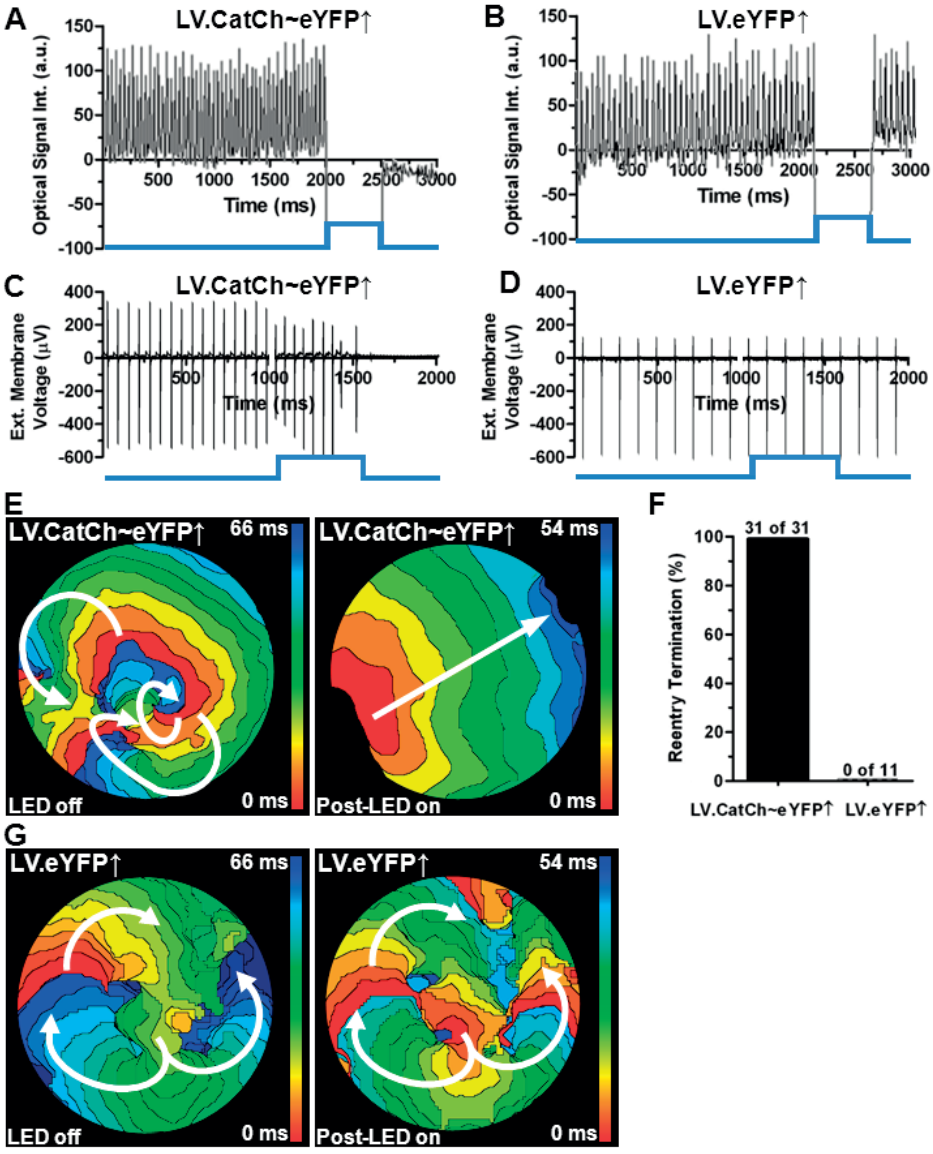

Figure 4. *Effective light-induced spiral wave termination by CatCh expression. Typical signal traces in reentrant tachyarrhythmic atrial cultures transduced with (A,C) LV.CatCh~eYFP↑ and (B,D) LV.eYFP↑ during (A,B) optical mapping or (C,D) MEA recordings, showing termination of tachyarrhythmic activity after exposure to blue light (500 ms-duration) in LV.CatCh~eYFP↑ cultures only. Typical activation map of (E) LV.CatCh~eYFP↑- and (G) LV.eYFP↑-transduced atrial cultures before (left panel) and after (right panel) exposure to a 500-ms blue light pulse, showing light-induced termination of reentrant activity. (F) Quantification of the success rate of light-induced spiral wave termination in LV.CatCh~eYFP↑- and LV.eYFP↑-transduced cultures. a.u., arbitrary units.*

Depolarization by activation of CatCh led to a reduction in overall excitability. The reduction in excitability caused by light-induced depolarization was confirmed by MEA mapping showing a strong decrease in peak-to-peak amplitude (Δpeak-to-peak amplitude 251.3±217.1 μV in LV.CatCh~eYFP↑-transduced cultures [n=6] vs 9.2±9.5 μV in LV.eYFP↑-transduced cultures [n=5]; *Figure 5C-E*), likely attributable to inactivation of the fast Na^+ current. As a consequence, the critical wavefront curvature (the curvature at which the conduction velocity becomes zero, *i.e.* the curvature near the spiral wave core) was decreased (first half winding distance was 2.6±1.1 before light exposure vs 5.0±2.5 mm during light exposure, n=6) (*Figure 5F* and Supplementary material online, *Figure S3*). Hence, during light exposure the critical wavefront curvature is reached at a greater distance from the spiral wave core than before light exposure. Since wavefront curvature cannot exceed the critical wavefront curvature, spiral wave core size increased after the decrease in excitability during light exposure. This was evinced by a reduction in AP amplitude and inhibition of excitation near the functional core (*Figure 5A*).

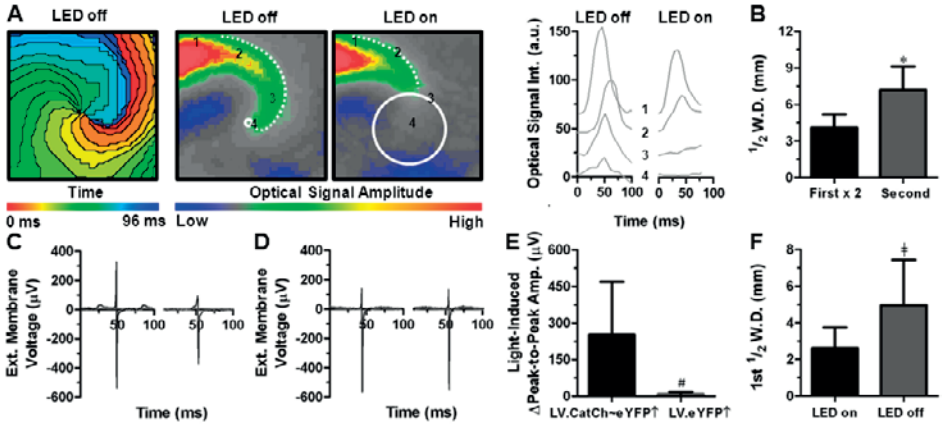

Figure 5. *Light-induced increase in functional core size. (A) Activation map (left panel) and snapshots (two middle panels) after spatial and high-pass filtering of optical signals of a LV.CatCh~eYFP↑-transduced atrial culture before and during exposure to a 500-ms blue light pulse (6-ms isochrone spacing). The optical signal traces (non-high-pass-filtered) are shown on the right. Numbers 1-4 correspond to the positions in the snapshots. White circles indicate estimated functional core sizes. (B) Quantification of the doubled first half winding distance (½ W.D.) of the wavefront and the second half winding distance as a measure of wavefront curvature during reentry in LV.CatCh.eYFP↑ transduced atrial cultures. (C) Typical MEA-recordings of LV.CatCh~eYFP↑- or (D) LV.eYFP↑-transduced atrial cultures during reentrant activity before (left) and at the beginning (right) of a 500-ms blue light pulse. (E) Quantification of MEA peak-to-peak amplitude changes upon exposure to blue light in LV.CatCh~eYFP↑- and LV.eYFP↑-transduced cultures. (F) Quantification of the first half winding distance in LV.CatCh~eYFP↑-transduced cultures prior to (LED off) and (LED on) during exposure to a 500-ms blue light pulse as a measure of wavefront curvature. *:p<0.05 vs doubled first half winding distance using a Wilcoxon signed rank test. #:p<0.05 vs LV.CatCh~eYFP↑-transduced cultures using a Mann-Whitney U test. ‡:p<0.05 vs LED on using a Wilcoxon signed rank test. a.u., arbitrary units.*

As a consequence of the lowered critical curvature, culture-wide expansion of the PS trajectory around the growing functional core occurred, which increased the probability of critical collisions of PSs with culture boundaries (*Figure 6A* and Supplementary material online, *Movie 1*) or with PSs of opposite chirality (*Figure 6B* and Supplementary material online, *Movie 2*), ultimately causing spiral wave termination.

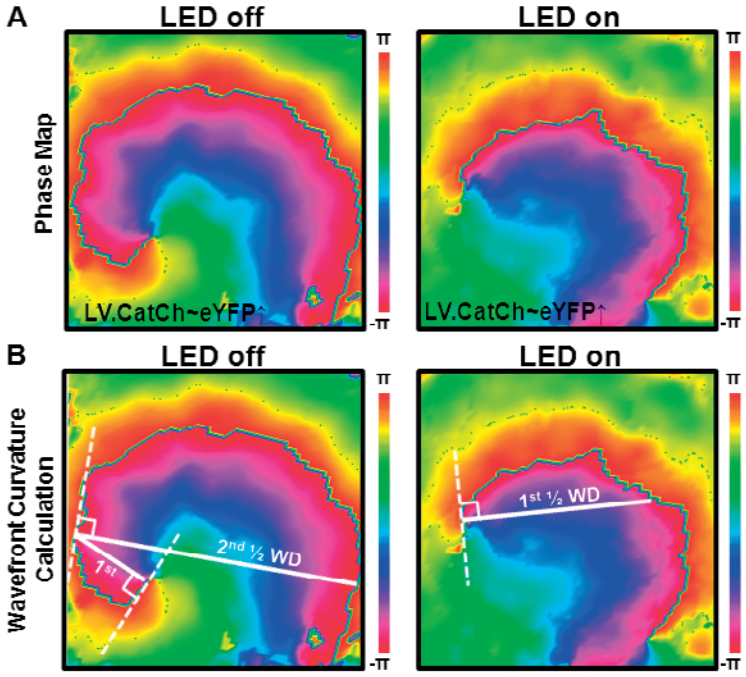

Supplementary Figure S3. *Wavefront curvature analysis. (A) Typical examples of phase maps of an LV.CatCh~eYFP↑-transduced aCMC culture before (left panel) and during (right panel) exposure to blue light. (B) The same phase maps as depicted in subfigure A including the lines used to measure the wavefront curvature. Dashed white lines represent tangent lines along the wavefront near the phase singularity. Uninterrupted white lines, perpendicular to the tangent line, represent the distance between the spiral wave tip and the wavefront at half winding (1st ½ WD). This shows that the 1st ½ WD is typically less than half of the second half winding distance, indicating an increase in wavefront curvature towards the phase singularity (left panel). The 1st ½ WD is increased during light exposure (right panel) indicating a decrease in wavefront curvature near the core.*

DISCUSSION

The key findings of this study are the following: First, neonatal rat aCMCs can be endowed with functional light-gated cation channels (*i.e.* CatCh) by lentiviral transduction without evident alterations in the characteristics of the AP or calcium transient. Second, activation of these channels by brief light pulses (10 ms/470 nm)

provides a depolarizing current strong enough to serve as suprathreshold stimulus for instant and synchronous electrical activation of CatCh-expressing cardiomyocytes in atrial monolayer cultures. Third, in such monolayers, stable rotors with PSs rotating around functional cores and maintaining fibrillatory activation, can be terminated effectively and repeatedly by prolonged activation of CatCh (500 ms). Fourth, mechanistically, prolonged CatCh activation reduces overall excitability of the fibrillating monolayers, followed by an increase in functional core size, resulting in PS drift, which ultimately leads to termination of the spiral wave arrhythmias. Finally, this is the first study to show that optogenetic engineering of neonatal rat aCMCs, by means of forced CatCh expression and subsequent photoactivation, allows fibrillating aCMC monolayers to generate themselves the electrical current needed for defibrillation. This proof-of-concept may give a strong impetus towards the design of shockless treatment strategies for AF.

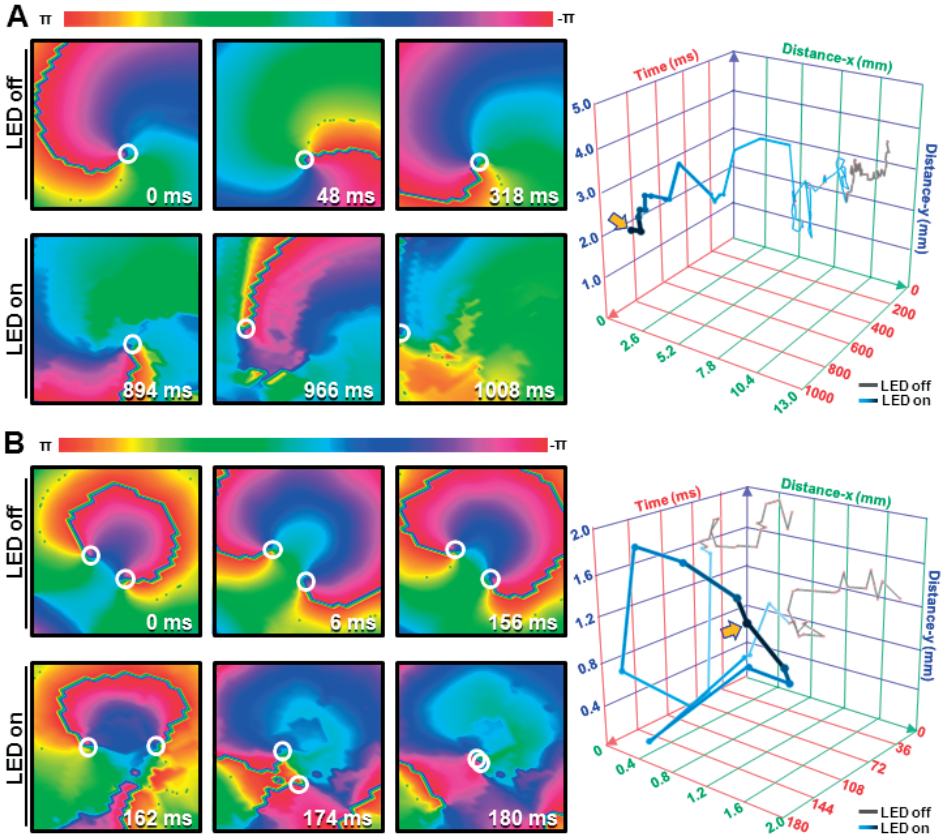

Figure 6. *Light-induced alteration of PS trajectory and arrhythmia termination. Typical phase map sequence of an LV.CatCh~eYFP↑-transduced atrial culture showing spiral wave phase progression before (upper sequences) and during (lower sequences) exposure to blue light leading to spiral wave termination by (A) PS-boundary collision and (B) PS-PS collision. White circles indicate PS positions. 3D graphs show the PS positions before (grey) and during (blue gradient) exposure to blue light, exemplifying PS drift leading to wave termination (yellow arrow).*

Optogenetic control of cardiac excitability

In the past, most studies that aimed to unravel the mechanisms underlying cardiac arrhythmias and to identify new anti-arrhythmic targets relied exclusively on the use of pharmacological and/or electrical interventions to modulate electrophysiological processes in cardiomyocytes, like de- and hyperpolarization.[12,16,18] More recently, genetic interventions including site-directed mutagenesis, gene knockdown/knockout and forced (trans)gene expression have been added to the repertoire of techniques to modulate cardiac ion channel activity and excitability in a more refined manner.[11] Nevertheless, even today's most sophisticated genetic interventions allow for only modest spatiotemporal, as well as, quantitative control of the target's functionality. Such

constraints hamper further progress in our mechanistic understanding and treatment of cardiac arrhythmias. However, optogenetic engineering allows modulation of cellular electrophysiological properties with superb spatiotemporal and quantitative control in a non-voltage-gated fashion by combining the advantages of photoactivatable ion channels and light.[6] As a result, optogenetics has become an indispensable tool in neuroscience to modulate the activity of neurons by light and thereby study the functional roles of specific neural pathways in the brain.[6]

More recently, optogenetics was introduced in the field of cardiovascular research by showing that channelrhodopsin-2 (ChR2)-expressing cardiomyocytes, either cultured *in vitro* or present in the intact heart, could be electrically excited by brief light pulses without obvious adverse effects on cardiac function.[7-9] These pulses caused depolarization of cardiomyocytes at the site of illumination, thereby triggering APs that were rapidly propagated across the cardiac tissue via gap junctions and merged into a spread of uniform electrical activation. Prolonged activation of light-gated cation channels in cardiomyocytes led to sustained depolarization of all cardiomyocytes without causing noticeable adverse effects.[7] However, thus far, the potential of optogenetics to counteract cardiac tachyarrhythmias has not been investigated.

Optogenetic termination of spiral waves

Based on current evidence, reentrant spiral waves play a major role in the maintenance of fibrillation in both atria and ventricles.[19] Hence, most strategies aiming to prevent or terminate AF involve the inhibition of reentry formation and the elimination of existing reentrant circuits, respectively. Previous studies have shown that during reentry, conduction velocity and excitability gradually increase from the rotor core towards the periphery. Paramount to the establishment of these gradients seem to be the inward rectifier K^+ current (I_{K1}) and the fast Na^+ current (I_{Na}), of which the amplitudes decrease towards the rotor core. The interplay between I_{K1} and I_{Na} determines reentry frequency and rotor stability as a decrease of either current slows and destabilizes the rotor, possibly leading to spiral wave termination.[16,20,21] The present study is consistent with these hypotheses, as a light-induced decrease in overall excitability increased the functional core size and terminated reentry. Due to the existing gradient in excitability, decreasing overall excitability will first prevent excitation near the core leading to its expansion thereby causing PS drift from a relatively stable position. Consequently, the chance for PSs to collide with each other or with physical boundaries will increase. Following light-triggered annihilation of all PSs in a culture, as found in our experiments, no spiral waves are generated anymore, allowing reestablishment of a regular cardiac activation pattern. Still, as optogenetic defibrillation is a new field of research, various aspects of this method need to be investigated in further detail in order to fully appraise its value as a research tool and to gain more insight into its therapeutic potential.

Potential advantages over established defibrillation strategies

While pharmacological blockade of I_{K1} and I_{Na} are well-accepted strategies to terminate reentry, they are associated with proarrhythmia, since the resulting chronic slowing of repolarization and conduction promote afterdepolarizations and reentry, respectively.[16,22] Optogenetic therapy would, however, decrease excitability only during photostimulation, leaving important electrophysiological parameters unaltered after spiral wave termination.

Several advantages of optogenetic therapy over electrical cardiac therapy have been previously postulated in the light of cardiac pacing, including a higher level of spatial control[7,8] and, more importantly, higher energy efficiency resulting in less tissue damage. For CatCh, the enhanced energy efficiency might be even more pronounced than for earlier ChR2 variants due to its improved light sensitivity. While optogenetic pacing might prove an interesting alternative for treatment of bradyarrhythmias, energy efficiency could be of even greater importance when trying to normalize heart rhythm during tachyarrhythmia. The possible applicability of optogenetics in the field of tachyarrhythmias was already hinted at in a study showing the ability to cause light-induced conduction block by overexpression of the hyperpolarizing light-sensitive Cl^- channel NpHR in zebrafish cardiomyocytes.[7] Moreover, using ChR2(H134R), Bruegmann *et al.* showed that through a depolarizing photocurrent spontaneous beating of embryonic stem cell-derived cardiomyocytes could be depressed, most likely as a result of fast Na^+ channel inactivation upon prolonged local illumination.[8] In the present study, the possibility to optogenetically suppress cardiac excitability was confirmed by prolonged light exposure of aCMCs expressing the Ca^{2+}-permeable and ultra-light-sensitive ChR2 mutant CatCh. The CatCh-dependent photocurrent was used to show that uniform light-induced depolarization can terminate spiral wave reentry, exemplifying the possibility to broaden the field of optogenetic control of myocardial function towards arrhythmia termination. In sharp contrast, traditional defibrillation is based on the delivery of high-energy electrical shocks to cause uniform depolarization. The use of high-energy electrical shocks is associated with severe discomfort in patients as well as tissue damage, increasing with stimulus strength and duration. A major improvement in electrical defibrillation has been the introduction of the biphasic waveform[23] and further technical refinements like multistage electrotherapy[24] are arising. Still, stimulus duration in traditional defibrillation must be confined to several milliseconds, whereas the optogenetic approach might enable the use of longer stimuli, such as applied in this study, without inducing tissue damage.

During traditional electrical defibrillation, reentry can be reinitiated at critical points in local electrical field strength, when shock strength is below the upper limit of vulnerability or when the shock causes the occurrence of virtual electrodes from which new fibrillatory waves can emanate.[5,25-27] Since optogenetic defibrillation, as presented in

this study, does not use an electric field to induce depolarization, it should not result in reinitiation of fibrillation by the formation of virtual electrodes. Under conditions of homogeneous transduction and illumination also reinitiation as a consequence of aforementioned critical points may be prevented by optogenetic arrhythmia termination. Concordantly, after light-induced spiral wave termination, no proarrhythmic reexcitations were found in our model. Thus, as shown in the present study, optogenetic therapy to control cardiac function and to terminate arrhythmias might provide several advantages over the traditional means of treating heart rhythm disorders.

Translational considerations and study limitations

This study shows that the endogenous electrochemical gradients present in cardiac tissue can be exploited for defibrillation by optogenetics, as an alternative to the external electrical current applied to interrupt reentrant circuits during conventional electrical defibrillation.[5] However, we acknowledge that translating this principle to the *in vivo* situation comes with some hurdles that need to be overcome before considering any clinical applications.

First, in the present study, a 2D model of AF was used to demonstrate proof-of-principle for the optogenetic termination of fibrillatory conduction. This *in vitro* model lacks the complexity found in the intact 3D atrium and thus does not suffer from factors such as a low transduction efficiency of the target cell population and poor light penetration into the target tissue that might limit the effectiveness of optogenetic arrhythmia termination *in vivo*. Moreover, as we found termination of reentry by light to depend on the collision of PSs with boundaries or with PSs of opposite chirality, at least an area including the PS and its nearest physical boundary or a counteracting PS has to be illuminated for successful arrhythmia termination. However, because in our model the position of the PSs causing reentrant activation cannot be predetermined and their trajectories cannot be controlled , homogeneous illumination of the entire aCMC cultures is required for consistent reentry termination by light. Still, earlier work in the field of ventricular fibrillation has shown that effective defibrillation does not require every cell in the myocardium to be depolarized,[5] hinting at the possibility that successful defibrillation may also be achieved in the case of incomplete light penetration and/or patchy transgene expression. This might even be more pronounced in AF, as rotors or drivers of AF usually localize to specific areas of the atrium such as the direct surroundings of pulmonary vein ostea, meaning that illumination concentrated on these areas might suffice for successful cardioversion. Hence, future studies testing the possibility of AF termination using local instead of global cation channel activation may provide an important next step in the realization of shockfree defibrillation *in vivo*.

Nevertheless, in tackling the possibility of insufficient light penetration *in vivo*, it may be critical to expand the optogenetic toolbox with improved/mutated light-gated cation

channels displaying greater light sensitivity or increased ion permeability. In addition, due to the absorption of especially short-wavelength visible light by tissue constituents like blood, it might be of interest to look into (optogenetic) tools that are excited by light of higher wavelength (*i.e.* near-infrared) or by other energy sources (radio waves/ ultrasound) and therefore allow deeper tissue penetration. These improvements are likely to arise in the near future through the ongoing research and advances in (opto) genetic technology.[6,28]

Second, it should be noted that the physical boundaries of culture dishes (necessary for extinguishing PSs by collision, in addition to the collision to PSs of opposite chirality) differ from the anatomical boundaries in the intact atrium. Nonetheless, in several clinical studies PS-boundary collisions have been identified as a mechanism of rotor termination in both atrial and ventricular fibrillation.[29,30] Hence, while in the intact atrium, the likelihood of a PS meeting a PS of opposite chirality may be diminished compared to that in our 2D model, light-induced rotor termination *in vivo* might be facilitated by the numerous anatomical boundaries contained within the atrium, such as the many walls of the microvasculature, the mitral/tricuspid valve rings, the ostea of the pulmonary veins and the epi- and endocardium.

Third, in the present study transgene expression was achieved by lentiviral vector-based gene transfer. Although lentiviral vectors are very efficient in inducing stable transgene expression *in vitro*, they are of limited use for *in vivo* cardiac gene therapy mainly because of their poor dissemination through myocardial tissue and their potential to cause insertional oncogenesis. These hurdles may be overcome by using adeno-associated virus (AAV) vectors for *in vivo channelrhodopsin* gene delivery to the heart as these vectors (i) can mediate long-term transgene expression in post-mitotic cells including cardiomyocytes without the need to integrate their DNA into the target cell genome, (ii) do not contain viral genes encoding potentially cytotoxic and/or immunogenic proteins, (iii) readily spread through myocardial tissue and (iv) are well known for their excellent *in vivo* safety. The utility of AAV vectors for *in vivo* gene transfer to the human heart has been illustrated by a recent clinical study in which heart failure patients received AAV vector particles encoding sarco/endoplasmic reticulum Ca^{2+}-ATPase 2a,[31] paving the way for optogenetic (or other genetic modifications) therapies in the field of cardiology.

Finally, also the delivery method of the necessary light (or any other excitatory energy source) *in vivo* needs to be perfected. In the field of neurology solutions to this problem have already been postulated, and lie in the use of, for example, fiberoptics.[32,33] Hence, the future might hold painfree implantable cardioverter defibrillator device therapy for AF, based on optogenetics and fiberoptic delivery of light, instead of electrical shocks applied via platinum leads, in specific areas of the atrial myocardium.

Without the intention to detract from this prospect, it should be noted that the conclusions drawn from the present study are only conceptual in relation to human AF and therefore cannot be readily extrapolated to the clinical setting. Hence, there is still a considerable amount of work to be done before optogenetic therapy (or any other therapy exploiting the electrochemical gradients that are endogenously present in myocardial tissue) becomes a realistic treatment option for patients with cardiac rhythm disorders.

Conclusions

In summary, forced expression of the light-gated cation channel CatCh in aCMCs allows for effective and repeated termination of reentrant conduction by photocurrent-induced functional core expansion. These results indicate that optogenetic control of cardiac electrical function could serve as a novel anti-arrhythmic strategy, in which the arrhythmogenic substrate itself provides the defibrillating current. This may trigger the exploration of a previously uninvestigated principle to develop safe and effective new therapies for cardiac arrhythmias.

Acknowledgements

We thank Karl Deisseroth and Charu Ramakrishnan (Stanford University, Stanford, CA) for providing the lentiviral vector shuttle plasmid pLenti-CaMKIIa-hChR2(L132C)-EYFP-WPRE, Ivan Kazbanov (Ghent University, Ghent, Belgium) for writing analysis software and Huybert van der Stadt for excellent technical support.

CONFLICT OF INTEREST

None declared.

FUNDING

This work was supported by the Dutch Heart Foundation (E. Dekker grant [2012/T023 to B.O.B.]) and the Netherlands Organization for Scientific Research (Mosaic grant [017007064 to M.C.E.]). D.A.P. is recipient of a Veni grant (91611070) of the Netherlands Organization for Scientific Research.

SUPPLEMENTAL MATERIAL

METHODS

Optical mapping of intracellular Ca2+

The effects of Catch activation on intracellular Ca^{2+} concentrations and dynamics were assessed by optical mapping using Rhod-2-AM (Life Technologies, Bleiswijk, the Netherlands) as calcium-sensitive dye. To this purpose, neonatal rat atrial cardiomyocyte (aCMC) cultures were incubated with 2.5 μM Rhod-2-AM in Dulbecco's modified Eagle's medium/HAM's F12 (DMEM/F12; 1:1, v/v; Life Technologies at 37°C for 30 minutes, after which cells were rinsed with DMEM/F12 to remove excess dye. Subsequently, cells were kept in the incubator for another 30 minutes to allow de-esterification of internalized AM esters after which optical signals were captured using the MiCAM ULTIMA-L imaging system (SciMedia, Costa Mesa, CA). During optical mapping of Ca^{2+}, cells were stimulated electrically with an epoxy-coated bipolar platinum electrode by delivery of 3 square suprathreshold electrical stimuli at 1000-ms intervals (1 Hz) prior to exposure to a 500-ms blue light pulse. Electrical pacing at 1 Hz was reinitiated 10, 20, 50, 100, 200, 500 and 1000 ms after the blue light had been switched off. The amplitude of the calcium transient, the basal Ca^{2+} signal and the occurrence of propagated calcium sparks were analyzed using BrainVision Analyzer 1101 software (Brainvision, Tokyo, Japan).

RESULTS

Optical mapping setup and light-emitting diode (LED)-induced shift in optical signal baseline

Using the setup depicted in Supplementary material online, *Figure S1A*, exposure of untransduced and unstimulated neonatal rat atrial cell cultures to blue light LED caused an immediate vertical drop in baseline optical signal (Supplementary material online, *Figure S1B*). The amplitude of the decrease in baseline optical signal depended on the light intensity. The temporal precision of the LED control by the pacing module was checked by calculating the exposure times detected by the charge-coupled device (CCD) camera. Upon a 500-ms blue light pulse, 94% of pixels showed an exposure time of 504 ms while for the remainder of the pixels the exposure time was 510 ms, exemplifying the tight control of the LED by the pacing module (Supplementary material online, *Figure S1C*). During reentry, optical signal baseline showed a similar downward shift as seen in the absence of activation. Importantly, during the downward shift (LED-on period) the action potential (AP) morphology remained unchanged (Supplementary material

online, *Figure S1D*). Offline adjustment of the baseline during the LED-on period did not principally alter optical signal distribution through the culture (Supplementary material online, *Figure S1E*). Thus, the optical mapping setup allowed direct correlation of events during the LED-on period with changes in electrophysiological parameters.

Electrophysiological effects of 500-ms light pulses on LV.CatCh~eYFP↑-transduced aCMC cultures

Because CatCh is permeable to Ca^{2+}, prolonged light exposure could lead to perturbations in intracellular Ca^{2+} in LV.CatCh~eYFP↑-transduced cultures, while the Na^{+} permeability of CatCh could lead to a decrease in excitability. As both effects, if persisting after turning off the LED, could be proarrhythmic, we tested the electrophysiological effects of the 500-ms blue light pulse used for termination of spiral wave reentry. To this purpose, aCMC cultures were paced electrically at 1 Hz prior to exposure to a 500-ms blue light pulse, during optical mapping using Rhod-2AM as Ca^{2+}-binding dye (n=10) or di-4-ANEPPS (n=10) as a voltage-sensitive dye. Electrical pacing at 1 Hz was resumed 10, 20, 50, 100, 200, 500 and 1000 ms after turning off the blue LED. Comparison of the calcium transients prior to and after exposure to blue light did not reveal significant differences irrespective of the length of the LED off-to-electrical pacing interval (*Figure S4A,B*). Calcium transient amplitude after exposure to blue light was not significantly different from that before CatCh activation (100% vs 100.2±4.6% after light exposure) (*Figure S4C*). In addition, no propagated Ca^{2+} sparks were found after the LED-on period. In 1 culture, reentry was induced by electrical pacing starting at 10 ms after the LED was turned off. In this particular case, pacing most likely occurred in the vulnerable window after repolarization from the LED-induced depolarizing current instead of being caused by perturbations in intracellular Ca^{2+} as no (propagated) calcium sparks or reexcitations were found after exposure to a 500-ms blue light pulse (*Figure S4A,B,D*). In addition, conduction velocity, AP duration at 80% repolarization (APD_{80}) and AP amplitude in LV.CatCh~eYFP↑-transduced aCMC cultures prior to light exposure did not significantly differ from those after exposure to blue light (conduction velocity: 100 vs 101.7±19.5% post LED-on, APD_{80}: 100 vs 103.4±10.5% after light exposure and AP amplitude: 100 vs 102.0±11.1% post LED-on) (*Figure S4E,F,G*). Together, these results indicate that prolonged (*i.e.* 500 ms) light exposure of LV.CatCh~eYFP transduced↑-cultures, at the given conditions, does not cause pro-arrhythmicity due to persistent electrophysiological disturbances.

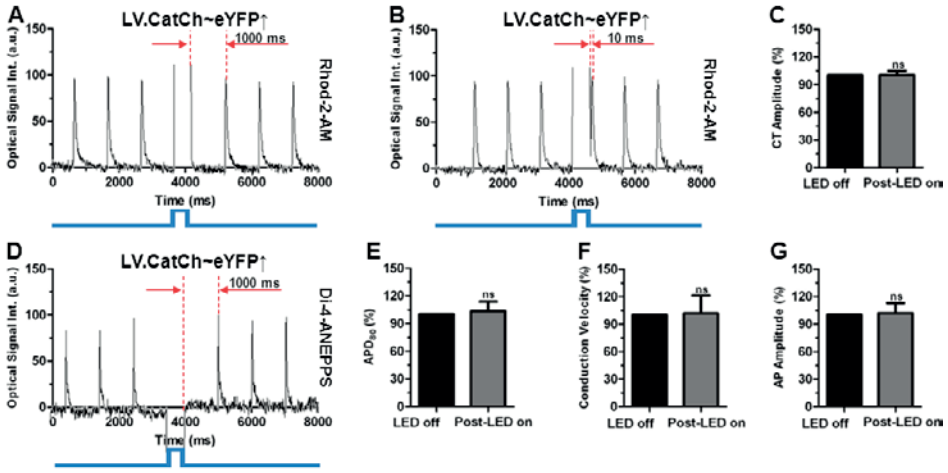

Supplementary Figure S4. *Electrophysiological effects of 500-ms light pulses on LV.CatCh~eYFP↑-transduced aCMC cultures. (A,B) Typical examples of the Rhod-2-AM optical signals in 1-Hz electrically paced LV-CatCh~eYFP↑-transduced aCMC cultures before and after exposure to a 500-ms blue light pulse. Electrical stimulation was resumed at 1000 ms (A) or 10 ms (B) after turning off the LED. (C) Quantification of calcium transient (CT) amplitude based on Rhod-2AM mapping. (D) Example of the di-4-ANEPPS optical signal in an LV.CatCh~eYFP↑-transduced aCMC culture before and after exposure to a 500-ms blue light pulse. Electrical stimulation was resumed at 1000 ms after turning off the LED. Quantification of (E) APD_{80}, (F) conduction velocity and (G) action potential (AP) amplitude, based on voltage-sensitive dye mapping, after exposure to blue light as a percentage of these characteristics prior to exposure to light. ns: non-significant vs LED off using a Wilcoxon signed rank test.*

Supplementary Movie 1. *Typical example from an optical mapping experiment in a neonatal rat aCMC culture transduced with LV.CatCh~eYFP↑during light-induced termination of spiral wave reentry. The upper part shows the high-pass-filtered optical signal in a 5-mm^2 square in the culture during spiral wave reentry induced by burst pacing, followed by a 500-ms blue light pulse causing spiral wave termination by a phase singularity-boundary collision. Note: High-pass-filtering caused the blue light-dependent downward shift in optical signal baseline to change into two short (±18 ms duration) artifacts occurring when the LED is turned on and when the LED is turned off only. The lower part displays the corresponding spatially filtered optical action potential progression prior to, during and after light-induced spiral wave termination.*

Supplementary Movie 2. *Typical example from an optical mapping experiment in a neonatal rat aCMC culture transduced with LV. CatCh~eYFP↑ during light-induced termination of spiral wave reentry. The upper part shows the high-pass-filtered optical signal in a 5-mm^2 square in the culture during spiral wave reentry induced by burst pacing, followed by a 500-ms blue light pulse causing spiral wave termination by a phase singularity-phase singularity collision. Note: High-pass-filtering caused the blue light-dependent downward*

shift in optical signal baseline to change into two short (±18 ms duration) artifacts occurring when the LED is turned on and when the LED is turned off only. The lower part displays the corresponding spatially filtered optical action potential progression prior to, during and after light-induced spiral wave termination.

REFERENCES

1. Lip GY, Tse HF, Lane DA. Atrial fibrillation. *Lancet* 2012;**379**:648-661.
2. Iwasaki YK, Nishida K, Kato T, Nattel S. Atrial fibrillation pathophysiology: implications for management. *Circulation* 2011;**124**:2264-2274.
3. Schotten U, Verheule S, Kirchhof P, Goette A. Pathophysiological mechanisms of atrial fibrillation: a translational appraisal. *Physiol Rev* 2011;91:265-325.
4. Wellens HJ, Lau CP, Luderitz B, Akhtar M, Waldo AL, Camm AJ, Timmermans C, Tse HF, Jung W, Jordaens L, Ayers G. Atrioverter: an implantable device for the treatment of atrial fibrillation. *Circulation* 1998;**98**:1651-1656.
5. Dosdall DJ, Fast VG, Ideker RE. Mechanisms of defibrillation. *Annu Rev Biomed Eng* 2010;**12**:233-258.
6. Deisseroth K. Optogenetics. *Nat Methods* 2011;**8**:26-29.
7. Arrenberg AB, Stainier DY, Baier H, Huisken J. Optogenetic control of cardiac function. *Science* 2010;**330**:971-974.
8. Bruegmann T, Malan D, Hesse M, Beiert T, Fuegemann CJ, Fleischmann BK, Sasse P. Optogenetic control of heart muscle in vitro and in vivo. *Nat Methods* 2010;**7**:897-900.
9. Jia Z, Valiunas V, Lu Z, Bien H, Liu H, Wang HZ, Rosati B, Brink PR, Cohen IS. Stimulating cardiac muscle by light: cardiac optogenetics by cell delivery. *Circ Arrhythm Electrophysiol* 2011;**4**:753-760.
10. Kleinlogel S, Feldbauer K, Dempski RE, Fotis H, Wood PG, Bamann C, Bamberg E. Ultra light-sensitive and fast neuronal activation with the Ca(2)+-permeable channelrhodopsin CatCh. *Nat Neurosci* 2011;**14**:513-518.
11. Bingen BO, Neshati Z, Askar SF, Kazbanov IV, Ypey DL, Panfilov AV, Schalij MJ, de Vries AA, Pijnappels DA. Atrium-Specific Kir3.x Determines Inducibility, Dynamics and Termination of Fibrillation by Regulating Restitution-Driven Alternans. *Circulation* 2013;**128**:2732-2744.
12. Askar SF, Ramkisoensing AA, Schalij MJ, Bingen BO, Swildens J, van der Laarse A, de Vries AA, Ypey DL, Pijnappels DA. Antiproliferative treatment of myofibroblasts prevents arrhythmias in vitro by limiting myofibroblast-induced depolarization. *Cardiovasc Res* 2011;**90**:295-304.
13. Salva MZ, Himeda CL, Tai PW, Nishiuchi E, Gregorevic P, Allen JM, Finn EE, Meuse L. Design of tissue-specific regulatory cassettes for high-level rAAV-mediated expression in skeletal and cardiac muscle. *Mol Ther* 2007;**15**:320-329.
14. Goncalves MA, Janssen JM, Nguyen QG, Athanasopoulos T, Hauschka SD, Dickson G, de Vries AA. Transcription factor rational design improves directed differentiation of human mesenchymal stem cells into skeletal myocytes. *Mol Ther* 2011;**19**:1331-1341.
15. Kubalak SW, Miller-Hance WC, O'Brien TX, Dyson E, Chien KR. Chamber specification of atrial myosin light chain-2 expression precedes septation during murine cardiogenesis. *J Biol Chem* 1994;**269**:16961-16970.
16. Bingen BO, Askar SF, Schalij MJ, Kazbanov IV, Ypey DL, Panfilov AV, Pijnappels DA. Prolongation of minimal action potential duration in sustained fibrillation decreases complexity by transient destabilization. *Cardiovasc Res* 2013;**97**:161-170.
17. Hou L, Deo M, Furspan P, Pandit SV, Mironov S, Auerbach DS, Gong Q, Zhou Z, Berenfeld O, Jalife J. A major role for HERG in determining frequency of reentry in neonatal rat ventricular myocyte monolayer. *Circ Res*. 2010;**107**:1503-1511.
18. Pijnappels DA, Schalij MJ, Ramkisoensing AA, van TJ, de Vries AA, van der Laarse A, Ypey DL, Atsma DE. Forced alignment

of mesenchymal stem cells undergoing cardiomyogenic differentiation affects functional integration with cardiomyocyte cultures. *Circ Res* 2008;**103**:167-176.

19. Jalife J. Inward rectifier potassium channels control rotor frequency in ventricular fibrillation. *Heart Rhythm* 2009;**6**:S44-S48.
20. Jalife J. Deja vu in the theories of atrial fibrillation dynamics. *Cardiovasc Res* 2011;**89**:766-775.
21. Pandit SV, Berenfeld O, Anumonwo JM, Zaritski RM, Kneller J, Nattel S, Jalife J. Ionic determinants of functional reentry in a 2-D model of human atrial cells during simulated chronic atrial fibrillation. *Biophys J* 2005;**88**:3806-3821.
22. Weiss JN, Garfinkel A, Karagueuzian HS, Chen PS, Qu Z. Early afterdepolarizations and cardiac arrhythmias. *Heart Rhythm* 2010;**7**:1891-1899.
23. Schneider T, Martens PR, Paschen H, Kuisma M, Wolcke B, Gliner BE, Russell JK, Weaver WD, Bossaert L, Chamberlain D. Multicenter, randomized, controlled trial of 150-J biphasic shocks compared with 200- to 360-J monophasic shocks in the resuscitation of out-of-hospital cardiac arrest victims. Optimized Response to Cardiac Arrest (ORCA) Investigators. *Circulation*. 2000;**102**:1780-1787.
24. Janardhan AH, Gutbrod SR, Li W, Lang D, Schuessler RB, Efimov IR. Multistage electrotherapy delivered through chronically-implanted leads terminates atrial fibrillation with lower energy than a single biphasic shock. *J Am Coll Cardiol*. 2014;**63**:40-48
25. Chen PS, Feld GK, Kriett JM, Mower MM, Tarazi RY, Fleck RP, Swerdlow CD, Gang ES, Kass RM. Relation between upper limit of vulnerability and defibrillation threshold in humans. *Circulation* 1993;**88**:186-192.
26. Efimov IR, Cheng YN, Biermann M, Van Wagoner DR, Mazgalev TN, Tchou PJ. Transmembrane voltage changes produced by real and virtual electrodes during monophasic defibrillation shock delivered by an implantable electrode. *J Cardiovasc Electrophysiol* 1997;**8**:1031-1045.
27. Frazier DW, Wolf PD, Wharton JM, Tang AS, Smith WM, Ideker RE. Stimulus-induced critical point. Mechanism for electrical initiation of reentry in normal canine myocardium. *J Clin Invest* 1989;**83**:1039-1052.
28. Entcheva E. Cardiac optogenetics. *Am J Physiol Heart Circ Physiol* 2013;**304**:H1179-H1191.
29. Ikeda T, Uchida T, Hough D, Lee JJ, Fishbein MC, Mandel WJ, Chen PS, Karagueuzian HS. Mechanism of spontaneous termination of functional reentry in isolated canine right atrium. Evidence for the presence of an excitable but nonexcited core. *Circulation* 1996;**94**:1962-1973.
30. Yamazaki M, Honjo H, Ashihara T, Harada M, Sakuma I, Nakazawa K, Trayanova N, Horie M, Kalifa J, Jalife J, Kamiya K, Kodama I. Regional cooling facilitates termination of spiral-wave reentry through unpinning of rotors in rabbit hearts. *Heart Rhythm* 2012;**9**:107-114.
31. Zsebo KM, Yaroshinsky A, Rudy JJ, Wagner K, Greenberg B, Jessup M, Hajjar RJ. Long Term Effects of AAV1/SERCA2a Gene Transfer in Patients with Severe Heart Failure: Analysis of Recurrent Cardiovascular Events and Mortality. *Circ Res* 2014;114:101-108.
32. Ahmari SE, Spellman T, Douglass NL, Kheirbek MA, Simpson HB, Deisseroth K, Gordon JA, Hen R. Repeated cortico-striatal stimulation generates persistent OCD-like behavior. *Science* 2013;**340**:1234-1239.
33. Tye KM, Prakash R, Kim SY, Fenno LE, Grosenick L, Zarabi H, Thompson KR, Gradinaru V, Ramakrishnan C, Deisseroth K. Amygdala circuitry mediating reversible and bidirectional control of anxiety. *Nature* 2011;**471**:358-362.

Chapter VI

Appendix III

CardioPulse: first evidence for shockless atrial fibrillation treatment

Cardiac optogenetics achieve defibrillation without the pain of electric shocks.

Taylor J.

Eur Heart J. 2014;35:2702

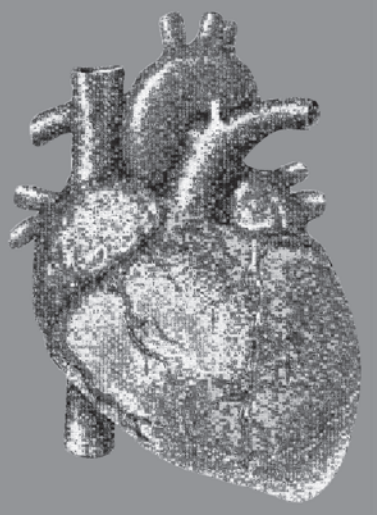

The first evidence for a shockless treatment for atrial fibrillation (AF) was presented at Frontiers in CardioVascular Biology 2014 in Barcelona, Spain. Electric shocks are the quickest way to bring AF patients back to normal sinus rhythm and prevent symptoms and complications. But shocks are very painful and require anaesthesia, which comes with its own possible adverse effects. Atrial fibrillation usually progresses froma paroxysmal form, in which episodes of AF last fromseveralminutes up to 7 days, to a persistent and eventually a chronic form. People with the latter are in AF 24 h a day, 7 days a week, and shock treatment no longer works. Dr Brian O. Bingen, first author, said: 'AF causes structural changes to the atrium which make patients more prone to subsequent induction of AF. That's another reason toget patients back into sinus rhythmas soon as possible'. The researchers devised a method of shockless defibrillation. They used optogenetics to genetically insert depolarizing ion channels into the heart that can be activated by light. Dr Bingen said: 'The theory was that we could just turn a light switch on and depolarize the entire myocardium without needing a shock. In theory, the patient could be given an implantable device with a mesh of light emitting diodes (LEDs) and when AF occurs you turn the light on and the AF stops'. During arrhythmias there is subepicardial activity, but the heart is a complex three-dimensional structure and it is only possible to directly observe the epicardium. To see howtheir method worked subepicardially, the researchers developed two-dimensional (2D) hearts. They isolated cardiac muscle cells from the rat atrium, replanted them in a culture dish and allowed the cells to form intercellular connections, creating a 2D heart. Atrial fibrillation was induced in 31 of these 2D hearts. The researchers used a lentivirus to insert a gene into the 2D hearts called calcium-translocating channelrhodopsin, which is a lightsensitive depolarizing channel. Dr Bingen said: 'Then it was just a matter of switching on the light and seeing what happened.We found that in all 31 of these 2Dhearts we were able to achieve the2Dequivalent of cardioversion into sinus rhythm. The mechanismwe sawwas slightly different than the normal defibrillation but was equally effective'. He continued: 'We nowhave to test our method in the 3D setting. In that scenario we won't be able to see the defibrillating mechanism in as much detail, but we hope that it will be possible to terminate AF in the complete heart.We will also test other types of light or energy sources that penetrate the body more deeply and could be applied externally, avoiding the need for an implanted device'. Dr Bingen concluded: 'This is the first evidence of a shockless defibrillation. Ourmethodof using optogenetics to defibrillate by light is completely painless and looks promising, but more research is needed before it can be applied in patients'.

FUNDING

This work was supported by the Dutch Heart Foundation [E. Dekker grant (2012/T023) to B.O. Bingen] and the Netherlands Organization for Scientific Research [Vidi grant (91714336) to D.A. Pijnappels and Mosaic grant (017007064) to M.C. Engels].

CONFLICT OF INTEREST

None declared.

Chapter VII

Summary, conclusions, discussion and future perspectives.

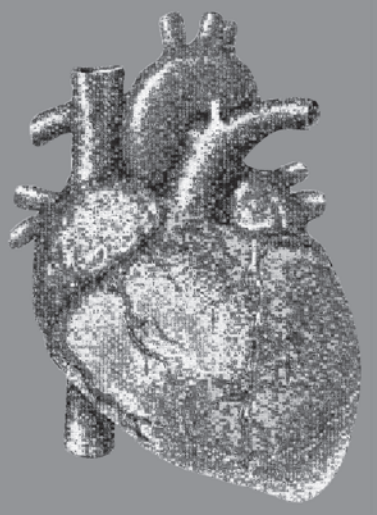

SUMMARY AND CONCLUSIONS

The general introduction of this thesis, **Chapter I**, described the basic electrophysiological mechanisms involved in the control of cardiac rhythm and contraction in the healthy heart. A multitude of disturbances in this control, which can lead to triggers or substrates for the maintenance of cardiac arrhythmias, are discussed in detail. This was followed by an overview of the anti-arrhythmic strategies that have been applied to date to prevent these triggers or disrupt the maintenance of the arrhythmias, and regain control of cardiac rhythm. Furthermore, disadvantages of current anti-arrhythmic treatment options, attributable to the incomplete understanding of pro-arrhythmic mechanisms, were addressed. Following from these disadvantages, the aim of this thesis was to dissect cellular and molecular pro-arrhythmic mechanisms, and to explore the possibilities for more specific, substrate-oriented and less harmful anti-arrhythmic strategies.

Chapter II evaluated the differences in pro-arrhythmic mechanisms between pathological cardiomyocyte hypertrophy and cardiac fibrosis, as well as their respective influence on the outcome of anti-arrhythmic strategies. As pathological hypertrophy and fibrosis occur simultaneously in the remodelled ventricular myocardium, which is prone to the development of arrhythmias, discerning between their individual contributions to the initiation of arrhythmias is very difficult *in vivo*. Therefore, neonatal rat ventricular cardiomyocyte cultures were incubated with phenylephrine to induce pathological cardiomyocyte hypertrophy, while permitting free proliferation of cardiac (myo)fibroblasts in separate cultures was utilized to mimic fibrosis. This approach allowed us to study the pro-arrhythmic mechanisms involved in the remodelled myocardium separately, *in vitro*. Interestingly, the mechanisms of arrhythmia initiation proved very similar in the hypertrophy and fibrosis models. Both conditions induced significant slowing of conduction and repolarization, leading to formation of early afterdepolarizations (EADs) causing focal tachyarrhythmias (as a consequence of EADs occurring repetitively at the edge of a sustained depolarized area) or reentrant tachyarrhythmias (as a consequence of unidirectional block between areas of phase II EAD initiation and areas still in action potential [AP] phase II). Also, arrhythmia incidence based on either focal or reentrant mechanisms was similar in both models. However, further investigation revealed that the mechanisms underlying EAD formation and conduction slowing differed. While protein levels of Cx43 and Kv4.3 in cardiomyocytes were decreased as a consequence of hypertrophy, no significant differences were found under fibrotic conditions. Conversely, depolarization of the maximal diastolic potential (MDP), through heterocellular coupling between cardiomyocytes and cardiac (myo)fibroblasts was found in fibrosis, while MDP was unaffected under hypertrophic conditions. As a consequence, targeting heterocellular coupling through administration of low doses of 2-aminoethoxydiphenyl borate (2-APB) and carbenoxolone only reduced the incidence of arrhythmias in fibrotic

cultures. Moreover, L-type calcium channel blockade prevented both focal and reentrant arrhythmias in hypertrophic cultures, but caused conduction block in fibrotic cultures. These findings have yielded novel mechanistic insights into the substrate-specific mechanisms integrated within the remodelled ventricular myocardium and how they might affect therapeutic efficacy.

Chapter III investigated the electrophysiological characteristics that determined the number of rotors (or complexity) maintaining sustained ventricular fibrillation (VF), and the possibilities to use this knowledge to alter key parameters that allow termination of rotors and a consequent reduction of VF complexity. To this purpose, a novel *in vitro* model of sustained VF was developed using monolayers of neonatal rat ventricular cardiomyocytes incubated with the gap junctional uncoupler 2-APB. 2-APB caused a dose-dependent increase in complexity of spontaneously induced spiral wave reentrant tachyarrhythmias, with very high stability resembling sustained VF (0.0±0.1 phase singularities [PSs]/cm^2 in control cultures vs 0.0±0.1, 1.0±0.9, 3.3±3.2, 11.0±10.1 and 54.4±21.7 PSs/cm^2 in cultures containing 5, 10, 15, 20 and 25 μM 2-APB, respectively). Arrhythmia complexity was inversely correlated with wavelength (robust standard deviation of the residuals=0.4). The wavelength could only be prolonged by agents that increased the AP duration (APD) at maximal activation frequencies (the minimal APD). Blockade of the inward rectifier potassium current (I_{K1}) by $BaCl_2$ and potentiation of the L-type calcium current (I_{CaL}) by BayK8644 significantly prolonged minimal APD, which also significantly decreased the complexity and activation frequency of VF *in vitro*. An increase in minimal APD during VF was found to cause a transient destabilization of rotors, leading to rotor termination following critical collisions of the wavefronts emanating from these rotors. Interestingly, similar 2-APB dose-dependent complexity increases could be induced in *ex vivo* Langendorff-perfused adult rat hearts. More importantly, increasing minimal APD by $BaCl_2$ also significantly reduced VF complexity in the *ex vivo* model. Together these results show that the stability of sustained fibrillation is highly dependent on minimal APD, which knowledge can be exploited to transiently destabilize VF and assist VF termination. As such, this might provide a novel conceptual framework for future anti-arrhythmic drug design and help to extend/refine therapeutic strategies for sustained VF.

Chapter IV described a study in which the effect of downregulation or blockade of Kir3.x channels on the initiation, maintenance and termination of atrial fibrillation (AF) was assessed. As pharmacological treatment of AF can be complicated by ventricular pro-arrhythmia, exploring the possibilities to alter atrial electrophysiology without affecting the ventricles may provide an opportunity to develop less hazardous anti-AF therapy. Kir3.x channels, responsible for the acetylcholine-dependent potassium current ($I_{K,ACh}$), are expressed in the atria but not in the ventricles. $I_{K,ACh}$ is known to become constitutively active (*i.e.* acetylcholine-independent) in patients suffering from persis-

tent AF, and might therefore be an interesting target for atrium-specific anti-AF therapy. Interestingly, blockade of $I_{K,ACh}$ by the specific pharmacological blocker tertiapin, was found to significantly increase the APD (56.5±12.5 to 145.5±20.6 milliseconds; $P<0.0001$) in primary neonatal rat atrial cardiomyocyte cultures in the absence of acetylcholine, which indicates the presence of constitutively active $I_{K,ACh}$ ($I_{K,ACh-c}$). Moreover, atrium specificity of both Kir3.1 and Kir3.4 was confirmed in western blot analyses comparing atrial and ventricular cardiomyocytes (Kir3.1 and Kir3.4 levels in homogenates of ventricular cardiomyocyte cultures were 18.3±0.7% and 7.8±2.0% of those in their atrial counterparts, respectively). Hence, tertiapin had virtually no effect on the APD in ventricular cardiomyocyte cultures. Spiral wave reentrant tachyarrhythmias could easily be induced by burst pacing in 89.2% of atrial cultures resembling 2-dimensional (2D) AF as a consequence of APD alternans at high activation frequencies. In these cultures, tertiapin significantly increased APD (from 54.7±24.0 to 128.8±16.9 milliseconds, $p<0.05$), and decreased rotor frequency (14.4±7.4 to 6.6±2.0 Hz; $p<0.05$) and complexity (6.6±7.7 to 0.6±0.8 PSs, $p<0.05$). Reentry was terminated by tertiapin treatment in 67.4% of cultures. Moreover, after tertiapin treatment spiral wave reentry could only be induced in 27.2% of cultures. Decreasing Kir3.1 of Kir3.4 expression using lentiviral vectors encoding short hairpin RNAs specific for *KCNJ3* and *KCNJ5*, yielded similar results as the pharmacological approach. Blockade or downregulation of $I_{K,ACh-c}$ or its molecular counterparts (Kir3.x) was found to prevent or terminate reentry by prolonging APD and moderating the slope in the APD and conduction velocity (CV) restitution, thereby lowering the probability of APD alternans and decreasing rotor stability.

Similarly, AF could easily be induced *ex vivo* in 90% of whole neonatal rat hearts, which was again reduced by more than 50% through blockade of $I_{K,ACh-c}$ by tertiapin.

Collectively, these results indicate that the induction, maintenance and ability to terminate AF are influenced by the atrium-specific $I_{K,ACh-c}$ through its effect on the slopes of the APD and CV restitution curves. This study thus has not only provided novel mechanistic insight into atrial tachyarrhythmias but has also identified Kir3.x as a promising atrium-specific anti-arrhythmic target.

Chapter V tested the hypothesis that constitutive activation of $I_{K,ACh}$ increases the energy necessary (*i.e.* threshold) to successfully convert AF to sinus rhythm by electrical cardioversion (ECV) and decreases the success rate of ECV. As the success rate of ECV is known to decrease with increasing AF duration, coinciding with an increase in $I_{K,ACh}$ through its constitutive activation, might play a key role in determining the ECV threshold and success rate. Therefore to test this hypothesis, we equipped neonatal rat atrial cardiomyocyte monolayers, in which we induced reentry by burst pacing with a custom-made electrical cardioverter. Indeed, incubating these monolayers with tertiapin resulted in a significantly increased success rate of electrical reentry termination (80.0 vs 36.3% at 50 V), coinciding with a decrease in threshold for reentry termination (35.5±10.9

vs 60.0±25.1 V in control cultures). Transduction with lentiviral vectors encoding short hairpin RNAs specific for *KCNJ5* yielded similar results. From a mechanistic point of view, $I_{K,ACh-c}$ determined ECV threshold through its effect on wavelength (0.48±0.14 cm in tertiapin-treated cultures vs 0.30±0.09 cm in control cultures), which correlated with the decrease in defibrillation threshold (R^2=0.65). Moreover, blockade of $I_{K,ACh-c}$ moderated the spatial shock-induced differences in depolarization and prevented propagation of shock-induced AP wavefronts, through the increase in wavelength. Optical mapping of ECV in *ex vivo* Langendorff-perfused neonatal rat hearts showed similar effects of tertiapin on the ECV threshold (27.2±0.66 vs 36.1±11.3 V in control hearts and success rate (100 vs 40% in control hearts at 30 V). These findings indicate that constitutive activation of $I_{K,ACh}$, as occurs during AF, can contribute to an increase in atrial defibrillation threshold and failure of ECV. Hence, $I_{K,ACh-c}$ may serve as an interesting target for lowering the energy requirements for ECV and increasing its effectiveness. Moreover, these results imply the possibility to alleviate ventricular pro-arrhythmia associated with drug-enhanced ECV in the context of primary ECV failure as $I_{K,Ach-c}$ is atrium-specific.

Chapter VI tested the hypothesis that direct cardioversion could be accomplished without electrical shocks by forced expression and subsequent activation of light-activated depolarizing ion channels into atrial cardiomyocytes. Because the electrical shocks employed to achieve cardioversion are very painful, ECV requires anesthesia, precluding its frequent use and hampering the applicability of device therapy for AF. Hence, exploring shockless direct cardioversion methods may provide significant improvements in AF treatment. To this purpose, neonatal rat atrial cardiomyocyte monolayers were transduced with a lentiviral vector encoding calcium-translocating channelrhodopsin (CatCh, a blue-light activated depolarizing ion channel) fused to enhanced yellow fluorescent protein (eYFP) to facilitate its detection. Monolayers transduced with a lentiviral vector encoding just the eYFP reporter were used as a control. Spiral wave reentrant tachyarrhythmias resembling 2D AF were induced by burst pacing. Indeed, exposing these monolayers to prolonged blue light pulses of 500 ms, terminated 100% of the tachyarrhythmias in the CatCh-transduced monolayers (n=31) compared to 0% in the control group (n=11). Mechanistically, CatCh activation caused uniform depolarization which led to a decrease in overall cardiomyocyte excitability as evidenced by a strong light-induced decrease in peak-to-peak amplitude in electrode recordings (251.3±217.1 μV in CatCh-transduced cultures vs 9.2±9.5 μV in control cultures). Consequently, the critical wavefront curvature decreased, coinciding with an increase in functional coresize, forcing the PSs to move towards the spiral wave periphery. The resulting light-induced PS drift led to reentry termination by PS-PS or PS-culture boundary collisions. Hence, this study shows that spiral waves in atrial cardiomyocyte monolayers can be terminated effectively by a light-induced depolarizing current, produced by the arrhythmogenic

substrate itself, upon optogenetic engineering. Taken together, these results provide the first proof-of-concept for shockless cardioversion or defibrillation.

In conclusion, cardiac tachyarrhythmias maybe counteracted by preventing the triggers that cause their initiation, altering the substrate that contributes to their maintenance, or promoting the factors that contribute to their termination. Based on the studies described in this thesis it is proposed that among other factors EADs can serve as the triggers for both focal and reentrant ventricular tachyarrhythmias in the context of cardiac remodelling. However, this thesis in the prevention of these triggers, emphasizes on the importance of taking the source of these triggers into consideration as this may affect the outcome of anti-arrhythmic interventions. Additionally, it is concluded that the minimal APD is a major factor contributing to the maintenance of cardiac tachyarrhythmias. This factor can be exploited to decrease the complexity of VF through for instance I_{K1} and I_{CaL}, but also to terminate AF in an atrium-specific manner through $I_{K,ACh-c}$. Moreover, termination of AF by ECV can be enhanced by preventing the post-shock re-emergence of PSs by slowing repolarization through blockade of $I_{K,ACh-c}$. Finally, based on the proof-of-concept provided in a study described in this thesis, immediate termination of AF may be achieved without the application of an electrical shock, through the insertion of depolarizing ion channels that are, for instance, activated by light.

DISCUSSION AND FUTURE PERSPECTIVES

In vitro and ex vivo experimental modelling of cardiac arrhythmias

Over the past decades our understanding of the mechanisms underlying cardiac arrhythmias has increased. Paramount to this development has been the introduction of the optical mapping technique using (among others) voltage-sensitive dyes. The exceptional spatiotemporal resolution provided by this technique allows researchers to get a detailed look into the propagation of APs throughout the myocardium before, during and after cardiac arrhythmias to investigate their initiation, maintenance and termination. As such, optical mapping has become an indispensable tool in the electrophysiological mapping of the heart.[1]

Still, when trying to use optical mapping to visualize AP propagation throughout the myocardium *in vivo* any researcher runs into two obvious problems: (1) Normally, the heart resides in the darkness of the inner body. Hence, both the excitation of the voltage-sensitive dye and the capture of any light emitted by the voltage-sensitive dye are precluded without surgical opening of the rib cage and pericardial cavity. (2) The heart is a very complex 3-dimensional (3D) structure. As such, while the entire heart can be incubated with a voltage-sensitive dye, the signal, if successfully captured, is only

the result of a depth-weighted average of the transmembrane potential. In other words, by far the largest component of the optical signal will be derived from epicardial heart muscle tissue. As many of the events that may be critical to the initiation, maintenance or termination of any arrhythmias likely occur supepicardially, the insights gained from whole-heart optical mapping studies is limited. Moreover, the 3D structure can hamper the interpretation of the epicardial signal as well, as the tissue from beneath the surface, by definition, emits light through a scattering volume of tissue and can therefore blur the epicardial signal.[2]

The methods used throughout this thesis provide innovative solutions to the aforementioned problems by employed *ex vivo* (*ad* 1) and *in vitro* (*ad* 1 and 2) models of cardiac arrhythmias. For *ex vivo* optical mapping the organism is removed from the heart (or *vice versa*) and subsequently perfused retrogradely using a Langendorff apparatus, to allow direct visualization of the epicardium, and capture of epicardium-derived signals. In the *in vitro* approach, the heart is (in parts) dissociated and the resulting isolated cardiomyocytes are replated on fibronectin-coated coverslips, after which they are allowed to reestablish their intercellular connections thereby forming a functional 2D syncytium. This specific configuration prevents overlooking of events important to arrhythmia initiation, maintenance and termination during optical mapping, facilitating data interpretation.

An example of events studied in the 2D *in vitro* model is presented in **Chapter IV**, in which the contribution of Kir3.x to the initiation, maintenance and termination of AF was studied. Here, it was shown that the occurrence of APD alternans produced the critical event for initiation of AF by enhancing the probability of unidirectional block formation, which depended on the expression on Kir3.x. Moreover, it was demonstrated that AF can be maintained by rotors showing either stable or unstable period dynamics, linked to the slopes in the restitution curves of the APD and CV, which were again modulated by Kir3.x. Finally, termination of AF, which could be elicited by blockade of Kir3.x channels, depended on the destabilization or rotors and consequent collision of PSs with each other or with the boundaries of the monolayer (*i.e.* the critical event for termination). The same study could serve to illustrate that studying these events in the intact, 3D heart is far more difficult.

In addition to the improved interpretability of critical events, the *in vitro* model allows for superior control of the investigated variables and are highly reproducible. An example in which this superior control is exploited is described in **Chapter II**, in which the individual contributions of pathological hypertrophy and cardiac fibrosis to the pro-arrhythmia associated with cardiac remodelling (as occurs in the context of cardiac pressure or volume overload,) were studied. As hypertrophy and fibrosis occur simultaneously during cardiac remodelling,[3] studying the individual contribution of these variables outside the *in vitro* situation is precluded.

However, regardless of the mechanistic insights offered through utilization of the *in vitro* model, it is important to remain apprehensive of overstating the implications of *in vitro* research. Hence, it is of essence to be cognizant of the methods involved in obtaining the *in vitro* results and how this relates to what they represent: As the *in vitro* model utilizes 2D monolayers, the electrotonic interactions made by each cell are less extensive than in the whole heart (3D) situation. Electrotonic interactions are known to determine the probability of deviations in the electrophysiological behaviour of single cells within the tissue from the average tissue behaviour.[4] Hence, solely changing the myocardial structure to the 2D state might alter the chance of initiating events such as EADs and APD alternans (as described in **Chapter II** and **Chapter IV**, respectively**)**. In addition, the 2D monolayers lack the anatomical boundaries found in the intact heart such as the coronary vasculature, the annuli fibrosi cordis and the epi- and endocardium (which are composed of different cell types such as endothelial cells, mesothelial cells and smooth muscle cells or contain increased amounts of fibroblasts), but are demarcated by the coverslip boundaries (which have the same cellular composition as any other area within the culture). Hence, boundary conditions found in the *in vitro* model may differ significantly from those found in the intact heart. As the occurrence of a collision between a PS and the boundaries determined the termination of arrhythmias, after for instance I_{K1} blockade (**Chapter III**), Kir3.x blockade (**Chapter IV**) or in many instances of optogenetic depolarization (**Chapter VI**), the boundary conditions of the *in vitro* model itself could in theory be critical for the termination described in these studies. Moreover, the absence in the *in vitro* model of several cell types found in the intact heart (such as endothelial cells or smooth muscle cells, as demonstrated in **Chapter IV**) could alter the outcome of the introduction of disease states such as pathological hypertrophy or cardiac fibrosis (**Chapter II**), as these states are known to modulate the behaviour of non-cardiomyocytes, as well as the (electrophysiological) effect of non-cardiomyocytes on cardiomyocytes.[5, 6]Nonetheless, as described in the studies presented in **Chapter III**, **Chapter IV** and **Chapter V** key results from the *in vitro* model (*i.e*. decreasing complexity of VF upon minimal APD increase, decrease in AF inducibility upon Kir3.x blockade and a decrease of atrial defribillation threshold after $I_{K,ACh-c}$ blockade, respectively) could be reproduced using the intact heart *ex vivo* model, which underlines the relevance of the *in vitro* model. Starting out with a simplified *in vitro* model of cardiac arrhythmias and then gradually increasing the complexity of the model thus allowed uncovering of pro-arrhythmic mechanisms and anti-arrhythmic strategies. Still, further increase of this complexity to the *in vivo* situation, large animals and eventually humans will still be necessary to establish the importance of these parameters for human disease.

Preventing arrhythmic triggers as an anti-arrhythmic strategy

As described in **Chapter I**, cardiac arrhythmias can be counteracted by preventing pro-arrhythmic triggers, by altering the substrate to prevent arrhythmia maintenance or by facilitating or forcing termination of ongoing arrhythmias. Of these three approaches, preventing arrhythmic triggers could be regarded as the preferential anti-arrhythmic strategy. Evidently, preventing an arrhythmia from occurring in the first place is the only approach that (when employed successfully) will alleviate all complications associated with allowing an arrhythmia to initiate, such as thromboembolic events in the case of AF.[7] Moreover, several studies have demonstrated that even the ectopic triggers of cardiac arrhythmias, such as premature ventricular complexes, can be a sufficient causal factor for cardiac remodelling and for the associated decrease in cardiac function and increase in pro-arrhythmic risk.[8, 9] To prevent such pro-arrhythmic triggers, it is essential to comprehend the origin of the trigger to allow the development of strategies for inhibition of critical steps within the pathway leading to its initiation. Still, it is essential to remain apprehensive of the secondary electrophysiological consequences inhibition of these pathways may have in order to select the right critical step for optimization of anti-arrhythmic treatment:

In **Chapter II** of this thesis it is demonstrated that EADs, dependent on I_{CaL}, are prime triggers for spiral wave reentrant tachyarrhythmias in the context of ventricular remodelling. Concordantly, preventing the trigger by inhibiting I_{CaL} effectively inhibited the occurrence of EADs and the consequent tachyarrhythmias caused by the pathological hypertrophic component/pathway of cardiac remodelling. However, this study also showed that using the same strategy to prevent EADs caused by the fibrotic component can lead to cardiomyocyte inexcitability, as the fibroblast-induced depolarized membrane potentials (causing inactivation of the fast sodium current) leave excitability fully dependent on calcium currents. As inexitability prevents subsequent activation and contraction of the involved myocardium, blocking I_{CaL} in the fibrotic myocardium could -in theory- severely hamper cardiac function. As such, iatrogenic inexcitability, apart from the effect I_{CaL} blockers may have on vascular tone and inotropy,[10] may contribute to the hemodynamic instability found after treatment of patients with cardiac mechanical dysfunction with I_{CaL} blockers.[10] On the other hand, if the EADs originate from a local fibrotic area, treatment with I_{CaL} blockers may be suitable for trigger prevention. Moreover, if the arrhythmia still proceeds to initiate, the resulting inexcitable area may, hypothetically, facilitate conversion to a fixed macro-reentrant circuit and thereby allow easier termination or ablation of the reentrant pathway. However, as demonstrated in **Chapter III**, a decrease in minimal APD, through I_{CaL} inhibition, during an arrhythmia can also prompt an increase in activation frequency, potentially worsening the cardiac output and possibilities for termination. Thus, prevention of I_{CaL}-dependent EADs by simply blocking I_{CaL} will mean walking a narrow tightrope between pro- and anti-arrhythmia. Hence, future

anti-arrhythmic therapy may benefit, for instance, from research exploring the possibilities to alter I_{CaL} without (substantially) affecting minimal APD and excitability. Conceptually, this may be achieved by modulating the I_{CaL} activation and inactivation dynamics, to decrease the overlap of the steady-state inactivation and activation curves and the resulting I_{CaL} window current or by increasing the time constant of I_{CaL} deinactivation (see also **Chapter I**). Hence, this thesis underlines that EAD prevention is an effective anti-arrhythmic strategy. However, selecting and modulating the right (specific) targets in the pathways that culminate into EAD-dependent arrhythmias, in order to prevent unwanted electrophysiological effect remains relatively elusive and therefore requires additional research.

Another example of trigger prevention as an anti-arrhythmic strategy is described in **Chapter IV**. Here, it is shown that APD alternans, dependent on the slope of the APD and the CV restitution curves, can serve to create unidirectional block and formation of spiral wave reentrant tachyarrhythmias. Decreasing the maximal slope in the restitution curves by blocking the constitutively active acetylcholine-dependent potassium currents ($I_{K,ACh-c}$) prevents this pro-arrhythmic trigger. Again, also with $I_{K,ACh-c}$ blockade, secondary electrophysiological consequences could, in theory, hamper therapeutic efficacy and underpin pro-arrhythmia. Since inhibition of $I_{K,ACh-c}$ lengthens APD, it may increase the probability of EADs. Be that as it may, evidence for EADs underlying AF is relatively scarce. Ventricular arrhythmias, on the other hand, are known to originate from EADs, whose incidence can increased by prolongation of the refractory period in an attempt to treat AF.[4] However, as in the heart, Kir3.x channels, which govern $I_{K,ACh-c}$, are almost exclusively present in the atrial cardiomyocytes, blockade of these channels does not lead to ventricular pro-arrhythmia.

Although the possible clinical success of this approach still has to be tested in humans, it underlines the significance of trigger prevention as a prime anti-arrhythmic strategy.

Getting to the core of cardiac tachyarrhythmias to facilitate termination

In this thesis, multiple approaches to modify arrhythmia maintenance to facilitate arrhythmia termination have been demonstrated. In **Chapter III**, it is shown that an increase in minimal APD can decrease VF complexity (*i.e.* the number of rotors) through transient rotor destabilization. Similary, in **Chapter IV** it is shown that blockade of $I_{K,ACh-c}$ can lead to rotor destabilization and termination. **Chapter VI** demonstrates how an increase in functional coresize through optogenetics can induce spiral wave drift and ultimately termination. Taken together, it seems that any intervention that causes PSs to collide with an anatomical boundary or PSs of opposite chirality leads to their termination. Hence, getting to the core of the reentrant tachyarrhythmia seems to be the key factor to facilitating its termination. Therefore, understanding what happens within and

around the core is regarded by many to be crucial, if we are to make progress in the treatment of cardiac arrhythmias through enhancing termination.

Many studies have attempted to describe, approach, or simulate the behaviour of cells within the core of a functional reentrant circuit. In 1973 the first observations of reentrant tachycardias in the absence of an anatomical obstacle led to the formulation of the 'leading circle concept'.[11-13] This theory proposed that in the absence of an anatomical obstacle the reentrant conduction would assume the shortest path length needed to sustain the arrhythmia. This minimal path length depends on the conduction velocity and refractory period, in such a way that there should be an excitable gap between the wavefront and the waveback. Under these conditions, excitation wavefronts are traveling through tissue with limited excitability. The core, in this case, is rendered refractory by electrotonic depolarization or centripetal activation from the circulating wavefront to the core.[11-13] In contrast, the spiral wave reentry theory proposed that the path of the wavefront's leading edge (or spiral wave tip) depends on the relationship between wavefront curvature and CV. An increased wavefront curvature decreases the source/sink ratio for AP propagation and therefore decreased CV.[14] Accordingly, if a reentrant circuit is to sustain without an anatomical obstacle, given homogeneous basal excitability, wavefront curvature has to increase towards the center of the circuit and CV (as a consequence) has to decrease, causing the wavefront to assume the form of an Archimedean spiral. The functional core is formed where the wavefront curvature hits the critical value and becomes zero. As at this critical curvature the wavefront cannot invade the functional core, tissue within the core is assumed to remain excitable but not excited in contrast to the state of the core as proposed in the leading circle concept.[14, 15] Moreover, while both theories describe different arrhythmia mechanisms, they do not necessarily exclude each other as cardiac arrhythmias comprise a heterogeneous group of disorders and can therefore be based on different mechanisms. This could imply that the state of the core has to be deduced or determined for each arrhythmia first, in order to apply the most effective therapeutic strategy.

In **Chapter V**, it is demonstrated that the amplitude of the shock-induced AP decreases at shorter pre-shock peak-to-peak intervals as a consequence of the local refractoriness of the tissue. Following from this relation between refractoriness and amplitude, it can be concluded that if the core is refractory (concordant with the leading circle theory), the electrical shock would induce the least depolarization at this location. As such, the core itself could be a cause for failed defibrillation. In contrast, both the core itself and the distance from the core had no effect on the shock-induced AP amplitude. Concordantly, complexity of fibrillation (*i.e.* the number of rotors) did not seem to determine the defibrillation threshold. In **Chapter VI** it is demonstrated that short decreases in excitability through optogenetics, can increase the functional coresize leading to termination of reentry. In this case, we hypothesised that the reduction in excitability

decreases the critical wavefront curvature, causing the PS to move to a more peripheral point. As the area between the PS before the excitability decrease and the new PS is not invaded as a consequence of the new critical wavefront curvature, the functional coresize is increased (to approximately the area between the old and the new PS). In this situation, the optical signal derived from the new core does not discriminate between refractoriness or absence of excitation. However, assuming that the core is depolarized and dependent on centripetal activation from a more peripheral wavefront, decreasing the excitability would only decrease the velocity of the wavefront, which decreases the wavefront-wavetail interaction, stabilizes the rotor and, importantly, leave the coresize unaltered or even diminished. The reentrant tachyarrhythmias in these cases thus seem to revolve around an excitable core in concordance with the spiral wave theory. Together, this illustrates that the state of the core can be leading in the (theoretical) efficacy of a chosen anti-arrhythmic strategy.

In contrast, in **Chapter III** and **Chapter IV**, different methods to achieve an increase in the minimal APD led to the termination of the rotors maintaining VF and AF, respectively. As this leads to an increase in wavelength both cores activated through centripetal activation or cores that remain unexcited would become destabilized as a consequence of the increased wavetail interaction of the wavefronts in their periphery. Therefore, if indeed arrhythmias exist based on both leading circle reentry and spiral wave reentry, the best way to treat arrhythmias (in absence of knowledge on the state of the core) may be not lie in tackling the core but its periphery.

Taken together, apart from providing proof-of-principle for strategies of reentry termination the results within this thesis can add to the understanding of the state of cells within the core as well as its periphery, which might help to develop new anti-arrhythmic strategies. Still, more research is necessary to fully elucidate the state of the core as well as the wavefronts in its periphery in different disease states, as well as their relation to therapeutic effects, in order to improve treatment of cardiac arrhythmias.

CONCLUSION

Understanding the mechanisms underlying cardiac tachyarrhythmias, including their triggers, maintenance and termination is crucial for their treatment. Additional efforts from the scientific community will be necessary to translate newly acquired knowledge on triggers and maintenance of arrhythmias into safe and effective ways to terminate or prevent them to thereby improve anti-arrhythmic therapy.

DUTCH SUMMARY - NEDERLANDSE SAMENVATTING

Algemene introductie van dit proefschrift, **Hoofdstuk I**, beschreef de basale electrofysiologische mechanismen die betrokken zijn bij het controleren van het hartritme en de contractie in het gezonde hart. Tal van verstoringen in deze controle, welke kunnen leiden tot ritmestoornis-initierende 'triggers' of 'substraten' voor het voortbestaan van een hartritmestoornis, werden in detail besproken. Dit werd gevolgd door een overzicht van de bijbehorende anti-aritmische strategieen die tot nu toe zijn bedacht om deze triggers te voorkomen of het substraat verantwoordelijk voor het voortbestaan van de ritmestoornis te doorbreken, om zo controle over het hartritme terug te winnen. Daarnaast, werden de nadelen van de huidige anti-aritmische behandelingen, te wijten aan het incomplete begrip van de pro-aritmische mechanismen, doorgenomen. Volgend uit deze nadelen was het doel van dit proefschrift het uiteenzetten van de cellulaire en moleculare pro-aritmische mechanismen, en het verkennen van de mogelijkheden tot meer specifieke, minder schadelijke anti-aritmische strategieen.

In **Hoofdstuk II** werden de verschillen in pro-aritmische mechanismen tussen pathologische hypertrofie van de hartspiercel en cardiale fibrose geevalueerd, alsmede hun onafhankelijke bijdrage aan het resultaat van een anti-aritmische behandeling. Aangezien hypertrofie en fibrose tegelijkertijd voor kunnen komen in de context van 'remodelling' van het ventriculaire myocard, hetgeen de ventrikels vatbaar maakt voor ritmestoornissen, is het onderscheid in hun individuele bijdrage aan ritmestoornissen moeilijk te maken. Om die reden werden neonatale ventriculaire hartspiercelkweken geincubeerd met phenylephrine om hypertrofie te induceren en werden in aparte kweken vrijelijk prolifererende fibroblasten gebruikt als model voor cardiale fibrose. Deze aanpak maakte het mogelijk om, *in vitro*, de pro-aritmische mechanismen in 'remodelled' ventriculair myocard separaat te onderzoeken. Verassend genoeg, bleken de mechanisme verantwoordelijk voor de initiatie van ritmestoornissen vrijwel gelijk in the modellen voor hypertrophy en fibrose. Beide condities induceerden een significante verlaging van de geleidingssnelheid en verlenging van de repolarizatie, wat aanleiding gaf tot het ontstaan van early afterdepolarizations (EADs). EADs lagen aan de basis van het ontstaan van zowel focale- (als gevolg van het repetitief optreden van EADs aan de grens van een continu gedepolariseerd gebied) als reentry-tachyaritmieen (als gevolg van unidirectioneel block tussen het gebied van fase II EAD initiatie en het aangrenzende gebied dat zich nog steeds in fase II van het actiepotentiaal bevond). Daarnaast, waren ook de incidenties van focale- en reentry-tachyartimieen vergelijkbaar in beide modellen. Nader onderzoek liet echter zien dat de mechanismen die ten grondslag lagen aan de vorming van EADs en de vermidering van de geleidingssnelheid wél verschilden. Terwijl de eiwit levels van connexine43 en Kv4.3 in de hartspiercellen waren verminderd als gevolg van hypertrofie, werden geen significante verschillen gevonden onder fibro-

tische condities. Aan de andere kant werd een depolarisatie van de maximale diastole potentiaal (MDP) alleen gevonden in fibrose, terwijl de MDP niet was aangedaan onder hypetrofe condities. Dientengevolge had het beinvloeden van de heterocellulaire koppeling door toediening van 2-aminoethoxydiphenyl boraat (2-APB) en carbenoxolon alleen anti-aritmische effect in het fibrotische model. Daarnaast verhinderde blokkade van het L-type calcium kanaal het ontstaan van zowel focale als reentry tachyaritmieen in hypertrofe kweken, maar veroorzaakte geleidingblok in fibrotische kweken. Deze resultaten verschaffen nieuwe inzichten in de substraat-specifieke mechanismen die geintegreerd zijn in 'remodelled' ventriculair myocard, en hoe deze mechanismen de effectiviteit van anti-aritmische strategieen kunnen beinvloeden.

Hoofdstuk III onderzocht welke electrofysiologische eigenschappen bepalend zijn voor het aantal rotors (ook wel de complexiteit genoemd) dat de ritmestoornis ventrikelfibrilleren (VF) onderhoudt. Daarnaast werden de mogelijkheden onderzocht deze kennis te gebruiken om deze bepalende parameters te veranderen teneinde rotors te termineren en daarmee de complexiteit van VF te verminderen. Met dit doel werd een nieuw *in vitro* model van VF ontwikkeld, waarbij monolagen van neonatale ratten ventriculaire hartspiercellen werden behandeld met 2-APB (een farmacologische ontkoppelaar van de gap junctions). 2-APB veroorzaakte een dosis afhankelijke toename in de complexiteit van spontaan geinduceerde spiral wave reentry tachyaritmieen, met een zeer hoge stabiliteit gelijkend op VF (0.0±0.1 phase singularities [PSs]/cm^2 in control tegenover 0.0±0.1, 1.0±0.9, 3.3±3.2, 11.0±10.1 and 54.4±21.7 PSs/cm^2 in respectievelijk 5, 10, 15, 20 en 25 µM 2-APB). Een inverse correlatie werd gevonden tussen de complexiteit en de wavelength. De wavelength kon alleen vergroot worden door middelen die de actiepotentiaalduur (APD) bij maximale activatiefrequentie (de minimale APD) konden verlengen. Blokkade van de inward rectifier kaliumstroom (I_{K1}) door $BaCl_2$ en vergroten van de L-type calciumstroom (I_{CaL}) door BayK8644 induceerde een significante verlenging van de minimale APD, hetgeen eveneens een significante verlaging van de complexiteit en de activatiefrequentie van VF *in vitro* veroorzaakte. Een toename van de minimale APD tijdens VF veroorzaakte een tijdelijke destabilisatie van de rotors, wat leidde tot terminatie van rotors door botsingen van de activatie fronten uitgaand van deze rotors. Een gelijkaardige dosis afhankelijke toename in de complexiteit kon ook worden geinduceerd door 2-APB in *ex vivo*, Langendorff geperfundeerde adulte ratten harten. Belangrijker nog, het verlengen van de minimale APD door $BaCl_2$ gaf eveneens een significante reductie van de complexiteit in het *ex vivo* model. Tezamen laten deze resultaten zien dat de stabiliteit van wordt gereguleerd door de minimale APD, welke kan worden gebruikt om VF tijdelijk te destabiliseren zodat VF kan worden getermineerd. Daarmee kunnen deze resultaten mogelijk voorzien in een nieuw conceptueel raamwerk voor toekomstige anti-aritmische medicatie en een uitbreiding in de rationale for therapeutische strategieen gericht tegen VF.

Hoofdstuk IV beschrijft een studie waarin het effect van downregulatie of blokkade van Kir3.x kanalen op de initiatie, het onderhoud en de terminatie van atriumfibrilleren (AF) werd bestudeerd. Aangezien farmacologische behandeling van AF kan worden gecompliceerd door pro-aritmische effecten ten aanzien van de ventrikels, kan het verkennen van de mogelijkheden tot het bijstellen van de atriale electrofysiologie zonder die van de ventrikels te veranderen mogelijkheden bieden tot het ontwikkelen van minder schadelijke behandelingen voor AF. Kir3.x kanalen, verantwoordelijk voor de acetycholine-afhankelijke kaliumstroom ($I_{K,ACh}$) worden alleen tot expressie gebracht in de atria en niet in de ventrikels. Van $I_{K,ACh}$ is het bekend dat deze constitutief actief wordt (oftewel acetylcholine onafhankelijk) in patienten met persisterend AF, en zou daarom een interessant doelwit kunnen zijn voor atrium-specifieke behandeling van AF. Blokkade van $I_{K,ACh}$ met de specifieke farmacologische blokker tertiapin resulteerde in een significante toename van de APD (56.5±12.5 naar 145.5±20.6 milliseconden; $p<0.0001$) in primaire neonatale ratten atriale hartspiercellen in afwezigheid van acetylcholine, wat de aanwezigheid van constitutief actieve $I_{K,ACh}$ ($I_{K,ACh-c}$) in deze cellen demonstreert. Daarnaast werd de atrium-specificiteit van zowel Kir3.1 als Kir3.4 bevestigd in Western blot analyses waarin atriale en ventriculaire cardiomyocyten werden vergeleken (Kir3.1 en Kir3.4 expressie waren respectievelijk 100.0±6.3% tegenover 18.3±0.7% en 100.0±2.8 tegenover 7.8±2.0% in atriale en ventriculaire hartspiercel lysaten). Om die reden had tertiapin vrijwel geen effect op de APD in de ventriculaire hartspiercel kweken. Spiral wave reentry tachyaritmieen, gelijkend op 2D AF, konden eenvoudig worden geinduceerd door middel van burst pacing in 89.2% van de atriale kweken als gevolg van APD alternans bij hoog frequente activatie. Tertiapin verlengde de APD (van 54.7±24.0 naar 128.8±16.9 ms), verlaagde de rotor frequentie (van 14.4±7.4 naar 6.6±2.0 Hz) en de complexiteit (van 6.6±7.7 naar 0.6±0.8 PSen) significant in deze kweken. Reentry kon worden getermineerd door tertiapin in 67.4% van de kweken. Daarnaast kon na behandeling met tertiapin in nog maar 27.2% van de kweken reentry worden geinduceerd. Downregulatie van Kir3.1 en Kir3.4 door middel van lentivirale vectoren met sort hairpin RNAs gericht tegen *KCNJ3* en *KCNJ5* resulteerde in soortgelijke resultaten als de farmacologische aanpak. Blokkade van $I_{K,Ach-c}$ of downregulatie van Kir3.x bleek reentry te voorkomen of te termineren door de APD te verlengen en de steilheid van de restitutiecurves van de APD en geleidingssnelheid te beperken, hetgeen de kans op APD alternans en rotor destabilisatie veranderde. AF kon eveneens eenvoudig worden geinduceerd in 90% van de *ex vivo* intacte neonatale ratten harten. Deze induceerbaarheid werd wederom meer dan 50% gereduceerd door behandeling met tertiapin.

Tezamen laten deze resultaten zien dat de inductie, het onderhoud en de terminatie van fibrillatie worden gecontroleerd door het atrium-specifieke $I_{K,ACh-c}$ door zijn effect op de steilheid van de restitutiecurves van de APD en geleidingssnelheid. Hiermee biedt deze studie nieuwe mechanistische inzichten in atriale tachyaritmieen en identificeert

deze studie Kir3.x als een veelbelovende atrium-specifiek doelwit voor toekomstige anti-aritmische behandeling.

Hoofdstuk V testte de hypothese dat constitutive activatie van $I_{K,ACh}$ de benodigde hoeveelheid energie (drempel) om AF succesvol te converteren naar sinus ritme door middel van electrische cardioversie (ECV) verhoogt en de kans op een succesvolle cardioversie verlaagt. Aangezien de kans op succesvolle cardioversie blijkt af te nemen naarmate AF langer bestaat, hetgeen eveneens aanleiding geeft tot een toename van $I_{K,ACh}$ door constitutieve activatie, zou $I_{K,ACh-c}$ een sleutelrol kunnen spelen in het bepalen van de drempel voor ECV. Om deze hypothese te testen werden monolagen van neonatale ratten atriale cardiomyocyten, waarin reentry was geinduceerd door middel van burst pacing, uitgerust met een speciaal vervaardigde *in vitro* electrische cardioverter. Incubatie van deze monolagen met tertiapin verhoogde inderdaad de kans op succesvolle ECV (36.3 tegenover 80.0% bij 50V), en verlaagde de drempel voor succesvolle electrische terminatie van reentry (35.5±10.9V tegenover 60.0±25.1V in controle kweken). Transductie met lentivirale vectoren, uitgerust met short hairpin RNAs tegen *KCNJ5* resulteerde in soortgelijke verhoging van de succeskans en verlaging van de drempel. Vanuit een meer mechanistisch oogpunt bleek $I_{K,ACh-c}$ de ECV drempel te controleren door zijn effect op de wavelength (0.48±0.14 cm in tertiapin behandelde kweken tegenover 0.30±0.09 cm in controles, wat correleerde met een afname in ECV drempel [R2=0.65]). Daarnaast voorkwam $I_{K,ACh-c}$ blokkade het opnieuw ontstaan van PSs door het afzwakken van de spatiële verschillen in depolarisatie die ontstaan na de shock en verhinderde het propagatie van wavefronts geïnduceerd door de schok via de verlenging van de wavelength.

Optical mapping in *ex vivo* intacte neonatale ratten harten liet overeenkomstige effecten van tertiapin op de succeskans en drempel van ECV zien (respectievelijk 36.1±11.3 tegenover 27.2±0.66V in controles en 100% vs 40% in controles bij 30V). Zodoende liet deze studie zien dat constitutieve activatie van $I_{K,ACh}$ kan bijdragen aan het verhogen van de ECV drempel en het falen van ECV. $I_{K,ACh-c}$ kan daarom een interessant mikpunt zijn om de benodigde hoeveelheid energie voor ECV te verlagen en de effectiviteit van ECV te verhogen. Daarnaast impliceren deze resultaten de mogelijkheid tot het voorkomen van ventriculaire ritmestoornissen geassocieerd met conventionele manieren van farmacologische ondersteuningvan ECV in de context van primair ECV falen omdat $I_{K,ACh-c}$ atrium specifiek is.

Hoofdstuk VI testte de hypothese dat de noodzaak voor een electrische schok voor directe cardioversie zou kunnen worden teniet gedaan door het forceren van de expressie van licht-geactiveerde depolariserende ionkanalen in atriale hartspiercellen. Omdat de schok die noodzakelijk is voor een ECV zeer pijnlijk is, is enige vorm van anaesthesie noodzakelijk voor ECV, wat frequent gebruik van ECV beperkt en ook de mogelijkheid tot implanteerbare device-therapie ontneemt. Derhalve kan het verken-

nen van de mogelijkheden tot schokvrije cardioversie significante verbeteringen opleveren in de behandeling van AF. Met dit als doel werden neonatale ratten atriale hartspiercellen getransduceerd met een lentiviralen vector uitgerust met calcium-translocating channelrhodopsin (CatCh, een depolariserend ion kanaal, dat activeerbaar is door blauw licht) gefuseerd met enhanced yellow fluorescent protein (eYFP) als een reporter gen. Monolagen van atriale hartspiercellen getransduceerd met een lentivirale vector uitgerust met uitsluitend het reporter gen werden gebruikt als controle. Spiral wave reentry tachyaritmieën werden geinduceerd door middel van burst pacing. Het blootstellen van CatCh getransduceerde kweken aan licht-pulsen van 500ms leidde inderdaad tot terminatie van 100% (n=31) van de aritmieen tegenover 0% in de controle groep (n=11). Activatie van CatCh leidden tot een uniforme depolarisatie, wat aanleiding gaf tot een vermindering van de exciteerbaarheid, hetgeen gedemonsteerd werd door een afname in de peak-to-peak amplitude in electrode recordings geinduceerd door licht (251.3±217.1 tegenover 9.2±9.5 μV in controle kweken). Als gevolg hiervan, nam de kritieke wavefront curvatuur af, waardoor de grootte van de functionele core toenam en de PS naar de periferie van de spiral wave geforceerd werd. De hierdoor ontstane PS drift leidde tot terminatie van reentry door botsingen tussen PSs met verschillende draairichting of een PS met de grenzen van de kweek. Deze studie laat daarmee zien dat spiral wave reentry tachyaritmieën in monolagen van atriale hartspiercellen kunnen worden getermineerd door een licht-geinduceerde depolariserende stroom, geproduceerd door het aritmogene substraat zelf doormiddel van optogenetische modificatie. Tezamen vormen deze resultaten het eerste bewijs voor het concept van shockvrije cardioversie of defibrillatie.

Samengevat kunnen hartritmestoornissen worden tegengegaan door het voorkomen van de triggers die initiatie veroorzaken, het veranderen van het substraat dat bijdraagt aan het onderhoud, of het bevorderen van factoren die bijdrage aan terminatie van een ritmestoornis. Op basis van de studies beschreven in dit proefschrift kan worden geconcludeerd dat onder andere early afterdepolarizations kunnen fungeren als trigger voor focale en reentry tachyaritmieen in de context van ventriculaire remodeling. In de preventie van deze triggers blijkt het echter belangrijk rekening te houden met de bron van de triggers omdat deze de uitkomst van anti-aritmische interventies kunnen beinvloeden. Daarnaast kon worden geconcludeerd dat de minimale APD een belangrijke factor is voor het onderhoud van ritmestoornissen. Deze factor kan worden uitgebuit om de complexiteit van VF te verlagen door het veranderen van de I_{K1} of de I_{CaL}, maar ook om AF te termineren op een atrium-specifieke manier door $I_{K,ACh-c}$ aan te pakken. Terminatievan AF door ECV van daarnaast worden bevorderd door het verminderen van het opnieuw ontstaan van PSs na de schok door het blokkeren van de $I_{K,ACh-c}$. Tenslotte, kan gebaseerd op het proof-of-concept geleverd in dit proefschrift, directe terminatie

van AF worden bewerkstelligd zonder een electrische schok, door geforceerde expressie van ion kanalen die geactiveerd worden door andere mechanismen dan extracellulair voltage, bijvoorbeeld via optogenetica.

DISCUSSIE EN TOEKOMSTPERSPECTIEVEN

In vitro en ex vivo experimentele modellen van hartritmestoornissen

In de afgelopen decennia is het begrip ten aanzien van het mechanisme dat ten grondslag ligt aan hartritmestoornissen sterk toegenomen. In deze ontwikkeling is de introductie van de optical mapping techniek, waarbij gebruik wordt gemaakt van (onder andere) voltage-gevoelige kleurstoffen. De hoge spatiotemporele resolutie van deze techniek maakt het voor onderzoekers mogelijk de propagatie van actiepotentialen door het myocard voor (het onderzoeken van triggers), tijdens (het onderzoeken van het onderhoud) of na (het onderzoeken van de terminatie) van hartritmestoornissen zeer gedetailleerd te bestuderen. Om die reden is optical mapping een onmisbaar hulpmiddel geworden in het in kaart brengen van de cardiale electrofysiologie.[1]

Desalniettemin, zal iedere onderzoeker wanneer getracht wordt de propagatie van actiepotentialen door het hart te visualiseren door middel van optical mapping tegen twee vanzelfsprekende problemen aanlopen: (1) In iedere fysiologische toestande is het hart omringd door een organisme. Derhalve worden zowel de excitatie van de voltage-gevoelige kleurstof als het vastleggen van het uitgezonden signaal vrijwel onmogelijk gemaakt. (2) Het hart is een zeer complexe 3-dimensionale (3D) structuur. Zodoende is, hoewel het hele hart kan worden geincubeerd met een voltage gevoelige kleurstof, het resulterende signaal slechts het resultaat van een voor de diepte gewogen gemiddelde van de transmembraan potentiaal. Met andere woorden, met afstand de grootste component van het signaal is afkomstig van het epicard. Aangezien veel van de verschijnselen die cruciaal zijn voor de initiatie, onderhoud of terminatie van een ritmestoornis subepicardiaal kunnen voorkomen, wordt de interpretatie van deze verschijnselen zeer bemoeilijkt. De 3D kan structuur ook de interpretatie van het epicardiale signaal belemmeren, doordat het weefsel onder de epicardiale oppervlakte, per definitie, licht uitzend door een hoeveelheid weefsel die verstrooing van dit licht teweeg brengt, hetgeen het epicardiale signaal kan vertroebelen.[2]

De methodes die door dit gehele proefschrift zijn toegepast bieden innovatieve oplossingen voor de hiervoor genoemde problemen, vertegenwoordigd door de *ex vivo* (*ad 1*) en de *in vitro* modellen (*ad 2*) van hartritmestoornissen. Voor het ex vivo optical mapping wordt het hart uit het organisme verwijderd en retrograad geperfundeerd gebruik makend van een Langendorff opstelling, waardoor directe visualisatie van het epicardium, en het vastleggen van het (overwegend) epicardiale signaal mogelijk

wordt. Voor de in vitro benadering wordt het hart (in delen) gedissocieerd en de hieruit voortgekomen geisoleerde hartspiercellen opnieuw uitgeplaat op fibronectine-gecoate dekglaasjes, waarna de cellen opnieuw hun intercellulaire connecties kunnen vormen zodat ze wederom een functioneel syncytium vormen. De cellen vormen op deze manier een functionele monolaag van hartspiercellen, hetgeen het onopgemerkt blijven van verschijnselen die bepalend zijn voor de initiatie, het onderhoud en de terminatie van ritmestoornissen op de multicellulaire schaal vrijwel onmogelijk maakt. Een voorbeeld van hoe deze verschijnselen onderzocht kunnen worden in het in vitro model is gegeven in **Hoofdstuk IV**, waarin de bijdrage van Kir3.x in de initiatie, onderhoud en terminatie van AF werd bestudeerd. Hier werd gedemonstreerd dat het optreden van APD alternans (m.a.w. het bepalende verschijnsel) de initiatie van AF veroorzaakte door het vergroten van de kans op unidirectioneel block, hetgeen afhankelijk bleek van de Kir3.x expressie. Daarnaast werd aangetoond dat AF kan worden onderhouden door rotors met stabiele en onstabiele period dynamics, wat gekoppeld is aan de steilheid van de restitutiecurves van de APD en de geleidingssnelheid, welke wederom werden bepaald door de Kir3.x expressie. Tenslotte bleek de terminatie van AF, die kon worden geinduceerd door IK,ACh-c blokkade, afhankelijk van de destabilisatie van rotors en de hieruitvolgende botsingen tussen PSen en de grenzen van de kweken (m.a.w. het verschijnsel bepalend voor de terminatie). Dezelfde studie kan gebruikt worden om te illustreren dat het bestuderen van dezeverschijnselen in het 3D, intacte hart vele malen moeilijker is.

Naast de toegenomen interpreteerbaarheid van bepalende verschijnselen geeft het invitro model ook de mogelijkheid tot superieure reporduceerbaarheid en controle van de onderzochte variabelen. Een voorbeeld van deze superieure controle is beschreven in **Hoofdstuk II**, waarin de individuele bijdragen van pathologische hypertrofie en cardiale fibrose aan de ritmestoornissen geassocieerd met ventriculaire remodeling (zoals ontstaat in de context van druk of volume overbelasting, bijvoorbeeld na een hartinfarct) werden bestudeerd. Doordat hypertrofie en fibrose simultaan voorkomen tijdens cardiac remodelling,[3] is het bestuderen van de individuele bijdrage van beide factoren buiten de *in vitro* situatie vrijwel onmogelijk.

Het is echter, ongeacht de mechanistische inzichten die geboden kunnen worden het gebruik van de *in vitro* modellen, belangrijk om te waken voor overschatting van de implicaties van *in vitro* onderzoeksresultaten. Het is daarom belangrijk om bewust te blijven van de methodes die gebruikt zijn om tot dergelijke resultaten te komen, en wat deze methodes vertegenwoordigen: Aangezien het in vitro model gebruikt maakt van 2D monolagen van hartspiercellen, zijn het aantal electrotone interacties per cell significant lager dan in het intacte (3D) hart. Van electrotone interacties is het bekend dat ze bepalend zijn voor de kans op deviaties in het electrophysiologische gedrag van enkele cellen van het gemiddelde gedrag van cellen binnen het weefsel.[4] Derhalve kan 'slechts'

het veranderen van de myocardiale structuur naar de 2D situatie de kans op initierende verschijnselen zoals early afterdepolarizations en APD alternans (zoals beschreven in respectievelijk **Hoofdstuk II** en **Hoofdstuk IV**) veranderen. Daarnaast ontbreken de normale anatomische barrieres uit het intacte hart zoals het epi- en endocard en de vasculatuur (die worden gevormd door verschillende celtypen als endotheelcellen, gladde spiercellen of toegenomen hoeveelheden fibroblasten) in het *in vitro* model, waar de barrieres in het in vitro model slechts the randen van het dekglaasje bedekken (en daarmee dezelfde cellulaire compositie hebben als alle andere gebieden binnen de kweek). De effecten van deze barrieres kunnen daarom verschillen in het *in vitro* model in vergelijking met het intacte hart. Aangezien de botsingen tussen PSen en anatomische barrieres onmisbaar lijken voor de terminatie van reentry tachyaritmieen in vitro, na bijvoorbeeld IK1 blokkade (**Hoofdstuk III**), Kir3.x blokkade (**Hoofdstuk IV**), of optogenetische depolarisatie (**Hoofdstuk VI**), kunnen de effecten van de aanwezige barrieres bepalend zijn voor de terminatie zoals beschreven in deze studies. Daarnaast kan het gebrek aan celtypes die worden gevonden in het intacte hart maar niet in het in vitro model (zoals endotheelcellen en gladde spiercellen, zoals aangetoond in **Hoofdstuk IV**) de uitkomst van het introduceren van ziekte-condities zoals pathologische hypertrofie of fibrose (**Hoofdstuk II**) beinvloeden, aangezien het bekend is dat deze condities ook effecten hebben op zowel het gedrag van niet-hartspiercellen als hun effecten op de hartspiercellen zelf.[5, 6] Desalniettemin was het mogelijk om de belangrijkste resultaten uit het in vitro model zoals beschreven in de studies die worden gepresenteerd in **Hoofdstuk III**, **Hoofdstuk IV** en **Hoofdstuk V**, worden gereproduceerd in het intacte hart, hetgeen de relevantie van het in vitro model onderstreept. Op deze manier kan door het starten met een vereenvoudigd in vitro modelvan hartritmestoornissen, om vervolgens de complexiteit te vergroten naar het intacte hart pro-aritmische mechanismen en anti-aritmische strategieen worden effectieve en relevante manier worden blootgelegd. Het vergroten van de complexiteit van deze modellen naar de in vivo en de humane situatie blijft echter noodzakelijk om de rol van de gevonden verschijnselen in humane ziekte ontegenzeglijk vast te stellen.

Het voorkomen van pro-aritmische triggers als anti-aritmische strategie.

Zoals beschreven in **Hoofdstuk I**, kunnen hartritmestoornissen worden tegengegaan door het voorkomen van de pro-aritmische trigger, door het veranderen van het substraat om zo het onderhoud van een ritmestoornis te voorkomen or door het faciliteren of forceren van terminatie van reeds ontstane ritmestoornissen. Van deze drie manieren van aanpak, zou preventie van trigger gezien kunnen worden als de preferentiele anti-arrhytmische strategie. Vanzelfsprekend is het beletten van het ontstaan van een ritmestoornis (wanneer met succes toegepast) de enige manier strategie die alle complicaties geassocieerd met het laten ontstaan van een ritmestoornis (zoals trom-

boembolische events in het geval van atriumfibrilleren) voorkomt.[7] Daarnaast is door verschillende studies aangetoond dat zelfs de ectopische triggers van ritmestoornissen, zoals premature ventriculaire complexen, een voldoende causale factor kunnen zijn voor het ontstaan van remodelling en hiermee geassocieerde vermindering in hartfunctie en pro-aritmie.[8, 9] Om een trigger te voorkomen is het essentieel de oorsprong van deze trigger te begrijpen, om zo te kunnen zoeken naar en in te grijpen op stappen die cruciaal zijn in de cascade die leidt tot deze trigger. Nogthans is het van groot belang om bedacht te blijven op de secundaire electrofysiologische consequenties die inhibitie van deze stappen heeft teneinde anti-aritmische behandeling te optimaliseren:

In **Hoofdstuk II** van dit proefschrift werd aangetoond dat early afterdepolarizations (EADs), afhankelijk van IcaL, de voornaamste triggers zijn van spiral wave reentry tachyaritmieen in de context van ventriculaire remodelling. Het voorkomen van deze triggers door het inhiberen van I_{CaL} bleek een effectieve manier om EADs en de hieruitvolgende ritmestoornissen in de context van de pathologisch hypertrofe component van remodelling. Dezelfde studie toonde echter ook dat dezelfde strategie, met als doel het voorkomen van EADs in de context van de fibrotische component van remodelling, inexcitability van de hartspiercellen kan veroorzaken, aangezien de fibroblast-geinduceerde depolarisatie van de rustmembraanpotentiaal (hetgeen inactivatie van het snelle natrium kanaal veroorzaakt) de exciteerbaarheid volledig afhankelijk van de calcium stromen maakt. Inexciteerbaarheid van de hartspiercellen maakt activatie en contractie van het betrokken myocard onmogelijk. Het blokkeren van de I_{CaL} in fibrotisch myocard kan daarom -in theorie- de hartfunctie significant beperken. Op deze manier zou iatrogene inexciteerbaarheid, buiten het effect dat I_{CaL}-blokkers hebben op de vasculaire tonus en inotropie,[10] kunnen bijdragen aan de hemodynamische instabiliteit die kan worden gevonden in patienten met cardiale mechanische dysfunctie na behandeling met I_{CaL}-blokkers.[10] Daarentegen, zou, mits de EAD hun oorsprong vinden in een lokaal fibrotisch gebied, I_{CaL}-blokkade geschikt kunnen zijn voor de preventie van triggers. Als de ritmestoornis in dat geval nog steeds wordt geinititieerd zou het inexiteerbare gebied, hypothetisch, conversie naar een gefixeerd macroreentrant circuit kunnen faciliteren en daarmee terminatie of ablatie van resp. reentry geleiding of het reentry circuit kunnen vergemakkelijken. Echter, zoals werd aangetoond in **Hoofdstuk III**, kan een vermindering van de minimale APD door I_{CaL}-blokkade tijdens een hartritmestoornissen juist een toename van de activatiefrequentie bewerkstelligen, hetgeen in potentie de cardiac output en de mogelijkheden tot terminatie kan verslechteren. Zodoende, werd aangetoond dat preventie van I_{CaL}-afhankelijke EADs, door simpelweg het blokkeren van de EADs, zou betekenen dat men opereert in een nauwe balans tussen pro- en anti-aritmische effecten. Om die reden zou anti-aritmische behandeling in de toekomst kunnen profiteren van onderzoek naar de mogelijkheden om I_{CaL} te moduleren zonder-, of met minimaal effect op de minimale APD en exciteerbaarheid. In

theorie zou dit kunnen worden bewerkstelligd door het corrigeren van de activatie en inactivatie dynamics van I_{CaL}, om zo de overlap in de steady-state inactivatie en activatie curves, en de hieruitvolgende I_{CaL}-window stroom te verminderen of door het reduceren van de tijdsconstante van I_{CaL}-deinactivatie (zie ook **Hoofdstuk I**). Dit proefschrift onderschrijft daarmee dat EAD-preventie een effectieve anti-aritmische strategie is. Het selecteren en corrigeren van de juiste (specifieke) targets in de cascades die resulteren in EAD-afhankelijke ritmestoornissen, teneinde ongewilde electrofysiologische effecten te voorkomen, blijft een relatief gecompliceerd doel en behoeft daarom additioneel onderzoek.

Een ander voorbeeld van trigger-preventie als anti-aritmische strategie is beschreven in **Hoofdstuk IV**. Hierin werd gedemonstreerd dat APD alternans afhankelijk is van de steilheid van de APD- en CV-restitutiecurves en kan bijdrage aan het onstaan van unidirectioneel geleidingsblok en ritmestoornissen op basis van reentry. Het verminderen van de maximale steilheid in deze curves door het inhiberen van de constitutief actieve acetylcholine-afhankelijke kalium stroom ($I_{K,ACh-c}$) voorkomt deze pro-aritmische trigger. Ook in het geval van $I_{K,ACh-c}$ blokkade zouden secundaire electrofysiologische effecten ongewenste pro-aritmische gevolgen kunnen hebben. Aangezien blokkade van $I_{K,ACh-c}$ de APD laat toenemen zou de kans op EADs kunnen toenemen. Desondanks, is het wetenschappelijke bewijs voor EADs als oorzaak voor AF schaars. Voor de relatie tussen EADs, die ook kunnen worden veroorzaakt door het verlengen van de refractaire periode in een poging AF te behandelen,[4] en ventrikulaire ritmestoornissen bestaat een duidelijk grotere bewijslast. Kir3.x kanalen, verandtwoordelijk voor $I_{K,ACh-c}$ komen echter binnen het hart alleen tot expressie in de hartspiercellen van de boezems. Blokkade van deze kanalen zal daarom niet leiden tot verntriculaire ritmestoornissen. Hoewel ieder mogelijk klinisch succes van deze aanpak nog onderzocht moet worden, onderschrijft deze studie wederom de mogelijkheid om ritmestoornissen te voorkomen door trigger-preventie.

Het aanpakken van de kern van de hartritmestoornis ten behoeve van terminatie

In dit proefschrift zijn meerdere methodes om het onderhoud van ritmestoornis te veranderen, teneinde terminatie te faciliteren aangetoond. In **Hoofdstuk III** werd gedemonstreerd dan een toename in de minimale APD een vermindering in de complexiteit van VF (m.a.w. terminatie van rotors) kan bewerkstelligen, door middel van transiente rotor destabilisatie. In **Hoofdstuk IV** werd eveneens aangetoond dat blokkade van $I_{K,ACh-c}$ eveneens kan leiden tot rotor destabilisatie en terminatie. Hoofdstuk VI laat zien hoe een toename in de grootte van de functionele kern van door middel van optogenetics kan leiden tot spiral wave drift en uiteindelijk terminatie. Tezamen lijkt het erop dat iedere interventie die ervoor zorgt dat PSen botsen met PSen van tegenover-

gestelde draairichting of anatomische grenzen leiden tot PS-eliminatie. Het aanpakken van de kern van de rotor lijkt daarmee de sleutel tot het faciliteren van terminatie. Om die reden is het begrijpen wat er gebeurt binnen en om de kern van de ritmestoornis cruciaal indien we de behandeling van hartritmestoornissen willen verbeteren.

Vele onderzoeken hebben getracht het gedrag van cellen in de kern van een functioneel reentry circuit te beschrijven, te benaderen of te simuleren. In 1973 leidden de eerste observaties van een tachycardie in afwezigheid van een anatomische obstakel tot de formuleren van het "leading circle concept".[11-13] Deze theorie veronderstelt dat in afwezigheid van een anatomisch obstakel het functionele reentry circuit de minimale lengte aanneemt de het voortzetten van de ritmestoornis toe laat. Deze minimale lengte hangt af van de geleidingssnelheid en de refractaire periode, op zo'n manier dat een klein exciteerbaar gebied blijft bestaan tussen de wavefront en waveback. De wavefront bewegen zodoende door weefsel met beperkte exciteerbaarheid. De kern van de rotor is in dit geval refractair/inexciteerbaar door electrotone depolarisatie of centripetale activatie van het circulerende wavefront naar de kern.[11-13] In tegenstelling hiermee, veronderstelt de spiral wave reentry theorie dat het pad van de spiral wave tip (de voorflank van het wavefront in functionele reentry) af hangt van de relatie tussen de wavefront curvatuur en de geleidingssnelheid. Een toegenomen wavefront curvatuur zorgt voor een afgenomen source/sink ratio voor propagatie van een actiepotentiaal en verlaagd daarmee de geleidingssnelheid.[14] Gegeven homogene exciteerbaarheid, kan een functioneel reentry circuit zodoende alleen in stand worden gehouden als wavefront curvatuur toeneemt en de geleidingssnelheid afneemt richting de kern van de rotor, waardoor de wavefront de vorm aanneemt van een Archimedische spiraal. De functionele kern wordt gevormd op de plek waar de wavefront curvatuur de kritieke waarde bereikt waarbij de geleidingssnelheid tot het nulpunt daalt. Aangezien het wavefront bij deze kritieke waarde niet kan worden voortgeleid richting de kern, wordt aangenomen dat de kern exciteerbaar maar niet geexciteerd wordt, in contrast tot de staat van de core volgens het leading circle concept.[14, 15] Hoewel deze theorieen verschillende mechanismen van ritmestoornissen beschrijven hoeven ze elkaar niet uit te sluiten omdat ritmestoornissen als geheel uit een heterogene groep afwijkingen bestaat en om die reden gebaseerd kunnen zijn op verschilllende pathofysiologie. Dit zou kunnen betekenen dat de staat van de kern voor iedere ritmestoornis zou moeten worden beredeneerd of bepaald teneinde de meest effectieve therapeutische strategie toe te passen.

In **Hoofstuk V** werd gedemonstreed dat de amplitude van de actiepotentiaal geinduceerd door een electrische schok afneemt bij korte pre-schok piek-tot-piek intervallen als gevolg van lokale refractoriteit in het weefsel. Uit deze relatie tussen refractoriteit en amplitude kan worden geconcludeerd dat als de kern van de ritmestoornis refractair is (zoals verondersteld in de leading circle theorie) zou de hoeveelheid depolarisatie

geinduceerd door een electroschok moeten afnemen richting de kern. De kern zou zou op zichzelf een reden kunnen zijn voor het falen van defibrillatie. Zowel de kern, als de afstand tot de kern bleken echter geen invloed te hebben op de amplitude van de actiepotentialen geinduceerd door electrische schokken. In overeenstemming met deze bevinding had leek de complexiteit (m.a.w. het aantal rotors) van een ritmestoornis weinig effect te hebben op de energie benodigd voor succesvolle defibrillatie. Hoofdstuk VI liet zien dat kortstondige reducties in de exciteerbaarheid door middel van optogenetics, de grootte van de functionele kern kunnen doen toenemen, wat uiteindelijk kan leiden tot terminatie van de ritmestoornis. In dit geval werd verondersteld dat de afname in exciteerbaarheid de kritieke waarde van de wavefront curvatuur doet afnemen, waardoor de PS zich naar een meer perifeer punt begeeft. Aangezien het wavefront niet kan worden voorgeleid naar het gebied tussen de PS voor de afname van de exciteerbaarheid en de nieuwe PS, als gevolg van de nieuwe kritieke wavefront curvatuur, neemt de kern toe in grootte (naar ongeveer het gebied tussen de oude en de nieuwe PS). In deze situatie kan het optische signaal uit de kern niet discrimineren tussen refractoriteit of afwezigheid van excitatie. Wanneer echter wordt aangenomen dat de core is gedepolariseerd en afhangt van centripetale activatie vanuit een meer perifere voorflank, zou het korstondig verminderen van de exciteerbaarheid mogelijk slechts de geleidingssnelheid vertragen, waardoor de wavefront-waveback interactie afneemt, de rotor stabiliseert en de groote van de kern niet verandert of juist verkleint. Deze ritmestoornissen op basis van reentry lijken daarmee te roteren rond een exciteerbare kern, in overeenstemming met de spiral wave theorie. Tezamen illustreert dit dat de staat van de kern leidend kan zijn in de (theoretische) effectiviteit van een gekozen anti-aritmische strategie.

In **Hoofdstuk III en IV** daarentegen, worden verschillende methoden gebruikt om de minimale APD te verlengen en daarmee rotors die respectievelijk VF of AF onderhouden te termineren. Aangezien deze interventie leidt tot een toename in de wavelength zouden zowel kernen van reentry die centripetaal worden geactiveerd als kernen die niet geexiteerd worden gedestabiliseerd als gevolg van de toegenomen interactie van de wavefronts en de wavebacks in hun periferie. Als ritmestoornissen inderdaad kunnen bestaan op basis van zowel de leading circle als spiral wave reentry mechanismen, zou de beste manier om ritmeproblematiek te behandelen mogelijk niet kunnen liggen in tackelen van de kern maar juist de periferie.

Tezamen biedt dit proefschrift, naast proof-of-principle for strategieen voor reentry terminatie, nieuwe inzichten in de staat van cellen in de kern en de periferie van functionele reentry, hetgeen kan helpen in de ontwikkeling van nieuwe anti-aritmische strategieen. Desondanks is meer onderzoek nodig om de staat van de kern (voor verschillende ritmestoornissen) volledig te begrijpen, alsmede het effect van deze staat op

de therapeutische effect, als we verbeteringen willen aanbrengen in de behandeling van hartritmestoornissen.

CONCLUSIE

Het begrijpen van de mechanismen die ritmestoornissen veroorzaken, met inbegrip van triggers onderhoud en terminatie is cruciaal voor hun behandeling. Additionele inspanningen van de wetenschappelijke gemeenschap zullen nodig zijn om gewonnen kennis met betrekking tot triggers, onderhoud om te zetten in terminatie of preventie van hartritmestoornissen om zodoende anti-aritmische behandelingen te verbeteren.

REFERENCE LIST

1. Efimov IR, Nikolski VP, Salama G. Optical imaging of the heart. *Circulation research*. 2004;95:21-33
2. Bishop MJ, Gavaghan DJ, Trayanova NA, Rodriguez B. Photon scattering effects in optical mapping of propagation and arrhythmogenesis in the heart. *Journal of electrocardiology*. 2007;40:S75-80
3. Jalil JE, Doering CW, Janicki JS, Pick R, Shroff SG, Weber KT. Fibrillar collagen and myocardial stiffness in the intact hypertrophied rat left ventricle. *Circulation research*. 1989;64:1041-1050
4. Weiss JN, Garfinkel A, Karagueuzian HS, Chen PS, Qu Z. Early afterdepolarizations and cardiac arrhythmias. *Heart rhythm : the official journal of the Heart Rhythm Society*. 2010;7:1891-1899
5. Shah AM, Grocott-Mason RM, Pepper CB, Mebazaa A, Henderson AH, Lewis MJ, Paulus WJ. The cardiac endothelium: Cardioactive mediators. *Progress in cardiovascular diseases*. 1996;39:263-284
6. Tian Y, Morrisey EE. Importance of myocyte-nonmyocyte interactions in cardiac development and disease. *Circulation research*. 2012;110:1023-1034
7. Wolf PA, Abbott RD, Kannel WB. Atrial fibrillation as an independent risk factor for stroke: The framingham study. *Stroke; a journal of cerebral circulation*. 1991;22:983-988
8. Bhushan M, Asirvatham SJ. The conundrum of ventricular arrhythmia and cardiomyopathy: Which abnormality came first? *Current heart failure reports*. 2009;6:7-13
9. Yarlagadda RK, Iwai S, Stein KM, Markowitz SM, Shah BK, Cheung JW, Tan V, Lerman BB, Mittal S. Reversal of cardiomyopathy in patients with repetitive monomorphic ventricular ectopy originating from the right ventricular outflow tract. *Circulation*. 2005;112:1092-1097
10. Epstein SE, Rosing DR. Verapamil: Its potential for causing serious complications in patients with hypertrophic cardiomyopathy. *Circulation*. 1981;64:437-441
11. Allessie MA, Bonke FI, Schopman FJ. Circus movement in rabbit atrial muscle as a mechanism of trachycardia. *Circulation research*. 1973;33:54-62
12. Allessie MA, Bonke FI, Schopman FJ. Circus movement in rabbit atrial muscle as a mechanism of tachycardia. Ii. The role of nonuniform recovery of excitability in the occurrence of unidirectional block, as studied with multiple microelectrodes. *Circulation research*. 1976;39:168-177
13. Allessie MA, Bonke FI, Schopman FJ. Circus movement in rabbit atrial muscle as a mechanism of tachycardia. Iii. The "leading circle" concept: A new model of circus movement in cardiac tissue without the involvement of an anatomical obstacle. *Circulation research*. 1977;41:9-18
14. Fast VG, Kleber AG. Role of wavefront curvature in propagation of cardiac impulse. *Cardiovascular research*. 1997;33:258-271
15. Karagueuzian HS, Athill CA, Yashima M, Ikeda T, Wu TJ, Mandel WJ, Chen PS. Transmembrane potential properties of atrial cells at different sites of a spiral wave reentry: Cellular evidence for an excitable but nonexcited core. *Pacing and clinical electrophysiology : PACE*. 1998;21:2360-2365

List of publications

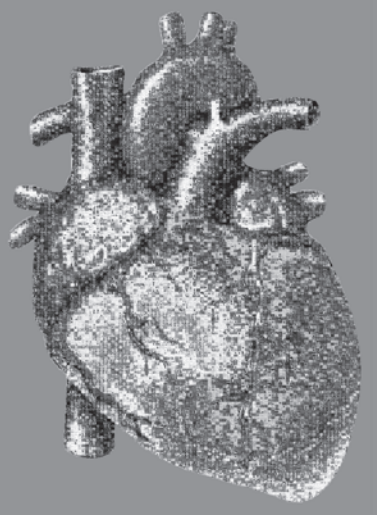

FULL PAPERS

Ray A, Huisman MV, Tamsma JT, van Asten J, **Bingen BO**, Broeders EA, Hoogeveen ES, van Hout F, Kwee VA, Laman B, Malgo F, Mohammadi M, Nijenhuis M, Rijkée M, van Tellingen MM, Tromp M, Tummers Q, de Vries L. *et al.* The role of inflammation on atherosclerosis, intermediate and clinical cardiovascular endpoints in type 2 diabetes mellitus. *European Journal of Internal Medicine*. 2009;20:253-60

Askar SF, Ramkisoensing AA, Schalij MJ, **Bingen BO**, Swildens J, van der Laarse A, Atsma DE, de Vries AA, Ypey DL, Pijnappels DA. Antiproliferative treatment of myofibroblasts prevents arrhythmias in vitro by limiting myofibroblast-induced depolarization. *Cardiovascular Research* 2012;90:295-304

Askar SF, **Bingen BO**, Swildens J, Ypey DL, van der Laarse A, Atsma DE, Zeppenfeld K, Schalij MJ, de Vries AA, Pijnappels DA. Connexin43 silencing in myofibroblasts prevents arrhythmias in myocardial cultures: role of maximal diastolic potential. *Cardiovascular Research* 2012;93:434-44

Askar SF, **Bingen BO**, Schalij MJ, Swildens J, Atsma DE, Schutte CI, de Vries AA, Zeppenfeld K, Ypey DL, Pijnappels DA *et al.* Similar arrhythmicity in hypertrophic and fibrotic cardiac cultures caused by distinct substrate-specific mechanisms. *Cardiovascular Research* 2013;97:171-81

Bingen BO, Askar SF, Schalij MJ, Kazbanov IV, Ypey DL, Panfilov AV, Pijnappels DA. Prolongation of minimal action potential duration in sustained fibrillation decreases complexity by transient destabilization. *Cardiovascular Research* 2013;97:161-70

Bingen BO, Neshati Z, Askar SF, Kazbanov IV, Ypey DL, Panfilov AV, Schalij MJ, de Vries AA, Pijnappels DA. Atrium-Specific Kir3.x Determines Inducibility, Dynamics and Termination of Fibrillation by Regulating Restitution-Driven Alternans. *Circulation* 2013;128:2732-44

Bingen BO, Engels MC, Schalij MJ, Jangsangthong W, Neshati Z, Feola I, Ypey DL, Askar SF, Panfilov AV, Pijnappels DA, de Vries AA. Light-induced termination of spiral wave arrhythmias by optogenetic engineering of atrial cardiomyocytes. *Cardiovascular Research* 2014;104:194-205.

Engels MC, Askar SF, Jangsangthong W, **Bingen BO**, Feola I, Liu J, Majumder R, Versteegh MI, Braun J, Klautz RJ, Ypey DL, De Vries AA, Pijnappels DA. Forced fusion of human

ventricular scar cells with cardiomyocytes suppresses arrhythmogenicity in a co-culture model. *Cardiovascular Research* 2015;107:601-612.

Bingen BO, Askar SF, Neshati Z, Feola I, Panfilov AV, de Vries AA, Pijnappels DA. Constitutively active acetylcholine-dependent potassium current increases atrial defibrillation threshold by favoring post-shock re-initiation. Sci Rep 2015;5:15187

LETTERS

Bingen BO, Askar SF, Schalij MJ, de Vries AA, Pijnappels DA. Prolongation of minimal action potential duration in sustained fibrillation decreases complexity by transient destabilization: reply. *Cardiovascular Research* 2013;98:156-157

Selected peer reviewed abstracts

Bingen BO, Askar SF, Ypey DL, van der Laarse AA, Schalij MJ, Pijnappels DA. Calcium-dependent repolarization abnormalities and early afterdepolarizations as basis for spontaneous reentrant tachyarrhythmias in cultured pathophysiological hypertrophic myocardial tissue. Published in *Europace* 2011;13:S3

Bingen BO, Askar SF, Ypey DL, van der Laarse AA, Schalij MJ, Pijnappels DA Early afterdepolarizations caused by calcium-dependent repolarization abnormalities as basis for spontaneous reentrant tachyarrhythmias in an in vitro model of pathological cardiac hypertrophy. Published in *European Heart Journal* 2011;32:S970

Bingen BO, Ramkisoensing AA, Neshati Z, Askar SFA, Kazbanov IV, Ypey DL, Panfilov AV, Schalij MJ, De Vries AA, Pijnappels. Atrium-specific Kir3.1 determines inducibility and dynamics of fibrillation by regulating voltage-dependent alternans in atrial cardiomyocyte Monolayers. Published in *Heart Rhythm* 2013;10:S393

Bingen BO, Ramkisoensing AA, Neshati Z, Askar SFA, Kazbanov IV, Ypey DL, Panfilov AV, Schalij MJ, De Vries AA, Pijnappels1 DA. Atrium-specific Kir3.x determines inducibility and dynamics of fibrillation by regulating voltage-dependent alternans in atrial cardiomyocyte monolayers. Published in *Europace* 2013;15:S2

Bingen BO, Engels MC, Neshati Z, Feola I, Ypey DL, Panfilov AV, Askar SF, Schalij MJ, Pijnappels DA, de Vries AA. Termination of reentrant tachyarrhythmiasby light: from electroshock towards shockless cardioversion. Published in *Cardiovascular Research* 2014;103:S52

Bingen BO, Askar SF, Neshati Z, Feola I, Ypey DL, Schalij MJ, de Vries AA, Pijnappels DA. Acetylcholine-dependent potassium current determines atrial defibrillation threshold by regulating post-shock refibrillation. Published in *European Heart Journal* 2014;35:S259

PUBLISHED INTERVIEWS

Taylor J. CardioPulse: first evidence for shockless atrial fibrillation treatment: cardiac optogenetics achieve defibrillation without the pain of electric shocks. *European Heart Journal* 2014;35:2702

Taylor J. European perspectives in cardiology: Funding: The Dutch Heart Foundation Dr E. Dekker programme. *Circulation* 2013; 128:f97-f102

Acknowledgements

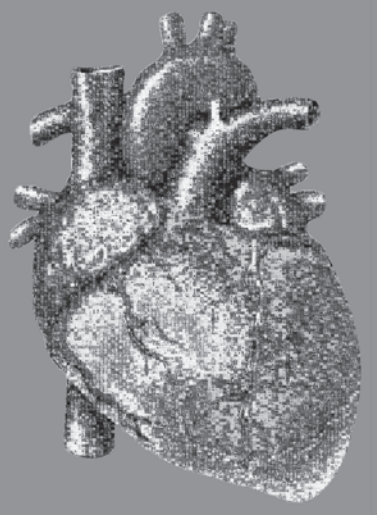

ACKNOWLEDGEMENTS-DANKWOORD

Hoewel mijn naam op de voorkant van dit boekje staat, zou dit proefschrift niet geworden zijn tot wat het nu is zonder de hulp van anderen. Ik wil daarom iedereen die betrokken is geweest bij de totstandkoming van dit boekje bedanken.

Een aantal mensen wil ik even apart noemen, te beginnen (natuurlijk) met Saïd: Ik hoef niet uit te leggen dat zonder jou dit boekje nooit was begonnen of anders niet afgemaakt. Dat jij mijn paranimf zou moeten worden staat inmiddels al een jaar of 4 vast. Macallan 35YO, opdat onze sinusoïde curves nog lang uit fase mogen blijven lopen! Daniël, hartelijk dank voor je lessen, adviezen en ondersteuning binnen en buiten de wetenschap. Twan, de hoeveelheid kennis binnen en buiten de biologie die jij tot je beschikking hebt overtreft al mijn eerdere schattingen over de grenzen van de humane opslagcapaciteit. Ik kan niet anders dan tegen je op kijken. Jouw moleculair biologische inbreng was zoals je weet onmisbaar! Dick, dank voor introductie in de basale electrofysiologie en de vele hieropvolgende interessante discussies. Minka, bedankt voor de behulpzaamheid en steun, zelfs tot aan de judomat. Cindy, ik heb je een aparte zin beloofd, dus bij deze, ik moet hem helaas hier ook alweer eindigen dus: bedankt voor alles! Margreet, Zeinab, Iolanda, Jia, Masaya and Rupa, many thanks for time spent on the much needed constructs and viruses, and valuable discussions, it was a pleasure working with you. Yoke, thanks for the daily lunchtime anecdotes, they very often made my day.

Professor Casadei, dear Barbara, many thanks for the opportunity to finish my PhD training in at your laboratory in beautiful Oxford. I sincerely hope we can continue collaborating in the future. I'd like to thank everybody else from Oxford University, especially Alice, Klemen, Xing, Rebecca and Ming, and the Oxford judo guys, Tew, Henry, Ifor and Rebecca for the good times, in and outside the Lab.

Graag wil ik ook mijn klinische collegae bedanken, in het bijzonder Maurits, Sebastiaan, Marieke, Aafke, Gijs en Jeroen. De wetenschappelijke discussies en gezamelijke congressen waren een verrijking van mijn promotietijd.

Talitha en Kariene, hartelijk dank voor jullie hulp bij alle bureaucratische rompslomp.

Ook de jongens van instrumentele zaken, Huybert, Sander en Alex kunnen niet ongenoemd blijven. Dank jullie wel!

Voeding is vanzelfsprekend van essentieel belang voor de hersenen en daarmee voor een succesvolle promotie. Daarnaast kan een goed diner met gelijkgestemden fungeren als perfecte uitlaatklep voor velerlei carrierefrustraties. Dus: Mariet, Russ, Wouter, Saïd, Kerem en Femke: Ik ben jullie bijdrage niet vergeten, en hoop dat de AYCE traditie nog lang op het menu blijft staan.

Lieve Wineke, het leven van een promovendus gaat niet altijd over rozen. Het leven mét een promovendus waarschijnlijk al helemaal niet. Ik ben blij dat jij er altijd was om toch wat bloemetjes aan het verhaal toe te voegen.

Papa, speciaal voor jou heb ik geprobeerd de inleiding van dit boekje wat begrijpelijker te maken. Als je deze keer verder leest dan de titel kunnen we misschien een keer een echte discussie over mijn werk hebben. Lieve papa, mama, Lilian en Eline bedankt voor jullie steun en support.

Curriculum Vitae

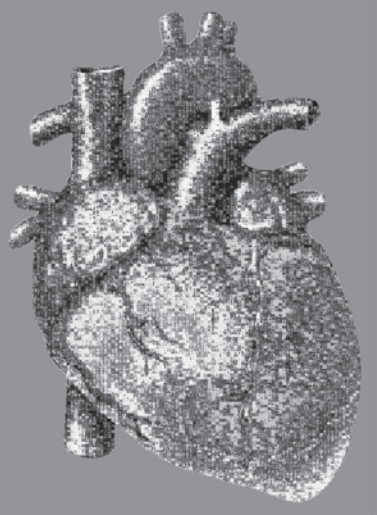

CURRICULUM VITAE

Brian O. Bingen was born on October 30, 1987 in Den Helder, the Netherlands. In 2004 he obtained his Gymnasium diploma from Visser 't Hooft Lyceum in Leiden, the Netherlands. After receiving his medical degree from Leiden University *cum laude* in 2011, he started his PhD training at the department of Cardiology, Leiden University Medical Center (LUMC), under the supervision of prof. dr. M.J. Schalij and dr. Pijnappels. During his training he focused on the molecular and cellular aspects of cardiac tachyarrhythmias. The results obtained during his PhD training are described in this thesis. He continued his research and training at the laboratory of prof. dr. B. Casadei at the Department of Cardiovascular Medicine, University of Oxford, United Kingdom. In this laboratory he studied the contribution of nitroso-redox imbalance to atrial fibrillation. In 2015 he became a LUMC cardiology resident under the supervision of prof. dr. M.J. Schalij and started his pre-cardiology phase in Internal Medicine at the Spaarne Gasthuis in Haarlem under the supervision of dr. W. de Ronde. He will return to the LUMC to finish his cardiology specialty training in 2018.

Selected scientific awards and honors

- 2011 Best moderated poster presentation, European Heart Rhythm Association, Madrid, Spain
- 2012 Best Presentation, Netherlands Heart Rhythm Association, Ermelo, the Netherlands
- 2012 Dr. E. Dekker Research grant, physician before specialty training, Dutch Heart Foundation
- 2013 Travel grant, European Heart Rhythm Association, Athens, Greece
- 2013 Best Presentation, Netherlands Heart Rhythm Association, Ermelo, the Netherlands
- 2013 Best Presentation, Rembrandt Institute of CardoVascular Science, Noordwijkerhout, the Netherlands
- 2014 Research Grant, Leiden University Fund
- 2014 Basic Research Fellowship, European Society of Cardiology
- 2014 Dr. Stiggelbout Travel Grant, Dutch Heart Foundation
- 2014 Young Investigator Award runner-up, Frontiers of CardioVascular Biology, Barcelona, Spain
- 2014 Press release selection (among others European Heart Journal, Healthline, ScienceDaily) Frontiers of Cardiovascular Biology, Barcelona, Spain
- 2014 Travel Grant, Working Group of Carciac Cellular Electrophysiology, Frontiers of CardioVascular Biology, Barcelona, Spain.
- 2014 Research Grant, Studiefonds Ketel 1

- 2014 Travel Grant, Council on Basic Science, European Society of Cardiology, Barcelona, Spain.
- 2014 Invited Lecture/Travel Grant, German Society of Cardiology, Herbsttagung und Jahrestagung der Arbeitsgruppe Rhythmologie, Düsseldorf, Germany.
- 2014 Young Investigator Award, Dutch German Joint Meeting on Molecular Cardiology, Groningen, the Netherlands